

Investigation of the binary protein-protein interactions of the yeast and the human nuclear pore complex

Dissertation zur Erlangung des akademischen Grades des
Doktors der Naturwissenschaften (Dr. rer. nat.)

eingereicht im Fachbereich Biologie, Chemie, Pharmazie
der Freien Universität Berlin

vorgelegt von

Luise Karin Apelt

eingereicht am 31.10.2014

Freie Universität zu Berlin
Fachbereich Biologie, Chemie und Pharmazie

Max-Planck Institut für molekulare Genetik
Otto-Warburg Laboratorium - Molecular Interaction Networks

1. Gutachter: Dr. U. Stelzl (Max-Planck Institut für molekulare Genetik)
2. Gutachter: Prof. Dr. M. Wahl (Freie Universität; FB – Biochemie)

Zeitraum der Anfertigung: 01.07.2010 – 31.10.2014

Disputation am 19.02.2015

Danksagung

An erster Stelle möchte ich mich bei Dr. Ulrich Stelzl für die hervorragende Betreuung während meiner gesamten Arbeit bedanken. Seine beständige Diskussionsbereitschaft, sowie seine umfassende Hilfsbereitschaft und seine immer freundliche Unterstützung ermöglichen mir eine hervorragende und motivierte Arbeitsatmosphäre. Des Weiteren möchte ich mich bei allen aktiven sowie ehemaligen Mitgliedern meiner Arbeitsgruppe: Nouhad Benslafer, Petra Birth, Anna Hegele, Arndt Großmann, Mareike Weimann, Josephine Worseck, Stefanie Jehle, Thomas Corwin und Jonathan Woodsmith für die immerwährende Unterstützung, Beantwortung jedweder Frage und die anregenden Diskussionen bedanken. Ein besonderer Dank gilt Jonathan Woodsmith, der unermüdlich meine Englischkenntnisse ertragen und verbessert hat. Auch allen Mitgliedern der Laboratorien unserer Etage möchte ich meinen herzlichsten Dank aussprechen. Egal in welcher Frage, es war stets Hilfe und Unterstützung anzutreffen.

Von ganzem Herzen möchte ich meiner Familie danken, die mich in jeder Situation unterstützt hat und mir in allen Lebenslagen mit Rat und Tat zur Seite stand. Ihr habt mir geholfen, alle Probleme anzugehen und zu meistern. Ohne euch wäre ich nicht da, wo ich jetzt bin. Danke!

Inhalt

1.	Introduction	9
1.1	The Nuclear Pore Complex – the nuclear gate keeper	10
1.2	The BBSome – a disease related transport protein complex	18
1.3	Mapping protein-protein interactions to investigate the architecture of protein complexes .	22
1.4	Aims of this study.....	24
2.	Materials and Methods	26
2.1	Materials.....	26
2.1.1	Chemicals	26
2.1.2	Lab ware.....	27
2.1.3	Organisms.....	29
2.1.4	Media.....	29
2.1.5	Vectors.....	32
2.1.6	Oligonucleotides.....	34
2.1.7	Databases.....	35
2.1.8	Software.....	35
2.2	Methods	35
2.2.1	Molecular biology of E.coli.....	35
2.2.2	Work with DNA	37
2.2.3	Molecular biology of <i>saccachomyces cerevisiae</i>	39
2.2.4	Molecular biology of human U2OS cells	42
2.2.5	Work with proteins	43
3.	Results	45
3.1	Identification of PPIs of the yeast and the human Nuclear Pore Complex	45
3.1.1	Defining the NPC clone set	45
3.1.2	Y2H system – Approach, Setup and Workflow	47
3.1.3	Identification of the human and yeast NPC PPIs	49
3.1.4	Validation of the NPC Y2H data.....	50
3.2	Characterization of PPIs within and between NPC subcomplexes	63
3.2.1	The Y2H interaction maps of the yeast and human NPC.....	63
3.2.2	Analysis of the Y2H PPIs within and between subcomplexes of the yeast NPC	65
3.2.3	Analysis of the cross species PPIs in the Y2H data set	70
3.2.4	High resolution Network of the yeast Y-complex and inter complex connections	72
3.2.5	NPC PPI network – summary.....	74
3.3	Confirmation of selected subcomplex PPIs of the yeast and the human NPC	74
3.3.1	Micro-scale Thermophoresis (MST) enables the validation of PPIs.....	75

3.3.2	Protein Complementation Assay (PCA) enables the validation of PPIs	83
3.4	Investigation of PPIs of the macromolecular protein complex BBSome	88
3.4.1	Defining the BBSome clone set	88
3.4.2	The BBSome Y2H screen – set up.....	90
3.4.3	Generation of the PPI network of the BBSome.....	91
3.4.4	Y2H data high resolution map of the BBSome components.....	92
3.4.5	The interacting domains of the BBSome.....	94
3.5	Investigation of the functional relationship between the human NPC and	95
3.5.1	Defining the human NPC-BBSome clone set.....	97
3.5.2	Identification of the NPC-BBSome PPIs with Y2H.....	97
3.5.3	Identification of the PPIs between BBSome and NPC.....	98
3.5.4	High resolution interaction map of BBSome and NPC components.....	99
3.5.5	Functional relationship between NPC and BBSome - summary.....	101
4.	Discussion	103
4.1	Aims and Structure of the discussion	103
4.2	The PPIs of the BBSome and the functional relationship between BBSome and NPC	103
4.3	The structure of the Nuclear Pore Complex	105
4.3.1	Binary PPIs of the yeast and the human NPC resulting in connections	107
4.3.2	Novel PPIs in the background of two major models describing NPC structure.....	111
4.3.4	Inter–Y-complex interactions can contribute to 16mer inner ring formation.....	117
4.3.3	Summary of the investigation of the binary PPIs of the human and the yeast NPC ...	119
4.3.4	Zusammenfassung der Untersuchung der binären Protein-Proteininteraktionen	120
5.	References	122
6.	Appendix	139

Abstract

To systematically elucidate how cellular processes are carried out it is necessary to gain insight into how proteins are organized into protein complexes. One such complex represents one of the largest protein assemblies in the cell called the Nuclear Pore Complex (NPC). The NPC consists of multiple copies of around 30 distinct proteins called Nucleoporins (Nups) that are grouped into subcomplexes whereas the largest, the Y-complex is suggested to be the structural given subcomplex. To emerge insight into the NPC subcomplex organization we utilized a high-throughput Y2H screen to determine binary protein-protein interactions (PPI). Besides yeast full length constructs the Y2H screen included fragments of yeast nucleoporins (nups) and several construct of human full length nups resulting in a network comprising 44 PPIs between 26 yeast nups and 16 PPIs between 15 human nups. The Y2H screen revealed direct connections within and between all subcomplexes of the yeast and the human NPC even on fragment level. While benchmarking the yeast Y2H data against previous published binary data set we confirmed highly reliable data. We validated selected inter and intra Y-complex PPIs with cell-based and biophysical experiments (protein-complementation assay for the human PPIs and MST for the yeast PPIs). The obtained PPI data were used to analyze the previous models based on Y-complex arrangement. We could fit our data in the latest model which arranges eight Y-complexes in an overlapping head-to-tail orientation whereas the Y-complexes are positioned in a 55° angle to the nuclear envelope, though many uncertainties remain, in particular steric constraint may arise that could exclude proposed interactions in the suggested arrangements. However, our validated inter Y-complex interactions allow the conclusion that more than two relative Y-complex positions within the NPC must exist. Taken together the Y2H data will assist further structural work on subcomplex organization.

Keywords: Nuclear pore complex, Yeast-2-Hybrid (Y2H), protein-protein interactions (PPI), Y-complex, PPI network, protein complex

Abbreviations

aa	Amino acid
AD	Activation domain
AP-MS	Affinity purification coupled to mass spectrometry
ATP	Adenosintriphosphate
BBS	Bardet-Biedel syndrome
bp	Base pair
CCT	Chaperonin containing TCP-1
CoA	Coenzyme A
Co-IP	Co-immunoprecipitation
Co-AP	Co-affinity purification
CPC	Ciliary pore complex
DBD	DNA-binding domain
DHFR	dyhydofolate-reductase
DMEM	Dulbecco's modified eagle's medium
DNA	Deoxyribonucleic acid
dNTPs	Desoxyribonukleosidtriphosphate
DPBS	Dulbecco's phosphate buffered solution
FBS	Fetal bovine serum
FG	Phenylalanine-glycine
FL	Full length
GAE	G-adaptin ear
GDP	Guanosine-5'-diphosphate
GSH	Glutathione
GST	Glutathione <i>S</i> -transferase
GTP	Guanosine-5'-triphosphate
His	Histidine
HTP	High-throughput
Ig	immunoglobulin
IFT	intraflagellar transport
IP	Immunoprecipitation
LB	Lysogeny broth
MPIMG	Max Planck Institute for Molecular Genetics
mRNA	Messenger RNA
MTP	Microtiterplate
MTX	Methotrexat
NCBI	National Centre for Biotechnological information

NE	Nuclear envelope
NES	Nuclear export sequence
NITE	National Institute of Technology and Evaluation
NLS	Nuclear localisation signal
NPC	Nuclear pore complex
Nup	Nucleoporin
OD ₆₀₀	Optical density at 600 nm
ORF	Open reading frames
PCA	Protein fragment complementation assay
PCR	Polymerase chain reaction
PH	Pleckstrin homology
PPIs	Protein-protein interactions
ProtA	Protein A
RNA	Ribonucleic acid
RRM	RNA recognition motif
SDS	Sodium dodecyl sulfate
SDS-PAGE	SDS-polyacrylamide gel electrophoresis
SOCS	Suppressor of cytokines signalling
TBE	Tris Borate EDTA
TBS	Tris-buffered saline
TBST	TBS supplemented with Tween 20
TM	Transmembrane
TPR	Tetratricopeptide repeats
TRiC	TCP-1 Ring Complex
TSS	Transformation and storage solution
UV	Ultra violet
Y2H	Yeast-two hybrid
YFP	Yellow fluorescent protein

1. Introduction

Macro-molecular protein complexes that are involved in protein transport

Most of the mechanisms that are required to drive cell functions are carried out by ‘modules’ made by different types of interacting molecules, the proteins (Hartwell et al., 1999). The knowledge of how protein complexes are assembled and their tasks is of major importance for the basic understanding of life on a molecular level. The detection of protein complexes is in rapid progress. There are already large scale approaches that are able to detect protein complexes throughout the cell. For instance, the group around Havugimana et al. 2012 identified approximately 3000 stably associated soluble proteins that form approximately 620 putative protein complexes with approximately 14000 highly confidential interactions. Approximately 20% of all predicted human reading frames are annotated as subunits of protein complexes and are reported in curated databases (Havugimana et al. 2012). Even if many protein complexes are known specific insights like their detailed architecture, their function and life cycle remain elusive and demand further investigations.

One of the largest protein assemblies is the Nuclear Pore Complex (NPC) with an estimated molecular weight of 60 MDa in yeast and 120 MDa in mammalian cells (Peters, 2005). The NPC is composed of approximately 30 proteins, called nucleoporins that occur in multiple copies totaling in at least 456 molecules per NPC (Rout et al., 2000; Cronshaw et al., 2002; Alber et al., 2007). The NPC controls the transport of molecules in and out of the nucleus (Bagley et al., 2000). Small molecules (>40 kDa) are able to diffuse freely through the pore whereas larger molecules are actively transported (Cook et al., 2007 & 2010). The BBSome is a smaller protein complex (450 kDa) that is composed of proteins encoded by BBS genes (Katsanis et al., 2004; Nachury et al., 2007). Homozygous mutations in any of the 12 BBS genes lead to the multi-symptom disorder Bardet-Biedle syndrome (BBS) (Katsanis et al., 2000; Badano et al., 2003). Besides forming the stable seven membered protein complex BBSome other BBS proteins are suggested to fulfill different functions in the cell (Kim et al., 2004; Nachury et al., 2007; Jin et al., 2010). The NPC as well as the BBSome are involved in protein transport whereby the NPC is a fixed macro-molecular basic machinery whereas the BBSome is a highly disease related mobile module (Bagley et al., 2000; Nachury et al., 2007). However, their components are composed of the same protein domains and share a similar domain arrangement suggesting a shared common ancestry origin (Obado et al., 2012).

1.1

The Nuclear Pore Complex – the nuclear gate keeper

1.1.1

Functions of the NPC – Transport of molecules and barrier characteristics of the NPC

The eukaryotic cell is divided in separate spatial compartments that allow different cell functions in special environments. The nucleus as largest cell organelle contains the genetic material and is completely separated from the rest of the cell by an intracellular membrane system, the nuclear envelope. Because of the separation, mechanisms such as protein synthesis comprising DNA replication, DNA transcription and translation take place in the nucleus and in the cytoplasm. To ensure the complete process of protein synthesis, the exchange of molecules between the nucleus and the cytoplasm must be trouble-free guaranteed. The transport of molecules is a controlled mechanism that occurs via nuclear pores spanning the inner and outer nuclear envelope. Within the nuclear pores large protein assemblies called nuclear pore complexes (NPC) are embedded and act as gatekeepers. On the one hand the major task of the NPC is the facilitation of nucleocytoplasmic traffic. On the other hand molecules have to be excluded and the separation of cytoplasm and nucleoplasm must be ensured. The major task of the NPC is to form a selective exclusion barrier (Bagley et al., 2000; D'Angelo and Hetzer, 2008). Approximately 500 – 1000 NPCs are distributed overall the nucleus (D'Angelo and Hetzer, 2008).

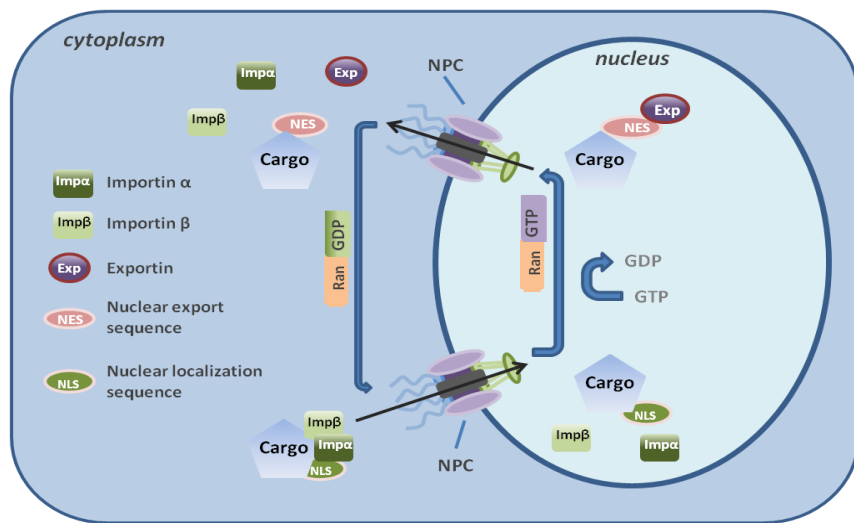


Fig 1.1 Major function of the NPC – Transport of molecules in and out of the nucleus: Import into the nucleus: The cargo binds via its NLS (nuclear localization sequence) to importin α and β that promotes the import of the cargo complex via by binding of the importins to the FG-repeat domains filling the inner channel of the NPC. Export: the export receptors bind via the NES (nuclear export sequence) to the cargo promoting its export into the cytoplasm. The directionality is controlled by Ran (a Ras-related nuclear protein) that binds to GTP (nuclear side) or GDP (cytoplasmic side).

Small molecules (< 40 kDa) are able to freely diffuse through diffusion channels with an estimated diameter of approximately $90 - 100$ Å (~ 10 nm) (Pante et al., 2002). The inner channel of the NPC is filled with a meshwork of protein domains containing different types of FG-repeats (Strawn et al.,

2004). Larger molecules (> 40 kDa) have to be transported actively through the NPC (Cook et al., 2007 & 2010). Transport receptors enable the passage of the cargo molecules by recognizing specific short sequence elements in the cargo molecules (Cook et al., 2007; Wagstaff et al., 2009). There are specific sequences for the import in the nucleus (NLS: nuclear localization sequence) and the export out of the nucleus (NES: nuclear export sequence) (Cook et al., 2007; McLane et al., 2009). The transport receptors belong to the family of karyopherins which are able to bind to specific domains of the nups that fill the inner channel. The karyopherins ‘ferry’ the cargo through the NPC by binding simultaneously the cargo and the components of the NPC (Macara et al., 2001; Cook et al., 2007; Chook et al., 2001). The whole transport process is GTP-driven. Thus the RanGTP concentration on each side of the nuclear envelope determines the directionality of transport. While the concentration of RanGTP is at high levels inside the nucleus, the cytoplasm only contains low concentrations (Cook et al., 2007; Debler et al., 2009; Cook et al., 2010). Besides determination of the transport direction, RanGTP is involved in the disassembly of the import complexes and assembly of the export complexes at nuclear side whereas the removal of RanGTP disassembles the export complexes at the cytoplasmic side (Cook et al., 2007; Chook et al., 2001; Hoelz et al., 2004; Debler et al., 2009; Cook et al., 2010). The translocation capacity of the NPC is by approximately 1000 molecules/s whereby a mass flow of nearly 100 MDa/s is achieved (Ribbeck and Görlich, 2001). In addition to nucleocytoplasmic transport components of the NPC are involved in many other cellular functions either as single proteins or as subcomplexes. They function in chromatin organization, DNA-repair and regulation of gene expression (Galy et al., 2000; Feuerbach et al., 2002; Akhtar et al., 2007; Ahmed et al., 2007; Palancade et al., 2007; Capelson et al., 2010; Strambio-de-Castillia et al., 2010; Pascual-Garcia et al., 2014).

1.1.2 Overall structure and architecture of the NPC

The NPC is a cylindrical formation that is embedded in the nuclear envelope. By microscopically observation the NPC was identified as eightfold rotational symmetrical along the nucleocytoplasmic axes with a diameter of approximately 1000 Å (Gall et al., 1967; Hinshaw et al., 2003). Nine- and tenfold rotational symmetrical NPCs were also observed indicating a flexible and modular architecture (Hinshaw et al., 2003). In comparison to the vertebrate NPCs, the NPCs of other species are smaller. Thus the vertebrate NPCs reach diameters of approximately 1250 Å, heights of approximately 950 Å and a diameter for the inner channel of approximately 550 Å. The yeast NPC has a diameter of approximately 960 Å and a height of approximately 350 Å. Thus the yeast NPC has less than half the height of its vertebrate counterpart reasoned by the different height of the nuclear envelopes (300 Å in yeast; 600 Å in vertebrates) (Akey et al., 1993; Frenkiel-Krispin et al., 2010; Yang et al., 1998). Despite different sizes the overall architecture of NPCs is well conserved throughout many species

(Kiseleva et al., 1998; Hinshaw et al., 1992; Yang et al., 1998). By using electron microscopy of Xenopus oocytes envelopes Unwin et al., 1982 determined several distinct NPC constituents. They observed two coaxial rings, one at the nuclear side and one at the cytoplasmic side. These ring-like formations are connected by eight elongated structures, termed spokes. A central plug was identified as transport channel (Jarnik et al., 1991; Stoffler et al., 2003). The NPC contains attachments extending in the cytoplasm and the nucleoplasm. Both formations are different in structure but are functionally related in releasing cargoes and providing binding sites for the transported cargoes (Cook et al., 2007). The nucleoplasmic extension is a basket-like formation providing a platform that is suggested to be an interaction interface for multiple proteins (Strawn et al., 2004; Cook et al., 2007). At the cytoplasmic site filaments, called cytoplasmic fibrils are attached extending in the cytoplasm. In summary the NPC comprises five main structures: the scaffold, the spokes, the central channel, the nuclear basket and the cytoplasmic fibrils (see Fig 1.2.). Structural rearrangements based on intrinsic conformational flexibility of the spokes of the *Dictyostelium discoideum* NPC were observed while translocating cargoes indicates structural modularity of the NPC core (Beck et al., 2004). It is formed from eight symmetric spokes that are connected and form five coaxial modules: a membrane ring, two adjacent inner rings, and two outer rings namely, the cytoplasmic and nucleoplasmic periphery (Martinez-Fernandez-Martinez et al., 2012). The modularity of the NPC was confirmed in more precise studies including integrative analyses indicating that the NPC is a highly organized protein complex (Beck et al., 2007; Fernandez-Martinez et al., 2012). The NPC is anchored to the nuclear membrane. A cryo-EM study of Akey and Radermacher in 1993 allowed a first insight into the anchoring of the NPC. They identified a luminal ring that was proposed to be responsible for the fixing the NPC to the nuclear envelope (Akey et al., 1993).

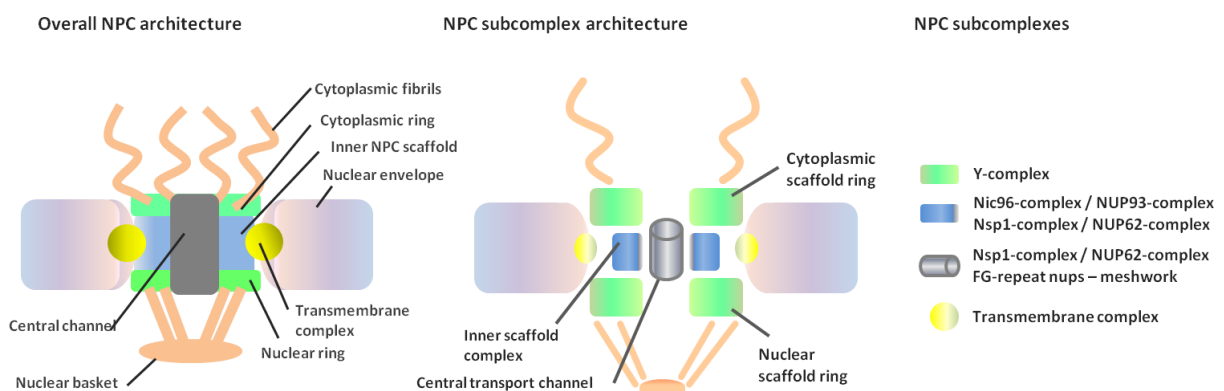


Fig 1.2 Overall NPC architecture; Shown is the schematic view of the structural building blocks of the NPC: cytoplasmic fibrils, cytoplasmic ring, inner NPC scaffold, transmembrane complex, nuclear ring, central channel and nuclear basket; and the localization of the distinct subcomplexes: Y-complex, nic96-complex/NUP93-complex, nsp1-complex/NUP62-complex, Transmembrane complex and FG-repeats filling the inner channel.

In 2000, Rout et al. assigned all nucleoporins of the yeast NPC and biochemically defined them into the discrete subcomplexes (Rout et al., 2000). Cronshaw et al., 2002 investigated the vertebrate NPC and assigned the nucleoporins to the according subcomplexes. Most of the nups are organized in

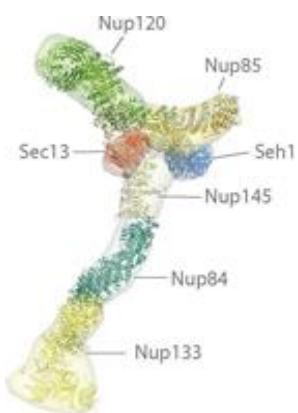


Fig 1.3 The nup84 complex of *Saccharomyces cerevisiae* (Figure of Fernandez et al., 2012); shown is a localization density map of the Y-shaped, seven-member nup84 complex: nup133, nup84, nup145C and sec13 form its base, and nup85, seh1 and nup120 comprise its arms.

discrete subcomplexes whereas the subcomplexes occur in multiple copies within the NPC. The NPC is highly conserved considering the subcomplex composition whereas the subcomplexes reflect the stable interactions of subsets of nucleoporins (Rout et al., 2000; Cronshaw et al., 2002). The symmetrical elements observed via microscopy are formed by the distinct subcomplexes. The cytoplasmic and a nucleoplasmic ring are the major scaffold units and are composed by the major scaffold subcomplex: the Y-shaped nup84-complex (nup107-complex in vertebrates). Multiple copies

of the Y-complex are ring-like arranged. However, the exact orientation of the subcomplexes is not known. The Y-complex is the best characterized subcomplex including six proteins: nup133, nup120, nup145C, nup85, nup84, sec13 and in some species seh1 (Siniossoglou et al., 1996; Lutzmann et al., 2002). The Y-complex is conserved throughout different species and the vertebrate Y-complex contains additional components: NUP37, NUP43, and ELYS (Belgareh et al., 2001; Franz et al., 2007; Loiodice et al., 2004; Rasala et al., 2006; Vasu et al., 2001).

The orthologous Y-complex of other fungi include also NUP37 and ELYS but not NUP43. Several electron microscopy studies were performed to investigate the architecture of the Y-complex (Kampmann and Blobel, 2009; Lutzmann et al., 2002; Alber et al., 2007; Thierbach et al., 2013). The overall Y-shaped structure could be determined as well as the localization of the distinct nups within the subcomplex (Fig 1.3). Crystallographic studies were performed leading to high-resolution structures of almost all Y-complex components and their interactions (Bilokapic and Schwartz, 2012b; Boehmer et al., 2008; Brohawn et al., 2008; Brohawn and Schwartz, 2009; Debler et al., 2008; Hsia et al., 2007; Leksa et al., 2009; Liu et al., 2012; Nagy et al., 2009; Seo et al., 2009; Whittle and Schwartz, 2009).

It was proposed that between the ring-like arranged Y-complexes another scaffold complex is embedded building the inner ring of the NPC, namely the nic96-complex (NUP93-complex in vertebrates) (Fig 1.2). The inner ring is connected with the membrane and is also linked to the inner channel building the bridge between membrane and inner channel (Vollmer and Antonin, 2014). The yeast nic96-complex (NUP93-complex in vertebrates) contains four large nups: nup192 (NUP205 in vertebrates), nup170 (NUP155 in vertebrates), nup188 (NUP188 in vertebrates) and nic96 (NUP93 in vertebrates). All nic96-complex members are highly connected with each other whereas nup192 and nup188 compete for one predicted α -helix as interaction site revealing two distinct binary subunits of the subcomplex (Sampathkumar et al., 2013). Structural studies in a eukaryotic thermophile possibly suggest that a supercomplex comprising nic96 (NUP93 in vertebrates), nup188 and nup192 is not formed (Amlacher et al., 2011). Moreover NUP93 (nic96 in invertebrates) might be part of two distinct subcomplexes either in interaction with nup188 or with nup192 (Theerthagiri et al., 2010; Vollmer and Antonin, 2014). In addition Amlacher et al. discovered that the structural nups of this

subcomplex were flexibly bridged by short linear motifs provided by nup53 and nic96. This suggests a new mode of interaction that enables the size flexibility of the NPC while transporting large cargoes. Crystal structures available for nic96 which revealing an unusual S-like morphology resembling in size, shape and curvature the karyopherin transport receptors (Jeudy and Schwartz, 2007; Schrader et al., 2008; Amlacher et al., 2011; Flemming et al., 2012; Sampathkumar et al., 2013).

The inner most subcomplex which is the pore-facing nspl-complex (NUP62-complex in vertebrates) (Grandi et al., 1995b; Bailer et al., 2001; Schrader et al., 2008; Ulrich et al., 2014). This subcomplex comprises three members: NUP62 (nspl in invertebrates), NUP54 (nup57 in invertebrates) and NUP58 (nup49 in invertebrates) which are essential for viability (Wente et al., 1992; Grandi et al., 1995b; Ulrich et al., 2014). The connection to the NPC scaffold is made by coiled coil domains connecting the binding partners (Bailer et al., 2001; Melcak et al., 2007). Besides coiled coil domains the members of the nspl-subcomplex contain N- or C-terminally FG-repeat domains that fill the inner channel and therefore ensure the selective transport through the NPC (Wente et al., 1992; Hu et al., 1996; Ulrich et al., 2014). Approximately 160 individual FG nups fill the inner channel (Alber et al., 2007; Ulrich et al., 2014). The coiled coil domains are well conserved in contrast to the FG-repeat domains (Ulrich et al., 2014). Nsp1 or NUP62 is part of another trimeric subcomplex comprising: nspl (NUP62 in vertebrates), nup82 and nup159 (NUP214 in vertebrates). This subcomplex was located at the entry and exit of the central channel and at the terminal ring of the nuclear basket (Fahrenkrog et al., 1998). Therefore it seems that nspl (NUP62 in vertebrates) is a member of two distinct subcomplex with different localizations. This nspl-subunit is suggested to be required for the assembly of other subcomplexes during assembly (Bailer et al., 2001). The transmembrane subcomplex comprises the nups ndc1, pom34 and pom152 in yeast and POM121, GP210, and NDC1 in mammalian cells (Wozniak and Blobel, 1994; Hallberg et al., 1993; Chial et al., 1998; Rout et al., 2000; Mansfeld et al., 2006; Stavru et al., 2006; Onischenko et al., 2009). Transmembrane nups are suggested to be crucial for NPC biogenesis (Suntharalingam and Wente, 2003). They are supposed to recruit the soluble NPC components to the nuclear envelope (Suntharalingam and Wente, 2003; Antonin et al., 2008; Onischenko et al., 2009). Further the yeast ndc1 is forming interactions with nup53 and nup59 of the nic96-complex (NUP93 in vertebrates) indicating a direct link between the membrane and the scaffold nic96-subcomplex (Onischenko et al., 2009).

1.1.3 Protein composition, domain architecture and origin of the NPC

The NPC contains only a small subset of approximately 30 different proteins, called nucleoporins (nups) that are conserved throughout distant eukaryotic species ranging from yeast to human (Rout et al., 2000; Cronshaw et al., 2002). All nucleoporins occur in multiple copies totaling in at least 456 molecules per NPC (Alber et al., 2007). NPCs are quite large with a molecular mass of 66 Mda in the

invertebrate organism *Saccharomyces cerevisiae* and 112 Mda in the vertebrate *Xenopus laevis* (Rout et al., 1993; Reichelt et al., 1990). Reasoned by the localization within the complex nups can be classified into four categories: scaffold nups, membrane nups, channel nups and miscellaneous nups comprising nuclear basket nups and cytoplasmic fibril nups (Rout et al., 2000; Rabut et al., 2004). Nups contain only a small number of different domains: α -solenoid folds (38% of the total nup residues), FG-repeat domains (29% of the total nup residues) and β -propeller (16% of the total nup residues). The rest of the protein residues are composed of the cadherin fold, the coiled-coil fold, the autoproteolytic nup98 domain and the RNA recognition motif (RRM) totaling in approximately 5% of all nup residues (Devos et al., 2006).

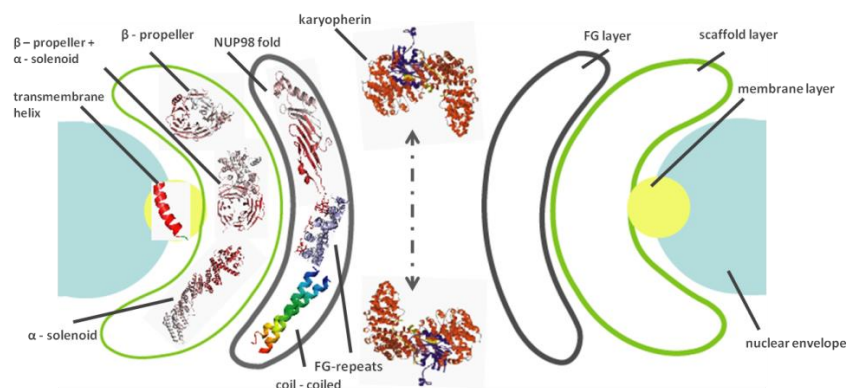


Fig 1.4 Overview of the localizations of NPC proteins containing similar domain composition (modified after Devos et al., 2006); The NPC is supposed to consist of several layers with similar protein domain compositions: the FG-layer containing proteins with FG-repeat domains, the scaffold layer contains proteins with β -propeller and α -helical domains and the membrane layer containing proteins with a transmembrane helix anchoring the large protein complex to the nuclear envelope. The nucleocytoplastic transport is done by proteins of the family of karyopherines.

A very small number of only three nups containing transmembrane domains anchor the NPC to the nuclear envelope and build the membrane layer (Devos et al., 2006). Therefore the major part of the nups is soluble. One third of all nups contain disordered N- and/or C-terminal regions that are rich in peptide stretches including FG repeats (phenylalanine glycine repeats) resulting in a total mass of 13% of the NPC (Brohawn et al., 2009). These FG-repeat nups fill the inner channel forming a dense meshwork and are rich in polar and charged residues possibly providing the biophysical properties to build the transport barrier. They include primary transport interaction sites and thus serve as docking sites for transport receptors (Hoelz et al., 2011). The FG repeat nups are held to the scaffold by nups composed of coil coiled α -helices that are arranged in zigzag fashion which differ enormously to canonical superhelical solenoids typically observed in transport receptors (Cook et al., 2007; Chook et al., 2002). A large portion of approximately 15 nups contain either α -helical regions or β -propellers whereas some nups include a combination of both. β -propellers are one of the most abundant class of proteins and involved in many different functions (Chaudhuri et al., 2008; Paoli et al., 2001). In general β -propellers are four to eight blades which are circular arrangements of antiparallel β -strands. The β -propellers of the NPC are mostly seven-bladed and N-terminal integrated. But there are unique variations of six-bladed β -propeller proteins, e.g. in sec13 and seh1. While protein interaction a

seventh blade is introduced to complete the domain *in trans* (Brohawn et al., 2008). β -propeller proteins are assumed to be architectural and serve as interaction sites to build the scaffold by connecting subcomplexes of the NPC (Brohawn et al., 2009). Nups including β -propeller are found in the NPC scaffold layer (Hoelz et al., 2011). In addition the scaffold layer also includes proteins containing either α -helices alone or tandem combinations of α -helices and β -propellers (Hoelz et al., 2011). More than half the mass of the NPC scaffold is made of α -helical domains (Brohawn et al., 2009; Hoelz et al., 2011). The α -helical proteins are composed of α -solenoids (Devos et al., 2006). Two- or three- helix units are repeatedly stacked to form an elongated super-helical domains whereby the N- and the C-terminal parts are often on opposite sides of the molecule (Kobe and Kajava, 2000; Devos et al., 2006). The nups contain three α -helical folds that are different from common α -solenoid arrangements (Boehmer et al., 2008; Jeudy et al., 2007; Leksa et al., 2009; Schrader et al., 2008; Whittle et al., 2009; Brohawn et al., 2009). The combination of β -propeller and α -helices are also found in several scaffolds such as the clathrin vesicle coats or the anaphase promoting complex (Brohawn et al., 2009). Indeed it was suggested that the NPC and the vesicle coats have a common ancestor (Devos et al., 2004). Based on the domain composition of the NPC scaffold a lattice model was proposed suggesting structural evidence for a common ancestry of the NPC and the COPI and II vesicle coats (Brohawn et al., 2008; Brohawn and Schwartz, 2009). There are several facts supporting this hypothesis: First, the occurrence of the unique β -propeller protein sec13 in the NPC scaffold. Sec13 was also found in the COPII coatamer as bona fide component. Second, sec13 has the same interaction mode in both complexes. While protein interaction between nup145C with sec13 the seventh propeller blade of sec13 is completed. The same occurs while interaction of Sec31 and sec13 in the COPII coat. This interaction mode is also found in the interaction between nup85 and seh1. Third, structural analyses of four scaffold proteins revealed a common 65 kDa domain (ACE domain – ancestral coatamer element domain) that is also found in SEC31 (Brohawn et al., 2008; Brohawn and Schwartz, 2009). Fourth, the overall protein domain composition of both complexes comprising a comparable distribution of β -propellers and α -solenoids is similar. This leads to fifth, the specific protein domain composition, namely the arrangement of amino-terminal β -propeller followed by specific α -solenoids is shared between coated vesicle proteins and proteins of the Y-complex (Devos et al., 2004). In summary, this hypothesis including the structural analyses are not only providing structural origin data moreover they propose how the NPC is assembled and anchored to the membrane by only three nups containing transmembrane domains. It was suggested that the shared characteristics of the COPII coatamer vesicle and the Y-complex form a membrane-curving module to form a coat that stabilize the highly curved membrane and allow that the large nuclear pore complex is hold to the membrane (Devos et al., 2004; Brohawn et al., 2008). Taken together, the protein domain composition and the distribution of the distinct nups within the NPC underline that the NPC is a structurally highly organized protein complex.

1.1.4 Assembly and disassembly of the NPC

The NPCs are embedded in the nuclear envelope. During the process of cell proliferation the nuclear envelope breaks down and reforms. NPCs are also affected by this process and they assemble and disassemble. There are two phases during cell cycle in which the NPC need to be assembled, first, at the end of mitosis while nuclear envelope is reforming around the segregated chromosomes and second during interphase while cells double their number of pores as preparation for next cell division. Both processes lead to new pores but the assembly occurs under different conditions. The mitotic NPC assembly is a highly organized step-wise process that occurs while the nuclear envelope is still broken down (Brohawn et al., 2008). Firstly, the nuclear envelope is the invaginated what seen in the outer membrane with electron microscopy (Kiseleva et al., 2001). When both nuclear membranes contact they fuse. This invagination is then stabilized by an electron-dense ring that might be part of the spoke complex containing Y-complex members to form a pore probably the ‘prepore’ (Kiseleva et al., 2001; Belgareh et al., 2001; Walther et al., 2003; Theisen et al., 2008). It is assumed that the chromatin-bound intermediate ‘prepore’ is formed that functions as binding platform for transmembrane nups and for more peripheral nups. Here structural nups of the Y-complex, a structural subcomplex, are recruited to the chromatin in a sequential manner starting in the early anaphase (Belgareh et al., 2001; Walther et al., 2003; Theisen et al., 2008). It was also shown that electron-dense material is inserted forming the central plug, the transport channel (Kiseleva et al., 2001). The NPC has already started to transport cargoes before it is totally assembled indicating that not all nups are essential for transport (Dultz et al., 2008; Bodoor et al., 1998). It seems that an intermediate the ‘star ring’ is then assembled and the cytoplasmic ring is build on top of it (Kiseleva et al., 2001). Lastly the cytoplasmic filaments were added (Kiseleva et al., 2001). In contrast the NPC assembly during the G1 and G2 phase of interphase occurs while the cytoplasm is completely physically separated from the nucleoplasm by an intact nuclear envelope. During interphase the cell prepares for re-entering mitosis and therefore NPCs were doubled. The knowledge of the assembly mechanism during interphase is very limited. What is known is that RanGTP and the karyopherin importin β are required and that nups were incorporated from both sides of the nuclear envelope indicating that the assembly requires coordination of nuclear and cytoplasmic events (Ryan et al., 2003; D’Angelo et al., 2006). Thus both assembly mechanisms include different parts. However both mechanisms involve coordinated interactions of chromatin-bound subcomplexes, transmembrane subcomplexes and cytoplasmic subcomplexes to assemble a stable nuclear pore complex into the double nuclear envelope. The disassembly of the NPC is assumed to be the reverse process to assembly since the same structural intermediates were observed in reverse order (Kiseleva et al., 2001). Many nups have been shown to be phosphorylated during mitosis (Doye 2011; Bui et al., 2013). Thus NUP98 was identified as a key target of CDK and other kinases. The phosphorylation removes NUP98 from the NPC that is followed by a stepwise ordered disassembly process (Laurell et al., 2011). The temporal progression is unknown and only one intermediate time

point could be identified (Kiselva et al., 2001). The process of disassembly seems to be more synchronous than that of assembly. The mitosis and nuclear envelope breakdown is a rapid and sudden triggered mechanism regulated by phosphorylation of nups (Macaulay et al., 1995). Thus the order of nup disassembly seems to reflect their accessibility to mitotic kinases.

1.2 The BBSome – a disease related transport protein complex

1.2.1 Functions of the BBS proteins

BBS describes a genetic disorder called Bardet-Biedle syndrome (Katsanis et al., 2004). The first BBS case was described in 1866 and a relation to specific genes was done in the 1990^{ties} (Leppert et al., 1994; Carmi et al., 1995a; Kwitek-Black et al., 1993). There are 14 different BBS genes described (Tobin and Beales, 2009). A homozygous mutation in any of the BBS genes will cause a multi-symptom disease pattern including blindness, obesity, polydactyl, kidney failure, deafness and retinal dystrophy, to name only a few (Green et al., 1989). The Bardet-Biedle syndrome is suggested to be caused by dysfunction of primary cilia (ciliopathies) (Mykytyn et al., 2004). The primary – or non-motile cilia are cell organelles extending as microtubule based protuberances from the cell body (Greenwood, 1892). Notably cilia are suggested to be signaling centers during vertebrate development setting investigations regarding cilia into spotlight of recent scientific work (Goetz et al., 2010). For instance, cilia are required for hedgehog signaling which plays an essential role in digit and limb formation (Huangfu et al., 2003). The BBS proteins are highly conserved throughout ciliated organisms, from the green algae Chlamydomonas to human and are absent in nonciliated organisms such as plants, fungi and amoeba (Nachury et al., 2007). A first relation between the primary cilia and BBS proteins was observed by Kim et al. in 2004. An Y2H experiment revealed a binary interaction between BBS4 and PCM1 (pericentriolar material 1). PCM1 is a large centrosome-associated autoantigen (228 kDa) and was reported to be part of the dynein-dependent, microtubule-based transport of proteins to the centrosome (Dammermann and Merdes, 2002). Expressed truncated forms of BBS4 lead to defectives in targeting of the pericentriolar proteins and further to microtubule disorganization indicating a relationship between BBSome proteins and the biogenesis of primary cilia via PCM1. A more detailed link to ciliogenesis reported Nachury et al. in 2007 & 2010. Their findings suggest the recruitment of the BBS components via Rabin8 to the centrosome or basal body and further the activation of the GTPase Rab8 that promotes the docking and fusion of vesicles close to the ciliary membrane. This allows the entry of Rab8_{GTP} and of the BBS proteins into the cilia indicating a role in ciliogenesis. Moreover they reported that PCM1 is transiently attached to a stable complex comprising seven BBS components (BBS1/2/4/5/7/8/9) that form a 450 kDa complex, termed

BBSome. It is suggested that the centriolar satellites transport the BBSome within the cytoplasm and transport is to the primary cilia where the BBSome interacts with Rabin8.

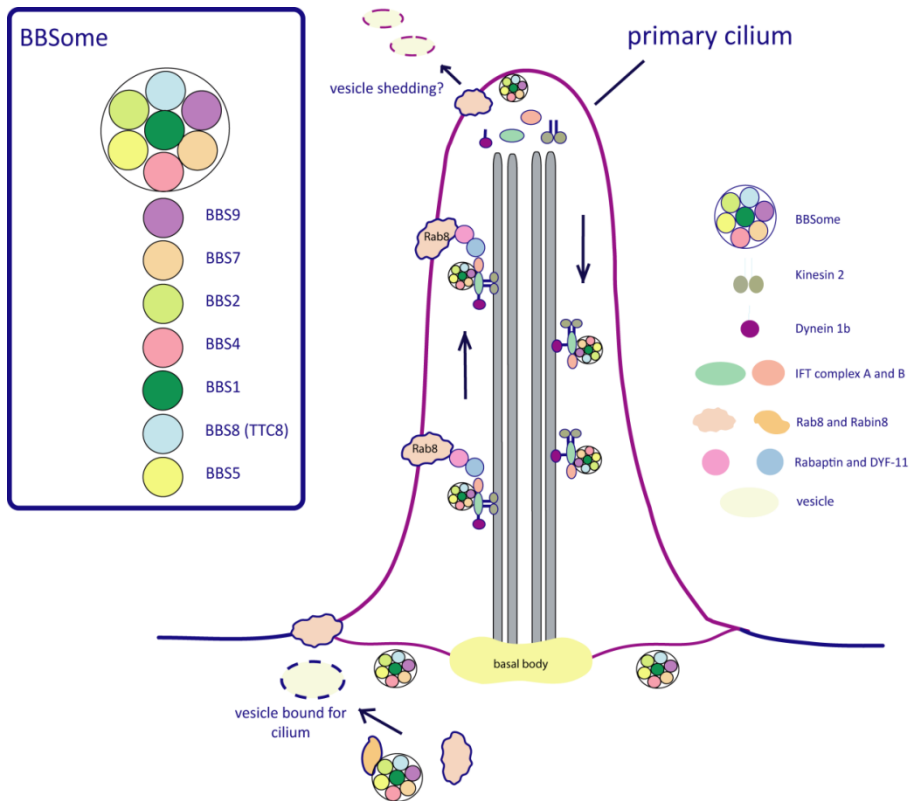


Fig 1.5 Schematic view of the localizations and tasks of the BBSome. The BBSome complex is found in the primary cilia as well as in the cytoplasm where it fulfills different functions. Within the cytoplasm it is suggested to be transported via Rab8 to the bottom of the primary cilium where it might be involved in vesicle shedding. Within the cilia the BBSome is proposed to control the intraflagellar transport (IFT) via binding to the IFT complexes A and B. See more details in the text.

In 2008, Loktev et al. discovered that the BBSome subunit BBIP10 that also located at the primary cilium and is suggested to be part of the stable protein complex (Loktev et al., 2008; Jin et al., 2010). They reported that BBIP10 is required for cytoplasmic microtubule polymerization and acetylation, functions that are not shared with any other BBSome subunits. However the depletion of BBSome components yields in characteristic BBS phenotypes in zebra fish linking dysfunction of the primary cilium to BBSome complex components. Beside ciliogenesis the BBSome has different tasks. Coat complexes resembling COPI, COPII and clathrin are suggested to be responsible for sorting membrane proteins to cilia (Jin et al., 2010; McMahon and Mills, 2004) (Fig. 1.5). It seems that the BBSome acts as coat complex. Besides tasks within the cytoplasm the BBSome fulfills several functions within the primary cilia. It was shown that the BBSome is part of the intra-flagella transport along the microtubules between the tip and the base of the cilia. BBS7 and BBS8 are reported to promote the cohesion between the IFT subcomplexes but no real interaction was shown (Ou et al., 2005). Moreover it seems to control the intraflagella transport (Wei et al., 2012). Taken together the BBSome proteins fulfill different tasks in the cell but all functions seem to be related to the transport of

molecules. However there are fundamental questions to be answered such as: How is the BBSome architecture? Which binding partner does it have? Are there unknown tasks within the cell? To address these questions the protein complex should be investigated on a molecular level, e.g. the specific BBS architecture should be determine as well as possible protein-protein interactions with other cell components.

1.2.2 Protein composition, domain architecture and assembly of the BBSome

The recently discovered octameric stable protein complex comprises seven highly conserved BBS components BBS1, BBS2, BBS4, BBS5, BBS7, BBS8, BBS9 and the novel protein BBIP10 (Loktev et al., 2008; Nachury et al., 2007 & 2008 & 2010; Jin et al., 2010). To investigate the BBSome protein architecture and determine similarities to coat complexes structural analyses were performed using sensitive structure-prediction algorithms (Jin et al., 2010). These investigations revealed a relatively simple domain architecture comprising mostly β -propeller, β -sandwiches, α -helices and α -solenoids (TPR domains) (Fig 1.6).

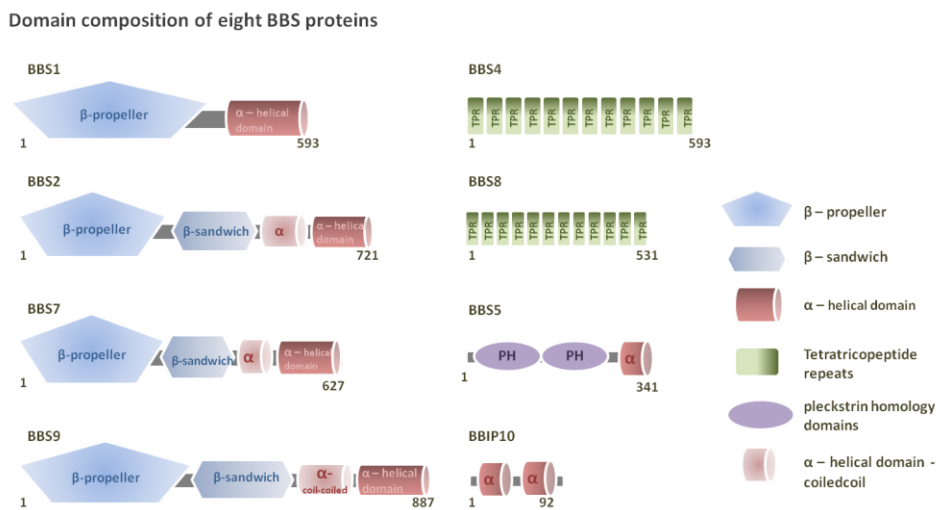


Fig 1.6 Domain compositions of eight BBSome components (modified after Jin et al., 2010). The BBSome components contain only a small number of different domains: α -helices, α -solenoids (TPR) and α -coiledcoils, β -propeller and β -sandwiches and PH domains. BBS2, BBS7 and BBS9 share architectural similarities as well as BBS1. However BBS1 is missing the β -sandwich that is inserted in the middle part of BBS2, BBS7 and BBS9. BBS4 and BBS8 (TTC) contain only TPR domains that fold into extended rod-shaped α -solenoids. BBS5 contains two PH-domains followed by an α -helical domain whereas BBIP10 contains only two α -helical domains. Both, BBS5 and BBIP10 are not included in our investigations. They were reported to be part of the architecture (see text for details).

Considering the structure BBS1, BBS2, BBS7 and BBS9 share similar domain architecture. All four proteins contain an N-terminal β -propeller. Except of BBS1 a β -sandwich is following the β -propeller. The β -sandwich fold was reported to be distantly related the immunoglobulin (Ig)-like β -sandwich of the γ -adaptin ear (GAE) motif in their C-termini (Jin et al., 2010). In addition BBS2, BBS7 and BBS9 include a α/β platform domain followed by a α -helix. The GAE motif is also found in several clathrin

adaptors and in the COPI coatamer either alone or fused to the α/β platform (McMahon and Mills, 2004). A first similarity to coatamer complexes was unraveled. COPII and clathrin cages contain rigid α -solenoids and β -propeller that form the scaffold of the vesicle coats (Stagg et al., 2007). Therefore the occurrence and the abundance of both domain folds suggest an ancient evolutionary relationship between the BBSome and the coatamer complexes (Jin et al., 2010). All four BBS components (BBS1, BBS2, BBS7 and BBS9) include an α -helical domain at their C-termini (Jin et al., 2010). In contrast BBS4 and BBS8 are entirely comprised of TPR domains that fold into extended rod-shaped α -solenoids (Jin et al., 2010).

To determine how the BBSome is assembled several approaches were performed by Zhang et al., 2012. By using RNAi against BBS genes to disrupt BBSome formation and overexpression of certain BBS components to assemble and accumulate distinct BBSome intermediates the BBSome assembly was characterized (Zhang et al., 2012). They reported that the BBSome assembly is an ordered stepwise process. Firstly a ternary complex is formed, consisting of BBS2, BBS7 and BBS9. Notably BBS9 and BBS7 are suggested to interact not directly (Zhang et al., 2012). This ternary complex is suggested to be the ‘core complex’ of the BBSome recruiting the other four members. In fact, during the next assembly step BBS5 and BBS8 are recruited, followed by BBS1. The last BBS component that is integrated into the stable complex is BBS4. However there remains the question of the function of the BBS proteins that are not incorporated into the stable complex. It was shown that the three BBS components BBS6, BBS10 and BBS12 share sequence homology to the CCT complex (chaperonin containing t-complex). The CCT (also known as TriC) family belongs to the group II chaperonins (Katsanis et al., 2000; Stoetzel et al., 2007). CCT proteins are forming a 900 kDa hetero-oligomeric complex that mediates protein folding in an ATP-dependent manner (Kubota et al., 1995; Spiess et al., 2004). 30% of the mutational load in BBS is distributed in these three genes (Seo et al., 2010). Seo et al. 2010 showed that all three BBS components are binding to each other building a ternary complex in conjunction with six CCT chaperonin proteins. Taken together it was reported that BBS6, BBS10 and BBS12 are required to assemble the BBSome while sharing sequence homology to the CCT proteins and thus fullfil chaperonin-like function in relation to BBSome assembly (Seo et al., 2010). Taken together the knowledge about the protein domain architecture of the BBSome is quite limited. However it seems that the BBS proteins which assemble the BBSome share sequence similarities to the vesicle coats whereas three other BBS proteins are required to assemble the BBSome and share sequence homology to chaperonins (Kim et al., 2004; Jin et al., 2010; Seo et al., 2010; Zhang et al., 2012).

1.3

Mapping protein-protein interactions to investigate the architecture of protein complexes

Most cellular processes are driven by coordinated protein actions in macro-molecular assemblies, the protein complexes. It is of fundamental importance to understand the molecular architecture of those protein complexes (Stelzl and Wanker, 2006; Vidal et al., 2011). To identify physical interactions between proteins several main technologies such as the Y2H system (Yeast-2-Hybrid), the Co-AP (Co-Affinity purification assay) pull downs and the PCA (Protein Complementation Assay) are used. The PCA is based on the reconstitution of either the DHFR-enzyme (dihydrofolate-reductase) leading to resistance to MTX (Methotrexat) or a fluorescence protein such as YFP (yellow fluorescence protein) leading to a fluorescence read-out both occurring in living cells (Sanderson 2008). Co-AP assays and pull downs can be performed differently, namely with different tags such as ProteinA or GST (Glutathione S-transferase). To address a GST pull down assay the protein of interest and GST are expressed as fusion protein. The strong affinity of GST to GSH (Glutathione) is exploited using GSH coated beads. The protein of interest will stick via GST to the beads and all bound proteins can be pulled down (Townsend et al., 2003). The Y2H screen is based on the reconstitution of a transcription factor via the protein-protein interaction (Fig 1.7). The Y2H system was developed by Stanley Fields in 1989 (Fields and Song, 1989) and is based on the reconstitution of two separable domains of a transcription factor. The DNA binding domain (DBD) recruits the transcription factor to the DNA whereas the activation domain (AD) initiates the transcription of the target genes, namely the reporter gene such as histidine that enables the yeast to grow on selective media. Both transcription factor domains are fused to the proteins of interest resulting in DBD and AD fusion constructs, also called bait and prey constructs, respectively.

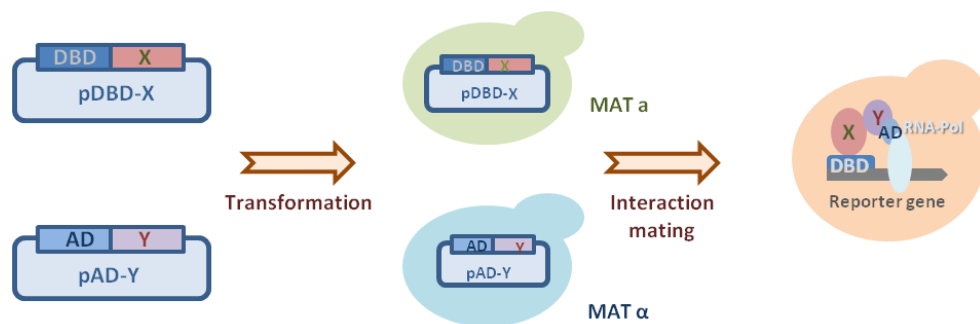


Fig 1.7 Schematic principle of the Y2H approach. The coding sequences for the proteins of interest (X and Y) are fused to the DBD (bait) and AD (prey) of a transcription factor. Two yeast strains of opposite mating types (MAT α and MAT α) are transformed with the bait and prey plasmids. After mating the diploid yeast strains express both hybrids proteins. While interaction of protein X and Y the DBD domain and the AD domain of the transcription factor come into close proximity leading to activation of gene activation of the reporter gene. The reporter gene activation enables the yeast to grow on selective media, namely in the absence of selected nutrient such as histidine or uracil or both (Stelzl and Wanker, 2006).

The reconstitution of both transcription domains occurs via the protein-protein interaction when AD and DBD come into close proximity. In summary a protein-protein interaction enables the yeast to

grow on selective media by reconstitution of a transcription factor and following transcription and synthesis of a reporter gene, mostly an amino acid or an intermediate of an amino acid synthesis pathway (Fig 1.7). The protein-protein interaction detection of the Y2H screen as well as the PCA provides heterologous environments either in yeast cells or in mammalian cells *in vivo*. The determination of protein-protein interactions with Co-AP assays occurs *in vitro* and therefore in a more natural cellular environment (Chaudhary and Mann, 2010). But highly abundant proteins are often identified as false positives (Mackay et al., 2008). Washing steps during co-APs and pull downs lead to loss of weak or transient interactions (Townsend et al., 2003). Strong interactions can be detected. GST pull downs reach affinities of 10 mM whereas the affinity for co-APs cannot be determined. They strongly depend on experiments conditions (Mackay et al., 2008). The Y2H approach is much more sensitive up to an affinity of 10-100 µM reasoned by the low expression levels of the tested proteins in the according expression vectors (Mackay et al., 2008). Moreover the proteins used in the Y2H approach are independent of endogenous expression levels leading to a preferred tool to analyze binary protein-protein interactions (Worseck et al., 2012). The Y2H system can be performed in two high-throughput (HTP) approaches: the matrix and the library approach. The matrix approach is based on an array in which either the bait or the prey have a fixed position in either a 96 or 384 well matrix, called bait or prey matrix. The separate bait or the prey constructs were then screened against the whole matrix. The interaction is detected by a growing spot in a specific position according to the interacting matrix construct. The matrix construct can be determined via its position in the matrix whereas the separate construct is already known (Worseck et al., 2012). In the library approach the baits are separately screened against a prey pool (prey library) that contains random cDNA fragments or open reading frames (ORFs) (Chien et al., 1991). In case of an interaction the prey is isolated from the growing yeast colonies and identified by Sanger sequencing (Chien et al., 1991). In summary both approaches differ in their read-out. While the library approach results in a sequencing read-out the interaction of the matrix approach is determined directly from its position in the array (Worseck et al., 2012; Chien et al., 1991). The proteins that are encoded by the matrix constructs are tested with equal probability than to the random protein encoding library constructs. The matrix constructs were normalized enhancing the detection efficiency of interactions in the matrix screen (Reboul et al., 2003). In addition the Y2H matrix screens can be easily repeated (Worseck et al., 2012). Reasoned by its easy handling in form of automated screens and the relatively low costs the Y2H approach belongs to one of the most powerful tools to generate quality-controlled, proteome-wide, binary PPI data (Worseck et al., 2012). Comprehensive proteome-wide screens have already been realized for yeast, fly, worm and human (Ito et al., 2001; Uetz et al., 2000; Yu et al., 2008; Giot et al., 2003; Li et al., 2004; Venkatesan et al., 2009; Bandyopadhyay et al., 2010; Rual et al., 2004; Stelzl et al., 2005). Although there are already proteome-wide studies specific knowledge about certain protein complexes remain elusive. To address the investigation of protein assembly architecture we performed a comprehensive well controlled Y2H matrix approach.

1.4 Aims of this study

Elucidating biochemical processes of the cell is of crucial importance to understand life on a molecular level. Many biochemical processes are constituted of proteins assembled to stable protein complexes, fulfilling several tasks such as proliferation or homeostasis. The knowledge of how the protein complexes are formed gives insight into the fundamental principles of molecular complex architecture. Additionally, the transport of molecules between and within cell organelles is of major importance to maintain cellular functions, e.g. the transport of mRNA, ribosome subunits or smaller cargoes such as proteins. The aim of this study is to map the protein-protein interactions of two transport complexes that seem to be very different at first glance: the Nuclear Pore Complex and the BBSome. While the nuclear pore complex is one of the largest protein assemblies with an estimated molecular weight of 120 Mda in mammalian cells the only recently discovered BBSome is much smaller with an estimated molecular weight of 450kDa (Cronshaw et al., 2002; Nachury et al., 2007). Besides the different sizes the NPC is, when functional, a relatively fixed protein assembly embedded in the nuclear envelope whereas the BBSome is a mobile module that is transported within cytoplasm and within the primary cilia where it transports cargoes by itself (D'Angelo and Hetzer, 2008; Brohawn et al., 2009; Nachury et al., 2007; Jin et al., 2010; Wei et al., 2013).

The NPC is subject of scientific research since the 1950ties and much information is available (Watson, 1959). The protein composition as well as the localization of protein within the NPC could be clarified (Rout et al., 2000; Cronshaw et al., 2002). Moreover the proteins could be assigned of the distinct subcomplexes (Rout et al., 2000; Cronshaw et al., 2002; Alber et al., 2007). However the specific arrangement of the subcomplexes within their predicted localizations remains unclear. This is evidenced by the fact that there are several structural models of the NPC. They are all based on the arrangement of the largest subcomplex, namely the Y-complex (Alber et al., 2007; Brohawn et al., 2008; Debler et al., 2008; Bui et al., 2013). The Y-complex is arranged either in a head-to-head or in a head-to-tail orientation (Alber et al., 2007; Brohawn et al., 2008). Besides large amounts of Co-AP data there is a large number of crystal data of individual components (Rout et al., 2000; Cronshaw et al., 2002; Alber et al., 2007; Bilokapic and Schwartz, 2012). However there is little information available regarding binary protein-protein interactions which would emerge insight into direct subcomplex contacts even for the Y-complex (Amlacher et al., 2011; Leducq et al., 2012). To address the investigation of NPC architecture a comprehensive Y2H screen was performed. The screen included almost all human and yeast nucleoporins even in fragments. The Y2H screen resulted in a very comprehensive PPI network of the NPC of *saccharomyces cerevisiae* and a good PPI network of the human NPC. The NPC is a well conserved structure and the PPIs of the yeast network can be used to complete the information of the human NPC and *vice versa*. In fact the PPI networks reveal data regarding protein contacts within and between all subcomplexes of the NPC. Using this information

we were able to determine inter-Y-complex contacts and therefore support the model of an overlapping head-to-tail arrangement based on four PPIs revealed from the human and the yeast network: nup85/nup133, nup120/nup120, SEH1/SEC13 and SEC13/SEC13. In fact we could recapitulate these PPIs with independent cell-based and biophysical methods: protein complementation assay (PCA) and microscale thermophoresis (MST).

The BBSome is a very recently discovered protein complex (Nachury et al., 2007 & 2010; Jin et al., 2010). The domain composition of the BBSome components share sequence homology to vesicle coatamers like the some of the NPC proteins do as well (Jin et al., 2012; Kee et al., 2013). It was reported that there is an ‘inner core’ comprising three BBSome components BBS2, BBS7 and BBS9 (Zhang et al., 2012). To investigate the specific protein-protein interactions we performed an Y2H analysis including six of the seven human BBS components that are suggested to build the stable complex (Nachury et al., 2007; Jin et al., 2010; Seo et al., 2012). The Y2H screen revealed a highly dense network comprising 20 interactions between 16 BBSome constructs combined to six PPIs between six BBSome components. We were able to recapitulate the ‘inner core’ proposed by Zhang et al. whereas BBS9 and BBS7 are not directly connected with each other. Rather BBS9 and BBS7 form homo-dimeric arrangements each, with BBS2 as the central molecule in the core complex. Moreover the network indicates the more peripheral components BBS1, BBS4 and TTC8 (BBS8) by interactions that seem to be more transient. It seems that the ‘inner core’ of the BBSome and BBS1 are connected via their C-termini whereas BBS4 and BBS8 are linked with their N-termini. Taken together our Y2H screen emerge a very first insight into the BBSome architecture.

2. Materials and Methods

2.1 Materials

2.1.1 Chemicals

- 4'6-Diamidino-2-phenylindole (DAPI) (Roth, Karlsruhe)
- Acetic acid (Merck, Darmstadt)
- Acrylamide/Bisacrylamide 40 % (37,5:1) (Roth, Karlsruhe)
- Agarose (Sigma-Aldrich, Taufkirchen)
- Ammonium persulfate (APS) (Merck, Darmstadt)
- Ammonium sulfate (Merck, Darmstadt)
- Ampicillin trihydrate (Sigma, Deisenhofen)
- Bacto agar (BD Biosciences, USA)
- Bacto peptone (BD Biosciences, USA)
- Bacto tryptone (BD Biosciences, USA)
- Bacto yeast extract (BD Biosciences, USA)
- Bovine serum albumin fraction V (Roche, Mannheim)
- Calcium chloride dihydrate (Merck, Darmstadt)
- Chloramphenicol (Sigma-Aldrich, Taufkirchen)
- Coomassie Brilliant Blue G-250 (Biomol GmbH, Hamburg)
- Dipotassium phosphate (Acros organics part of Thermo Fisher Scientific Inc., Geel, Belgium)
- Dithiothreitol (DTT) (Roth, Karlsruhe)
- Dulbecco's modified eagle medium (DMEM+GlutaMAX™-I) (Gibco BRL, Gaithersburg, USA)
- Dulbecco's phosphate buffered saline (DPBS) (Gibco BRL, Gaithersburg, USA)
- Ethylenediaminetetraacetic acid (EDTA) (Roth, Karlsruhe)
- Ethanol (Merck, Darmstadt)
- Fetal bovine serum (FBS) (qualified FBS, south 26itrate26) (Gibco BRL, Gaithersburg, USA)
- Glucose monohydrate (Merck, Darmstadt)
- Glycerol (Merck, Darmstadt)
- Glycine (MP Biochemicals, Aurora, USA)
- Glycogen (Roche, Mannheim)
- Histidine (Sigma-Aldrich, Taufkirchen)
- Isopropanol (Merck, Darmstadt)
- Kanamycin sulfate (Sigma-Aldrich, Taufkirchen)
- Leucine (Sigma-Aldrich, Taufkirchen)
- Lithiumacetate (LiOAc) (Sigma-Aldrich, Taufkirchen)
- Magnesium chloride (Roth, Karlsruhe)
- Magnesium sulfate (Roth, Karlsruhe)
- Methanol (Merck, Darmstadt)
- Monopotassium phosphate (Roth, Karlsruhe)
- Opti-MEM I (Gibco BRL, Gaithersburg, USA)
- Paraformaldehyde (PFA) (Roth, Karlsruhe)

- Polyethylene glycol (PEG) 3350 (Sigma-Aldrich, Taufkirchen)
- Polyethylene glycol (PEG) 8000 (Sigma-Aldrich, Taufkirchen)
- Potassium acetate (Merck, Darmstadt)
- Potassium chloride (Roth, Karlsruhe)
- Protease inhibitor (Roche, Mannheim)
- Sodium carbonate (Merck, Darmstadt)
- Sodium chloride (Roth, Karlsruhe)
- Sodium citrat (Roth, Karlsruhe)
- Sodium dihydrogen phosphate (Merck, Darmstadt)
- Sodium dodecyl sulfate (SDS) (Roth, Karlsruhe)
- Sodium hydrogencarbonate (Merck, Darmstadt)
- Sodium hydroxide (Roth, Karlsruhe)
- Sorbitol (Sigma-Aldrich, Taufkirchen)
- Spectinomycin dihydrochloride pentahydrate (Sigma-Aldrich, Taufkirchen)
- SYBR Gold Nucleic Acid Gel Stain (Invitrogen, Darmstadt)
- Tetracycline hydrochloride (Sigma-Aldrich, Taufkirchen)
- Tetramethylethylenediamine (TEMED) (Invitrogen, Darmstadt)
- Tris (hydroxymethyl) aminomethane (Tris Base) (Roth, Karlsruhe)
- Tris (hydroxymethyl) aminomethane hydrochloride (Tris HCl) (Sigma-Aldrich, Taufkirchen)
- Triton X-100 (Sigma-Aldrich, Taufkirchen)
- Tryptophan (Sigma-Aldrich, Taufkirchen)
- Tween 20 (Sigma-Aldrich, Taufkirchen)
- Uracil (Sigma-Aldrich, Taufkirchen)
- Yeast nitrogen base (Difco part of BD Biosciences, USA)

2.1.2 Lab ware

- NanoDrop ND-1000 (Thermo Fisher Scientific Inc.)
- Mini-protean tetra cell electrophoresis system (Bio-Rad Laboratories)
- Sunrise 96 horizontal gel electrophoresis apparatus (Biometra GmbH)
- Kby robooter (Cambridge, UK)
- BiomekNX (Beckman Coulter GmbH)
- Biophotometer plus (Eppendorf AG)
- Thermomixer comfort (Eppendorf AG)
- Centrifuge 5810 R (Eppendorf AG)
- E.A.S.Y 429k digital camera (Herolab GmbH Laborgeräte)
- Tetrad PTC-225 thermo cycler (MJ Research Inc.)
- Titramax 1000 (Heidolph Instruments GmbH & Co. KG)
- Incubator 1000 (Heidolph Instruments GmbH & Co. KG)
- Innova44 shaker (New Brunswick Scientific)
- InfiniteM200 multimode microplate reader (Tecan Group Ltd.)
- 96well MTPs, tissue culture test plates (TPP Techno Plastic Products AG, 92096)
- 96well MTPs, PS, flat bottom, crystal clear (Greiner Bio-One GmbH, 655101)
- 96well MTPs, PS, flat bottom, TC, μclear, black, sterile, with lid, (Greiner Bio-One GmbH, 655090)
- 96well MTPs, PS, flat bottom, TC, white, sterile (Greiner Bio-One GmbH, 655073)

- 96well MTPs, PS, flat bottom, lumnitrac600, high binding, white, sterile (Greiner Bio-One GmbH, 655074)
- 384well MTPs, PS, flat bottom, clear, sterile, with lid (Greiner Bio-One GmbH, 781186)
- Tissue culture flask (TPP Techno Plastic Products AG, 90076)
- Omnitrays (Nunc GmbH & Co. KG, 165218)
- Agar-plates (241 x 241 x 20) (Nunc GmbH & Co. KG, 240845)
- 96well PCR plate (Costar part of Corning Incorporated, 6511)
- 96well deepwell plates (2000 µl/well) (Eppendorf AG, 0030 501.322)
- Plastic tape for sealing PCR plates/MTPs
- (Costar part of Corning Incorporated, 6524 or Thermo Fisher Scientific Inc., AB-5558)
- Sterile breathable sealing films (Aeraseal, Excel Scientific Inc., BS-25)
- Polyvinylidene fluoride (PVDF) membrane (Bio-Rad Laboratories, 162-0177)
- Nitrocellulose membrane (Bio-Rad Laboratories, 162-0115)
- Glass beads, acid-washed <106 µm (Sigma-Aldrich, G4649)
- Pin tools with 96 and 384 pins. The steel pins are cylindrical with a diameter of 1.3 mm and the edge of the flat top that is touching the agar is 28itrate 45°at 0.2 mm. Sterilize by heating the pins until they glow red. Let them cool in a sterile environment.
- Confocal fluorescence microscope LSM700 (Zeiss)
- Monolith NT.115 (microscale thermophoresis)

2.1.2.1 Enzyme, proteins, DNA, kits

- 1 Kb Plus DNA ladder (Invitrogen, USA)
- Prestained protein ladder, PageRuler™ Plus (Fermentas GmbH, St. Leon-Rot)
- Phusion hot start high-fidelity DNA polymerase (Finnzymes, Vantaa)
- QIAquick PCR purification kit (Qiagen GmbH, Hilden)
- Western lightning plus-ECL (PerkinElmer, Massachusetts)
- PfuTurbo DNA polymerase (Stratagene, Santa Clara)
- PureYield plasmid midiprep system (Promega, Madison)
- QIAprep spin miniprep kit (Qiagen GmbH, Hilden)
- dNTP-Mix (Fermentas GmbH, St. Leon-Rot)
- Salmon sperm carrier DNA (Sigma-Aldrich, Taufkirchen)
- FastDigest Bsp1407I (Fermentas GmbH, St. Leon-Rot)
- Trypsin-EDTA (Gibco BRL, Gaithersburg, USA)
- Lipofectamine 2000 (Invitrogen, USA)
- BP Clonase enzyme mix (Invitrogen, USA)
- LR Clonase enzyme mix II (Invitrogen, USA)
- Proteinase K solution (Invitrogen, USA)
- Zymolase 20T (Seikagaku Corporation)
- Monolith NT™ Protein Labeling Kit BLUE-NHS 647

2.1.3 Organisms

2.1.3.1 Bacteria strains

- DH10B: F⁻mcrA Δ-(mrr hsd RMS-mcr BC) φ80dlacZΔM15 ΔlacX74 deoR recA1 araD139 Δ(ara leu)7697 galU galK λ-rpsL endA1 nupG (Invitrogen)
- BL21B (DE3)-RIL: F⁻ ompT hsd(r₈⁻m₈⁻) dcm⁺ Tet^c gal λ(DE3) endA Hte [argU ileY leuW Cam^c]

2.1.3.2 Yeast strains

- L40ccU: MAT_a his 3Δ200 trp1-901 leu 2-3,112 LYS 2 :: (lex Aop)4-HIS3 ura3:: (lex Aop)8-lacZ
ADE 2 :: (lexAop)8-URA3 GAL4 gal 80 could 1 cyh 2 (Goehler et al., 2004)
- L40cc: MAT_a his3Δ200 trp1-910 leu2-3,112 ade2 LYS2::(lexAop)4-HIS3 URA3::(lexAop)8-lacZ
GAL4 gal80 can1 cyh2 (Goehler et al., 2004)
- L40c MAT_a: MAT_a his3_200 trp1-901 leu 2-3,112 ade2 lys2-801am can1 LYS2::(lexAop)4-HIS3
URA3::(lexAop)8-lacZ
- L40ccU2 MAT_a: MAT_a his3_200 trp1-901 leu 2-3,112 ade2 lys2-801am gal4 gal80 cyh2 can1 LYS2::(lexAop)4-HIS3 ura3::(lexAop)8-lacZ (Goehler et al., 2004)
- L40cc_ MAT_: MAT_ his3_200 trp1-910 leu2-3,112 ade2 GAL4 can1 cyh2 LYS2::(lexAop)4-HIS3
URA3::(lexAop)8-lacZ (Goehler et al., 2004)
- W303 B124: MAT_a/MAT_ leu2-3,112 trp1-1 can1-100 ura3-1 ade2-1 his3-11,15 [phi+] (Markus Ralser, Ralser laboratory, MPI for Molecular Genetics)

2.1.3.3 Mammalian cell lines

The human osteosarcoma cell line U2OS was used for the PCA assay. It was derived in 1964 from a moderately differentiated sarcoma of the tibia of a 15-year-old girl. The U2OS cells are characterized by chromosomal instability, structural rearrangements and alterations. Additionally the two tumor suppressive genes p53 and pRb are functional in U2OS cells (Niforou et al., 2008). U2OS cells are adherent fibroblastoid cells growing as a monolayer.

2.1.4 Media

2.1.4.1 E.coli growth medium and medium supplements

LB-medium

- 10 g Bacto tryptone
- 5 g Bacto yeast extract

LB-agar

- 10 g Bacto tryptone
- 5 g Bacto yeast extract

- 10 g NaCl
 - pH 7.2 (with NaOH)
 - ad 1000 ml H₂O
 - ad 1000 ml H₂O
- 10 g NaCl
pH 7.2 (with NaOH)
20 g Bacto agar

SOB-medium

- 20 g Bacto tryptone
- 5 g Bacto yeast extract
- 0.5 g NaCl
- ad 1000 ml H₂O
- ad after autoclaving:
- 10 ml 1 M MgCl₂
- 10 ml 1 M MgSO₄

SOC-medium

- 99 ml SOB-medium
1 ml 20x Glucose

2YT-medium

- 16 g Bacto tryptone
- 10 g Bacto yeast extract
- 5 g NaCl
- pH 7.2 (with NaOH)
- ad 1000 ml H₂O

Transformation and storage solution (TSS)

- 85 % LB-medium
10 % (w/v) PEG 8000
5 % DMSO
50 mM MgCl₂
Filter sterilize through a 0.22 µm pore filter

Antibiotic stock solutions

- Ampicillin
- Tetracycline
- Kanamycin
- Spectinomycin

Stock concentration

- 100 mg/ml in H₂O
12.5 mg/ml in 50% EtOH
30 mg/ml in H₂O
25 mg/ml in H₂O

Final concentration

- 100 µg/ml
20 µg/ml
15 mg/l
50 µg/ml

2.1.4.2 S. cerevisiae growth medium and medium supplements

1.25 x YPD liquid medium

- 5 g Bacto yeast extract
- 10 g Bacto peptone
- ad 400 ml H₂O
- ad 400 ml H₂O
- 2.5x Yeast liquid medium (NB)
- 6.7 g Yeast nitrogen base
- ad 400 ml H₂O

1.25 x YPD agars

- 5 g Bacto yeast extract
10 g Bacto peptone
10 g Bacto agar

2.5x Agar
10 g Bacto agar
ad 200 ml H₂O

1.25x Yeast liquid medium (NB)

- 3.35 g Yeast nitrogen base
- ad 400 ml H₂O

1.25x Yeast storage medium (NBG)

- 3.35 g Yeast nitrogen base
250 ml Glycerol (99 %)
29.44 g Betain

ad 400 ml H₂O

20x Glucose stock solution

- 200 g Glucose monohydrate
- ad 500 ml H₂O

100x Amino acid stock	Stock concentration	Final concentration
• 100x Leucine	10 g/L Leucine	100 mg/L Leucine
• 100x Histidine	2 g/L Histidine	20 mg/L Histidine
• 100x Uracil	2 g/L Uracil	20 mg/L Uracil
• 100x Tryptophan	2 g/L Tryptophan	20 mg/L Tryptophan

2.1.4.3 Mammalian cell culture medium and medium supplements

- **Cell culture medium**
- Dulbecco's modified eagle medium (DMEM+GlutaMAX™-I)
- 10 % FBS (fetal bovine serum)

2.1.4.4 Solutions

2.1.4.4.1 E.coli and yeast miniprep buffers

Buffer P1	Buffer P2
• 50 mM Tris pH 8.0	200 mM NaOH
• 10 mM EDTA pH 8.0	1 % (w/v) SDS
• add 50 mg/l	RNase A after autoclaving
Buffer P3	Buffer H1
• 300 ml 5 M Potassium acetate pH 5.5	50 µl Zymolase 20T (20mg/ml)
• 57.5 ml Acetic acid	940 µl SCE-buffer
• ad to 500 ml H ₂ O	10 µl 1 M DTT
SCE-buffer	
• 1 M Sorbitol	
• M Sodium 31itrate pH 5.8	
• 10 mM EDTA pH 8.0	

2.1.4.4.2 Agarose gel electrophoresis buffers

10x Tris/Borate/EDTA (10x TBE)	10x Orange G sample buffer
• 108 g Tris Base	50 % (w/v) Sucrose
• 55 g Boric acid	0.5 % (w/v) Orange G
• 40 ml 0.5 M	EDTA pH 8.0
• pH 8.3 (with HCl)	
• ad to 1000 ml H ₂ O	

2.1.4.4.3 Yeast transformation

10x Tris/EDTA buffer pH 7.5 (10x TE)	Carrier DNA
• 100 mM Tris pH 7.5	5 mg Salmon sperm DNA
• 10 mM EDTA pH 8.0	1 ml 1x TE

Mix I	Mix II
• 1 ml 1 M LiOAc	6 ml 1 M LiOAc
• 0.5 ml 10x TE	6 ml 10x TE
• 5 ml 2 M Sorbitol	40 ml 60 % PEG 3350
• ad to 10 ml H ₂ O	ad to 60 ml H ₂ O

2.1.4.4.4 SDS polyacrylamide gel electrophoresis buffers

4x SDS gel loading buffer	10x Electrophoresis buffer
• 200 mM Tris pH 6,8	30,2 g Tris Base
• 4 % SDS	144 g Glycine
• 40 % Glycerine	10 g SDS
• 0,4 % Bromphenol blue	ad to 1000 ml with H ₂ O
• ad prior to use:	
• 200 mM DTT	

2.1.4.4.5 Immunofluorescence buffers

- % Paraformaldehyde solution
- g Paraformaldehyde
- ad to 100 ml with Dulbecco's phosphate buffered saline

2.1.5 Vectors

2.1.5.1 Entry vectors

pDONR221

Size: 4762 bp

Sequencing primers M13 forward/M13 reverse

Negative selection: ccdB

Bacterial resistance: Kanamycin

Reference: Invitrogen

pDONR223

Size: 5005 bp

Sequencing primers: M13 forward/M13 reverse

Negative selection: ccdB

Bacterial resistance: Spectinomycin

Reference: Invitrogen

2.1.5.2 Expression vectors for *S. cerevisiae*

pBTM116-D9

Gateway compatible
Size: 8176 bp
Promoter/terminator: Truncated ADH
DNA binding domain: LexA (N-terminal)
Selection marker: Tryptophan (TRP1)
Bacterial resistance: Tetracycline
Sequencing primers: BTM-5plus/BTM-3min
Properties Y2H vector: 2 μ plasmid
Reference: Goehler *et al.* (Goehler, et al., 2004)

pASZ-CN-DM

Gateway compatible
Size: 8525 bp
Promoter: *S. cerevisiae* Cup1 promotor
Terminator: *S. cerevisiae* CYC1 terminator
Nuclear localization sequence (N-terminal)
Selection marker: Adenine (ADE)
Bacterial resistance: Ampicillin
Sequencing primers: CUPSeq-5p/CycT-5m
Properties Y2H vector: ARS-CEN plasmid
Reference: modified from Stotz *et al.*
(Stotz and Linder, 1990)

pBTMcC24-DM

Gateway compatible
Size: 10871 bp
Promoter/terminator: Truncated ADH
DNA-binding domain: LexA (C-terminal)
Selection marker: Tryptophan (TRP1)
Antibiotic marker: Tetracycline
Sequencing primers: BTM-5plus, BTM-3min
Properties Y2H vector: 2 μ plasmid
Reference: Stelzl laboratory (not published)

pACT4-DM

Gateway compatible
Size: 9613 bp
Promoter/terminator: Truncated ADH
Activation domain: GAL4 (N-terminal)
Selection marker: Leucine (LEU2)
Bacterial resistance: Ampicillin
Sequencing primers: Prey-5p
Properties Y2H vector: 2 μ plasmid
Reference: Goehler *et al.* (Goehler, et al., 2004)

pASZ-C-DM

Gateway compatible
Size: 8459 bp
Promoter: *S. cerevisiae* Cup1 promotor
Terminator: *S. cerevisiae* CYC1 terminator

Selection marker: Adenine (ADE)
Bacterial resistance: Ampicillin
Sequencing primers: CUPSeq-5p/CycT-5m
Properties Y2H vector: ARS-CEN plasmid
Reference: modified from Stotz *et al.*
(Stotz and Linder, 1990)

2.1.5.3

Expression vectors for mammalian cells

pVEN-F2N-DM

Gateway compatible
Size: 7889 bp
Promoter: Human cytomegalovirus (CMV)
Terminator: Bovine growth hormone (BGH)
Bacterial resistance: Ampicillin
Venus fragment 2 (C-terminal) (Nagai, et al.,
Sequencing primers: T7-for/BGHrev
Reference: Eduard Stefan (University of

pVEN-F1C-DM

Gateway compatible
Size: 8092 bp
Promoter: Human cytomegalovirus (CMV)
Terminator: Bovine growth hormone (BGH)
Bacterial resistance: Ampicillin
Venus fragment 1 (N-terminal) (Nagai, et al.,
Sequencing primers: T7-for/BGHrev
Reference: Eduard Stefan (University of

pVEN-F2C-DM

Gateway compatible
Size: 7861 bp

pVEN-F1N-DM

Gateway compatible
Size: 8119 bp

Promoter: Human cytomegalovirus (CMV) P
Terminator: Bovine growth hormone (BGH)
Bacterial resistance: Ampicillin
Venus fragment 2 (N-terminal) (Nagai, et al.,
Sequencing primers: T7-for/BGHrev
Reference: Eduard Stefan

Promoter: Human cytomegalovirus (CMV)
Terminator: Bovine growth hormone (BGH)
Bacterial resistance: Ampicillin
Venus fragment 1 (C-terminal) (Nagai, et al.,
Sequencing primers: T7-for/BGHrev
Reference: Eduard Stefan

2.1.6 Oligonucleotides

2.1.6.1 Oligonucleotides for sequencing

Primer	5'-Sequence-3'
M13 forward	GTAAAACGACGGCCAG
M13 reverse	CAGGAAACAGCTATGAC
T7 forward	TAATACGACTCACTATAAGGG
BGHrev	TAGAAGGCACAGTCGAGG
Prey-5p	CCAAAGCTTCTGAATAAGCC
BTM-5plus	TCGTAGATCTCGTCAGCAG
BTM-3min	AGCAACCTGACCTACAGG
Barcode_Uptag	GATGTCCACGAGGTCTCT
Barcode_Downtag	CGGTGTCGGTCTCGTAG

2.1.6.2 Oligonucleotides for knock-out PCR

Primer 5'-Sequence-3'

Δnup85fwd
ATGACAATCGATGATTCAAATCGATTACTTATGGACGTCGATCAAAGCTTGCCTGTCCCCGCCG

Δnup85rev
TTACATGAACGCTTGACATAATTGAAATTAGTTCTTCTTAAATCGACACTGGATGGCGGGCGT

Δnup84fwd
ATGGAATTATCCCCTACTTATCAAACAGAACGCTTCACAAAGTTCAGCTTGCCTGTCCCCGCCG

Δnup84rev
TCAGTTGAAAGGGTTGCTGTGCGAGCAACGAGATCCAGATACTCTGACACTGGATGGCGGGCGT

Δnup120fwd
ATGGCATGCCCTCTAAGAATTGATGCAAATTGCTCCAATATAGCGGTCTTGTCCCCGCCG

Δnup120rev
CTATAGACCTCGTAACTCATCTCTTAAATCAGTTAAAGTAACCACACTGGACACTGGATGGCGGGCGT

Δnup133fwd
ATGAGTGAACCAAGTACATCTCGTTGCGGAAGGAACCTAGCAGCTTGCCTGTCCCCGCCG

Δ nup133rev
TTAGTATTCTACAGTGTGGTTCATAGTTGATGGTATAGTTTTGCACACGTGATGGCGGCGT

2.1.7 Databases

- Swissprot <http://www.ebi.ac.uk/swissprot/>
- HPRD <http://www.hprd.org/>
- Expasy <http://us.expasy.org/tools/>
- MultiAlin <http://multalin.toulouse.inra.fr/multalin/>
- PDBD <http://www.rcsb.org/pdb/home/home.do>

2.1.8 Software

- VectorNTI Invitrogen
- SnapGene
- Microsoft Office (Excel, Access, PowerPoint)
- Visual Grid
- Adobe Illustrator
- Cytoscape
- yED Graph Editor
- NT analysis (provided by Nanotemper technologies)
- Costum made perl script (network randomisztion)
- R plot

2.2 Methods

2.2.1 Molecular biology of *E.coli*

2.2.1.1 Growth and storage of *E. coli*

In general *E.coli* stocks were grown in liquid. To create a growth culture 1mL of LB medium was inoculated with a single colony of *E.coli* and incubated on an Incubator 1000 for 16-20h at 37°C. To store the *E.coli* stocks for long-term, glycerol stocks were created whereas the overnight cultures with 50% glycerol were mixed in a ratio of 1:1, e.g. 60µL overnight culture and 60µM glycerol. The mixture should be mixed well and immediately be frozen by -80°C. The short-term storage occurs on agar. For this purpose, the *E.coli* strains were streaked on LB-plates and incubated for 16-20h at 37°C. The storage occurs at 4°C.

2.2.1.2 Preparation of competent *E. coli*

2.2.1.2.1 Chemically competent cells

Chemically competent DH10B cells were generated using TSS (Transformation and storage solution). As a start a single freshly grown *E.coli* colony was inoculated in 20 ml 2YT-medium and incubated at 37°C over night. The next day, 2000 ml 2YT medium were inoculated with the overnight culture. The culture was grown until an OD₆₀₀ of 0.7-0.8 was reached and the portioned in four 500 ml flasks. These flasks were centrifuged at 4000 rpm for 15 min at 4°C. The supernatants were removed and each pellet was resuspended in 40mL sterile TSS. To ensure a proper storage of the cells glycerol stocks were created by mixing the resuspended pellets with 4 ml 87% autoclaved glycerol. The storage occurs at -80°C. In general, chemical-competent DH10B cells should have a transformation efficiency of up to 1x 10⁵ cfu/µg.

2.2.1.2.2 Electro-competent cells

Electro competent DH10B cells were generated using cold, sterile 15 % glycerol and several incubation and centrifugation steps. As a start 50 ml LB medium were inoculated with a single freshly grown *E.coli* colony over night. After 16-20 h, 1500 ml LB medium were inoculated with 45 ml overnight culture and the cells should grow until an OD₆₀₀ of 0.3-0.4 is reached. The culture was portioned in six 250 ml flasks and incubated on ice for 30 min. Afterwards the cultures were centrifuged at 3500 rpm for 10 min at 4°C. The supernatants were removed and each pellet was resuspended in 100 ml cold, sterile 15% glycerol and incubated on ice for 20 min and centrifuged as before. This procedure was repeated two times whereas the pellet was resuspended first in only 10 ml and in the second step in 2 ml cold, sterile 15% glycerol to obtain the final competent cell suspension that was aliquoted and stored at -80°C.

2.2.1.3 Transformation of competent cells

2.2.1.3.1 Chemical transformation of *E. coli*

The protocol is adapted to a 96-well format transformation of DH10B *E.coli* cells. In general, LR and BP reactions containing plasmid DNA were used to transform bacteria. To address this, a certain amount of DNA containing solution (2.5 – 5 µl) was pipetted into each well of the 96-well PCR plate. Competent bacterial cells were thawed on ice and 30 µl added into each well followed by incubation on ice for 30 min. Next, a heat shock at 42°C for 90 seconds was applied. The cell-DNA mixture was transferred in the according wells of a deep well plate in which 130 µl were prefilled with 130 µl prewarmed SOC-medium. The cells were incubated at 37°C for 1 hour at 220 rpm. The solution was then pipetted with a multipipette on selective LB-agar plates resulting in five or six rows of drops on each plate. The LB-agar plates were incubated at 37°C for 16-20h.

2.2.1.3.2 Electroporation of *E. coli*

In general, 1-2 µl of a LR or BP reaction was used to transform electro-competent DHB10 cells. Electro-competent cells were thawed on ice while aliquoting the DNA-solution into 2 ml micro-centrifuge tubes. 30 – 50 µl of cells were added to the DNA solution. The mixture of cell and DNA was then transferred into a 0.1 cm gap electroporation cuvette. With a Gene Pulser apparatus a pulse with a field strength of 1.7 kV and a time constant of approximately 4-5 msec (25 µF and 200) was applied to the cuvette. Immediately after applying the pulse 200 µl of prewarmed SOC-medium was added. The cell suspension was transferred into a sterile 2 ml micro-centrifuge tube and incubated at 37°C for at least one hour. After that the cell suspension was spread on selective LB-agar plates and incubated at 37°C.

2.2.1.4 Plasmid isolation of *E. coli*

The protocol is adapted to a 96-well plasmid isolation procedure of *E.coli*. 96-deep well plates containing 1.2 ml LB-medium were inoculated with one *E.coli* colony of interest and sealed with breathable sealing film. The plate was incubated at 37°C for 16-20 h. Afterwards it is possible to create glycerol stocks following the protocol described in section 2.2.1.1. The remaining cell suspension was centrifuged at (1258 x g) at 4 °C for 30 minutes to collect the cells. The supernatant was removed and the cell pellets were resuspended in 300 µl of cold buffer P1. 300 µl Buffer P2 was added to each well, mixed by inverting 3-4 times and incubated at room temperature for 5 min. 300 µl of buffer P3 was added, mixed and centrifuged (3220 x g) for 1 h. In the meantime a new deep well plate was filled with 530 µl isopropanol. After finishing the centrifugation step 750 µl of the cleared lysate were transferred into the according wells of the new deep well plate containing the isopropanol, mixed thoroughly and centrifuged (3220 x g) at room temperature for 1 h to precipitate the plasmid DNA. The supernatant was removed and 1 ml 70% ethanol was added to each well and centrifuged (3220 x g) at 4°C for 1 h. After removing the supernatant the DNA pellets were dried for 30-60 min and dissolved in 70-100 µl sterile water. The verification of the plasmid DNA occurs with BsrG I restriction analysis.

DNA plasmid isolation of single samples were done using the commercially available mini-prep kits (Qiagen) and mid-prep kits (Promega) according to the standard protocol in the manufacturers guidelines.

2.2.2 Work with DNA

2.2.2.1 Restriction digest of plasmid DNA

To perform restriction digest on DNA the restriction endonuclease FD-Bsp 1407I was used. It is a fast digest isoschizomer of BsrGI and mostly used to verify the plasmid DNA isolation. In general, 300 ng DNA sample were mixed with restriction endonuclease mix (1x FD-buffer, 0.1 µl FD-Bsp1407I) and incubated for 30 min at 37°C.

2.2.2.2 Separation of DNA fragments by agarose gel electrophoresis

To control the plasmid insert size obtained by the restriction digest agarose gel electrophoresis was performed. To address this, agarose was added to 0.5 x TBE buffer to a final concentration ranging from 1-2 % and heated up until it dissolved. According to the amount of DNA samples the size of gel was chosen. Approximately 100 ng of DNA are required to be visualized and 200 ng of the restricted DNA were supplemented with Orange G Sample buffer and loaded onto the agarose gels. Additionally to the DNA samples 5 µl of a 1 Kb DNA ladder was loaded to estimate the DNA band size. Electrophoresis was applied at 130 V for 1 h in 0.5 x TBE buffer as running buffer. Following the agarose gels were stained 15 min in a 1:20000 dilution of SYBR Gold nucleic acid gel stain and were visualized using an ultra violet light source.

2.2.2.3 Determination of DNA concentration

The concentration of DNA in samples was measured using a spectrophotometer (Nanodrop 2000) that determined the absorbance at 260 nm. As standard nuclease free water was used. The DNA was solved in sterile water. 1 µl DNA solution was pipetted onto the Nanodrop.

2.2.2.4 Polymerase chain reaction (PCR)

To generate yeast knock-out strains PCR was used as initial step (see section 2.2.3.6). Therefore primer pairs were generated containing the complementary DNA sequence of the gene encoding nourseothricin on both ends of the gene). Further the primer included recombination sites of the gene region of interest of the yeast (see section 2.1.6.2). The PCR mix was pipetted for each knock-out following the protocol:

PCR reaction mix (Phusion reaction mix):

- Primer (each): 1.5 µl
- Buffer (5x): 10 µl
- dNTPs: 0.5µl
- Phusion: 0.25 µl
- DMSO: 0.75 µl
- DNA: 1-10 ng
- H₂O: ad 50 µl

PCR – procedure:

- Initialization step: 30 seconds – 98 °C
- Denaturation step: 8 seconds – 98 °C
- Annealing step: 20 seconds – 55-62 °C
- Extension/elongation step: 30 seconds – 72 °C
- Final elongation: 480 seconds – 72 °C
- Final hold: ∞ 4°C

The resulting PCR products were controlled using agarose gel electrophoresis (see section 2.2.2.2) and sequencing.

2.2.2.5 Gateway cloning technology

The Gateway clone technology of Invitrogen allows fast and uncomplicated cloning. A well constructed system including different types of vectors allow the shuttling of the gene of interest between these vectors depending on the use of the gene. The gene of interest is flanked with certain att-sites according to the vector the gen is inserted in. With a BP or LR reaction the gene can be transferred to every other vector containing att-sites.

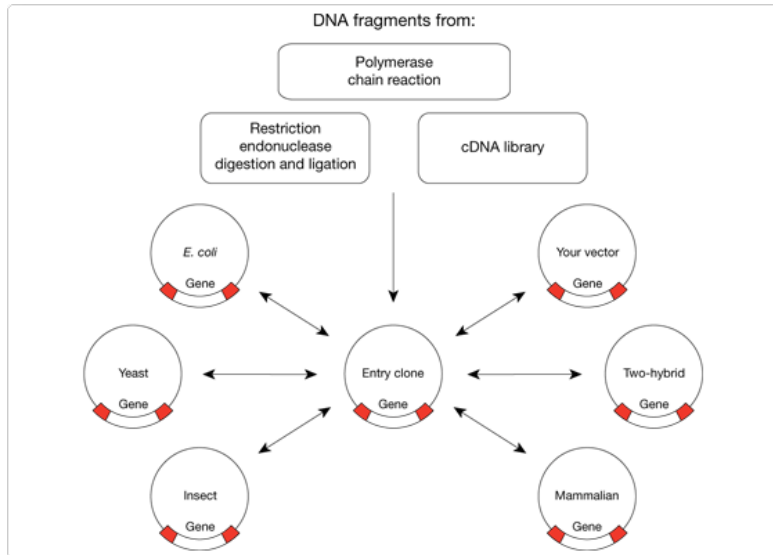


Fig 2.1 The gateway cloning strategy; DNA fragments of different origins can be inserted into the Entry clone and thus a library can be generated. Once a gene is cloned into an Entry clone the DNA fragment can be transferred into one or more destination vectors simultaneously; the picture was taken from Invitrogen Gateway® Recombination Cloning Technology

2.2.2.5.1 LR Reaction

In order to transfer the NPC and BBSome cDNAs from their initial entry vector pDONR221 and pDONR223 to the destination vectors pBTM116-DM, pBTMCC24-DM and pACT4-DM a LR reaction was performed. The reaction was done as described in the manual of Invitrogen. It composed 75 ng of the destination vector, 200-300 ng of the entry vector containing the gene of interest and 1 μ l LR clonase enzyme mix. The reaction was incubated at 25°C for 1-24 h. The LR reaction was either stored at -20°C or immediately used in bacterial transformations.

2.2.3 Molecular biology of *saccachomyces cerevisiae*

2.2.3.1 Preparation of yeast media

In order to work with yeast in the lab different media has to be provided that differs in amino acid composition. The content of amino acids is dependent on the vectors the yeast strains were transformed with. In general, the media were named after the amino acids that are missing and added in the medium. Thus the amino acids are labeled with a single letter: "H" for histidine, "A" for adenine, "U" for uracil, "L" for leucin and "T" for tryptophan. The missing amino acid had a minus in

front. For instance medium lacking tryptophan but included all other amino acids was declared as: -T /HAUL. Following medium preparations were used:

Liquid medium: 25 ml 20x glucose stock solution and 5 ml of each required 100x amino acid or nucleoside stock solution were added to 400 ml 1.25x NB or 1.25x NBG. Liquid medium was adjusted to a final volume of 500 ml with sterile water.

Solid medium: 200 ml 2.5x NB, 25 ml 20x glucose stock solution and 5 ml of each required 100x amino acid or nucleoside stock solution were added to 200 ml 2.5x agar. Solid medium was adjusted to a final volume of 500 ml with sterile water and dissolved using a microwave. After the medium was cooled down to 60 °C agar plates were filled with 200 ml medium under a sterile hood.

YPD liquid medium: 25 ml 20x glucose stock solution were added to 400 ml 1.25x YPD. YPD liquid medium was adjusted to a final volume of 500 ml with sterile water.

YPD solid medium: 25 ml 20x glucose stock solution were added to 400 ml 1.25 x YPD agars. Solid medium was adjusted to a final volume of 500 ml with sterile water and dissolved using a microwave. After the medium was cooled down to 60 °C agar plates were filled with 200 ml medium under a sterile hood.

2.2.3.2 Growth and storage of *S. cerevisiae*

Yeast cultures can either be stored as liquid or on solid agar whereas the liquid storage was used for long-term storage (many years) and the solid storage was used for short-term storage (several days up to four weeks).

To generate liquid storage, according amount of liquid medium (NP medium) was inoculated with yeast colonies and mixed thoroughly followed by a growing time of 16 – 20h on a shaker (Innova44, 250 rpm) at 30°C. Before storing the yeast at -80°C glycerol was added. Beside this it was also possible to use media containing glycerol in the first place, namely NBG medium. The glycerol stocks are limited in thawing. Thus each created glycerol stock can be thawed twice.

To store the yeast in a short-term solid way agar was used. To address this, the yeast strains were streaked on agar and incubated at 30°C for 1-5 days. The storage occurred in the cold room at 4°C. In general stored yeast was on agar to have an extra generation before beginning an Y2H experiment. Native, untransformed yeast strains were grown in YPDA medium at a temperature of 30°C.

The knock-out yeast strains were grown according to their temperature sensitivity (see section 2.2.3.6).

2.2.3.3 Transformation of *S. cerevisiae* with plasmid-DNA

The yeast strains MAT α and MAT α were transformed either with the bait plasmids pBTM116-DM, pBTMCC24-DM or the prey plasmid pACT4-DM. The following transformation is adapted to a 96-well transformation protocol whereas the transformation of one 96-well plate requires 60 ml of a freshly grown yeast culture.

- fresh yeast strains were inoculated in liquid YPDA medium, vortexed and grown at 30°C for 16-20 h in a shaking incubator (Innova44, 250 rpm)
- 60 ml YPDA medium were inoculated with the overnight culture to an OD₆₀₀ of 0.10 – 0.15 and incubated at 30°C until an OD₆₀₀ of 0.6 – 0.8 was reached
- adding of 5 µl of the DNA in each well of the 96-well plate
- adding of 5 µl carrier DNA (10.5 mg/ml heat denatured salmon testis DNA) to each well

- centrifugation at 1258 x g of 50 ml of the culture for 5 min at room temperature to harvest the yeast cells
- the supernatant was removed and the pellet resuspended in 20 ml sterile 1 x TE to wash the residual medium away
- centrifugation at 1258 x g for 5 min at room temperature
- removing of the supernatant and resuspension of the pellet in 2000 µl Mix I
- incubation at room temperature for 10 min
- ad 22 µl of the Mix I / cell suspension to each well containing plasmid DNA and Carrier DNA
- ad 120 µl of Mix II
- incubation at 30°C for 30 min
- ad 16 µl DMSO to each well
- incubation at 42°C for 30 min applying a heat shock to transfer the plasmid DNA into the yeast cells
- mixing of the plate and stamping onto selective solid medium (bait plasmid: -T/HAUL and prey plasmid: - L/HAUT)
- incubation for 3-5 days at 30°C

In order to prepare an Y2H screen four biological replicas were generated. To address this, the transformed yeast was stamped four times onto different agar plates. These replicas were then used in the screen. Besides creating replicas one copy of the transformed yeast replicas was used to perform an auto-activation screen. The obtained yeast colonies were stored as glycerol stock for long-term.

2.2.3.4 Auto-activation test of the bait-constructs

To avoid false positives the bait constructs have to be tested to be non-autoactive. The autoactivation of the reporter gene was tested by mating the four replicas of the MAT *andi* strain including the bait constructs with a MAT *alpha* strain carrying the prey plasmid (Gal4-AD fusion, pACT4-DM) without insert. Auto-active baits were able to grow on –HAULT and the diploid strain is able to grow on –H medium since the autoactivation activated the HIS-reporter gene. Following protocol was applied:

- one day before mating 25 ml of liquid medium –L/HAUT was inoculated with a freshly prey strain containing a prey plasmid without insert and incubated for 16-20h
- 100 µl of the overnight culture was added to each well of a 96-well MTP
- using a pin tool the bait strains freshly grown on –T/HAUL were stirred into the MTP containing the prey strain
- the bait and prey strain mixture was stamped on YPD agar and incubated at 30°C for 36-44 h
- when the yeast spots were grown the yeast was resuspended in –LT/HAU and transferred on – HAULT (SD4) medium
- Yeast spots including bait constructs that were still grown were removed from the screening set up. They are autoactive

2.2.3.5 Screening bait constructs against a prey matrix

The Y2H screen was done in a matrix approach by testing a yeast strain containing one bait construct against a whole array of haploid yeast cells containing the prey constructs. To address this, a

replication robot was used. Prey and baits were replicated in 384- or 96-well format to handle them, respectively. To create the prey matrix three or four biological replicas of the MAT α strain including the prey constructs were arranged in the 96- or 384-well format. Three days before mating the prey matrix and the baits were freshly stamped on -L/HAUT or -T/HAUL. One day before mating two of each bait constructs were inoculated in 30 ml of NB -T/HAUL medium by picking two colonies of the fresh grown baits. They were incubated for 18-22h at 30°C in a shaker to the early stationary phase ($OD_{600} = 1.5-3$). At the mating day the fresh liquid bait cultures were transferred into the 96- or 384-well plates with the pipetting robot. The bait constructs were stamped with the replication robot over the solid fresh grown prey matrix onto YPDA plates. The YPDA plates were incubated at 30°C for 36-44 h. Yeast was resuspended in -LT/HAU and transferred with the robot onto -HULT agar. To control for efficient mating some yeast plates were additionally transferred onto -LT/HU agar. The agar plates were incubated at 30°C for 5-7 days. The growth of a colony indicates an interaction between the bait construct and the prey construct. As mentioned above over the position in the matrix the prey can be determined.

2.2.3.6 Generation of yeast knock-out strains

The gene to be knocked-out is substituted with a nourseothricin cassette that additionally allows the selection of the altered strains. The cassette was obtained by amplifying it out of the vector **xxx** with the primer pairs: $\Delta nup85$ fwd/rev, $\Delta nup84$ fwd/rev, $\Delta nup120$ fwd/rev and $\Delta nup133$ fwd/rev with PCR. The insertion of the cassette into the yeast genome occurred via homolog recombination. To ensure that the yeast can insert a gene of interest by homolog recombination matching complementary DNA sequences to the gene region of interest comprising ~40 bp are required. These are attached at the according site of the primer pairs that were used to amplify the nourseothricin cassette. After amplifying the nourseothricin cassette with the primer containing the cDNA sequences of the yeast gene region of interest a yeast transformation was performed. This yeast transformation was a standard yeast transformation. However, two things were done differently. Thus, the amount of initial DNA solution was increased to 20 μ l and an incubation time of 1 h in YPDA was introduced between the transformation procedure and spreading the transformed yeast onto agar plates enabling the yeast to produce nourseothricin that allows growing on agar containing concentration of **xxx** nourseothricin. After incubation for several days (5-16) at different temperatures (20°C -37°C) the growing yeast spots were picked and transferred to a 96-well plate format. Then the knock-out yeast strains could be used for following transformations.

2.2.4 Molecular biology of human U2OS cells

2.2.4.1 Growth of mammal cells

U2OS cells were cultured in a humidified 5 % CO₂ atmosphere at 37 °C in Dulbecco's modified eagle medium (DMEM) supplemented with 4500 mg/L D-glucose, 110 mg/L sodium pyruvate and 5 % fetal bovine serum. Cells were maintained by growing to ~80 % confluence in 75 cm² flasks prior trypsinisation and splitting at a 1:10 dilution every 3-4 days as appropriate.

2.2.4.2 Co-Transfection of U2OS cells

The U2OS cells were seeded either in 96well plates or in 24well plates on cover slips to reach 40-50% confluence at the time of transfection. The cells were transiently transfected with 50 ng of each F1 and F2 plasmid DNA per well using Lipofectamine 2000 (Invitrogen) according to the manufacturer's instructions. Two mixtures were combined. Mix 1 includes 30 μ l Opti-MEM I and 1.5 μ l of 100 ng plasmid DNA. Mix 2 contains 30 μ l Opti-MEM and 0.8 μ l Lipofectamine. Both mixtures were incubated for 5 min and then mixed and incubated for at least 30 min. After 30 min 50 μ l of the mixture is added to each well and the cells were incubated at 37°C for 24h. After 24h the transfection medium was removed and Dulbecco's modified eagle medium (DMEM) supplemented with 4500 mg/L D-glucose, 110 mg/L sodium pyruvate and 5 % fetal bovine serum was added for an additional growth time of 24h at 37°C to ensure cell proliferation.

2.2.4.3 Protein Complementation Assay (PCA)

U2OS cells were seeded either in 96well plates or in 24well plates on cover slips and co-transfected with 50 ng Venus F1 and 50 ng Venus F2 plasmid DNA. After the transfection time of 12-24h with following additional growth time of 24h the DMEM medium was removed and the cells fixed with 2% paraformaldehyde (PFA) in DPBS. To fix the cells 50 μ l (96 well plate) or 120 μ l (24 well plate) 2% PFA was added to each well and incubated in the dark at room temperature for 10 min. The DPBS with 2% PFA was removed and the fixed cells were washed two times with 120 μ l (96 well plate) or 500 μ l (24 well plate) DPBS. To stain the nucleus DAPI was diluted in DPBS to a final concentration of 16 μ g/ml and 50 μ l (96-well plate) or 200 μ l (24 well plate) were added and incubated for 2 min at room temperature. The fixed cells were washed with DPBS two times as described above and stored at 4°C. To visualize the protein interactions a confocal fluorescence microscope (LSM700, Zeiss) at excitation wave length 525 nm was used. A positive interaction was only assumed when fluorescence was observed at the nuclear rim. Negative controls were done including empty vectors and construct that are strongly assumed to not interact.

2.2.5 Work with proteins

2.2.5.1 Protein purification (protocol is adapted to methods of Brohawn et al., 2008)

All protein fragments from *saccharomyces cerevisiae* were cloned into pET-Duet-derived plasmids using the BamHI/NotI restriction sites,respectively, resulting in N-terminally His-tagged constructs. The resulting plasmid was transformed into E. coli BL21 (DE3)-RIL for protein expression. Cells were grown at 30°C in Luria-Bertani broth supplemented with 0.4% glucose to OD600= 0.8 and induced with 0.2 mM IPTG at 18°C for 18 hours. Cells were harvested by centrifugation, resuspended in 40 mM potassium phosphate pH 8.0, 500 mM NaCl, 20 mM imidazole, and 3 mM β -mercaptoethanol, and lysed using a french press. The crude lysate was centrifuged at 15,000g for 15 minutes. The soluble fraction was then incubated with 1 ml Ni-NTA per 1000 Ods for 30 minutes at 4°C and loaded onto a disposable column (Pierce). The column was washed with four bed volumes of 50 mM potassium phosphate pH 8.0, 400 mM NaCl, 30 mM imidazole, and 3 mM β -mercaptoethanol

and the construct complex eluted in 4 bed volumes of 50 mM potassium phosphate pH 8.0, 250 mM NaCl, 250 mM imidazole, and 3 mM β -mercaptoethanol. The eluted protein constructs were dialyzed against 10 mM Tris/HCl pH 8.0, 150 mM NaCl, 0.1 mM EDTA, and 1 mM DTT and the 6xHis-tag cleaved with PreScission protease. The protein constructs were purified by anion exchange chromatography on a HiTrapQ column (GE Healthcare) via a linear NaCl gradient and twice by size exclusion chromatography using a Superdex S200 26/60 column (GE Healthcare) run in 10 mM Tris/HCl pH 8.0, 150 mM NaCl, 0.1 mM EDTA, and 1 mM DTT. The protein constructs were concentrated to 2.6 – 29.5 mg/ml. The quality of the protein constructs was checked with SDS gels.

2.2.5.2 Microscale thermophoresis (MST)

Before applying the thermophoresis protocol one protein or protein constructs of the protein pair to test has to be labeled. The labeling procedure was performed following the manual of Nanotemper technology: Monolith NTTM Protein Labeling Kit BLUE-NHS 647. After this procedure the concentration of labeled protein construct is approximately 50 – 100 nM. To prepare the MST measurements dilution series of the unlabeled protein constructs including 16 dilutions steps were created using 1:2 dilutions whereas the highest dilution step included the undiluted protein construct: 15 tubes were prefilled with 10 μ l of the experiment buffer (e.g. HEPES, gel filtration buffer). 10 μ l of the undiluted protein construct were added in the first tube and carefully mixed using the pipette. 10 μ l were transferred in the next tube and so on. After the dilution the labeled protein constructs were added in an equal amount of the dilution volume (10 μ l) to create again 1:2 dilution of each dilution step. The final volume of each dilution step should be 20 μ l. 16 capillaries were filled with the 15 diluted and the one undiluted protein constructs and loaded into the Monolith NT.115. The thermophoresis was performed using the Monolith NT.115 of the company NanotemperTM Technology. It should be ensured that all measurements were performed at similar temperature. Further it should be ensured that the initial fluorescence is a certain range (200-1000 fluorescence units). The read-out and the analysis occurred with the NT analysis software provided by Nanotemper.

3. Results

3.1 Identification of PPIs of the yeast and the human Nuclear Pore Complex

3.1.1 Defining the NPC clone set

The Nuclear Pore Complex is one of the largest protein assemblies in the cell comprising ~30 distinct proteins called nucleoporins (nups) occurring in multiple copies with a total number of ~500 molecules per NPC (Alber et al., 2007). The majority of nups are grouped into six discrete subcomplexes building the NPC scaffold, the transport channel, the cytoplasmic fibrils and the nuclear basket (Rout et al., 2000; Schwartz et al., 2005). The NPC scaffold of the yeast and the human NPC is constituted by three subcomplexes, namely the Y-complex, the nic96-complex (NUP93-complex in vertebrates) and the nsp1-complex (NUP62-complex in vertebrates) whereas the inner channel is formed by a differently composed nsp1-complex. The inner channel is filled with several types of FG-repeat containing nups realizing the active transport of molecules above 40kDa through the NPC (Bagley et al., 2000). The connection to the membrane presumably occurs only via a small subset of three nups including only one classical transmembrane domain each (Rout et al., 2000; Cronshaw et al., 2002; Mansfeld et al., 2006).

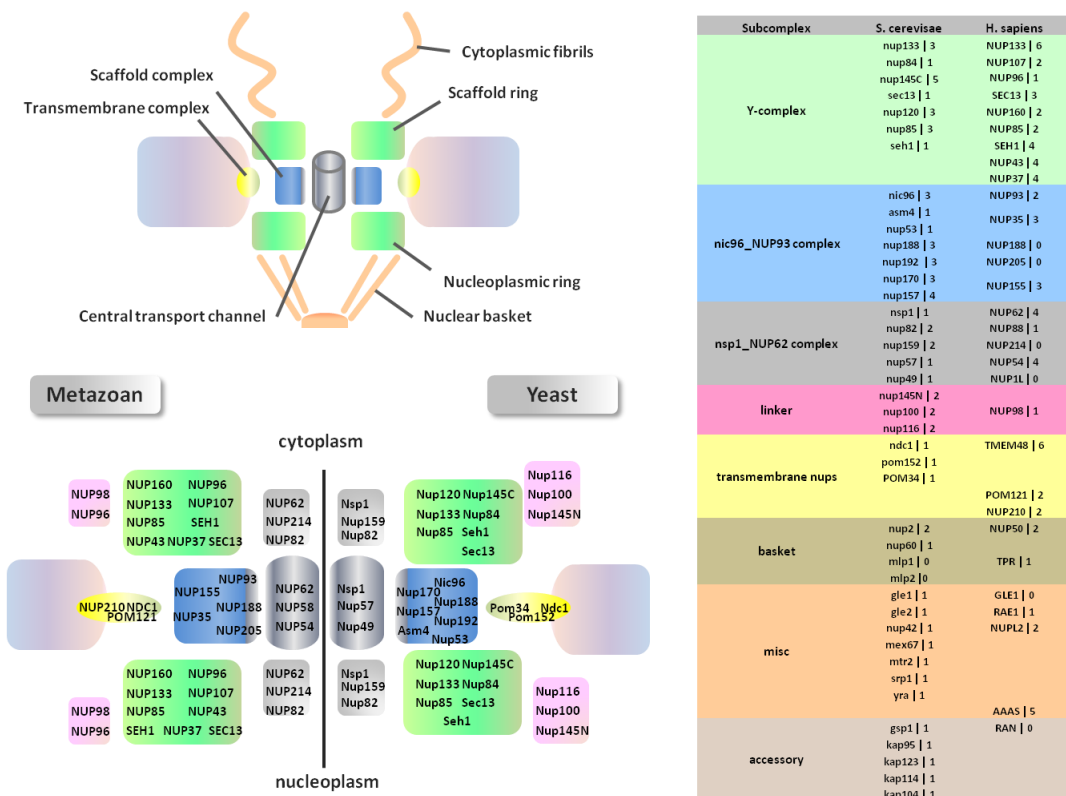


Fig 3.1 Schematic overview of the localizations of nucleoporins within yeast and metazoan NPC subcomplexes. The subcomplexes are boxed and indicated by different colors (green: Y-complex, blue: nic96_NUP93

complex, grey: nsp1_NUP62 complexes, pink: linker nups, yellow: membrane nups). The list of all nups included in the screen. At the left side: yeast nups, at the right side: human. The numbers declare the number of included constructs in the Y2H screen. The Y2H screen included almost all human and yeast nups and

An extensive Y2H screen could enlighten the connections between subcomplexes and therefore also the architecture of the NPC that is vigorously debated. There are only three nups in yeast and human that contains a transmembrane domain (Rout et al., 2000; Cronshaw et al., 2002). The rest of the nups are soluble making an investigation with the conventional Y2H approach possible. The yeast subcomplexes are thought to be linked by multiple copies of three linker nups, whereas there are only two in the human NPC (Alber et al., 2007). Nups could be successfully assigned to the several subcomplexes (Rout et al., 2000; Cronshaw et al., 2002). To systematically investigate the binary interactions of the yeast NPC with an Y2H approach cDNAs of all yeast nups from Thomas Schwartz (MIT, Dep. Biology, Boston MA) were collected. Beside full length constructs, additionally cDNA fragments cloned according to their domain structure were obtained. Protein interactions are often mediated by domains and that appropriate domain constructs interact better may be due to the lack of certain folding restraints, in particular in the case of large proteins (Stein et al., 2011). Additionally, FG-repeat amino acid stretches which are known to be aggregation prone and may disturb PPIs were removed from several fragments.

To study further the binary interactions in the human NPC we obtained all human nups as full length cDNAs from our lab collection that is mainly composed of human ORFs from the CCSB collection (Rual et al., 2004; Lamesch et al., 2004) or specifically purchased from the NITE consortium (Goshima et al., 2008; Maruyama et al., 2012). Human full length proteins were included in the screen using several different constructs for the nups, *e.g.* investigated were six clones for nup62 that differ in their cDNA sequence regarding to isoforms (Fig 3.1). As described above it was possible to obtain constructs for almost all human and yeast nups. Some human constructs were not available and therefore not included in the screen. For example, the two human linker nups (NUP98 and NUP96), two members of the human NUP93-complex (NUP188 and NUP205) and two members of the human NUP62-complex (NUP58 and NUP214) were not obtained. Additionally several miscellaneous nups of the human and yeast NPC could not be included in the screen. The yeast clone set is complete with regards to the bona fide structural nups, the linker nups and the transmembrane nups, except of gp210. Taken together the screen included 39 yeast proteins and 25 human proteins representing the bona fide nups as well as transiently bound nups. The yeast nups were represented by at least one full length protein. In addition 27 yeast protein fragments were introduced into the PPI analysis. 72 human full length constructs were integrated into the Y2H analysis. At all 138 constructs of the human and the yeast NPC were investigated (Fig 3.1).

3.1.2 Y2H system – Approach, Setup and Workflow to analyze the protein-protein interactions of the NPC

To systematically analyze the human and yeast NPC PPIs a well-controlled, stringent, automated, yeast two-hybrid setup was used that allowed the generation of systematic PPI data with high precision (Worseck et al., 2012). The quality of a Y2H screen is based on the stringency of the system that is dependent on internal system parameters like, the low expression of bait and prey fusion proteins, a background-free setup to unambiguously distinguish interaction and non-interaction and the improvement of the data quality by using replicas (Worseck et al., 2012). To ensure a stringent Y2H approach, a well controlled Y2H screen set up was created that included the usage of at least two biological replicas of the bait and three of the prey constructs. Beside the internal parameters a well designed experimental setup ensures high quality data. The experimental setup comprises the creation of the clone set, the appropriate application of the Y2H screen, the data processing, the data validation and finally the discussion of the obtained data in the context of the current scientific knowledge (Fig 3.2).

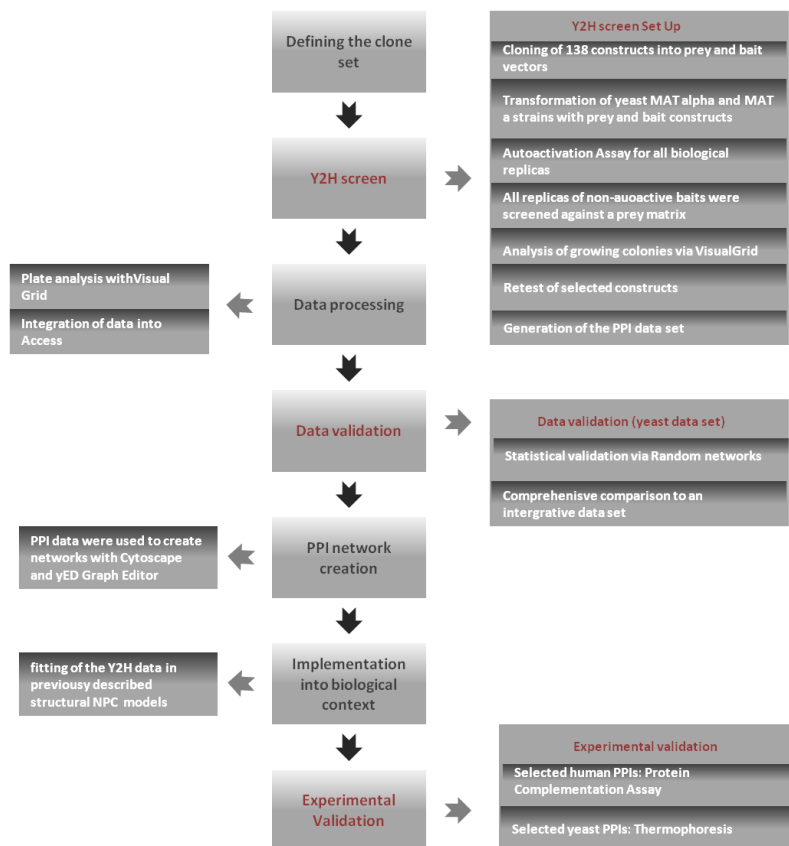


Fig 3.2 Schematic project overview of the entire protein-protein interaction analysis of the NPC. The workflow indicates the experimental strategy: starting with the creation of the NPC clone set followed the NPC Y2H screen and by data analysis, finally leading to the implementation of the Y2H data into the current scientific background and the experimental validation of the resulting hypotheses.

After generation of an appropriate cDNA clone set 138 clones were subcloned into the two low-expression Y2H bait and one Y2H prey destination vectors via gateway cloning (Invitrogen). The two

bait vectors differ in arrangement of the DNA-binding domain with respect to the bait ORF. In pBTM116-DM it is located N-terminal and in pBTMCC24-DM it is fused to the C-terminus of the ORF. Using more than one vector combination increases the number of true positives which increases data coverage. The prey vector (pACT4-DM) contains the activation domain on the N-terminus of the ORF. A MAT *alpha* strain was transformed with the prey constructs and a MAT *a* strain with the two bait vectors. To avoid false positives the autoactivation of the bait constructs was tested. Autoactivation is the detectable bait-dependent reporter gene activation in the presence of any prey plasmid, even without insert (Walhout and Vidal, 1999). To detect autoactive baits, the MAT *andi* strain including the bait construct was mated with a MAT *alpha* strain carrying the prey plasmid (Gal4-AD fusion, pACT4-DM) without insert. 68 bait constructs showed autoactivation in both vectors. Thus the ratio of the autoactive baits in the NPC Y2H screen is approximately 26%. In general, 20% of randomly selected full length bait ORFs tends to be autoactive (Nakayama, et al., 2002; Uetz, et al., 2000). The autoactive bait constructs were removed from the construct list resulting in a final bait construct list of 208 for both bait vectors. Each bait construct was tested twice against a 384-prey matrix including biological triplicates of 128 preys. The PPI screen was undertaken in all possible combinations of human and yeast baits and preys. In total the number of the possible colonies counted up to 79872. After the mating the yeast colonies were spotted on SD4 medium to detect interactions via growing colonies resulting in 1016 of grown spots (Fig 3.3).

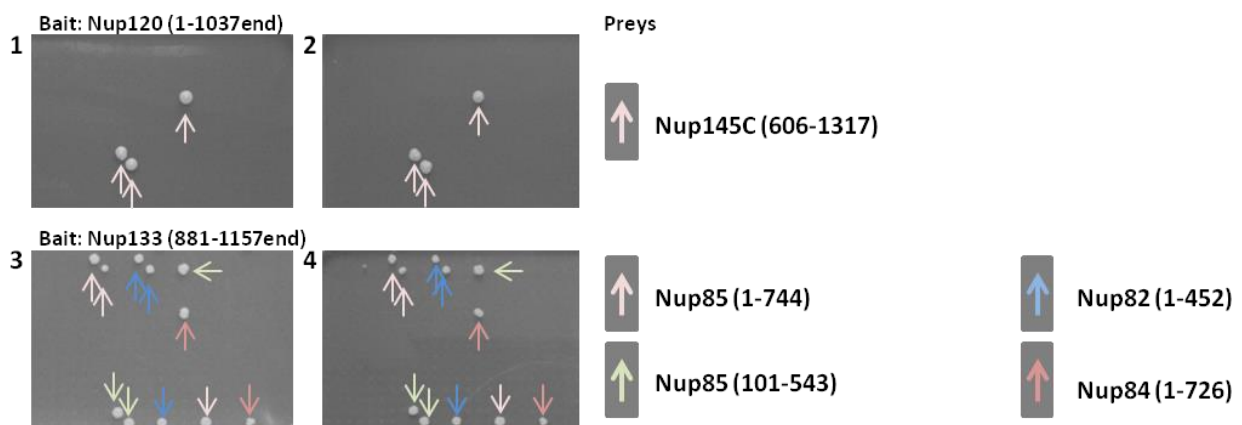


Fig 3.3 Identification of Y2H – protein-protein interactions. Shown are six selective Y2H agar plates (day 5) of three bait replicas. The yeast baits nup120 (aa 1-1037), nup133 (aa 881-1157) and the human bait NUP54 were mated with the 384-well prey matrix containing 128 preys in three replicas. The colonies which grew on -HAULT medium indicate a protein-protein interaction. The plates 1, 2: growth of colonies in position: K9, L10 and F15 indicates interaction between nup120 (aa 1-1037end) and nup145C (aa606-1317end); plate 3, 4: growth of colonies in positions: B7,B8,P17; B15,O9,P10; A11,A12,P13 and L10,P20 indicate interactions between nup133 (aa 881-1157end) and nup85 (1-744), nup85 (101-543), nup82 (1-452) and nup84 (1-726end).

All plates were analyzed with Visual Grid and the resulting grid information transferred into a Microsoft Access data base. Additionally all plates were visually assessed. The grown spots were assigned to the constructs over the position in the matrix. To make the Y2H analysis systematically more stringent, only two or more grown colonies of each bait-prey construct pair were included in the analysis. This resulted in a final colony data set of 289 colonies. To obtain a data set of interacting

construct pairs the grown spots of the replica were summarized. Finally the Y2H approach resulted in 97 interactions between 16 human and 43 yeast constructs (Fig 3.3).

3.1.3 Identification of the human and yeast NPC PPIs

The Y2H screen resulted in 97 interactions between 43 yeast and 16 human constructs. Almost all nucleoporins are represented by more than one construct. Therefore the Y2H screen resulted in 60 PPIs between human and yeast nucleoporines (Fig 3.4).

	Yeast proteins	Yeast constructs	Human proteins	Human constructs
Constructs	39	66	24	72
Interactions	44	65	16	32
One-directed	37	55	13	23
Both-directed	5	8	1	4
Dimerization	2	2	2	5

Fig 3.4 Shown is the overview of the yeast and human constructs and the resulting interactions. Listed are the initial numbers of yeast and human constructs and proteins and the resulting interactions after the transformations and autoactivation test. The Y2H screen resulted in 44 protein-protein interactions between 26 yeast proteins and 16 protein-protein interactions between 15 human proteins.

To ensure a comprehensive screening setup and decrease the number of false negatives the constructs were tested in bait-prey and prey-bait configuration. This should increase the success rate like the usage of different vectors (Chen et al., 2010). Additionally, if an interaction occurs in both directions it adds up to the normalized interaction count. Nevertheless one-directed interactions are sufficient to indicate PPIs. 37 one-directed interactions were detected for the yeast constructs and 23 interactions for the human constructs followed by 5 both-directed interactions for yeast and 4 both-directed interaction for human constructs and finally the 2 and 5 dimers for yeast and human respectively (Fig 3.4).

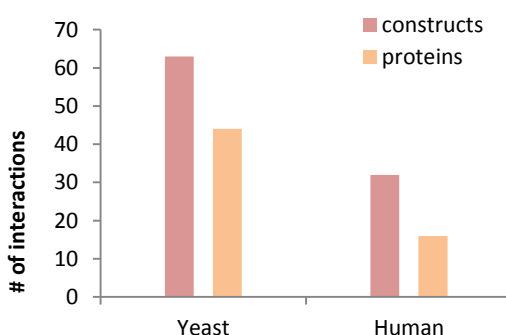


Fig 3.5 Distribution of interactions with regards to constructs and proteins of the human and yeast screen. Shown are the number of yeast and human interaction either on construct level or on protein level. The inclusion of yeast fragments increased the number of interactions. In contrast even by a higher number of human full length constructs the total amount of interactions is lower.

Besides the usage of different vectors and screening in both configurations the incorporation of fragments might increase the number of true positives further. The yeast Y2H screen resulted in 66 interactions between 43 fragments giving information about 44 PPIs between 26 yeast nucleoporins. In contrast, only 11 interactions between full length yeast proteins were detected. The screen revealed

more interactions between yeast constructs than for human construct whereby the initial amount of human constructs was larger (66 yeast constructs and 72 human constructs). This suggests that the inclusion of fragments increases the success rate of the Y2H approach. Taken together the Y2H data set comprises 44 interactions between 26 yeast nups and 16 interactions between 15 human nups.

3.1.4 Validation of the NPC Y2H data

The Y2H system is one of the most applied methods to determine PPIs (Walhout et al., 1999). It considers a variety of advantages, e.g. it is done in *in vivo* (e.g. in *saccharomyces cerevisiae*) and the minimal requirement of material to name only a few (Worseck et al., 2012). Nevertheless the Y2H system has restrictions, like a third protein could bridge the interaction, or the high sensitivity of the reporter system may detect weak interactions that might not have any biological relevance (Brückner et al., 2009). To avoid false positives the PPIs discovered with Y2H assay need to be experimentally validated. It is possible to validate single PPIs. The Y2H screen revealed a large data set and therefore it is, for a more global validation of the data set as such, also suitable to compare the entire data sets to previously published data sets.

3.1.4.1 Comparison of the Y2H data to previously published binary PPI data

To apply a first validation the literature was searched to find previously described NPC PPIs. Databases were mined like CPDB and PubMed. In fact, there are two large binary PPI data sets of the NPC published (Amlacher et al., 2011; Leducq et al., 2012). The group around Amlacher performed a Y2H screen with yeast nups and several fragments resulting in 18 PPIs between 13 nucleoporins (Fig 6.1, appendix). With an initial Y2H screen followed by affinity purification and gel filtration they performed *in vitro* binding studies to reconstitute the inner pore ring consisting of nic96-complex (NUP93-complex in vertebrates) members. The aim of their study was to emerge insight into the architecture of the NPC. Therefore they perform crystallization studies in the fungi *Chaetomium thermophilum*. The proteins of this organism seem to be more stable (Amlacher et al., 2011). They investigated only structural components of the NPC, namely members of the Y-complex and of the Nic93-complex (NUP62-complex in vertebrates). A preceding Y2H screen resulted in a binary PPI data set of *saccharomyces cerevisiae* comprising 19 PPIs related only to these two subcomplexes. 10 PPIs of the Amlacher data set are only describing intra-complex connections of the nic96-complex. The nic96-complex contains seven members (nic96, nup170, nup53, nup57, nup157, nup192 and nup188) whereas their membership was not absolute clarified unless there were several evidences. For instance it was shown that the nup170/nup53-nup59 subcomplex is essential for NPC architecture and therefore is suggested to be part of the scaffold (Marelli et al., 1998; Makio et al., 2009).

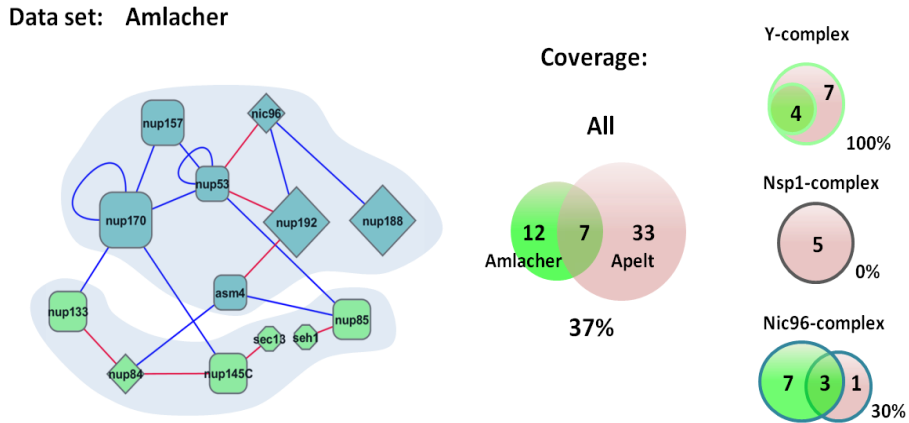


Fig 3.6a PPI network of Amlacher et al., 2011 and coverage of the whole data set and the subcomplexes to our data; The Amlacher data set contains 19 PPIs of which we could recapitulate 7 PPIs (red links). The coverage of the PPIs of the Y-complex is 100% and 30% for the nic96-complex (NUP93-complex in vertebrates). In contrast there was no coverage detected between the PPIs regarding the nsp1-complex (NUP62-complex in vertebrates).

The Amlacher data set and our Y2H data set include these PPIs supporting the suggestion of a nup170/nup53-nup59 subcomplex. Fahrenkrog et al., 2000 implied a connection between nic96 and the nup170-complex via the interaction nic96/nup53. This PPI was found by Amlacher et al. as well as we found this PPI. Further substoichiometric interactions were detected between nic96 and nup188 or nic96 and nup192 indicating a functional relationship within one subcomplex comprising nic96, nup170, nup53, nup57, nup192 and nup188 (Kosova et al., 1999; Nehrbass et al., 1996). Interactions between nic96, nup192 and nup188 were detected by the Amlacher Y2H screen but not by ours. But we were able to recapitulate two PPIs regarding nup192 (nup192/nup53 and nup192/asm4). The Amlacher data set revealed two homodimerizations of nup53 and nup170. We could not find these in our data set. In summary we were able to recapitulate three of 10 PPIs describing connections within the nic96-complex indicating coverage of 30% (Fig 3.6a). The data set of Amlacher did also reveal PPI information of the Y-complex. At all four Y-complex PPIs were described (nup84/nup145C, nup84/nup133, nup145C/sec13 and nup85/seh1). Our Y2H screen revealed all of these PPIs resulting in coverage of 100%. In addition five PPIs were reported by Amlacher describing inter-complex connections between the nic96-complex and the Y-complex. Our Y2H screen revealed also two PPIs between these two complexes (see section 4.3.2.) but none of the Amlacher PPIs were found. However we were able to recapitulate seven of 19 PPIs resulting in coverage of approximately 37%.

The group around Leducq applied a systematic yeast DHFR protein-fragment complementation assay (DFHR-PCA) to show that most protein-protein interactions are highly conserved between species and are not perturbed in hybrids. To address this they performed a comprehensive DHFR-PCA screen in *saccharomyces cerevisiae* resulting in 225 PPIs between 15 yeast nucleoporins. An interaction score was introduced by the authors resulting in a final data set of 44 PPIs between 13 yeast nucleoporins (Fig 6.1, appendix). They engineered a strong PPI reporter by fusing the DHFR fragments downstream of the coding sequence of the protein of interest. After the mating step the yeast is stamped onto medium containing methotrexate (MTX). MTX is lethal to cells. If an interaction occurs and the

DHFR enzyme is reconstituted the yeast is able to survive on the MTX containing medium (Tarassov et al., 2008). The assay is able to detect an interaction if the C-termini of both proteins are in closer proximity than 80 Å. The PCA approach was performed in four different yeast species: *S. cerevisiae* (*Scer*), *S. paradoxus* (*Spar*), *S. uvarum* (*Suva*) and *S. kudriavzevii* (*Skud*). The strongest signal to noise ratio of the assay was measured in *Scer* and *Skud*. Therefore they focused their study on these both species. They examined the robustness of protein complexes throughout close related species. To address this, PPIs were measured within the NPC and RNApII protein complexes within species and their hybrids. The PPIs were identified by estimating the colony size whereby the measurements were performed in triplicates and averaged resulting in a mean growth signal index (SI). To make their system more stringent a threshold was defined that should remove the background growth of the yeast from real interactions. The resulting data set for the *scer* PPIs comprises a highly interconnected network of 44 PPIs between 14 nups.

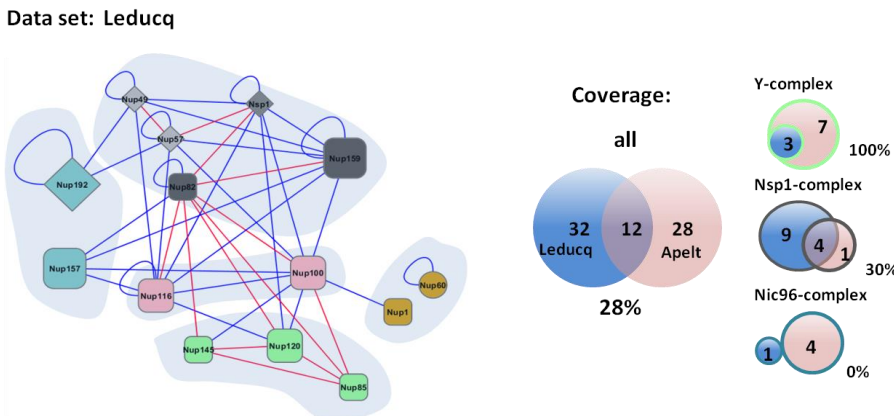


Fig 3.6b PPI network of Leducq et al., 2013 and coverage of the whole data set and the subcomplexes to our data; The Leducq data set contain 44 PPIs of which we could recapitulate 12 PPIs (red links). The coverage of the PPIs of the Y-complex is 100% and 30% for the nsp1-complex (NUP62-complex in vertebrates). In contrast there was no coverage detected between the PPIs regarding the nic96-complex (NUP93-complex in vertebrates).

The majority, 28 PPIs refer to the nsp1-complex (NUP62-complex in vertebrates). 13 PPIs describe interactions within the subcomplex and 15 PPIs between the nsp1-complex and other NPC components such as the linker and the nic96-complex (NUP93-complex in vertebrates). We could recapitulate four of the 13 PPIs (nsp1/nup57, nsp1/nup82, nup82/nup49 and nup82/nup159) of the Leducq data set indicating coverage of 30% between both data sets. The data of Leducq suggests homodimerizations of all five members (nsp1, nup49, nup57, nup159 and nup82). None of these homodimerizations were found in our data set. Our entire yeast data set included only two homo dimerizations. All members of the nsp1-complex in the Leducq data set are connected to at least one of the linker nups (nup100 and nup116) suggesting a highly interconnected nsp1-complex – linker character. Indeed we could recapitulate two PPIs nup82/nup100 and nup82/nup116 showing also here coverage. The Leducq data set includes only one intra-nic96-complex connection, namely the homodimerizations of nup192 that was not recapitulated. Three connections were detected between three members of the nsp1-complex (nup159, nup49 and nup57) and two members of the nic96-

complex (nup157 and nup192). None of these connections were found in our Y2H screen. The Leducq data set revealed connections between the nic93-complex member nup157 and the two linker nups nup100 and nup116 that are not seen in our Y2H screen. The data set comprises three PPIs between the three Y-complex members nup120, nup85 and nup145. If these are intra-Y-complex PPIs our Y2H screen did reveal these as well. The PPI nup120/nup85 was also found in our Y2H screen. All three intra-Y-complex connections were recapitulated indicating coverage of 100% of the Leducq data set by our Y2H data set. In summary we could recapitulate 11 of the 44 PPI regarding the nsp1-complex, the Y-complex and connections between them and the linker nups. This results in coverage of approximately 28% which is comparable to recapitulation rates of interactions from orthologous screens (Braun et al., 2009).

Beside previous comprehensive data sets several structural analyses were performed to create crystal data of protein contacts of the NPC (Brohawn et al., 2008 and 2009; Boehmer et al., 2008; Nagy et al., 2009; Whittle and Schwartz 2009; Yoshida et al., 2011). Crystallized PPIs are considered to be a highly trustworthy PPI information source if a crystal contact was found and the resolution is beyond a certain threshold (3-4 Å). This is supported by lines of evidence: *first*, the two proteins of interests are mostly co-purified and therefore disturbing influences are eliminated; *second*, an interaction surface is specifically determined and *third*, the resolution is high enough to determine interaction residues resulting in specific interaction sites. Therefore we decided to curate a binary data set based on crystal structures. We collected all crystal information that include PPI information of the NPC resulting in a data set of 23 crystal data (see Fig 6.2, appendix). Some of the data is redundant; five PPIs were crystallized in different labs or at least in different approaches. For instance the PPI between the NUP107/NUP133 was crystallized twice in the Schwartz lab but with two different fragments of NUP133 (NUP133 (aa 517-1156) and NUP133 (aa 935-1156) in different resolutions of 3.53 Å and 2.53 Å (Boehmer et al., 2008; Whittle et al., 2009). We decided to include all available data in the table to ensure a comprehensive data set. The PPI network in Fig 3.6c includes only combined PPI information.

The crystal data give information about protein-protein interactions of five different structural components of the NPC, namely the structured scaffold subcomplexes Y-complex and nsp1-complex (NUP62-complex in vertebrates) and the more unstructured parts of the NPC: the linker nups, miscellaneous nups building the cytoplasmic fibrils and the basket and the family of karyopherines. Most of the data (10 crystals) refer to the Y-complex including nup84, sec13, nup145C, nup85 and seh1 of the NPC of *saccharomyces cerevisiae*, nup37 and nup120 of the NPC of *Schizosaccharomyces pombe* and NUP107 and NUP133 of the human NPC. In all five of seven PPIs forming the Y-complex were crystallized (nup84/sec13, nup84/nup145C, nup85/seh1, NUP133/NUP107 (nup133/nup84 in yeast) and nup120/NUP37). Four co-crystals comprise information about three PPIs of the outer nsp1-complex including nup82 (*s.cer*), nup159 (*s.cer*), NUP62 (*r.nor*), NUP58 (*r.nor*) and NUP54 (*r.nor*).

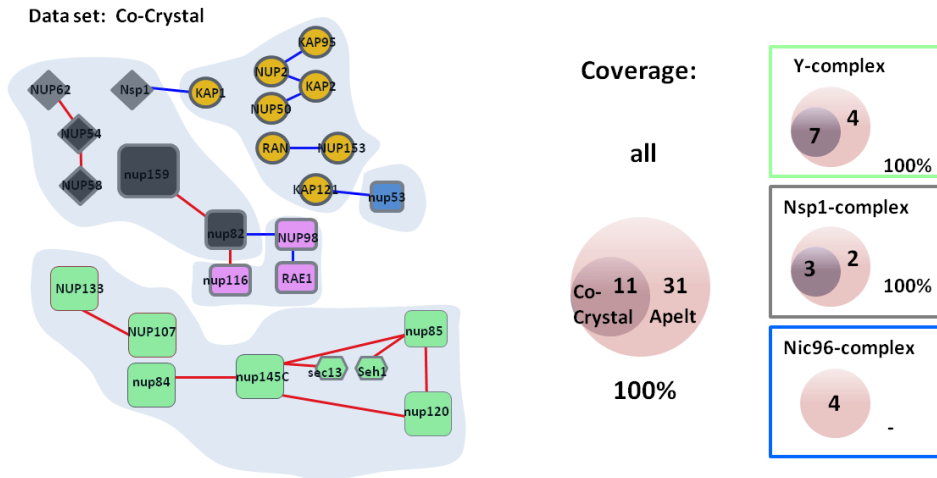


Fig 3.6c Overview of all crystal data comprising PPI information of the NPC; By mining the literature we found 18 PPIs that describe connections between 27 nups comprising the nsp1-complex (NUP62-complex in vertebrates), the nic96-complex (NUP93-complex in vertebrates), the Y-complex, linker nups and karyopherines. 11 of the 18 PPIs could be included in our screen and all 11 could be recapitulated (red links). Three of the Y-complex PPIs are unpublished data of the Schwartz-lab: nup145C/nup120, nup145C/nup120 and nup145C/nup85. The coverage is for all subcomplexes 100%.

The Y2H screen detected the PPIs nsp1/nup57 and nup57/nup49 which are the yeast interologs to the mammalian PPIs NUP62/NUP54 and NUP54/NUP85 and also were detected in the cross species PPI screen (see Fig 3.11). We could recapitulate all inner nsp1-complex (NUP62-complex in vertebrates) with our Y2H screen also resulting in coverage of 100%. There are four crystals describing PPIs between the nsp1-complex (NUP62-complex in vertebrates) members nsp1, nup82 and nup159 and the linker nup116 of *s.cer* and NUP98 of *mus musculus*. One linker PPI we were able to recapitulate was nup116/nup82 that was suggested previously (Ho et al., 2000). The crystal data contain PPI information about the more unstructured part of the NPC. Connections to miscellaneous nups (nup1, nup2 and nup50) and karyopherines (KAP1, KAP2 and KAP95) were reported. A crystal comprising an interaction between nsp1 (*saccharomyces cerevisiae*) and KAP1 (human) describes a cross species. There are four more crystals describing three PPIs between the miscellaneous nups NUP1, NUP2, NUP50 and the kaps KAP1, KAP2 and KAP95. Our Y2H screen included neither the human karyopherines nor most of the miscellaneous nups such as NUP1. Therefore we could not recapitulate any of these five PPIs. Taken together the 23 previous crystallization studies comprise information about 18 PPIs. In summary we tested 10 of the 18 PPIs in our screen and could recapitulate all 10 resulting in coverage of 100% of the co-crystal data set.

All data sets are focussing on different subcomplexes. The Leducq data set is concentrating on data about the nsp1-complex (NUP62-complex in vertebrates) whereas the Amlacher data set is focussing on data about the nic96-complex (NUP93-complex in vertebrates). The crystal data contains mostly data regarding the Y-complex. The coverage between our data set and the Leducq data set regarding the nic96-complex is approximately 30%. We were able to recapitulate three of ten PPIs. The coverage regarding the nsp1-complex is much higher. Here our Y2H data set covers approximately 40% of the Amlacher data. The coverage regarding the Y-complex is 100%. The comparison revealed high

coverage and therefore indicates high reliability of our Y2H screen. This shows that our yeast Y2H data withstands a comprehensive comparison to single PPIs of other binary data sets. Moreover the coverage of 100% of the co-crystal data suggests indeed a remarkably high quality of our Y2H data.

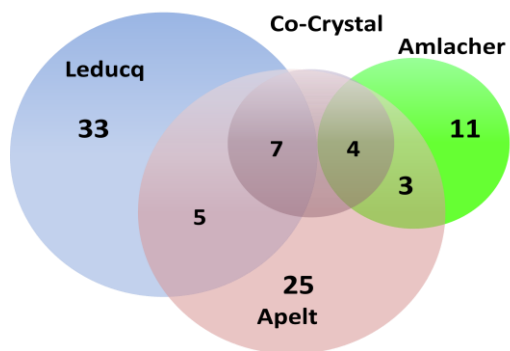


Fig 3.6 Overlap of the yeast Y2H data to the binary PPI data sets of Amlacher et al., 2011 and Leducq et al., 2012 and collected Co-Crystal data from PDB; The numbers indicate the number of PPIs measured in the according studies and therefore represent the overlaps between all three studies. The highest overlap to our data set was found with the structural data with 11 overlapping PPIs. The Amlacher data set and our data set share seven PPIs and the Leducq data set 11 PPIs.

Normalized to the total number of PPIs the overlap of all data sets ranges from of 36 % (7 of 19 PPIs) for the Amlacher data set, 30 % (11 of 44 PPIs) for the Leducq data set and 100% for the collected co-crystal data set (Fig 3.6). In summary there is a relatively high overlap to all three data sets. However the overlap to the crystal data set is remarkably high. There is no binary data set for the human NPC. Hence we were not able to perform an equal comparison with the human data set. However all crystal data of human PPIs were recapitulated. The same experimental conditions were applied for the human screen as they were for the yeast screen therefore we assume an equal quality for the human data set. A total of 73 PPIs were reported by the three other binary data sets. Information about inter-complex connections includes 11 PPIs. Our Y2H screen contains 18 out of 40 PPIs that are describing inter-complex connections. Our Y2H data set complements well the known literature with regards to inter-complex PPI data.

3.1.4.2 Comparison of the yeast Y2H data set to the comprehensive co-AP data set of Alber et al., 2007

In addition to the three previously described binary data sets, large amounts of Co-Immunoprecipitation (Co-IP), pull down and affinity purification results are available revealing complex data of the NPC (Rout et al., 2000; Fahrenkrog et al., 2000; Cronshaw et al., 2002; Alber et al., 2007). To further elucidate the quality of our Y2H screen we compared the Y2H data set with a large complex data set. We chose the data set of Alber et al., 2007. To obtain the Co-AP data, nups were tagged with Protein A (PrA) and then assayed which other nups could be co-purified. The affinity purified PrA-tagged nups and attached proteins were resolved by SDS-PAGE to be identified. The co-AP experiments comprise 82 co-APs containing 36 nups, whereby scaffold nups and more

transiently nups are included. Each resulting Co-AP blot of a tagged protein was called composites by the authors. Gel pictures of 71 composites were available and are included in our analysis. The raw data were extracted directly from the Co-AP gels and complex data for 435 protein constructs pairs could be obtained. The composites include replica of tagged proteins. The number of replicas ranges from one co-AP for nup192 and nup170 up to five co-APs for nup82. 10 composites contain only one attached protein suggesting binary interactions. Three composites were reproducible in both bait-prey and prey-bait orientation, giving seven non-redundant PPIs: gle2/nup116 (and *vice versa*), nup188/nic96, nup192/nic96, seh1/nup85 (and *vice versa*), gle1/nup42 (and *vice versa*), nup53/nup170 and nup84/nup145C. We could recapitulate three of the seven protein pairs in our Y2H screen resulting in coverage of around 40% (seh1/nup85, gle1/nup42 and nup84/nup145C). The other composites include more than one attached protein and thus result in complex data. The nups differ in occurrence in the data set. Nsp1 was co-purified and tagged in at all 33 composites and nup82 (31 composites), nup84 (30 composites), nup192 (29 composites) and nic96 (27 composites) appeared in most co-APs. The occurrence of several nups in many composites could indicate strong interactions that are easy to co-purify or this could be due to the high number of replica for each nup. Otherwise this could indicate that they are part of many interactions and should be reflected in our Y2H data set. Indeed nup82 is the protein which has the most interaction partners revealed by our Y2H screen (eight interaction partners). The most commonly identified protein in the co-AP data set was nsp1 and it has only three interaction partners in the Y2H network. Also the other three proteins that are mostly identified in the co-AP data set such as nic96 (three Y2H interaction partners), nup84 (four Y2H interaction partners) and nup192 (five Y2H interaction partners) did not report exceptionally many interaction partners. Thus the number of occurrences is only partially reflected in our Y2H data set. The composites indicate the composition of nups of the distinct subcomplexes of the NPC. The attached proteins mostly belong to the same subcomplex as the tagged protein. For instance almost all composites with tagged nups of the Y-complex include only nups of the Y-complex. Thus there are 10 composites with a tagged Y-complex nup. Six of them only contain members of the Y-complex whereas the other four composites include additionally members of other subcomplexes. Binary interactions between the tagged nups and the subcomplex members are not obvious. The co-APs revealed only complex data. For an adequate comparison of the co-AP data set with our data set we had to transform the complex data into data that come close to binary data. To address this we introduced a formula that was developed by Hegele et al., 2012 and was used to assign to each protein pair a so called Co-AP score. The co-occurrences of two proteins in one composite were determined and normalized for the total number of composite proteins. Co-occurrences in composites containing fewer proteins were favored. Thus the formula considers the specificity of the two proteins by favoring the co-occurrences of more specific proteins and weights the score by the number of co-occurrences of two proteins in all AP-composites.

Protein 1	Protein 2	Co-Crystal	Amlacher	Leducq	co-AP	contFreq
nup145C	sec13	x		x	0.45	0.50
nup145C	nup120	x		x	0.33	0.50
nup145C	nup85	x		x	0.33	0.35
nup84	nup120				0.28	0.49
nup84	nup145C	x		x	0.5	1.00
nup84	nup133	x		x	0.23	0.57
nup85	nup133				0.22	0.48
nup85	nup120	x		x	0.35	0.60
nup85	seh1	x		x	0.61	1.00
nup120	nup120				nd	nd
nup145C	nup192				0.02	0.29
nup120	nup192				0.03	0.26
nup133	nup82				0.05	0.21
nup145C	nup82			x	0.03	0.17
nup85	nup82			x	0.02	0.19
nup85	nup116				0.02	0.05
nup85	nup100			x	0	0.02
nup84	nup100				0.04	0.03
nup145C	ndc1				0	0.11
asm4	nup192		x		0.18	0.56
asm4	nic96				0.07	0.44
nup53	nup192		x		0.1	0.28
nup53	nic96		x		0.08	0.23
nup188	nup100				0.06	0.45
nup188	nup116				0.08	0.22
nup192	nup116				0.11	0.23
nup170	nup116				0.1	0.10
nup145N	nup145N				nd	nd
nup82	nup100			x	0.09	0.40
nup82	nup116	x		x	0.28	0.95
nup49	nup145N				0	0.04
nup57	nsp1	x		x	0.27	1.00
nup82	nsp1			x	0.36	1.00
nup49	nup57	x		x	0.49	1.00
nup82	nup159	x		x	0.42	0.95
nup49	nup82				0.07	0.07
nup53	nup82				0.08	0.01
asm4	nup49				0.05	0.05
nic96	nup57				0.35	0.42
asm4	nsp1				0.04	0.09
gle1	ndc1				0	0.00
nup42	gle1				1	1.00
nup2	gsp1				nd	nd
nup42	gsp1				nd	nd

Fig 3.7 Overview of all yeast Y2H PPIs with the calculated Co-AP scores and the assigned contact frequencies. 40 Y2H PPIs resulted in a Co-AP score and a contact frequency ranging from 0-1; also shown are the overlapping PPIs that were found in the other three data sets of Amlacher et al., 2011, Leducq et al., 2012 and the golden standard set comprising co-crystal data. The nups are colored according to their subcomplex membership: green: Y-complex, grey: nsp1-complex, blue: nic96-complex, pink: lonker nups, yellow: transmembrane nups, brown: miscellaneous nups including nuclear basket and cytoplasmic fibrils

As such higher Co-AP scores are given to protein pairs involving proteins that are found rarely (i.e., in fewer complexes) and in more stringent preparations (i.e., in complexes with fewer proteins). We calculated the complex scores for each protein pair of the Co-AP data set, then assigned the score to all protein pairs of our Y2H data set, ranging from 0-1 (see Fig 3.7). There is only one Y2H PPI that resulted in a Co-AP score of 1, namely the PPI *nup42/gle1* indicating co-occurrence as heterodimer in every complex. In contrast the protein pairs *ndc1/gle1*, *nup85/nup100*, *nup49/nup145N* and *ndc1/nup145C* revealed a co-AP score of zero indicating that all proteins never occur in the same composite. The co-AP scores ranges from 0-1 with an average co-AP score of the whole data set of 0.19. To assess the quality of the calculated and assigned Co-AP scores a basic statistical analysis was performed based on random networks. In general random networks were used to empirically confirm the nonrandom character of a PPI network and therefore also for the PPIs. To create a random network the Y2H network was randomized whereby the degrees of the nodes (number of interactions per protein) as well as the size of the network (number of nodes) were maintained.

To ensure a significant analysis we created 1000 random networks. The co-AP scores were assigned to the PPIs of the random networks and the distribution of co-AP scores across all 1000 random networks defined. The Co-AP scores of the random networks were depicted as a distribution with an average Co-AP score of 0.09 (Fig 3.8). The distribution revealed a standard deviation of 0.015.

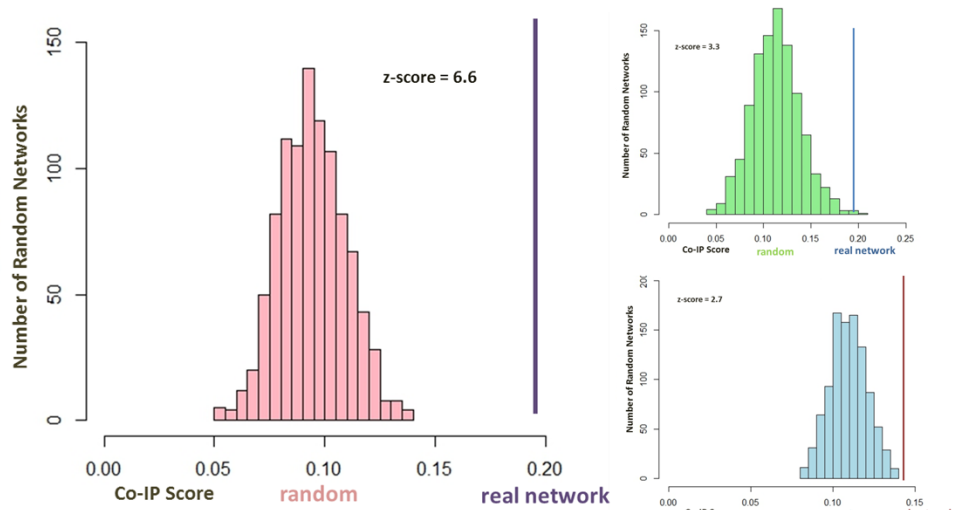


Fig 3.8 Co-AP scores of real networks and of 1000 random networks of all three data sets. Shown are the distributions of the average Co-AP scores of 1000 random networks of the different data sets represented by the bars (Y2H: pink, Amlacher: green and Leducq: blue). The Co-AP scores of the Y2H network are represented by the line. The Z-scores are depicted in each histogram and indicate the significance of the data sets to the mean of the groups of random networks via the distance. The higher the Z-score the higher the difference of the according data set to the random networks. The Y2H data are the most different data compared to random networks indicated by a Z-score of 6.6.

The random network scores approximated a normal distribution; therefore we could use a z-score to test whether our score was significantly distinct or approximated random network co-AP scores. The z-score is a statistical measurement of the relationship of a value to the mean of a distribution, taking into account the variance of the data. Here it is calculated using the distance of the Y2H co-AP scores to the mean of the distribution, as a function of the variance of that distribution. It shows the distance of a value in form of standard deviations. If a given mean and standard deviation of a normal distribution determine the range of values that encompass 95% of the probability density the z-score reaches 1.960 (Woolf et al., 2004). We propose that a z-score above 1.960 indicate significant difference to the normal distribution of the co-AP scores of the random networks. The analysis revealed that the Z-score of the average co-AP score of the random networks compared to the co-AP score of the Y2H network is quite high at 6.6 indicating a significant difference between the values. Taken together this difference implies that the calculation of the co-AP scores is meaningful and represents an opportunity to assess the quality of the Y2H PPI network with regards to a typical statistical analysis, namely to show that the Y2H network has nonrandom character. We performed the same analysis with the other two binary data sets of Amlacher et al, 2011 and Leducq et al., 2012 to compare the quality of the data sets. Therefore distributions of the Co-AP scores of the random networks were created and compared to the Co-AP scores of the real PPI data sets. The randomly generated co-AP scores range from 0.04-0.20 for the Amlacher data set and 0.08-0.14 for the Leducq data set. The real data sets achieved average Co-AP scores of 0.19 for the Amlacher data set and 0.14 for the Leducq data set. Therefore the average Co-AP score of the Leducq data set is lower than the average Co-AP scores for our Y2H data set (0.19) indicating that the protein pairs of the Leducq data set achieved lower co-AP scores. To determine the nonrandom character of both data sets 1000 random networks were created for each the Amlacher and the Leducq data set. Also here normal distributions were obtained with average scores of 0.13 for the Amlacher data set and 0.12 for the Leducq data set. The z-scores were calculated for both cases and resulted in 3.3 for the Amlacher data set and 2.7 for the Leducq data set. These z-scores indicate significant differences between the co-AP scores of the random networks and the real networks. Taken together the analysis showed that the Y2H data set revealed protein pairs with high co-AP scores indicating co-occurrences in many composites leading to a higher probability of interaction. Further it shows that the Y2H PPIs are certainly distinguishable from random PPIs indicated by the nonrandom character of the whole Y2H data set.

3.1.4.3 Comparison of the yeast Y2H data set to the integrative data set of Alber et al., 2007

Alber et al., analyzed the architecture of macromolecular assemblies through performing several experimental procedures and combining them to an integrative analysis. Because of the usage of different methods and the resulting large data set we compared our yeast Y2H data set to the final data set of Alber et al. This comprises information about the proximities of any two proteins in the structure in form of ‘contact frequencies’. These ‘contact frequencies’ were defined by how often both proteins have contact with each other in the whole NPC ensemble. The data set comprises 435 protein pairs which revealed contact frequencies ranging from 0-1. Alber et al., hypothesize that “Contact frequencies reflect the likelihood that a protein interaction is formed given the data considered and are calculated from the ensemble of optimized structures”. The protein pairs that revealed a contact frequency of one should represent a binary PPI. The data set was divided into three ranges by the authors. Most of the protein pairs fall into the low range of contact frequencies from 0-0.25. The medium range from 0.25-0.65 contains 79 protein pairs. The highest range from 0.65-1 includes only 32 protein pairs whereas 13 protein pairs resulted in a contact frequency of 1. Of the 13 protein pairs with a contact frequency of one we found six protein pairs in our Y2H data set (nup85/seh1, nup84/nup145C, nup57/nup49, nsp1/nup82, nsp1/nup57 and gle1/nup42) resulting in coverage of approximately 47%. This indicates that the binary data sets are able to recapitulate protein pairs with a contact frequency of one.

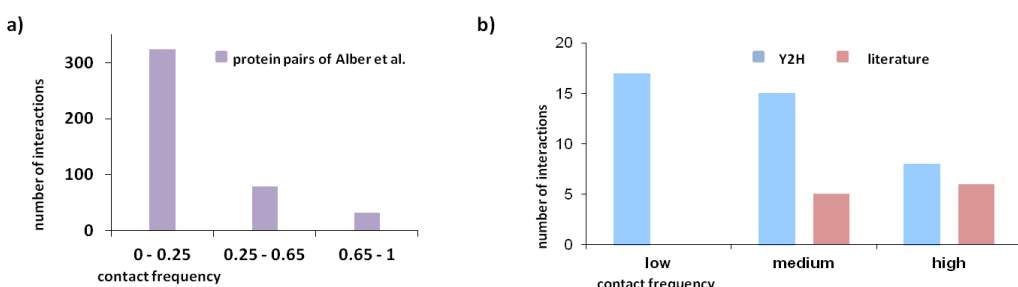


Fig 3.9 Distribution of the contact frequencies of the Alber data protein pairs, the Y2H PPIs and the crystallized PPIs. Shown in a) is the distribution of the contact frequencies of the protein pairs of the Alber data set. Most contact frequencies of the Alber protein pairs were found in the low range followed by the medium and lastly the high range. Shown in b) are the distributions of the contact frequencies of the Y2H protein pairs and the co-crystal protein pairs. The contact frequencies of the Y2H protein pairs are mostly found in the low range followed by the medium and the high range. In contrast are the contact frequencies of the co-crystal protein pairs located in the high range, as expected. No co-crystal protein pair was found in the low range.

To determine the quality of the whole yeast Y2H data set we then made a systematic comparison between our Y2H data and the contact frequency data. The contact frequency data set is based on a comprehensive and integrative experimental set up with extensive analytical and interpretational parts. Similarities between both data sets would indicate also high quality for our data set. Therefore we determined if both data sets share similarities in contact frequency distribution. To address this we split our protein pairs with the assigned contact frequencies into the three ranges given by the authors:

high (1-0.65), medium (0.65-0.25) and low (0.25-0). Next we determined the fractions of Y2H protein pairs in each of the three ranges and analyzed similarities. The distribution of the Y2H protein pairs in each range showed that most of the protein pairs are in the low range (17 PPIs) followed by the medium range (15 PPIs) and the low range (8 PPIs). The Y2H data set includes binary PPI data. We would expect most of the Y2H PPIs in the high range because they describe ‘real’ protein contacts. However most of the Y2H PPIs were found in the low range and only a few PPIs in the high range. Contact frequencies reflect only the probability that a protein interaction is formed by “defining how often the two proteins contact each other” in the Alber structure. Thus it is not excluded that protein pairs with a lower contact frequency form interactions. In addition the probability that there are 17 of 324 protein pairs in the low range that form PPIs is conceivable. Therefore to apply an adequate comparison the total number of Alber protein pairs for each range has to be included in the analysis. The fraction of Y2H protein pairs could be determined in each range leading to an exact comparison of the proportions of protein pairs in each range. When considering the fractions of protein pairs, the high range includes relatively many protein pairs indicated by a fraction of 0.27 in contrast to the low range containing only a fraction of 0.05. The medium range included a fraction of 0.2. In summary, the analysis shows the overall distributions of fractions in each range are similar in both data sets. Furthermore, the Y2H data set revealed a relatively large fraction of high contact frequencies. This shows that the Y2H data set revealed protein pairs that achieved high contact frequencies in the Alber data set. In summary both outcomes indicate that our Y2H data set is comparable to the contact frequency data set of Alber et al. after normalization and it is able to obtain protein pairs with high contact frequencies.

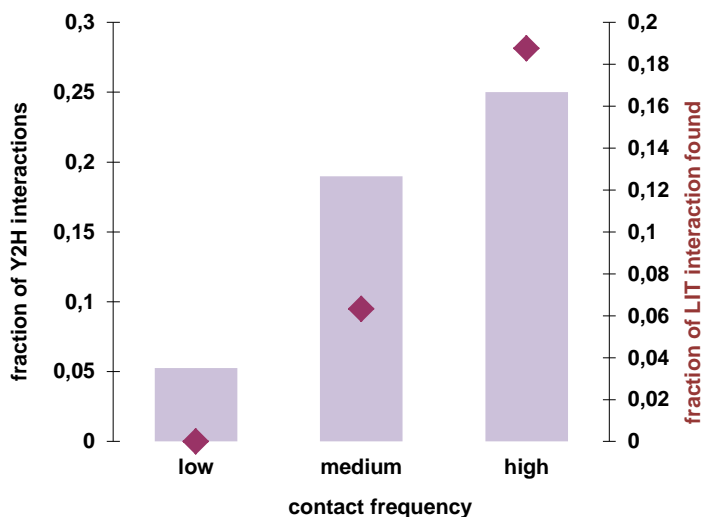


Fig 3.10 Fractions of contact frequencies of the protein pairs of Alber, of the Y2H screen and of the Co-Crystal protein pairs. Shown is the normalization of the number of Y2H interactions and Co-crystal interactions with regards to number of protein pairs of Alber in the according ranges. The highest fraction of Y2H protein pairs was found in the high range followed by the medium and the low range (purple bars). Same applies for the protein pairs of the co-crystal data set (dark red points).

A contact frequency of one indicates a very high probability of a binary interaction. All previously crystallized PPIs should theoretically achieve high contact frequencies. Indeed two of the protein pairs mentioned above that belong to the Y-complex reached contact frequencies of 1 and were previously crystallized (nup85/seh1 and nup84/nup145C). In addition two other Y-complex PPIs were crystallized before, namely nup145C/Sec13 and nup133/nup107 whereas nup107 is the human homolog to the yeast nup84 and resulted in contact frequencies of only 0.57 for nup84/nup133 and 0.50 for nup145C/Sec13. Our Y2H data set includes crystal data and therefore this comparison would show the quality of our data set. We assigned the contact frequencies to the protein pairs of the crystal data set and split them into the three ranges. There was no protein pair in the low range but five in the medium range followed by six protein pairs in the high range (Fig 3.9). This shows that the distribution of protein pairs in the crystal data set in all three ranges is different to the distribution of protein pairs in the Alber data set. It further shows that the data set of Alber is reflecting real protein contacts by means of high contact frequencies. Also by involving the total number of protein pairs of the Alber data set this trend is observable. Thus the high range contains the highest fraction of protein pairs with 0.145 followed by the medium range with 0.04. In summary ‘real’ protein contacts from crystal data are observable in the Alber data set by high contact frequencies.

Taken together a direct comparison between the contact frequencies of the protein pairs of our Y2H and the Alber data set seems to be difficult because the contact frequencies are by definition not “real interactions”. We observed a general trend between both data sets by normalization to the total number of all protein pairs in each range. This was also observed by comparing the contact frequencies of the protein pairs of the co-crystal data set to the contact frequencies of the Alber protein pairs. This shows that there are similarities in all three data sets indicating that all three are comparable to each other. In summary the comparison of the Y2H data and the Alber data is mostly meaningful by protein pairs with a contact frequency of one. We could recapitulate 47% of protein pairs with a contact frequency of 1 indicating that both data sets revealed high quality data.

3.1.4.4 Validation of the yeast data set – summary

As figured out above, the yeast data show agreement with three other binary data sets, a co-AP data set and a data set comprising contact frequencies. This starts with the overlap analysis resulting in an overlap up to 100 % to the binary co-crystal data set. Next, the comparison with the comprehensive co-AP data set resulted in appropriate average co-AP score of the Y2H PPIs that was confirmed by a statistical validation using random networks and showed that the calculated co-AP scores are significantly different to those from 1000 random networks. Finally a comparison to an integrative data set resulted in similar fractions of protein pairs within the same range of contact frequencies. Taken together the different validation approaches revealed high confident yeast data. The same Y2H

setup was used to determine human PPIs suggesting a similar quality also for the human network. Nevertheless, single human and yeast PPIs were experimentally validated (see section 3.3.1.).

3.2 Characterization of PPIs within and between NPC subcomplexes

3.2.1 The Y2H interaction maps of the yeast and human NPC

Basic parts of the NPC structure and the localization of the yeast and human nups are well described, likewise their membership to the discrete subcomplexes (Rout et al., 2000; Cronshaw et al., 2002). Nups are largely conserved between human and yeast and it is assumed that the human NPC is similar to the yeast NPC in its structural arrangement as well as in its overall shape (Beck et al., 2004). In addition to the Y2H data set obtained with the 66 yeast constructs of 39 yeast nups also the human NPC components were investigated for protein interactions using full length construct. At all 72 human constructs of 24 human nups were screened against each other. With the obtained data of the yeast and the human screen two networks were designed that are depicted next to each other to underline the homology of nups, PPIs and the possible homolog functions of nups. The human Y2H network consists of 16 PPIs between 15 nups and the yeast data set comprises 44 PPIs between 26 nups (Fig 3.11).

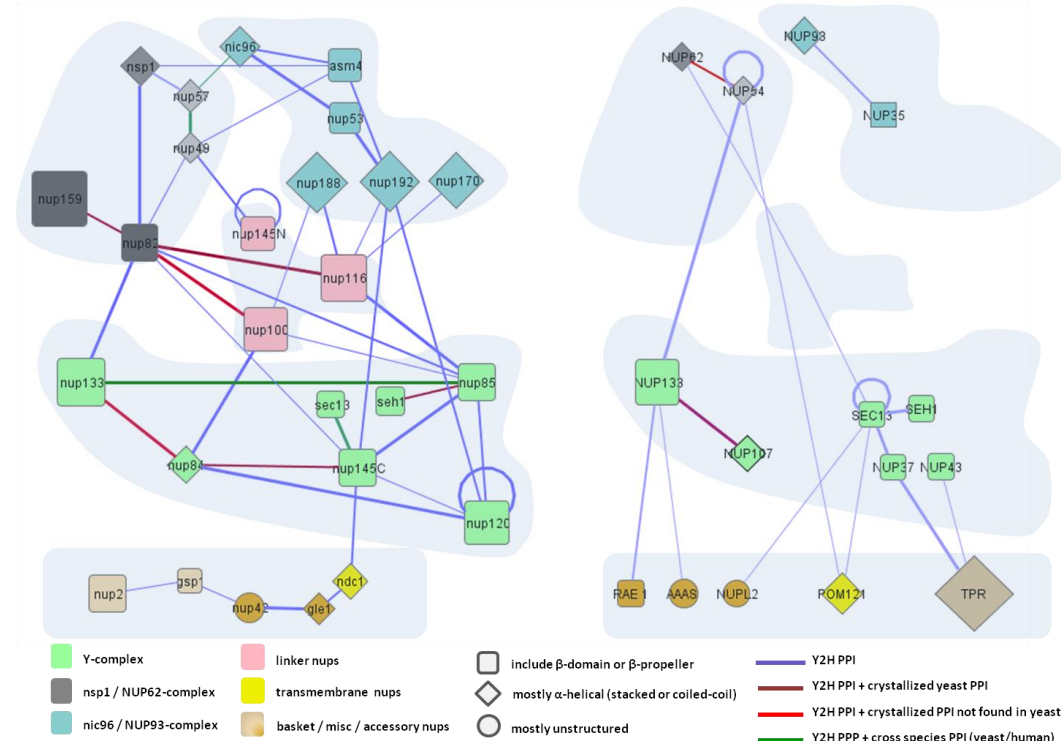


Fig 3.11 Entire PPI networks of yeast and human NPC. The PPI network of yeast NPC comprises 44 PPIs between 26 nups, the human NPC network 15 PPI between 16 nups. All subcomplexes are indicated by blue shaded areas and colored

nodes (the Y-complex in green, the nic96_NUP93-complex in blue, the two nsp1_NUP62-complexes in light and dark grey and the linker nups in pink). The shapes of the nodes declare roughly the structural architecture: rectangle: β -propeller containing proteins diamond and circles: alpha-helical domain containing proteins. The links are colored as well: blue: Y2H PPIs, red links: PPIs found in either the screens and are also previously described as co-crystals, darker red lines: found in either the screens and as co-crystals in other organisms not in yeast or human, green links: PPIs found in either the screens and as cross species PPI between human and yeast. In the yeast network all subcomplexes are connected whereas the human interaction map is much sparser.

The network view includes all previously described subcomplexes indicated in the figure as blue shades. The nodes are colored according to their membership to the discrete subcomplexes, e.g. the Y-complex in green, the nic96_NUP93-complex in blue, the two nsp1_NUP62-complexes in light and dark grey and the linker nups in pink. The links are colored as well. Blue links indicate PPIs found in the yeast or the human screen; red links declare PPIs found in either the screens and are also previously described at atomic resolution in co-crystal structures in literature (see Fig 6.2, appendix) whereas the lighter red lines indicate previously described PPIs in other organisms not in yeast or human.

The screen recapitulated nine previously described PPIs in the yeast network and two in the human network. The fraction of recapitulated PPIs (11 PPIs in yeast and human) underlines the high quality of the Y2H data sets. Human and yeast constructs were also screened against each other and PPIs found in the cross species screen are indicated as green lines. The Y2H screen could identify four cross species PPIs that are also discussed in section 3.3.3. The thickness of the links is reasoned by the internal Y2H score that was introduced to judge a PPI with regards to the amount of growing spots of one construct pair. It ranges from one to three. The Y2H screen revealed PPIs between all previously described subcomplexes in the human and yeast network. Links to the membrane in both networks could be shown, e.g. nup145C/ndc1 in yeast and NUP54/POM121 and SEC13/POM121 in human. Additionally the networks depict the connection to the basket and the cytoplasmic fibrils. Both networks are fully connected, except for the NUP93/NUP35 PPI in human. All subcomplexes are linked within themselves as well as they are connected with each other. Nevertheless more PPIs within the subcomplexes were found than between them, at least for the Y-complex. Given the high symmetry of the NPC homo dimers may be expected but only two dimers in each network were found, e.g. nup145N/nup145N and nup120/nup120 in yeast and NUP54/NUP54 and SEC13/SEC13 in human. This suggests mostly heterogeneous connections between all nups. In contrast to the dense Y2H data set of the yeast NPC the human PPI network is much sparser. It contains 16 PPIs between 15 nups. However, three well studied interactions were corroborated which were picked up in the human and the yeast screen: *first*, the Y complex interaction between NUP133/NUP107 (human) and nup133/nup84 (yeast) were found (Belgareh et al., 2001; Boehmer et al., 2007). *Second*, the NUP54/NUP62 interaction in the NUP62-complex was observed (Solmaz et al., 2011) and the homologous interaction with the yeast proteins nup57 and nsp1 (Grandi et al., 1995). *Third*, the interaction between NUP93 and NUP35 found with the human protein corresponds to the nic96 asm4/nup53 interactions (Fahrenkrog, et al., 2000). This suggests that reliable data are obtained in the

human screen as well. Several interactions are found that complement the yeast network because the homologous interactions were not detected with the yeast proteins and because the interactions involve human specific proteins such as the Y-complex proteins NUP37 and NUP43.

3.2.2 Analysis of the Y2H PPIs within and between subcomplexes of the yeast NPC

As previously described the NPC consists of several subcomplexes: the Y-complex, the nsp1-complex, the nic96-complex and the linker nups. Using the Y2H data we were able to obtain specific PPI information about connections within and between them.

The nic96-complex is one of the major subcomplexes of the NPC and constructs the inner scaffold ring (Kosova et al., 1999; Alber et al., 2007). It is an evolutionarily conserved subunit containing four architectural nucleoporins: nic96, nup157/170, nup188, and nup192. In addition the more disordered proteins nup53 and nup59 belong to the nic96-complex (Zabel et al., 1996; Grandi et al., 1995). There are different architecture options discussed. It was suggested that nic96, nup188, nup170/nup157, nup192, asm4 and nup53 are organized in a subcomplex (Andersen et al., 2013). But it was also suggested that nic96, nup192 and nup188 are not connected directly to each other. Moreover the group around Amlacher provided insight into the interactions of the large structural proteins nup192, nup188 and nup170/nup157 with nic96 and nup53 (Amlacher et al., 2011). Their studies suggest that a complex consisting of nup192, nup188 and nic96 is not possible. The binding of one helix motif of nic96 to nup192 and nup188 is mutually exclusive (Amlacher et al., 2011). They are linked by short linear motifs provided by linker nups (Amlacher et al., 2011). In contrast previous studies suggested interactions between nic96, nup188 and nup192 but a direct link could not be shown (Andersen et al., 2013, Theerthagiri et al., 2010). Thus they suppose two separate modules.

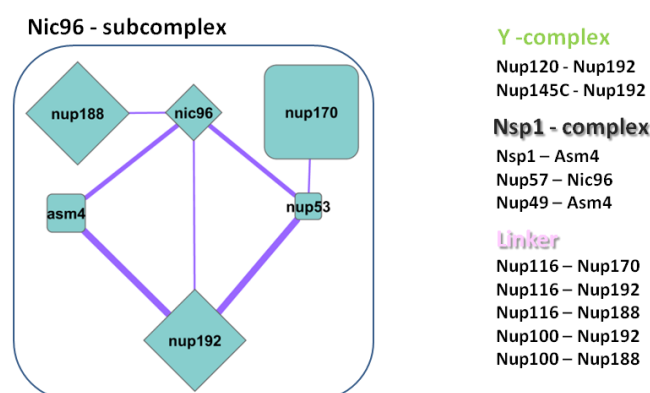


Fig 3.12a The PPI network of the yeast nic96-complex. Shown are the direct binary protein-protein interactions revealed by our extensive Y2H screen. The screen resulted in seven PPIs between six members of the nic96-complex. The shapes of the nodes are dependent on the domain composition of each protein whereas the thickness of the lines indicates the internal count (see Fig text 3.11). The nic96-complex shows direct connections to all other subcomplexes of the NPC (the Y-complex, the nsp1-complex and the linker nups).

Our Y2H screen clearly resulted in PPIs between nic96, nup188 and nup192. This suggests another binding site at nic96 that enables the binding to nup192 and nup188 simultaneously. In summary the Y2H screen revealed a nic96-subcomplex consisting of all suggested nups (nic96, nup188, nup170/nup157, nup192, asm4 and nup53) by connecting all of them with binary PPIs. Nic96 is an essential, conserved nucleoporin that is known to recruit the nsp1-nup49-nup57 complex, a module with Phe-Gly (FG) repeats, to the central transport channel of the NPC (Grandi et al., 1993; Grandi et al., 1995; Bailer et al., 2001; Schrader et al., 2008). We found that nic96 interacts with nup57, a member of this hetero-trimeric complex which is one of two subunits of the whole nsp1-complex. Thus we could confirm previous data. Nup53 and asm4 (nup59) are both FG-repeat domain nucleoporins and similar in structural organization (Fahrenkrog et al., 2000). They share two of at all six interaction partners, i.e. nic96 and nup192. The two largest members of the nic96-complex nup188 and nup192 contain high structural domain similarities (Flemming et al., 2012; Andersen et al., 2013) and it is assumed that they are most likely paralogs that originate from an early gene duplication event (Mans et al., 2004). Nevertheless they have evolved different functions in the NPC (Mans et al., 2004; Andersen et al., 2013). Depletion of nup188 resulted in an increase of the size limit for molecules transported through the NPC whereas depletion of NUP205 (homolog of nup192 in vertebrates) did not show any changes in transport limiting (Theerthagiri et al., 2010). Nup192 and nup188 seem not to share interactors except of nup116. Nup188 interacts additionally with nup100. Nup188 and nup192 connect the nic96-complex to the linker nups. In addition nup192 couple the nic96-complex to another scaffold subcomplex, namely the Y-complex via nup145C and nup120. Thus nup192 connects both structural major subcomplexes of the NPC whereas nup188 is part of the connection of the nic96-complex to the linker family. Taken together the PPIs of the nic96-complex members suggest that this complex seem to act like a scaffold module (Schrader et al., 2008). Namely it looks like the different parts of the nic96-complex are responsible for specific connection with several other NPC modules, e.g. one part (including asm4, nup53, nic96) are connected to the nsp1 complex and the structurally similar proteins nup192, nup170 and nup188 are linked to the Y-complex.

The NPC included two hetero-trimeric subunits, both containing the nucleoporin nsp1. Both subunits were classified as nsp1-complex but they have different localizations and tasks (Fahrenkrog et al., 1998). The innermost layer of the central channel of the NPC comprises the nsp1-nup49-nup57 complex – the inner nsp1-complex (Belgareh et al., 1998). All three components contain FG-repeats which fill the inner channel and are involved in the active transport of molecules (Grandi et al., 1993; Grandi et al., 1995). In contrast the other subunit of the nsp1-complex is localized at the cytoplasmic fibrils and comprises the nsp1-nup159-nup82 complex, thus often also referred to nup82 complex (Fahrenkrog et al., 1998; Yoshida et al., 2011). Apart from nup82 all other complex members are FG-nups (Grandi et al., 1995). The function of this nsp1-subunit is suggested to be required for assembly of nucleoporin subcomplexes (Bailer et al., 2001).

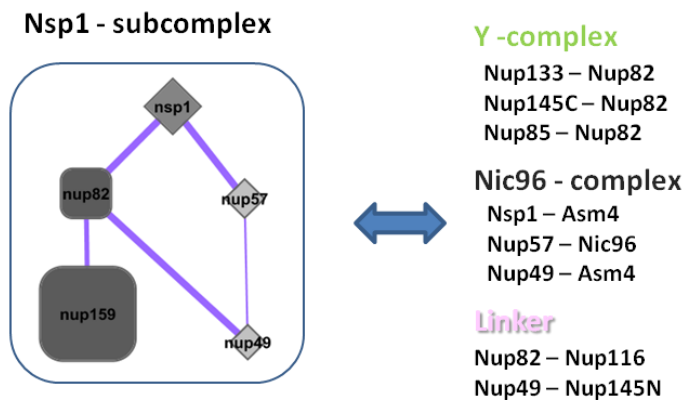


Fig 3.12b The PPI network of the nsp1-complex of the yeast NPC. The inner nsp1-complex is indicated by lighter grey whereas the outer nsp1-complex is colored in darker grey. The Y2H screen revealed five PPIs between five members (nsp1, nup82, nup57, nup159 and nup49) of both subunits. Almost all complex members (except nup159) showed connections to other subcomplexes, e.g. the Y-complex, the nic96-complex and the linker nups.

Although different localizations were suggested, two members of both subunits showed an interaction nup49/nup82 suggesting either a direct association of both nsp1-subunits or the occurrence of nup82 or nup49 in both subunits. The inner nsp1-subunit is known to be recruited by the nic96-complex (Bailer et al., 2001). We found several interactions of the inner nsp1-subunit members with components of the nic96-complex; e.g. nsp1/asm4, nup49/asm4 and nup57/nic96. Thus the inner channel of the NPC is associated with the nic96-complex. The outer nsp1-subunit showed PPIs between two members: nup159 and nup82 an inner subunit connection that was already reported before (Belgareh et al., 1998). Nup82, specifically the N-terminal part, showed most of all PPIs in the network. It suggests the connection of the outer nsp1-subunit with the inner subunit and imply connections to members of the nic96-complex, the Y-complex and both linker nups. Therefore it seems that the outer nsp1-subunit might act as an adaptor linking several other subcomplexes. In summary the nsp1-complex is suggested to fulfill two different tasks: *first*, it builds the inner channel of the NPC and *second*, it acts like a scaffold which connects almost all subcomplexes with each other. Nevertheless both subunits are associated via nup49/nup82 and might form an nspl-complex comprising both subunits.

The linker nups fill the inner cannel and are known to bind transport factors with their FG-repeats (Wente et al., 1992). It was shown that they are involved in the active transport of proteins through the NPC (Wente et al., 1993; Iovine et al., 1995). Additionally to their export task they are assumed to link distinct subcomplexes (Wimmer et al., 1992; Bailer et al., 2000). The linker nup100 and nup116 showed connections between all scaffold given subcomplexes whereby they partly share the same interactors, e.g. nup82 (outer nsp1-complex), nup85 (Y-complex), nup188 (nic96-complex). This is not unlikely as they contain high domain similarities and are assumed to be evolutionarily related by gene duplication (Wente et al., 1992). Both linker nups seem to connect the Y-complex with the nic96-complex. While both linker nups are suggested to bind to nup188 and nup85, nup100

additionally bind nup84. In contrast nup116 shows connections to nup192 and nup170. Thus they might link the nic96-complex and the Y-complex with the outer nsp1-complex by nup82.

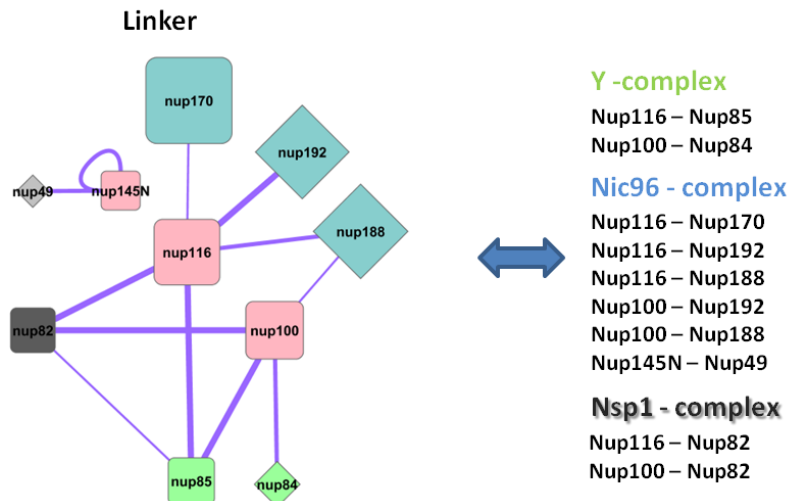


Fig 3.12c The Y2H interaction map of the yeast NPC linker family. The yeast linker family comprises three members and is indicated by pink colored nodes. At all there were 11 PPI detected to directly interact with at least two members of three different subcomplexes, namely the Y-complex, the nic96-complex and both nsp1-complexes.

It was suggested that nup116 associates with the nup82-nsp1-nup159-complex (Bailer et al., 2000). Additionally Yoshida et al., 2011 observed the binding of the nup82 β -propeller to other yeast nup116 family members, nup145N and nup100. A binary interaction between nup116 and nup100 with nup82 could be recapitulated. We were able to confirm the suggested link-function of nup116 and nup100 to all NPC subcomplexes. Another member of the linker family is nup145N. It is derived by proteo-catalytic cleavage of the precursor protein nup145 (Teixeira et al., 1997 and 1999). The C-terminus (aa 606-1317) is part of the Y-complex whereas nup145N (aa 1-605) is part of the linker family and share structural similarity to nup116 and nup100 (Ratner et al., 2007). Lutzmann et al., 2005 reconstituted nup145N into the Y-complex which was not confirmed by our Y2H screen. Nup145N seems to show two PPIs in the screen. First it seems to build a dimer and is therefore one of two nups (nup120 and nup145N) that showed dimerization in the screen. Second it is interacting with the inner nsp1-complex member nup49, a FG-nup that is part of the inner channel of the NPC. We suggest a connection between the linker family and the inner channel of the NPC. Taken together the results of the Y2H screen support the suggested function of the linker nups that is to connect all subcomplexes of the NPC. The linker nups themselves showed no connection to each other in our Y2H screen.

The subset of transmembrane domain containing nups comprises three nups in the yeast NPC (Rout et al., 2000). PPIs between membrane nups and scaffold nups might emerge insight into the anchoring. Interactions of transmembrane nups were detected in our Y2H screen. Ndc1 seems to binary interact with nup145C, a member of the Y-complex. It seems that the NPC is anchored via the ‘hub’ of the Y-complex to the membrane. The ‘hub’ of the Y-complex is the C-terminal connection of the three Y-complex proteins nup145C, nup85 and nup120 that build the hinge of the Y-complex (Thierbach et al.,

2013). Ndc1 seems to interact with members of the nuclear basket, in fact with gle1 that is localized at the nucleoplasmic side of the NPC suggesting the connection between the NPC and the basket occurs via the membrane. We found gle1 interacting with nup42 that is known to be localized at the cytoplasmic fibrils and nup2 (Dingwall et al., 1995) that is localized at the nuclear basket. Taken together the NPC is might be fixed to the membrane via the Y-complex. Furthermore the association of the fibrils and the basket are reflected in the Y2H network.

The largest and major structural given subcomplex is the Y-complex. The Y-complex includes six or seven members (nup133, nup85, nup84, nup120, nup145C, sec13 and seh1) and has a molecular weight of approximately 450kDa (Siniossoglou et al., 2000). The stable membership of seh1 throughout organisms is discussed. Seh1 could be identified in human and some yeast organisms such as *saccharomyces cerevisiae* and *schizzosaccharomyces pombe*. However it could not be found in all *ascomycetes*; at least it could not be detected (Neumann et al., 2010).

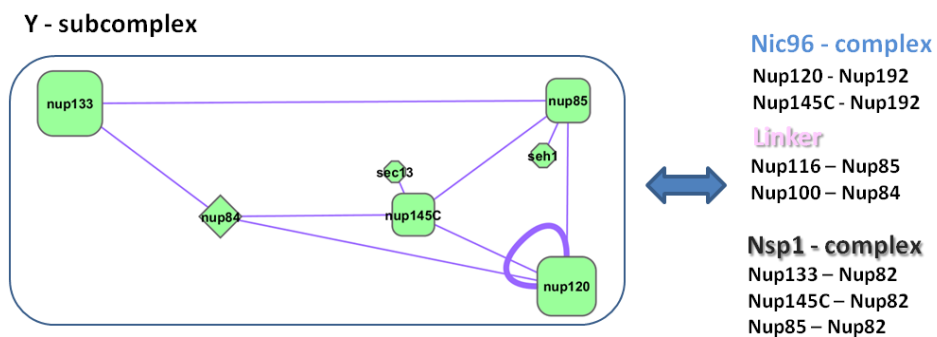


Fig 3.12d The PPI interaction map of the yeast Y-complex. The Y-complex comprises seven members and the screen revealed 10 PPIs between them. In addition the screen revealed direct connections to all other NPC subunits such as the nic96-complex, the nsp1-complex and the linker family.

The Y-complex seems to be highly interlinked. All members of the Y-complex showed at least one interaction with another member in our Y2H screen. Three of the seven yeast PPIs were already described by previously reported crystallization experiments in yeast, namely nup145C/sec13, nup145C/nup84 and nup85/seh1 whereas NUP107/NUP133 (interolog to nup84/nup133) was found in human (see Fig 6.2; appendix). Other three intra-molecular associations could also be resumed with the Y2H screen: nup145C/nup120, nup145C/nup85 and nup120/nup85. Beside the six previously shown interactions we received data for three novel PPIs; nup120/nup120, nup85/nup133 and nup84/nup120. These PPIs are unlikely to have intramolecular character given the localization of the according nups. Actually they seem to be intermolecular which may give rise to the link between two Y-complexes. The Y2H screen revealed connections to other subcomplexes such as the links between the Y-complex and nic96-complex via nup120/nup192 and nup145C/nup192. Two links between the structural subunit of the nsp1-complex and the Y-complex could be suggested via nup133/nup82 and nup85/nup82. It seems that the connection to both other subcomplexes occur via several Y-complex members but only to one nsp1-complex and one nic96-complex member. Beside attachments between

structural subcomplexes the network seems to reveal connections of the Y-complex to the linker nups nup100 and nup116. Nup85 is interacting with both linker nups whereas nup84 is only interacting with nup116. Taken together the results showed the role of the Y-complex as a structural component that seems to be associated to all structural subcomplexes building the scaffold of the NPC as well as the connection to the linker.

In summary the Y2H screen revealed connections within all subcomplexes as well as between them. Some of already in literature described PPIs could be confirmed and all of the Y-complex connections obtained by crystallization could be recapitulated. Additionally the Y2H screen revealed novel findings such as the bridging the two nsp1-complexes by members of the nic96-complex or the link to the membrane via ndc1/nup145C.

3.2.3 Analysis of the cross species PPIs in the Y2H data set

As described above the NPC might be largely conserved between human and yeast (Beck et al., 2004). We screened human and yeast nups against each other to detect possible cross species PPIs that could give insight into the conservation of PPIs or at least give information about the functionality of homolog proteins in the yeast and the human NPC. The entire screen revealed 20 cross species PPIs (Fig 6.5, appendix). However in the analysis only these cross species PPIs were included for that additionally yeast or a human PPI could be found.

In the network view (Fig 3.11) cross species PPIs are indicated as green lines. We could recapitulate the crystallized cross species PPI between the human nup SEC13 and the yeast nup145C (Nagy et al., 2009) of which the screen also revealed the yeast PPI between sec13 and nup145C. For another previously described PPI between NUP58 and NUP54 in *rattus norvegicus* a cross species PPI between the yeast nup49 (homolog of NUP58) and the human NUP54 was detected. The screen resulted in a cross species PPI between the human NUP133 and the yeast nup85 that could lead to the assumption of an inter-molecular Y-complex link. This PPI was also observed with the yeast PPI nup85/nup133.

Notably the screen resulted in a read out in which the interaction patterns on agar plates of the bait constructs hNUP133/ynup120 and hNUP107/ynup85 looked very similar (Fig 3.13). This suggests different homolog relationships between human and yeast Y-complex members as suggested (D'Angelo et al., 2009). This is not unlikely as the domain architecture of all nucleoporins is similar and contains only different kinds of alpha helices, β-propeller and FG-repeat domains (Rout et al., 2000) especially within subcomplexes which impede an exact structural analysis. To investigate this hypothesis knock-out strains were transformed with different human and yeast nup constructs. Human proteins may rescue temperature sensitive phenotypes in so called complementation experiments

(Osborne et al., 2007). In general, knock out strains of the BY4741/BY4742 yeast library were used (Tong et al., 2001). A U2 Δ 85 knock out strain could be created with a nourseothricin cassette by decreasing the growth temperature from 30°C to 24°C and prolongation of the growth time up to 12 days. The control of the knock out occurred with sequencing and with the rescue of the according yeast nup (Fig 3.13.).

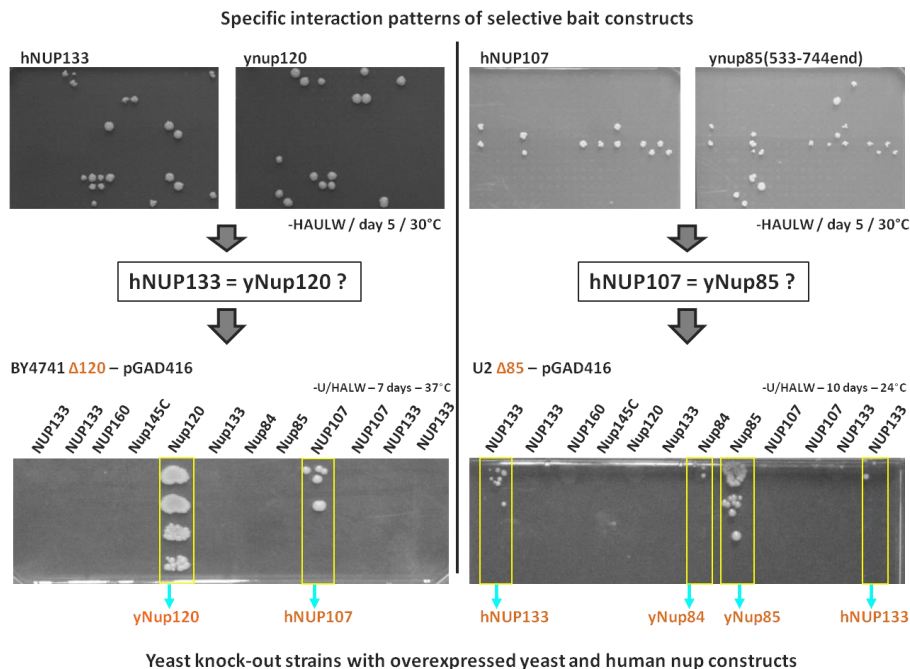


Fig 3.13 Experimental set up to investigate the same Y2H interaction patterns of yeast and human nucleoporins. Shown are the interaction patterns of *ynup120* and *ynup133* that are shared with *hNUP133* and *hNUP107* and the resulting homolog-hypothesis. Below: two agar plates are shown of knock out strains transformed with the according yeast and human nups

After creating the knock out strains, they were transformed with all structural nups of the yeast Y-complex, namely *nup120*, *nup145C*, *nup84*, *nup85* and *nup133*. Additionally the strains were transformed with different constructs of the human Y-complex members *NUP133*, *NUP107* and *NUP160*. The results showed that the yeast *nup120* can be rescued by itself but by no other yeast nup. To support the initial finding of the similar interaction patterns of *nup120* and *NUP133* it would be expected that *NUP133* would rescue the *nup120* knock out. This is not the case. Instead the *nup120* knock out is rescued by the human *NUP107* which is suggested to be the homolog to the yeast *nup84* (D'Angelo et al., 2008). In case of *nup85* the initial hypothesis could also not be substantiated. Thus the *nup85* knock out could be rescued with the yeast *nup85* and with the human *NUP133* whereas *NUP107* was expected from the interaction pattern. The results obtained with delta 85 are not conclusive. However the results of rescuing the delta *nup120* knock-out strain are in agreement with the literature (D'Angelo et al., 2008) and refute our hypothesis. The results underline the complexity of the nup function in contrast to their architecture indicating the importance of PPI analysis.

3.2.4 High resolution Network of the yeast Y-complex and inter complex connections

The Y2H screen of the yeast NPC did not only include full length proteins, it also contains fragments of all nups according to their structural domain organization. This allows deeper insights into the structural organization of the NPC, a high resolution view. The most structural given subcomplex of the NPC is the Y-complex. With the PPI fragment data we could support previously described co-crystal data as well as we could define novel connections between either Y-complexes or between Y-complexes and other subcomplexes of the NPC. The Y-complex of *s.cer* includes at least six members (nup133, nup85, nup84, nup120, nup145C and sec13). The membership of seh1 is still discussed (Neumann et al., 2010). With the obtained Y2H data we generated a network comprising 15 interacting fragments resulting in 24 interactions (Fig 3.14).

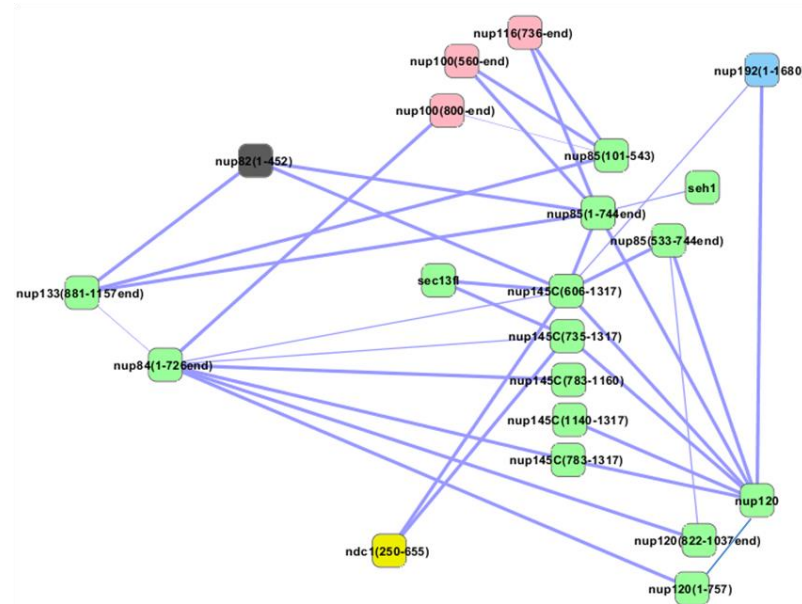


Fig 3.14 the high resolution interaction map of the Y-complex. Shown are connections within the Y-complex and to other subcomplexes. Green nodes = Y-complex; pink = linker; blue = nic96 complex; grey = nspl-complex; yellow = transmembrane nups. The interaction map comprises 21 fragments, 15 constructs belong to the Y-complex. All previous crystallization data could be confirmed with our Y2H screen even on a fragment level (see text for details). In addition the Y-complex shows connections to the nic96-complex member nup192 via nup145C (both full length). The nspl-complex is attached via the N-terminal part of nup82 (aa 1-452) to the Y-complex members nup133 (aa 881-1175end), nup85 and the ‘hub’ nup nup145C. There is also a ‘hub’ connection to the membrane via ndc1 (aa 250-655) /nup145C (aa735-1317end). The linker nups are connected as well. The linker nups seems to be attached via the N-terminal part of nup85 (aa101-543)

The Y2H screen revealed connections to other subcomplexes. We could detect two links between the Y-complex and the nic96-complex via nup120(f.l.)/nup192(f.l.) and nup145C (f.l.)/nup192(f.l.). Furthermore a link between the structural subunit of the nspl-complex was shown via nup133 and the N-terminal of nup82 (aa 1-452) whereas the C-terminal part of nup82 (aa 452-713end) is linked to the nspl-complexes and the linker (Fig 3.14). Beside attachments between structural subcomplexes the network revealed novel and specific connections of the Y-complex to the linker nups 100 and nup116. The N-terminal part of nup85 (aa 101-543) is interacting with the C-terminal part of both linker nups:

nup116 (aa 736-end) and nup100 (aa 800-end). Another novel finding is the connection of nup145C (aa 735-1317end) to the middle part of Ndc1 (aa 250-655). Taken together the results showed specific connections to other structural components of the NPC at high resolution.

The high resolution data could be used to validate the three yeast and one human crystallization results of the Schwartz lab with regards to following interacting proteins and their fragments:

Protein 1	Residues 1 (crystallization)	Y2H fragment 1 (s.c.)	Protein 2	Residues 2 (crystallization)	Y2H fragment 2 (s.c.)	PDB_Entry
nup84	1-460	1-726 (f.l.)	nup145C	731-1158	783-1160	3IKO
seh1	1-349 (f.l.)	1-349 (f.l.)	nup85	1-564	1-744 (f.l.)	3EWE
sec13	1-297 (f.l.)	1-297 (f.l.)	nup145C	731-1158	735-1317	3JRP
NUP133 (human)	935-1156	881-1157 (yeast)	NUP107 (human)	658-925	1-744 (yeast) (f.l.)	3CQC

Fig 3.14 Co-Crystal data containing members of the yeast and the human Y-complex. Shown are the interacting Y2H fragments and the residues obtained by crystallization

The screen confirmed the three existing crystallization data of the yeast Y-complex: nup84/nup145C, nup85/seh1, nup145C/sec13 and the human PPI NUP133/NUP107. Moreover the Y2H interacting fragments of nup145C (aa 783-1160 and aa 735-1317) are matching to the residues found in the crystallization experiments, namely nup145C – aa731-1158 (Fig 3.14). The interaction nup133/nup84 was only crystallized in human (NUP133/NUP107). However, high conservation between the human and the yeast NPC allows the comparison of the interacting yeast fragments (D'Angelo et al., 2008). The fragment of nup133 (aa 881-1157) overlaps with the human residues of NUP133 (aa 935-1156). Thus we could confirm with perfect agreement previous crystallization results of the four PPIs. In addition to the four PPIs mentioned above three other Y-complex PPIs were revealed by the Y2H screen, namely nup145C/nup120, nup145C/nup85 and nup85/nup120 (Rout et al., 2000; Alber et al., 2007). They were known to build the 'hub' of the Y-complex but binary PPI information were not available (Leksa et al., 2009; Schwartz et al., 2009). However it was assumed that the 'hub' consisting of nup145C-nup120-nup85 is linked by all three C-termini of the proteins (Thierbach et al., 2013). Indeed we found that the C-terminal fragment of nup85 (aa 533-744end) interacts with the C-terminal fragment of nup120 (aa 822-1037). Further the C-terminal part of nup145C (aa 1140-1317end) interacts with the full length construct of nup120 and full length construct of nup145C (aa 606-1317) is linked to the C-terminal part of nup85 (aa 533-744end). In summary at least one interacting construct of each interaction is the C-terminal part of a protein supporting the suggestion of a C-terminal link of all three 'hub'-proteins. Thus the Y2H results are also here in perfect agreement and confirm previous knowledge. In summary the screen revealed and confirmed all seven PPIs that build the Y-complex even on a fragment view.

Beside confirmation of previously described interactions the screen revealed three novel PPIs: nup133 (aa 881-1157end)/nup85 (aa 101-543), nup84aa (aa 1-726end)/nup120 (aa 1-757) and nup120 (aa 1-757)/nup120. The nup120 dimerization occurs via the N-terminus: nup120 (f.l.)/nup120 (aa 1-757)

whereas the connection to the ‘hub’ occurs via the C-terminus nup120 (aa 822-1037). This indicates that both parts of nup120 are involved in protein interactions. The screen revealed also a connection between nup84 and nup120. Two non-overlapping fragments of nup120 (aa 1-757 and aa 822-1037end) interact with nup84 indicating that there might two binding sites for nup84. The interaction between nup133 and nup85 occurs via the N-terminus of nup133 and the C-terminus of nup85. As described above the architecture of the Y-complex is determined by seven PPIs (Alber et al., 2007; Beck et al., 2007; Kampmann et al., 2009). The three novel interactions might describe connections between Y-complexes and are therefore inter-complex connections.

Taken together we were able to confirm all previously described inner Y-complex PPIs that were obtained by previous studies such as crystallization even at the fragment level resolution. Further we obtained novel data that could describe inter-molecular Y-complex connections.

3.2.5 NPC PPI network – summary

Taken together we obtained PPI data for 26 yeast nups and 16 human nups comprising yeast 44 PPIs and 15 human PPIs. By analyzing the created PPI networks it was possible to confirm previous PPI data, e.g. the yeast intra-molecular Y-complex connections and the connection of basket and cytoplasmic fibrils to the NPC. In addition novel PPIs and thus connections between NPC subcomplexes could be unraveled. By including fragments a high resolution view especially to the Y-complex was possible confirming all previous co-crystal data. Further novel Y-complex PPIs were obtained that are very unlikely to be intra-molecular Y-complex connections. Moreover they seem to be inter-molecular connections between two or more Y-complexes.

3.3 Confirmation of selected subcomplex PPIs of the yeast and the human NPC

Our yeast data set belongs to one of the most comprehensive NPC PPI data sets. The results have to be validated experimentally. In general the application of an independent method is necessary to recapitulate at least some of the obtained PPIs. Different interaction assays can be used to detect distinct sets of protein interactions and are of complementary nature (Stelzl and Wanker, 2006). However different methods can be used to detect same interactions. It is helpful to use different protein tags, *in vivo* or *in vitro* environments and mechanisms of interaction as readout. Consequently, each assay has its own false-positive and false-negative rates. Thus it is not expectable that all physiologically meaningful Y2H interactions can be detected in other biophysical or cell-based assays such as surface plasma resonance (SPR) experiments, pull downs or protein fragment

complementation assays (PCAs) (Braun, et al., 2009). However, an interaction which is seen in different assays is less likely to be false-positive.

To address this issue, PPIs belonging to the Y-complex were chosen as it is one of the best characterized subcomplexes of the NPC and provides already well reported PPIs that could be used as positive test if the method is able to detect nup interactions. In contrary the novel inter Y-complex PPIs should be experimentally validated. As described above PPIs of the Y-complex were previously investigated to high extend with crystallization and with cryo-tomography (Nagy et al., 2009; Brohawn et al., 2009; Leksa et al., 2008; Beck et al., 2007). Thus a high overlap to these data supported by the results of the validation experiments would indicate a valid Y2H data set.

3.3.1 Micro-scale Thermophoresis (MST) enables the validation of PPIs of the yeast Y-complex

In addition to the *in silico* validation of the whole yeast data set, we set out to recapitulate selected yeast and human PPIs with independent biophysical and cell-based methods, focusing on PPIs belonging to the Y-complex of the yeast NPC. The Y-complex is the largest subcomplex of the NPC building the base of NPC architecture (Alber et al., 2007; Brohawn et al., 2009; Debler et al., 2008). The entire Y2H screen revealed 10 PPIs between seven Y-complex nups (Fig 3.15). Seven of them were previously described as intra-complex connections which build the yeast Y-complex: nup133/nup84, nup84/nup145C, nup145C/Sec13, nup145C/nup85, nup145C/nup120, nup85/seh1 und nup120/nup85 (Alber et al., 2007; Brohawn et al., 2009; Kampmann et al., 2009, Fernandez-Martinez et al., 2012). Three of them (nup84/nup145C, nup145C/Sec13, nup85/seh1) even could be crystallized (Rout et al., 2002; Alber et al., 2007; Brohawn et al., 2008 and 2009; Kampmann et al., 2009, Fernandez-Martinez et al., 2012). The Y2H screen revealed all previously reported connections within the Y-complex. The Y2H screen revealed additionally three PPIs that are both unreported and, based on the overall structure of the sub-complex, are highly unlikely to be intra Y-complex connections: nup133/nup85, nup120/nup84 und nup120/nup120. Nup133 and nup85 are on the opposite sites of the Y-complex. The architecture of the Y-complex is well defined and it is unlikely that both proteins are in close proximity within a single subcomplex to interact with each other (Kampmann et al., 2012). The same applies for nup84/nup120 (Fig 3.15). If the PPI nup120/nup120 is present in one Y-complex it must be assumed that nup120 occurs as an intra-complex homodimer. However, several biochemical purification studies suggested only one nup120 molecule per Y-complex (Leksa et al., 2009; Brohawn et al., 2009). These three PPIs are the first described inter-Y-complex PPIs and as such could give hints to the arrangement and orientation of Y-complexes.

To validate the Y-complex PPIs different methods were discussed. For instance SPR experiments using purified proteins were performed. SPR is based on the charge-density oscillation at the interface between two media that generate a surface plasmon wave (SPW) if two molecules of interest bind to each other. This occurs at real-time and in a label-free medium and enables the detection of binding kinetics resulting in on- and off-rates. To prepare the SPR measurements, a nanobody was covalently attached to the sensing surface. The nanobody attachment should enable the exchange of bait protein constructs from the sensing surface. A bait protein construct should bind via an integrated EPEA (glutamic acid – proline – glutamic acid – alanine) – tag to the nanobody to be fixed to the surface. Finally the prey protein construct was added. The binding of bait and prey constructs result in a change in the refractive index that should be detected resulting in a shift of the reflectivity curve versus wavelength of source light or angle of reflected light. It was not possible to remove the bait protein constructs from the nanobody by washing. The exchange of bait protein constructs from the surface was not possible and for each interaction a new chip has to be used. Therefore the method was not applicable because for financial reasons. Another technique that could be used to validate the Y2H PPIs with purified proteins was pull-down experiments on sepharose beads. Therefore nanobodies covalently bound to sepharose beads should be used to fix the bait protein construct to the sepharose beads via the EPEA-tag. By adding the prey protein construct a protein complex should be assembled that could be visualized with SDS-PAGE. In some experiments the prey protein constructs bind to the matrix or no binding between bait and prey could be detected. Therefore also the pulls-down experiments were not appropriate for the validation of the interactions. Finally, a recently developed method called thermophoresis was used (Jerabek-Willemsen et al., 2011). It is a physical phenomenon observed in fluids where proteins exhibit different behavior to the force of a temperature field implemented by a laser. A PPI would quite likely change the formation of the hydration shell of bound proteins which than leads to changes in movement in comparison to two separate unbound proteins. An inferred laser creates a precise micro scale temperature field within thin glass capillaries filled with a solution containing the proteins of interest in a serial dilution (Fig 3.15). One of the proteins of interest is labeled with a fluorescence marker (NHS 647, Nanotemper). The change of movement is detected in each of the 16 capillaries with varying amount of untagged protein by with fluorescence. The readout is shown as correlation between fluorescence of the labeled protein and the concentration of the non-labeled protein resulting in a binding curve. The big advantages of this method are *first*, the amount of protein input is quite low (~50 nM for the labeled protein and 10-200 μ M for the titrated protein in a 5 μ l sample); *second*, the procedure is easily to handle and not time consuming (15min for one measurement) and *third*, it is a biophysical method that yields a K_D . A K_D is the Dissociation constant that is used to describe the affinity between two molecules. The MST measurements in each capillary were done at equilibrium state. Here the Dissociation constant K_D is defined at half saturation of bound and unbound fraction of the titrated protein. The lower the K_D the stronger is the interaction (Fig 3.17).

3.3.1.1 Constructs and proteins used in the MST experiments

To apply MST purified proteins were needed. To address this, the proteins of interest (Fig 3.15) were purified during my visit in the lab of Thomas Schwartz at the MIT. Initially SPR was tried (see section 3.3.1). Therefore an EPEA-tag was introduced at the C-terminus of the DNA sequence of the protein constructs by PCR and the bait protein constructs were generated. The bait construct plasmids (pET-Duet) were closed by Gibson- and conventional cloning. The bacteria expression strain (BL21) was transformed with the according plasmids. The protein constructs were purified on nickel beads, dialyzed, followed by ion exchange and gel filtration. Finally the proteins were concentrated (see methods). Almost all proteins were not stable if they are expressed alone as such co-expression was necessary (Fig 3.15). The prey protein constructs were taken from the protein bank of the Schwartz lab.

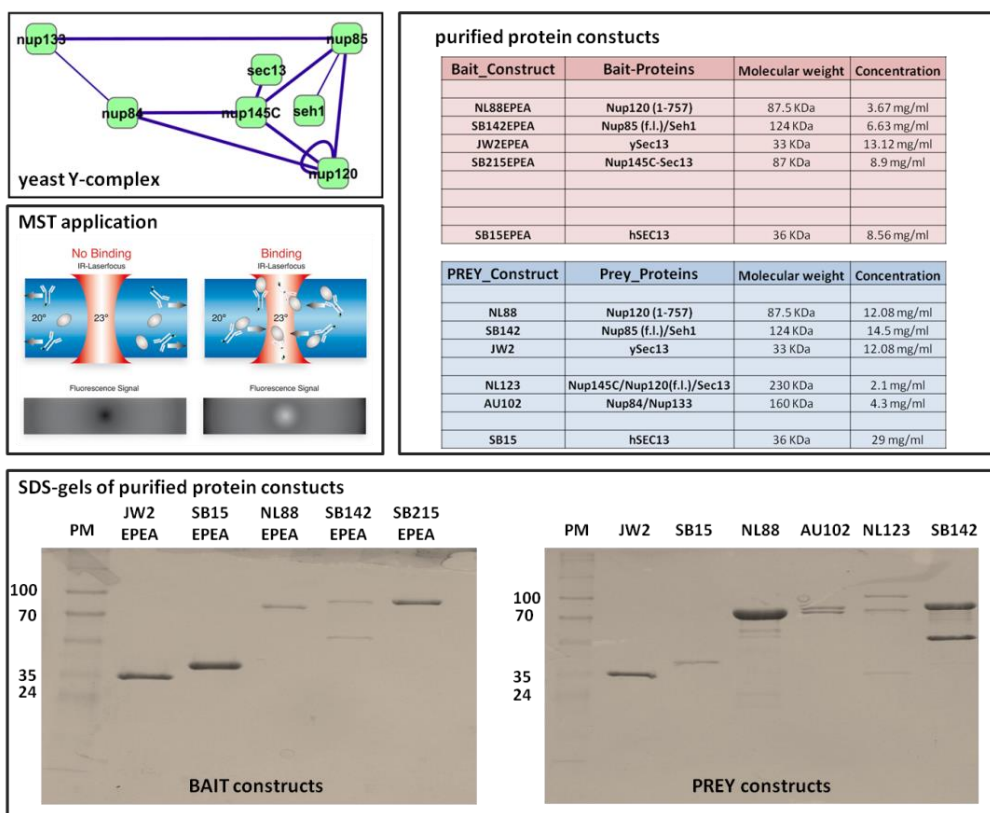


Fig 3.15 Overview of the MST based experimental workflow. Shown is Y2H PPI network of the Y-complex. The network of the Y-complex visualizes the connections between the proteins of interest that should be tested in the MST approach. The MST application shows the basic principle of thermophoresis (picture of Nanotemper; see detailed information in the text). The table contains all purified and co-purified protein constructs of the yeast Y-complex which were used in MST experiments. The SDS-PAGE gels (coomassie stain) are also shown that control the purified and co-purified proteins according to their size.

In all five bait-constructs were purified: nup85(f.l)-seh1(f.l.) = SB142EPEA; nup120(aa1-757) = NL88EPEA; nup145C(f.l.) covalently bound to sec13(f.l.) = SB215EPEA; sec13(f.l.) = JW2EPEA alone and the human SEC13(f.l.) = SB15EPEA. The prey constructs include partially the same proteins such as nup85(f.l.)-seh1(f.l.) = SB142; nup120(aa1-757) = NL88; yeast sec13(f.l.) = JW2 and

the human SEC13(f.1.) = SB15 but additionally different protein fragments are included in the constructs like nup145C(aa643-1317)-nup120-sec13 = NL123 and nup133(aa521-1157)-nup84 = AU102. As described above the purification occurred on nickel beads and resulted in protein concentrations ranging from 2.1 – 29 mg/ml. The controlling SDS-PAGE gels look clean with single bands with the expected size.

3.3.1.2 Protein-protein interactions of the Y-complex to be assayed with MST

As described above the yeast Y-complex PPIs should be validated including the seven intra-complex connections: nup84/nup133, nup84/nup145C, nup145C/nup120, nup145C/nup85, nup145C/sec13, nup85/nup120 and nup85/seh1. In addition following six inter-complex PPIs were assayed in the MST system: nup133/nup85, nup120/nup120, nup84/nup120, yeast sec13/sec13, yeast seh1/sec13, human SEC13/SEC13 and human SEH1/SEC13. Notably, the SEC13 homo-dimerization and the SEH1/SEC13 PPI were found in our human Y2H data set (see Fig 3.11). Additionally to the yeast inter-complex connections these two human PPIs are suggested to be inter-molecular Y-complex PPIs.

Considering the available co-expressed and co-purified protein constructs it was possible to test the ‘hub’ interactions, namely nup85/nup145C, nup84/nup145C and nup85/nup120 (Fig 3.16.). Some of the NPC proteins do not stably express alone hence three of the intra-complex connections could not be tested: nup133/nup84, nup85/seh1 and nup145C/sec13. They are included in the same constructs, namely constructs AU102 (nup84-nup133), SB142/SB142EPEA (nup85-seh1), SB215EPEA (nup145C-sec13) and NL123 (nup84-nup145C-sec13).

		constructs labeled	proteins labeled	not labeled
	'hub' interactions	labeled	labeled	not labeled
Intra-complex connections	nup120/nup120	NL123	nup145C/sec13/nup120	nup85/seh1
		SB142	nup85/seh1	nup145C/sec13/nup120
		NL123	nup145C/sec13/nup120	nup85/seh1
		SB142EPEA	nup85/seh1	nup145C/sec13/nup120
	nup85/nup133	NL88	nup120 (aa 1-757)	nup120 (aa 1-757)
		NL88	nup120 (aa 1-757)	nup120 (aa 1-757)
		NL88EPEA	nup120 (aa 1-757)	nup120 (aa 1-757)
		NL88EPEA	nup120 (aa 1-757)	nup120 (aa 1-757)
Inter-complex connections	nup120/nup84	AU102	SB142	nup133 (aa571-1157)/nup84
		AU102	SB142EPEA	nup133 (aa571-1157)/nup84
		SB142	AU102	nup85/seh1
		SB142EPEA	AU102	nup133 (aa571-1157)/nup84
	ysec13/ysec13	AU102	NL88	nup133(aa571-1157) / nup84
		AU102	NL88EPEA	nup133(aa571-1157) / nup84
		NL88	AU102	nup120 (aa 1-757)
		NL88EPEA	AU102	nup120 (aa 1-757)
	ysec13/yseh1	JW2EPEA	JW2EPEA	sec13
		JW2EPEA	JW2	sec13
		JW2	JW2EPEA	sec13
		JW2	JW2	sec13
	hSEC13/hSEC13	SB142	JW2	Seh1
		SB142EPEA	JW2	Seh1
		JW2	SB142	sec13
		JW2EPEA	SB142EPEA	sec13

Fig 3.16 Overview of constructs tested with micro scale Thermophoresis. The PPIs are divided in intra- and intermolecular PPIs. Given are all 30 construct combinations of 10 different constructs tested with MST. The protein

constructs includes more than one protein. Some proteins are only stable while co-purification. Therefore the non interacting construct is grey whereas the interacting protein is written in black. The ‘hub’ interactions include two possibilities: nup145C/nup85 and nup120/nup85. In addition the PPI sec13/seh1 could lead to a positive MST read-out. However this is not distinguishable.

All intermolecular Y-complex connections could be tested in various combinations, namely: nup120/nup120, nup85/nup133, nup120/nup84, ysec13/ysec13, yseh1/ysec13 and hSEC13/hSEC13 represented by the constructs: NL88, NL88EPEA, SB142, SB142EPEA, AU102, JW2, JW2EPEA, SB15 and SB15EPEA (Fig 3.16). In summary 10 construct in at all 30 combinations were tested to get information about two intra- and six inter- Y –complex connections (Fig 3.16).

3.3.1.3 MST enables the detection of intra molecular Y-complex PPIs

First of all a method must give a positive read-out, here resulting in binding curves. Therefore the intra-molecular ‘hub’ PPIs of the Y-complex were chosen that are well known : nup145C/nup85 and nup120/nup85 represented by the constructs NL123, SB142/SB142EPEA. To address this one construct of each construct pair has to be labeled. All construct pairs can be tested in two configurations. All labeled constructs are marked with a star. The labeling occurs following a standard labeling procedure of a kit provided by Nanotemper. The fluorophor NHS 647 was covalently attached to free lysines on the protein surface. To address this, a buffer exchange was performed followed by the labeling reaction. In a last step free fluorophor molecules were removed and the labeling controlled on SDS-gels with a fluorescence reader (Fig 3.17). After confirmation of correct labeling and determination of the concentration of the labeled protein it could be used for measurements. To address the measurements, the non-labeled proteins were serially diluted (16 times) and the labeled protein was added to each dilution. The mixture was filled into 16 capillaries and the measurements were performed with the MST Monolith NT112 (Nanotemper, Munich).

Five constructs in five combinations were examined to test if MST is applicable (Fig. 3.17). Exemplarily two binding curves and the determination of one K_D are shown in detail in Fig. 3.17. As mentioned above MST measurements in each capillary occur in an equilibrium state of the fractions of bound and unbound proteins. Because of increasing concentrations of the titrated protein construct in each capillary there are different concentrations of bound and unbound proteins and therefore different changes in movement of the single and assembled protein molecules that result in changes in fluorescence by applying an inferred laser. In general the concentration of labeled protein constructs ranges between 20 – 100nM. It must be ensured that the initial concentration is below the K_D . The concentration of the titrated protein constructs ranges from ~ 15 - 1 mg/ml in the highest concentrated dilution step. The read-out of the MST is given by the change of fluorescence (in fluorescence units) in relation to the concentration of the unlabeled protein (titrated protein) where each data point represents one capillary.

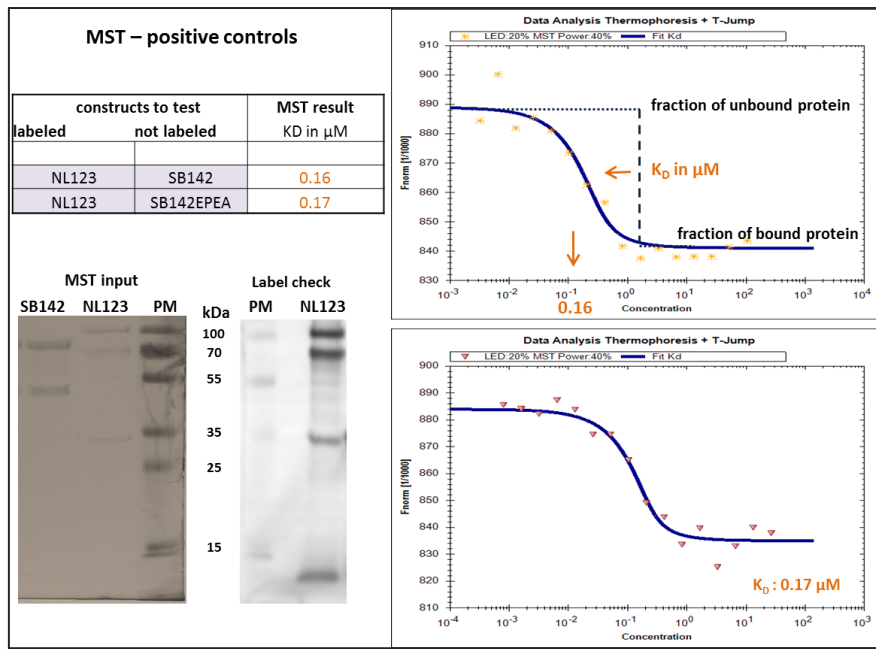


Fig 3.17 The MST measurement workflow for the positive controls with read-out. Shown are the binding curves of well characterized intra-complex interactions of the Y-complex to determine the applicability of MST. To test for protein input and correct fluorescence labeling the input was loaded on a gel. Two are exemplarily shown. The MST binding curves were obtained with the NT analysis software provided by Nanotemper. The ‘hub’ PPIs: nup145C-nup85 and nup145C-nup84 resulted in $K_{D\text{S}}$ of 0.16-0.17 μM (orange). PM = protein marker

If an interaction takes place a clear distinction between bound and unbound protein fraction was seen as a curve. To determine the K_D the half saturation was taken (Fig 3.17). The fitting of the binding curve and the K_D -calculation were done using the Nanotemper software. In this example the K_D of the ‘hub’-interaction is 0.16 μM .

The obtained binding curves of the positive controls differ in direction. However if a binding curve was detected, saturation was achieved and a K_D could be determined we considered this as a positive read-out. All previously charctarized Y-complex interactions resulted in a binding curve. Five construct pairs (NL123*/SB142, NL123*/SEB142EPEA, SB142*/NL123 and SB142EPEA) were tested yielding in five binding curves resulting in the ‘hub’ interactions: nup145C/nup85 and nup120/nup85 with a $K_D = 0.16 - 0.17 \mu\text{M}$. Both PPIs are well described in literature and confirmed that the MST is able to detect PPIs of the NPC Y-complex.

All constructs must be negatively controlled to avoid false positives. To address this different constructs combinations were tested including a protein construct that might not interact, e.g. NL88EPEA with SB2142EPEA (nup120 (aa 1-757)/nup85-seh1) or AU102 with JWEPEA (nup133-nup84/sec13).

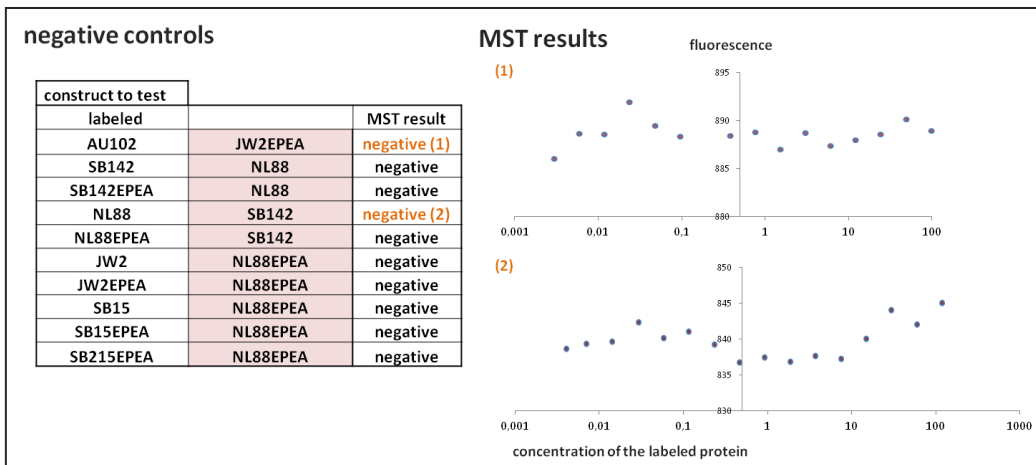


Fig 3.18 Shown is the overview of the negative controls and the according MST results. Shown are exemplarily two MST results of negative controls. By testing all the listed construct pairs no binding curve could be observed and therefore no K_D was obtained.

We tested all ten constructs that should yield in inter Y-complex PPIs with constructs which are not likely to interact. Exemplarily shown is AU102*/JWD2 that represents the interaction nup84-nup133/sec13. Neither nup84 nor nup133 is suggested to interact with sec13. Another example is the construct pair NL88*/SB142 that represents the interaction nup120(aa 1-757)/nup85-seh1. Also here neither nup85 nor seh1 should interact with nup120 (aa 1-757). The MST measurements revealed for these two construct pairs only minor changes in fluorescence that did not yield in fractions of bound and unbound protein constructs. No K_{DS} could be obtained and no interaction was observed. Therefore we can conclude with this protein set MST is able to distinguish between interaction and non-interaction.

3.3.1.4 Detection of inter molecular Y-complex PPIs with MST

It was shown that MST is able to detect PPIs and did not yield in false positives at least for the ten construct pairs we tested. A systematic screen was performed that should give information about the six Y-complex PPIs that are suggested to be inter-molecular, namely nup120/nup120, nup133/nup85, nup120/nup84, ysec13/ysec13, ysec13/yseh1 and hSEC13/hSEC13 (Fig 3.19). The construct pairs including the labeled constructs SB142, SB142EPEA and NL88 were tested three times, the labeled construct NL88 was tested twice and the labeled construct AU102 was tested four times in independent experiments. Some interactions could be easily recapitulated, e.g. SB142*/AU102 and *vice versa* AU102*/SB142 whereas others could only be positively tested once, e.g. SB142EPEA*/AU102. Parameters have to be determined to distinguish between interaction and non-interaction. These parameters are: *first*, the fluorescence signal differs in at least five units between the unbound and bound protein fraction; *second*, the fluorescence signal has to be in a certain detection range (400 – 1000 fluorescence units); *third*, a clear saturation must be observed (flatten of the curve)

and *fourth*, at least 11 of the 16 data points must be included in the analysis. To recapitulate the results all labeled protein constructs in a positively tested construct pair were labeled again and measured under the same conditions as in the first experiment. This could be due to the ratio of active labeled protein in the sample. Even if the concentration seems high enough, only a small fraction of the labeled protein could be active and therefore is capable to build interactions. Increasing the concentration of active protein is not always possible. Seven protein constructs were covalently labeled at least two times to create replica and provide independent experiments. In total 71 measurements were performed, with 38 experiments assaying the three Y2H positive PPIs: nup120/nup120 (13 measurements), nup84/nup133 (14 measurements) and nup84/nup120 (11 measurements). All included protein constructs were labeled (NL88, NL88EPEA, SB142, SB142EPEA and AU102) and tested resulting in four combinations for each interaction. All four combinations were tested three times in independent measurements. The different protein construct combinations of the PPIs nup120/nup120 and nup84/nup120 resulted in at least three binding curves with K_{D_s} of 0.9 – 4 μM and 1.4 - 2.3 μM . In contrast three protein construct combinations of the PPI nup133/nup85 revealed seven binding curves with K_{D_s} of 1.0 – 4.0 μM . Overall the K_{D_s} and thus the binding affinities of all three PPIs seem to be in a similar range, namely in the low μM -range. K_{D_s} can range from fM for enzyme/inhibitor interactions to μM for transient interactions between large proteins (Kastritis et al., 2011). The NPC as large distinct protein complex provide multivalent binding opportunities for the nups. Multivalent binding indicates that multiple proteins interact with each other simultaneously and therefore produce a greater biological effect, in the context of the NPC to generate a stable but somehow flexible scaffold (Sulcik et al., 2009). Often multivalent binding results in a remarkable increase of affinity and create additional specificity. However the binding remains much more dynamic and susceptible to competition than the corresponding tight monovalent interaction (Ruthenburg et al., 2007). Therefore the affinities of the weak interactions measured with MST could be enhanced within the NPC structure while the according nups are binding to several other nups simultaneously. However there remains the question of why not all measurements result in a positive read out. Using different protein preparation the MST readouts were variable and the exact reasons for that cannot be defined. But regarding the fact that three experiments per protein construct combination were performed and result in only one binding curve underlines the possibility that the affinity of the PPIs are in the sensitivity range of MST. The success of the MST measurements strongly depends on experimental conditions like buffers, protein concentrations and temperature but also on conditions regarding the purified proteins. For instance the proteins could aggregate and therefore inhibit interaction forming. Additionally the active fraction of a protein is of high importance. Thus the concentration of a protein construct can be high in solution but the active fraction is quite low and therefore too low to form an interaction. This is very difficult to experimentally ascertain, yet could explain why not all MST experiments result in positive read-out.

constructs		proteins			KD (μM)
labeled	not labeled	labeled	not labeled		
NL88	NL88EPEA	nup120	nup120	2.9	
NL88	NL88	nup120	nup120	4.2	
NL88EPEA	NL88EPEA	nup120	nup120	3.27	
NL88EPEA	NL88	nup120	nup120	3.88 (1)	
AU102	SB142	nup133	nup85	3.0	
AU102	SB142EPEA	nup133	nup85	-	
SB142	AU102	nup85	nup133	2.94	
SB142EPEA	AU102	nup85	nup133	2 (2)	
AU102	NL88	nup84	nup120	1.3	
AU102	NL88EPEA	nup84	nup120	-	
NL88	AU102	nup120	nup84	1.6	
NL88EPEA	AU102	nup120	nup84	1.4 (3)	
JW2EPEA	JW2EPEA	sec13	sec13	-	
JW2EPEA	JW2	sec13	sec13	-	
JW2	JW2EPEA	sec13	sec13	-	
JW2	JW2	sec13	sec13	-	
SB15EPEA	SB15EPEA	hSEC13	hSEC13	-	
SB15	SB15	hSEC13	hSEC13	-	
SB15EPEA	SB15	hSEC13	hSEC13	-	
SB15	SB15EPEA	hSEC13	hSEC13	-	

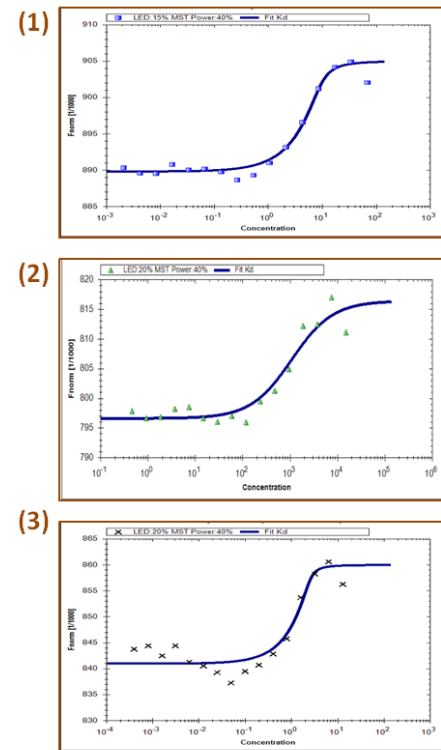
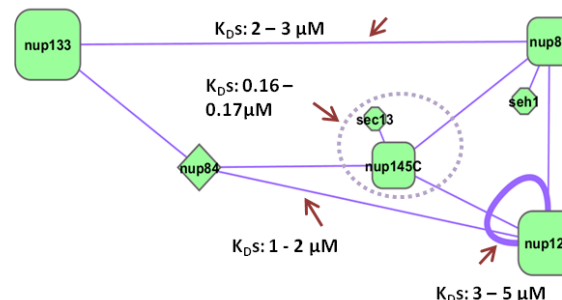


Fig 3.19 MST results for the inter-complex PPIs of the Y-complex. Shown is the list of tested construct pairs of the six inter-Y-complex PPIs nup120/nup120, nup133/nup85, nup120/nup84, ysec13/ysec13, ysec13/yseh1 and hSEC13/hSEC13 and the detected K_D . For each PPI one binding curve is exemplarily shown (number in the brackets indicate the MST curve on the right). Down right: interaction map of the Y-complex: seven PPIs are already declared as intra-Y-complex connections whereas three PPIs are detected with our Y2H screen and were validated with MST; the resulting binding affinities range from 1-4 μM .



Through optimization of the experiments conditions and enhancing the number of experiments these weak PPIs can be measured with MST. In addition all negative controls did not result binding curves. In summary MST, is capable of distinguishing between interactions and none interactions and therefore to be applicable as detection method for PPIs. Using MST we were able to validate the three interactions nup120(aa 1-757)/nup120(aa 1-757), nup85/nup133 and nup84/nup120(1-757) which could potentially describe connections between two or more Y-complexes.

3.3.2 Protein Complementation Assay (PCA) enables the validation of PPIs of the human NPC

After the validation of some yeast Y2H PPIs the focus was set on the validation of human Y2H PPIs. Protein fragment complementation assays (PCAs) are eligible in detecting transient and dynamic protein interactions in intact living cells with sub cellular resolution (Remy, et al., 2004). The PCA is

based on the assisted folding of two fragments of the yellow fluorescent protein (YFP) variant Venus (Nagai, et al., 2002; Michnick et al., 2007). For that purpose, non-fluorescent F1 and F2 fragments of Venus are fused to the coding sequence of two proteins of interest and expressed in mammalian cells, e.g. U2OS cells. In case of a protein-protein interaction, the fragments are in such close proximity leading to folding and reconstitution of YFP *in vivo* (Fig 3.21). Reasoned by inability of self-folding of both YFP domains, no fluorescence is measured without a protein-protein interaction (Magliery et al., 2005). Even sole co-localization does not lead to PCA based fluorescence (Lalonde et al., 2008). In contrast, co-localization studies performed with antibodies bound to proteins showed fluorescence within a co-localization volume even if there is no physical interaction (Vogel et al., 2006). Unspecific reconstitution of the two Venus fragments can occur reasoned by high local protein concentrations during several cellular processes, e.g. protein degradation or endoplasmatic reticulum- dependent folding. Therefore it is necessary to observe the fluorescence signal carefully. Ultimately a positive PPI was considered when fluorescence was observed at the nuclear rim. To address this, confocal microscopy was used. The confocal (*conjugated focus*) microscopy has a second focus point, the pinhole that rejects efficiently fluorescent light that is out of focus. The practical effect is that the image comes from a thin section of the sample (the nuclear rim in our case).

3.3.2.1 Human protein-protein interactions to be assayed with PCA

We recapitulated all PPIs of the human NPC scaffold. Thus the PPIs comprising miscellaneous nups were left aside from the PCA screen. The validation of the Y2H data with PCA comprises ten human PPIs of two major scaffold subcomplexes, namely the NUP62-complex and the Y-complex (Fig 3.20). The Y2H screen revealed four interactions with SEC13, a conserved β-propeller located at the ‘hub’ of the Y-complex. SEC13 showed interaction with other conserved β-propeller proteins SEH1, NUP37 and SEC13 itself. In addition SEC13 showed interactions to NUP62 (nsp1 in invertebrates). Further the connection to the membrane via POM121 was tested.

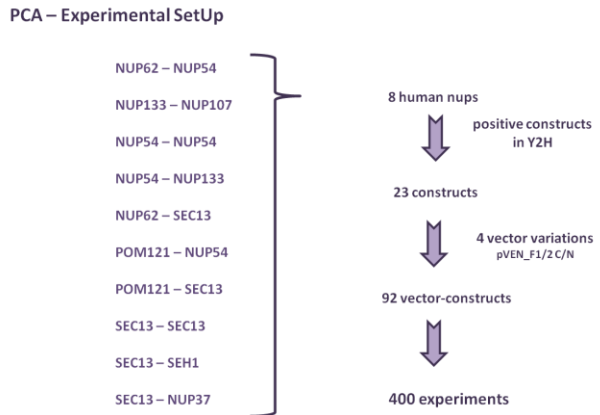


Fig 3.20 Overview of human proteins included in the PCA analysis and the workflow of the PCA set up. Shown is the workflow of the PCA set up. At all eight human nups resulting in 10 Y2H PPIs were tested. Only the positively tested human construct were used and transferred into the four PCA vectors resulting in 92 vector constructs that were tested in over 400 combinations.

PCA is accomplished with the gateway system. The vectors (pVEN-F2N-DM, pVEN-F1N-DM, pVEN-F2C-DM, and pVEN-F1C-DM) and their extensive analysis were done by Josephine Worseck and described in her thesis (Worseck, 2012). All 23 cDNAs were transferred from the gateway entry vector into the Venus gateway destination vectors that resulted in tagging the proteins on their N- or C-terminus with the YFP fragments F1 and F2. It should be noted that ORFs without stop codon can be transferred into all four vectors whereas ORFs with stop codon can only be introduced into N-terminal Venus fragment fusions. After subcloning of all cDNAs in the suitable destination vectors, the plasmid DNA was used to co-transfect U2OS cells. U2OS cells are characterized by a relatively large nucleus which is advantageous when observing staining of the nuclear envelope. After 12-24h of transfection the transfection medium was removed, new medium was added and cells grew additionally for 24h to ensure the breakdown and reformation of the nuclear envelope with simultaneously assembly of the NPC and incorporation of the YFP-tagged proteins. The cells were fixed and stained with DAPI (4', 6-Diamidin-2-phenylindol) to visualize the nucleus. The samples were analyzed with the confocal laser scanning microscope LSM700 (Zeiss). Several different fluorescent signals could be observed in U2OS cells (Fig 3.21). For instance, fluorescence could be equally distributed through the nucleus, the cytoplasm or both. It could appear as puncta in either the nucleus or the cytoplasm or in both. However, only if the localization of the fluorescence was observed at the nuclear envelope (as rim staining) a positive PPI was considered. Most of the construct combinations did not result in any fluorescence. In average one of eight vector combinations resulted in detectable fluorescence.

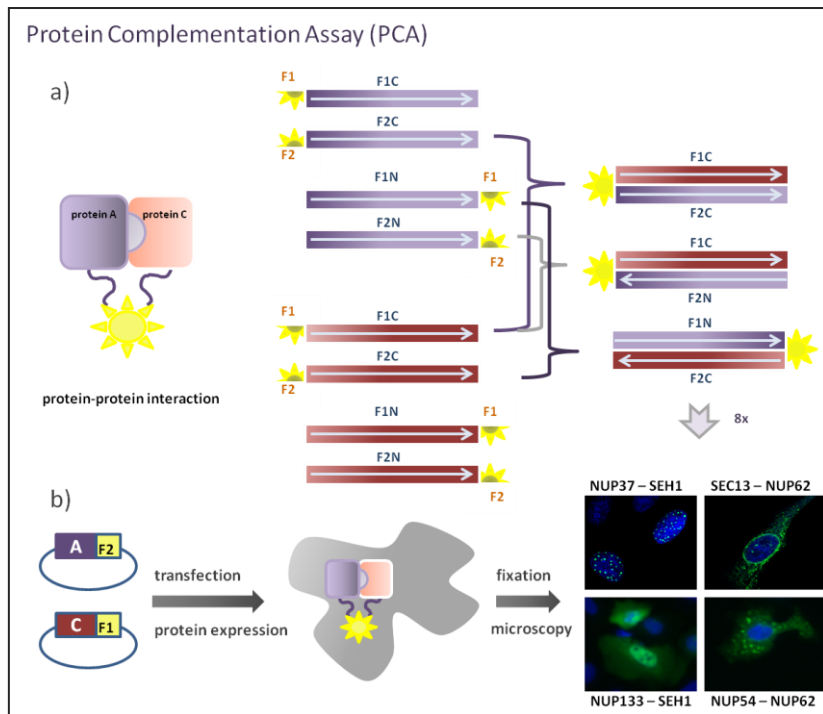


Fig 3.21 Shown is the principle of the PCA strategy to detect interactions *in vivo*. a) Non-fluorescent N-terminal (1-158 aa; F1) and C-terminal (159-239 aa; F2) Venus fragments are fused to the coding sequence of two proteins (indicated purple and red). If the coding sequence contains no stop codon four fusion proteins can be created. In order to determine a protein interaction Venus F1 and Venus F2 fusion proteins were combined up to eight combinations. b) Venus F1 and Venus F2 fusion proteins were transiently co-expressed in U2OS cells. In case of an interaction of the fusion proteins A and C, the fragments come into close proximity and YFP is reconstituted resulting in fluorescence that can be observed with confocal microscopy.

Due to the high sensitivity the assay had to be negatively controlled carefully. All positives were controlled using the respective constructs in other pairings. For each positive construct combination at least one other pairing resulted in no fluorescence showing the specificity of each positive tested construct (Fig 3.21). Ten PPIs were investigated with at all 23 constructs in 400 tested combinations (Fig 3.21). As a positive control we were able to visualize the intra-Y-complex PPI NUP107/NUP133 that was reported several times even as crystallized PPI (Belgareh et al., 2001; Boehmer et al., 2008; Whittle and Schwartz, 2009). The PPIs of SEC13 with SEH1, NUP62 and SEC13 itself could be visualized as co-localization at the nuclear rim. In 2012 the group around Fernandez-Martinez investigated the Y-complex and solved its structure to a precision of 1.5 nm. The most significant increase in precision was related to SEC13 and SEH1. They suggested a localization closer to each other that enables a direct interaction. Therefore this PPI could also describe an intra-Y-complex connection. Unpublished data of the Schwartz lab however demonstrate that SEC13 and SEH1 are distant pointing towards an inter-Ycomplex interaction. The SEC13/SEC13 interaction could take place in other subcellular structures. SEC13 is also part of the vesicle coats COPII where it interacts with SEC31 (Brohawn et al., 2009).

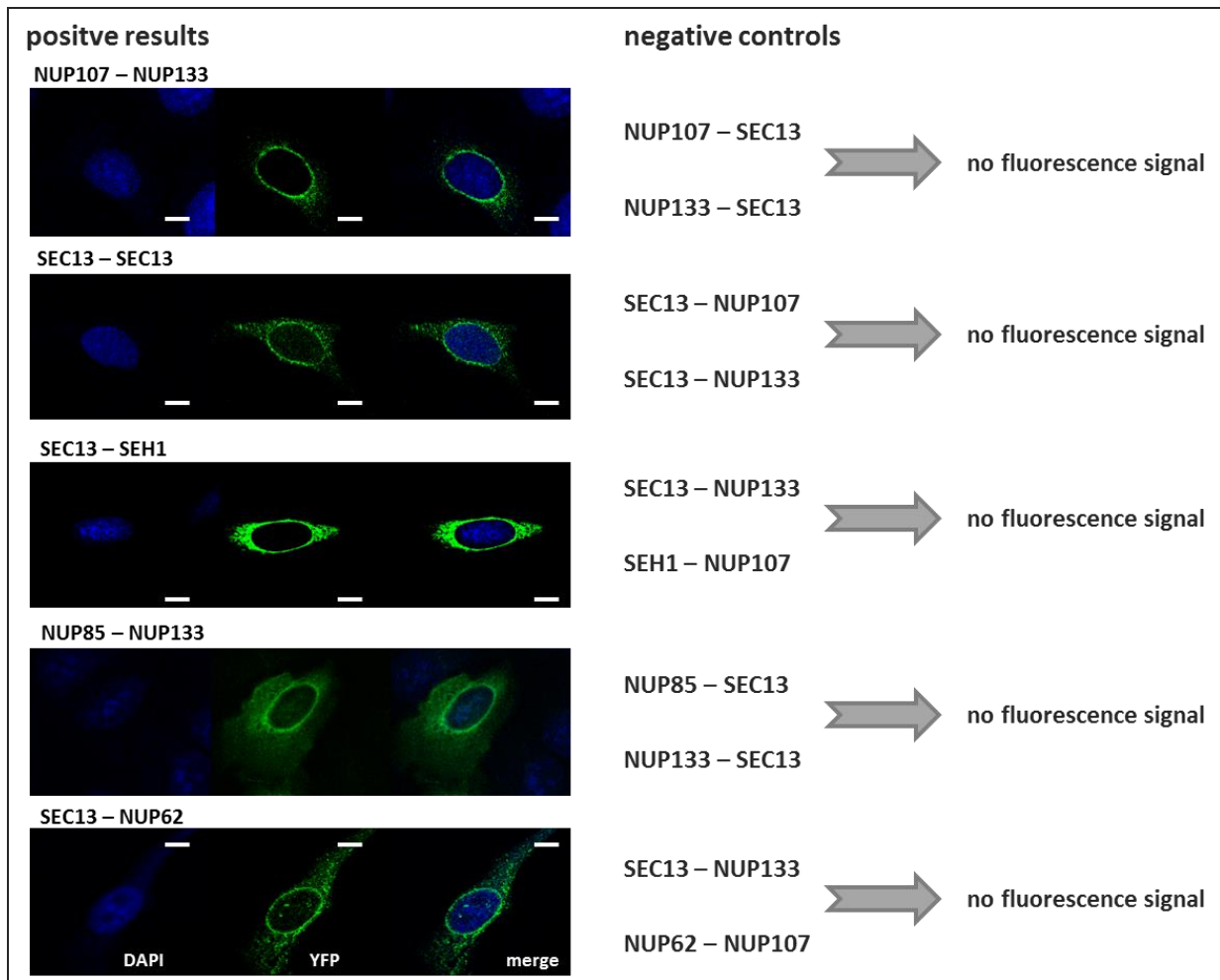


Fig 3.22 Overview of the positive tested PPIs of the PCA. For each positively tested PPI is exemplarily a photo shown. The measurements were done with a confocal LSM700 microscope from Zeiss, the scale bar is 4 μM ; a positively tested PPI is considered by staining of the nuclear envelope (rim staining). On the right: examples of negative controls are shown: every positively tested construct was tested with a construct that is assumed to not interact.

However the SEC13/SEC13 interaction was predominantly observed in the nuclear rim indicating that the homo-dimerization is stabilized within the NPC and therefore contributes to inter-Y-complex contacts. PPIs with SEC13 even with other NPC components could suggest a specific NPC architecture. Another inter-Y-complex PPI which validation could be used to emerge insight into NPC architecture is nup85/nup133 that was detected in our yeast Y2H screen and in the biophysical method PCA with yeast purified proteins. Assuming that the NPC is structurally conserved and therefore this PPI may be relevant in the human NPC we include this PPI in our PCA approach. Indeed we observed a nuclear rim staining in intact human cells and therefore could validate an interaction including nups of opposite sites of the structural given subcomplex providing a substantial constraint towards the arrangement of the Y-complexes with respect to each other. Taken together the PCA experiments revealed rim staining for five, namely NUP107/NUP133, SEC13/SEC13, SEH1/SEC13, NUP85/NUP133 and SEC13/NUP62 (Fig 3.22).

Besides staining of the rim three construct pairs resulted in staining of cytoplasm (SEC13/NUP62), nucleus (SEC13/SEC13) or both (NUP85/NUP133). The constructs of the PPIs NUP107/NUP133 and

SEC13/SEH1 showed only rim staining. Regarding SEC13/SEH1 it seems that aggregated protein is enriched in the endoplasmatic reticulum around the nucleus. However, a clear rim staining was observed as well. No rim staining was detectable for following Y2H PPIs: NUP54/NUP54, NUP54/NUP62, NUP37/SEH1, NUP133/NUP54 and NUP62/POM121. The promiscuity of isolated coil-coiled domains of NUP54 might be problematic in order to obtain stable NUP54 binding (Ulrich et al., 2014). The PPIs containing constructs of NUP54 and NUP62 resulted in puncta staining occurring in the cytoplasm (Fig 3.22). Also for the PPI NUP37/SEC13 fluorescence was observed not as rim staining but as puncta in the nucleus. The same fluorescence pattern was observed for the PPI between POM121 with SEC13 whereas the puncta also occur in the cytoplasm leading to the suggestion of subcomplex formation but no incorporation into the NPC

Taken together we were able to confirm five of the 10 initially tested human PPIs of the Y2H approach resulting in a success rate of approximately 50 %.

Taken together all validation steps revealed the high quality of the Y2H data and allowed a detailed view to single PPIs. With the Y2H data a detailed view into the subcomplexes connections as well as the connections between the subcomplexes was possible. Further we could interpret the novel inter-Y-complex connections and fit these data into previously published models.

3.4 Investigation of PPIs of the macromolecular protein complex BBSome

3.4.1 Defining the BBSome clone set

The BBSome was only recently discovered and it is suggested that most of the BBS proteins are present in a stable complex containing seven members BBS1, BBS2, BBS4, BBS5, BBS7, BBS9 and TTC8 (Nachury et al., 2007). A suggested protein composition was already reported as well as the assembly steps (Nachury et al., 2007; Jin et al., 2010; Zhang et al., 2012). To address an investigation of the protein-protein interactions within the BBSome a Y2H screen was performed. We received human full length proteins for six of the seven BBSome components from the lab of Thomas Schwartz: BBS1, BBS2, BBS4, BBS7, BBS9 and TTC8 (BBS8). Thus one BBSome component is missing in our clone set, namely BBS5. Beside human full length protein constructs protein fragments were included created according to the domain structure. The structural anatomy of the BBSome was explored by using sensitive structure-prediction algorithms (Jin et al., 2010). Thus we obtained 27 fragments for all six BBSome components which were prepared by Kevin Knockenhauer of the Schwartz lab (Fig 3.23). Considering the analysis of Jin et al. 2010 it became clear that BBS9, BBS2,

and BBS7 have a shared domain architecture. Specifically, all three proteins appear to have an N-terminal β -propeller (WD40) domain, followed by a β -sandwich fold (GAE domain), an α/β platform domain, a predicted coiled coil and a N-terminal alpha helical domain. To ensure that the complete β -propeller folding is included in the construct, two constructs of BBS2 and BBS7 were designed including the predicted β -propeller plus one additional strand as well as subsequent strands in the protein (BBS2(1-397), BBS2(1-538), BBS7(1-327) and BBS7(1-504)). BBS1 also contains a predicted N-terminal β -sheet, but it has a shorter C-terminal domain (predicted to be a beta-sandwich fold) compared to BBS9, BBS2, and BBS7. It was cut according to this organization resulting in three different constructs. BBS8 and BBS4 are homologous to one another and are predicted to be super alpha-helical stacks (TPR repeat proteins). Both proteins were cut in half expecting to localize interactions either to the N or the C-terminal half of the protein.

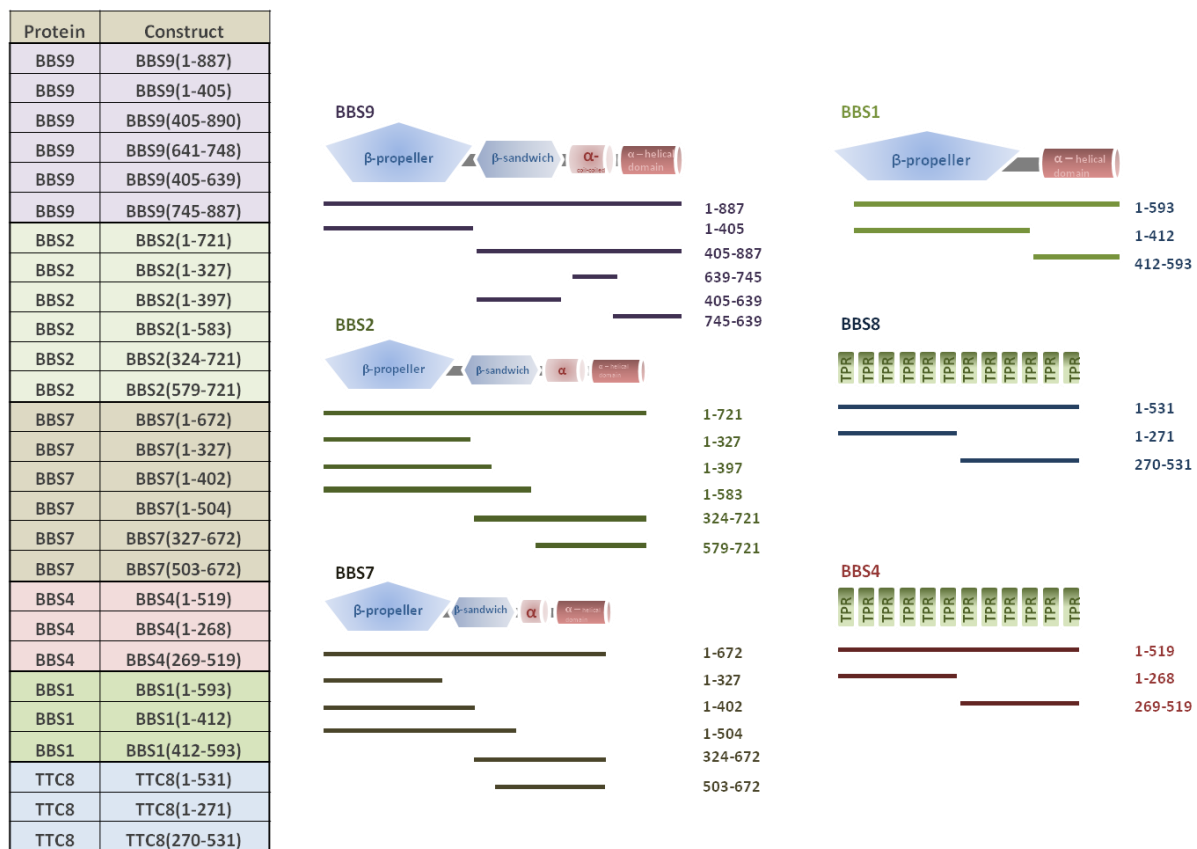


Fig 3.23 Overview of BBSSome components and BBSSome fragments included in the Y2H screen. The screen included six BBS proteins in all 27 constructs. The protein domain composition is simple and comprises only three different types: β -propeller, α -helical domains and TPR domains.

Thus all structurally ordered parts that are suggested to build the PPIs of the BBSSome were investigated. The inclusion of fragments should increase the success rate of the screen and further substantially decrease the false negative rate and gives rise to high resolution information with regards to interacting protein fragments. Taken together the screen included six human BBSSome proteins in 27 fragments (Fig 3.23).

3.4.2 The BBSome Y2H screen – set up

The human BBSome Y2H screen was performed like the NPC screen: a well-controlled, stringent automated yeast two-hybrid setup was used generating systematic PPI data with high precision. All BBSome cDNAs were subcloned into both bait vectors (pBTM116-DM and pBTMCC24-DM) that differ in arrangement of the DNA-binding domain with respect to the bait ORF (pBTM116-DM: N-terminal of the ORF; pBTMCC24-DM: C-terminal of the ORF). In total the subcloning gave 81 constructs (54 bait constructs and 27 prey constructs) which could be tested. A MAT *alpha* strain was transformed with the prey constructs and a MAT *a* strain with the two bait vectors. Due to the small clone set an auto-activation test was not performed. All probable auto-actives were removed after the screen. Autoactive baits are detectable when all colonies on an agar plate are grown. An autoactive prey construct can be identified when every construct pair that included this prey resulted in a grown colony. In the high quality interaction screening protocol each bait construct was tested twice (108 baits) against a 96-prey matrix including biological triplicates (81 preys). The screen of PPIs was performed in all possible combinations. At all the number of possible colonies achieved 8748. After mating of 108 liquid baits with 81 prey colonies (prey matrix) the possible yeast colonies were spotted on SD4 medium (see methods) to detect interactions via growing colonies resulting in 239 grown spots (Fig 3.24.).

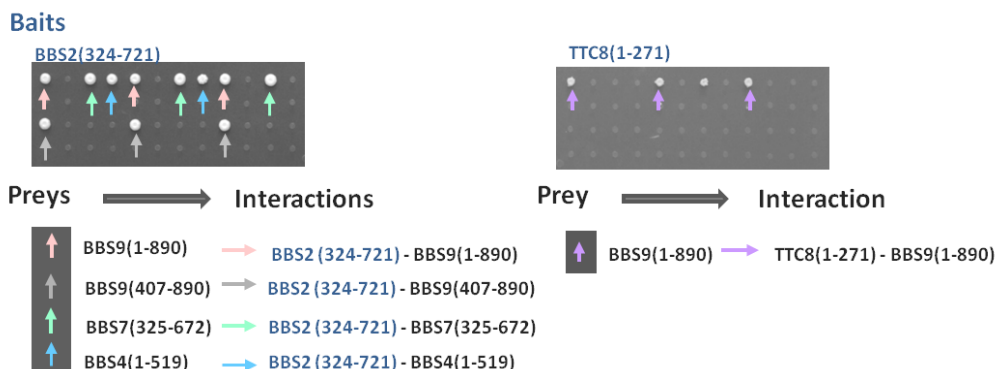


Fig 3.24 Identification of the Y2H interactions of the BBSome components. Shown are two selective 96-well Y2H agar plates of two baits: BBS2 (aa 324-721) and TTC8 (aa 1-271). The baits were mated with a 96-well prey matrix containing 27 preys in three replicas giving 72 prey constructs. Colonies growing on -HAULT indicate a protein-protein interaction which are indicated by the colored arrows.

All plates were analyzed with Visual Grid and judged visually as well. The grown spots were assigned to the constructs over the position in the matrix. To reduce the false positive rate and stringent the Y2H system systematically only two or more grown colonies of each prey construct were integrated into analysis resulting in 58 colonies. To get a PPI data set the colony information for all prey and bait constructs and further for all proteins were summarized. Thus the final data set contained 37 interactions between 16 BBSome constructs (Fig 3.24).

3.4.3 Generation of the PPI network of the BBSome

The Y2H screen resulted in 37 interactions between 16 constructs and in six PPIs between all six BBSome components. As in the NPC Y2H screen all constructs were tested in both configurations against each other, namely as bait construct as well as prey construct. Therefore it is possible to distinguish between one directed and both directed PPIs whereas a both directed PPI occurs between the bait and prey constructs of the same protein construct. The screen resulted in 24 one directed PPIs. In contrast to the NPC screen the BBSome Y2H screen resulted in a much higher amount of both directed PPIs, namely 13. This supports the suggestion of the stable complex (Nachury et al., 2007). The interactions could be combined with regards to their configuration revealing a PPI network of 22 interactions between 13 constructs (Fig 3.25). All fragments belonging to one BBS protein are indicated with the same node color whereas the numbers in the brackets indicate the amino acid residues. All BBS proteins revealed PPIs with at least one fragment. Moreover, except BBS1 two fragments of each BBS component gave PPI information, up to four fragments (dark blue nodes – BBS9).

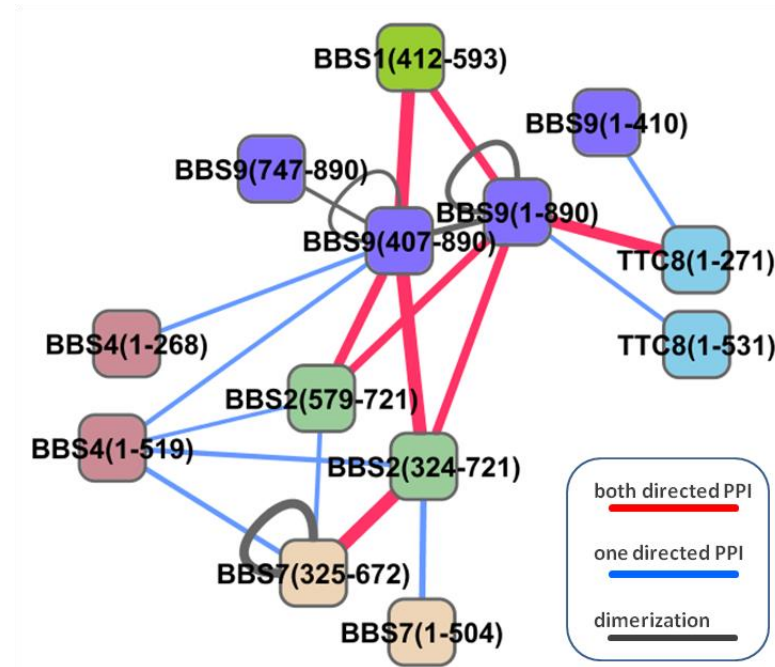


Fig 3.25 The BBSome interaction map. The interaction network comprises 22 interactions between 13 constructs. The nodes are colored according to the protein they belong to: green = BBS1, dark blue = BBS9, light blue = TTC8 (BBS8), brown = BBS4, dark green = BBS2, beige = BBS7. The links are colored by their character: red: both directed, blue: one directed, dark grey: homo dimerization; the thickness of the links indicate their internal count.

To differentiate the PPI configurations labeled links were used. One directed PPIs are highlighted in blue whereas both directed PPIs are highlighted in red. The screen resulted also in three homo dimerizations (BBS7(325-672), BBS9(407-890) and BBS9 full length) and dimerizations between two BBS9 constructs and the full length construct of BBS9. These are highlighted in grey. The BBSome components seem to be highly interconnected (Fig 3.25). More than one PPI connects each

BBSome protein with other BBS components. A ‘core complex’ was previously suggested based on same structural characteristics of BBS2, BBS7 and BBS9 (Nachury et al., 2007) (Fig 3.23). In addition it was shown that BBS2, BBS7 and BBS9 form the first ternary intermediate during BBSome assembly (Zhang et al., 2012; Seo et al., 2012). The Y2H data support the suggestion of an ‘inner core’ complex comprising BBS2, BBS7 and BBS9. These three proteins are highly interconnected with interactions occurring in both directions. BBS9 and BBS7 (aa 325-672) showed homodimerizations, BBS9 with two constructs, BBS9 (aa 1-890) and BBS9 (aa 407-890). This suggests a stoichiometry of more BBS7 and BBS9 molecules per BBSome complex. No connection was previously reported between the BBS9 and BBS7 constructs (Zhang et al., 2012). That was reflected in our Y2H data where no interaction between BBS7 and BBS9 could be observed. BBS9 was proposed to be the central scaffold and it showed connections to BBS2, BBS1, BBS5 and BBS8 (TTC8) (Zhang et al., 2012). The Y2H screen revealed also that BBS9 is the most connected BBS component within the PPI network (connections to four other BBS components). Taken together the suggestion of a core complex of the BBSome comprising BBS2, BBS7 and BBS9 by Zhang et al. was confirmed by the Y2H results. BBS4 is connected to all three ‘core’ complex members. BBS4 is suggested to be among the last subunits that are incorporated into the BBSome (Zhang et al., 2012). It was also reported that BBS4 binds independent of BBS2 and BBS7 to non BBSome components underlining an adaptor function (Kim et al., 2004). The connection of BBS4 to all three BBSome ‘core’ components underlines the anchoring via BBS4 of non BBSome components to the stable BBSome complex (Kim et al., 2004). None of the BBS4 constructs showed both directed PPIs. The constructs of BBS1 and TTC8 seems to be attached to the inner core complex with only connections to BBS9. These interactions were already shown in 2012 by Zhang et al. It was reported that BBS1, BBS5 and BBS8 are incorporated into the BBSome after the ‘inner core’ was established. The screen resulted also in interactions between BBS1 and BBS8 and therefore previous PPIs could be confirmed (Nachury et al., 2007; Jin et al., 2010; Zhang et al., 2012; Seo et al., 2010). The screen also implies that BBS1 and TTC8 are only connected to one other protein (BBS9) whereas all other BBS components might have connection to at least three other BBSome proteins indicating an attachment to the BBSome via BBS9.

Taken together the PPI data revealed a highly dense suggesting an ‘inner core’ complex containing BBS2, BBS7 and BBS9. Attached to each of the ‘inner core’ proteins is BBS4. More peripheral are the BBSome components BBS1 and TTC8 which are only linked to BBS9.

3.4.4 Y2H data high resolution map of the BBSome components

Three full length constructs gave PPI information, namely BBS9, BBS4 and TTC8. The PPI information would be much sparser by only including full length constructs. Including fragments in

the screen increased the density of the overall interaction map. Additionally it was possible to obtain specific PPI data with regards to interacting domains. With the PPI data a high resolution map was created that allows a detailed insight into structural interaction domains.

fragment view of the Y2H data of the BBSome components

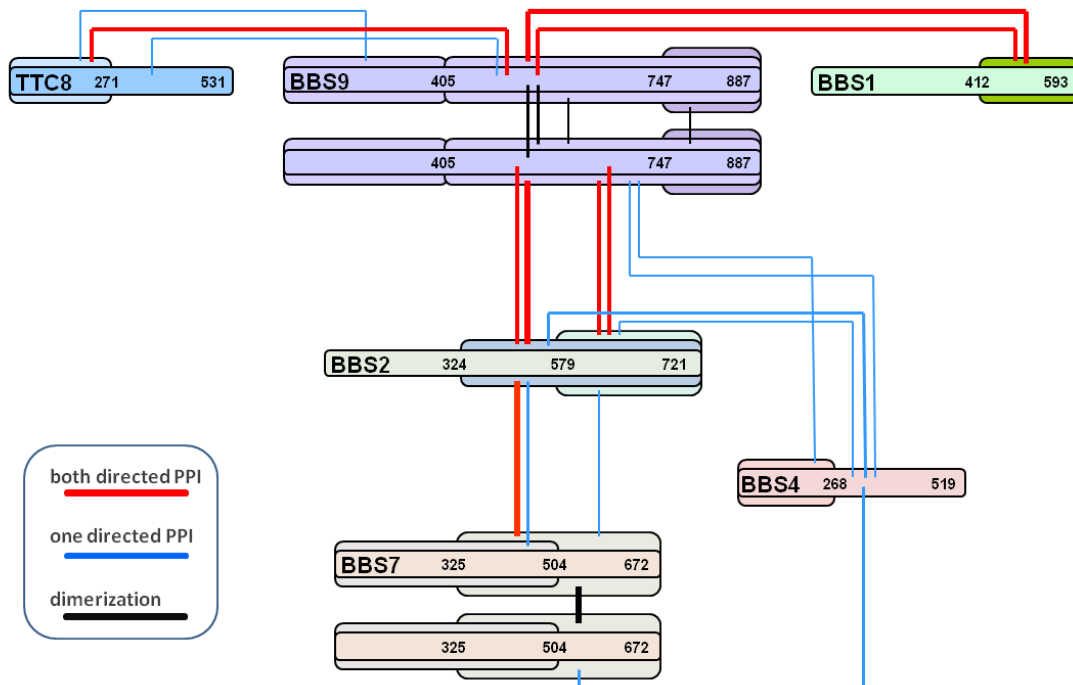


Fig 3.26 High resolution view of the PPIs between BBSome components. Shown are the interacting BBSome fragments. The dimerizations are indicated by two depicted BBSome components. The numbers indicate the amino acid residues of the fragments. The links are colored according to the PPI configuration: red: both directed, blue: one directed, black: dimerization. The thickness of the links indicates the intern count of the interactions. Based on the interacting fragments it can be assumed that the BBSome is mostly connected via the C-termini of the components.

To visualize information about the interacting fragments a high resolution interaction map was created only depicting the interacting BBSome fragments. The edges are colored according to the configuration of the interaction. Blue lines indicate one-directed and red lines denote both directed interactions. Each BBSome protein that is depicted by the same color contains the interacting fragments whereas the homo-dimerized BBS components are displayed with two sets of fragments in the map. The screen reveals homo dimerizations of the two ‘inner core’ BBS components BBS7 and BBS9. BBS9 showed two homo-dimerizations between the full length protein BBS9(aa 1-887) and the larger C-terminal part – BBS9(aa 405-887). Additionally two dimer-interactions of different fragments were uncovered. The full length construct interacted with the larger C-terminal part, BBS9(aa 1-887) – BBS9(aa 405-887) and further the larger C-terminal fragment BBS9(405-887) interacted with the C-terminal end fragment BBS9(aa 747-887). This suggests that the interaction domain is the C-terminus as it is the only part of the protein that is common to all homo dimers. Another interaction site could be possible but our data does not clarify whether or where it would be. BBS7 shows only one homo-dimerization between BBS7(aa 325-672) indicating an interlink of the C-terminal protein parts of two

BBS7 proteins. The Y2H homo dimerization data suggests the occurrence of two or more BBS7 and BBS9 proteins in one BBSome complex. BBS7 and BBS9 seem to be not directly connected within the BBSome as no PPI was discovered in the screen. Moreover the screen suggested that BBS2 is bridging BBS7 and BBS9 with at least three interacting constructs. The links of BBS2 with BBS7 and BBS9 occur on all three proteins via at least one C-terminal construct suggesting a C-terminal attachment. Considering the high interconnection of the three proteins BBS2, BBS7 and BBS9 the ‘inner core’ hypothesis is supported by a large number of both directed interactions between them. In all seven interactions connect the three proteins. BBS4 showed five interactions to all three ‘inner core’ members. Four of them were detected with the full length construct. Thus the exact protein part interacting with BBS7 remains unclear. In contrast BBS4 interacts with its full length construct as well as with its N-terminal fragment (aa 1-268) with BBS9 suggesting a N-terminal attachment. Moreover it is interacting with all three BBSome ‘core complex’ members and seems to be attached there C-terminally. The investigated BBS components BBS1 and TTC8 are only attached to BBS9. The screen revealed connections of the C-terminus of BBS1 (aa 412-593) with the full length construct and the large towards the C-terminus directed construct of BBS9. Both interactions are both directed. TTC8 is attached with three interactions to BBS9. Two of three PPIs were detected between the N-terminus of TTC8 (BBS8) with the full length construct and the N-terminus of BBS9: TTC8(aa 1-271) – BBS9(aa 1-405) suggesting an N-terminal attachment of both proteins.

Taken together the high resolution map shows the interactions between BBSome component fragments resulting in four main observations due to the architecture of the BBSome: *first*, BBS9, BBS7 and BBS2 are highly interlinked via their C-termini. *Second*, BBS9 and BBS7 homo-dimerize also at their C-termini but are not directly connected with each other. *Third*, BBS4 is attached to BBS7, BBS9 and BBS2 with its N-terminus to the C-termini of the three proteins. *Fourth*, BBS1 (via C-terminus) and TTC8 (via N-terminus) are only attached to BBS9 and show no connection to any other BBSome components in the screen. With this data and the structural information it is now possible to create a probable BBSome composition model.

3.4.5 The interacting domains of the BBSome

The inclusion of BBSome fragments in the screen is accompanied with big advantage to obtain specific knowledge about interacting protein parts besides increasing the success rate. Previously data were published giving information about the structural organization of the BBSome components BBS2, BBS7, BBS9, BBS4, BBS1, BBS8 (TTC8) and BBS5 (Jin et al., 2010 and Fig 3.23). With the high resolution Y2H data it was possible to assign the PPIs to the according domains and therefore characterize the interaction sites of the BBSome components and their architecture. To address this, the detected interacting fragments were combined to one probable PPI (Fig 3.27.). This is only possible if the fragments are overlapping, e.g. if the full length construct and the C-terminal part of a

protein are interacting with a second protein this suggests the C-terminal connection between both proteins. However, it could not be absolutely excluded that there are two separate links. But based on the assumption of one link between all BBSome components a map was created combining all PPIs (Fig 3.27).

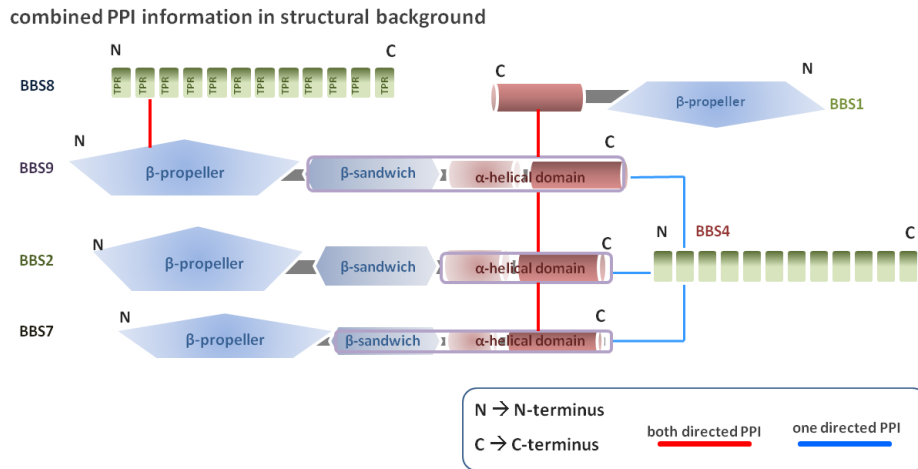


Fig 3.27 Combined PPI information in the structural background of the BBSome components. Depicted are the interactions between the separate domains based on PPI information obtained by including BBSome fragments in the Y2H screen. The domains are declared as well as the configuration of the PPIs.

As described above BBS9, BBS2, and BBS7 have shared domain architecture (Fig 3.23.). The Y2H data suggest a connection via their middle part and their C-termini which contain β -sandwiches and α -helical domains. The combined interaction data of BBS2 propose a connection to BBS9 and BBS7 via their alpha-helical domains. Same applies for BBS1 that is linked to BBS9 via its C-terminus also containing alpha-helical domains. Whereas BBS8 and BBS4 are attached to BBS2 and BBS9 via their N-termini containing stacked alpha-helical TPR repeat domains. But while BBS4 is linked to the C-terminal alpha-helical containing domain of BBS2 TTC8 is attached to the N-terminal beta-propeller part of BBS9. Taken together the Y2H PPI data support a C-terminal linkage of the ‘inner core’ components BBS2, BBS7 and BBS9 via their α -helical domains whereas an N-terminal attachment of the peripheral BBSome components BBS1 and TTC8 is suggested but also to the α -helical domains of the ‘inner core’ complex of the BBSome. Further the two peripheral BBSome components (BBS4 and BBS1) are attached to the C-terminal parts of the ‘inner core’ BBSome components except of BBS8 that is attached to the N-terminal part of BBS9.

3.5 Investigation of the functional relationship between the human NPC and the human BBSome

It was shown in a high profile report that the cilium is a separate cell organelle and the transport of soluble proteins is restricted to its size (Hu et al., 2010). The question has raised which mechanism could be responsible for protein exclusion or in more detail, how is the protein transport between cilia

and cytoplasm controlled. It was previously shown that BBS components are involved in vesicle coating and further that they share sequence homology to vesicle coats such as COPI, COPII and clathrin (Jin et al., 2010). The group around Jin showed that BBS3, a small ARL6-GTPase which is not part of the stable octameric BBSome complex but still belongs to the BBS gene encoding proteins (Fan et al., 2004; Chiang et al., 2004) recruits the BBSome onto membranes. Here the BBSome builds a coat complex that sorts membrane proteins to cilia. The NPC's core scaffold also resembles coatomer structures that are suggested to have a common structural ancestor (Brohawn et al., 2008). Thus the BBSome and the NPC components share key structural elements composed entirely of a β -propeller-type protein fold, an α -solenoid fold, or a distinctive arrangement of both (Brohawn et al., 2008; Jin et al., 2010). It was shown that the localization of retinitis pigmentosa 2 to cilia is regulated by importin- β (Hurd et al., 2011). This was one of the first indicators of a common transport process of ciliary and nucleocytoplasmic proteins.

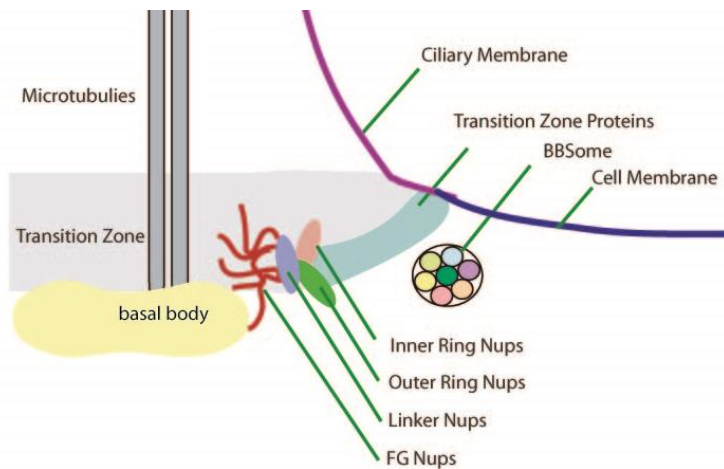


Fig 3.28 Schematic view of suggested mammalian Ciliary Pore Complex (CPC) at the bottom of a primary cilium (modified after Obado et al., 2012). It is assumed that the transport of molecules in and out of the cilia is controlled with a pore complex that contains NPC and BBS components (Kee et al., 2013).

Finally, investigations of Lee et al., 2012 implied a size-dependent diffusion barrier and the localization of six human nucleoporines at the base of primary and motile cilia, namely NUP358, NUP214, NUP35, NUP37, NUP62 and NUP93. This suggests functional parallels between nuclear and ciliary protein transport. A ciliary pore complex (CPC) was hypothesized (CPC) that is build of BBSome and NPC components (Kee et al., 2012) (Fig 3.28). The question has risen if there is a direct functional link between NPC and BBSome and further do NPC components and BBSome components build a CPC. To address this question a Y2H screen was performed to determine possible PPIs between nups and BBSome components.

3.5.1 Defining the human NPC-BBSome clone set

To examine the hypothesis of a ciliary pore complex comprising BBSome and NPC components a Y2H screen was performed. Tested were human full length nucleoporines against human full length BBSome proteins. Moreover all 21 human BBSome fragments were included to ensure a comprehensive analysis that includes all structurally ordered parts of the BBSome complex. Also by increasing the number of probable true positives and decrease the number of false negatives. Taken together 27 construct of six BBSome components and 72 full length constructs of 24 human nucleoporines were examined.

3.5.2 Identification of the NPC-BBSome PPIs with Y2H

The human NPC-BBSome Y2H screen was performed like the NPC and the BBSome screen. A well-controlled, stringent automated yeast two-hybrid setup was used generating systematic PPI data with high precision. Because all BBSome and NPC components were already subcloned into the bait and the prey vectors and the according yeast strains were transformed with the constructs the screen could be performed immediately. In the high quality interaction screening protocol the screen was realized testing the BBSome baits against a NPC prey matrix and the NPC baits against a BBSome prey matrix. Thus bait constructs of each complex were tested against a 96-prey matrix including biological duplicates of the NPC constructs or triplicates of BBSome constructs (81 preys of the BBSome and 96 of the NPC). After the mating of 222 liquid baits with the 177 prey colonies (two prey matrices) the possible yeast colonies were spotted on SD4 medium (see methods) to detect interactions via growing colonies. At all the number of possible colonies achieved 39294. The number of actually grown spots was 80 (Fig 3.29).

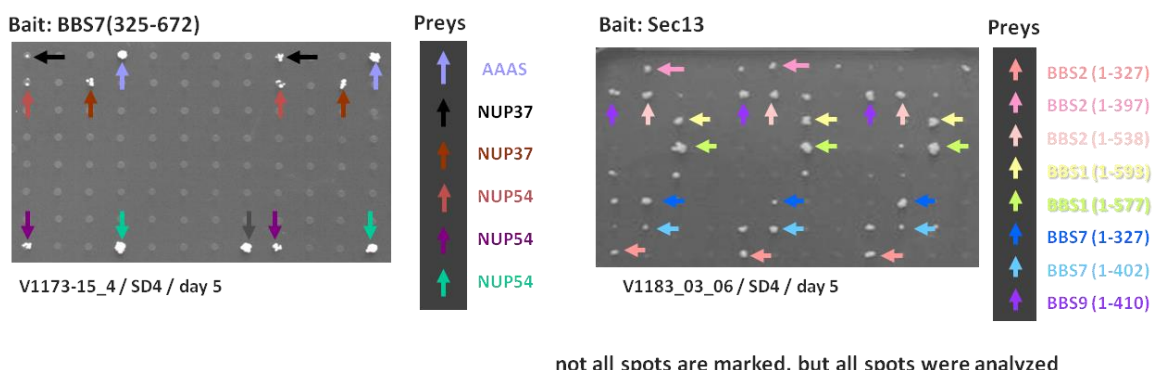


Fig 3.29 Shown are two 96-well agar plates of the BBSome-NPC Y2H screen. Two baits (BBS7 (325-672) and SEC13) are interacting with six NPC prey constructs and several BBSome constructs (indicated by the different colored arrows). The plates represent the Y2H results at day 5 on selective -HAULT medium.

All plates were analyzed with Visual Grid and judged individually as well. The grown spots were assigned to the constructs over the position in the matrix. To reduce the false positive rate and

stringent the Y2H system systematically only two or more grown colonies of each prey construct were integrated into analysis. The potential integration of bait constructs into the final data set given by grown colonies was judged individually. This resulted in a final colony data set of 40 colonies. To get an interaction data set the colony information for all prey and bait constructs and further for all proteins were summarized. Thus the final data set revealed 27 interacting construct pairs.

3.5.3 Identification of the PPIs between BBSome and NPC

The Y2H screen resulted in 27 interactions between human NPC and human BBSome constructs. Like in the previous Y2H screens all constructs were tested in both configurations against each other, namely all NPC baits were tested against BBSome preys and *vice versa*. Only one directed interactions were detected. With the obtained data set it was possible to create a PPI network (Fig 3.30).

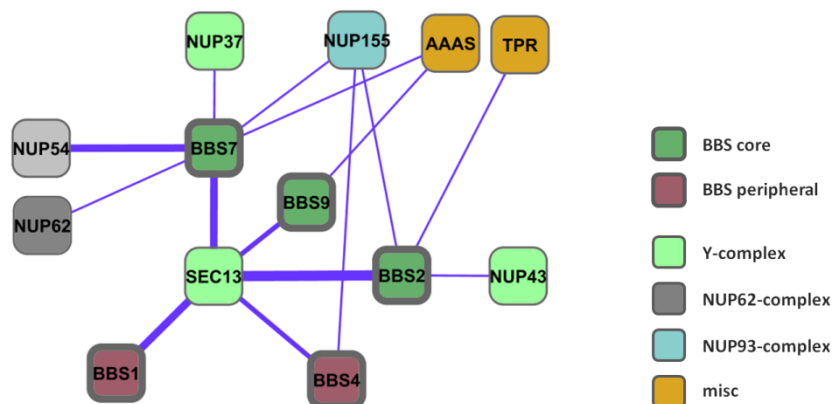


Fig 3.30 PPI interaction map of BBSome and NPC components obtained with Y2H screens. The Y2H screen resulted in 15 interactions between eight NPC and five BBSome components. The nodes are colored according to their membership to subcomplexes of each protein complex. The thickness of the links indicate the intern interaction count – the thicker the link, the more often an interaction was found even with more different constructs. The screen showed that the core as well as peripheral BBSome components interacts with the β -propeller protein SEC13 a member of the scaffold subcomplex, the Y-complex of the NPC

The Y2H screen revealed interactions between 16 constructs of the BBSome and 11 constructs of the NPC resulting in 15 PPIs between five BBSome proteins and eight NPC proteins (Fig 3.30). No interaction was detected in both configurations, namely bait-prey and prey-bait direction. The number of interacting constructs of BBSome and NPC were summarized and are indicated by the thickness of the links, e.g. one construct of SEC13 (CCSB_4052) seems to interact with four different fragments of BBS2 but only one construct of BBS2 resulted in an interaction with a construct of NUP43. Considering the number of interacting constructs it is obvious that SEC13 and NUP54 belong to the constructs of the NPC resulting in the largest number of interactions indicated by the thickness of their links. Whereas only one construct of all other NPC components showed interactions to one BBSome fragment of each BBSome protein. Apart of BBS8 (TTC8) all BBS components showed interactions with NPC components of the Y-complex, NUP93-complex and NUP62-complex. In addition a

connection to a member of the inner transport channel, namely NUP54 of the NPC was observed as well as to miscellaneous nups, part of the nuclear basket like TPR and AAAS (Aladin). It seems that the ‘inner core’ of the BBSome comprising BBS2, BBS7 and BBS9 are connected to the NPC components whereas the more peripheral BBSome components only share two NPC interaction partners. In detail, BBS2 and BBS7 are linked to the NPC components whereas BBS2 is connected to the Y-complex member NUP43 and the NUP93-complex member NUP155. BBS7 is linked to the Y-complex member NUP37 and additionally attached to the NUP62-complex members NUP62 and NUP54. Further BBS2 and BBS9 showed connections to the miscellaneous nups TPR and AAAS. AAAS is also connected with BBS9. The Y-complex member SEC13, a small β -propeller protein of the NPC Y-complex seems to interact with all five BBS components. The peripheral BBSome components BBS1 and BBS4 showed interactions to SEC13. However BBS4 is additionally attached to NUP155. The connection between SEC13, the BBSome ‘inner core’ and the peripheral BBSome components suggest a link between the inner core complex and the periphery of the BBSome via SEC13.

Taken together BBSome components interact with members of different parts of the NPC, namely the NPC scaffold, the inner channel and miscellaneous nups. On the other hand, the interactions are almost restricted to the core complex of the BBSome. SEC13 seems to interact with both parts of the BBSome, the inner core as well as the periphery.

3.5.4 High resolution interaction map of BBSome and NPC components

The incorporation of BBSome fragments into the screen allows the creation of a high resolution map emerging insight into the binding of NPC components to certain parts of the BBSome components. Thus it enables a better characterization of the resulting interactions between BBSome and NPC (Fig 3.32.). Depicted are all interacting BBSome constructs with the suggested interacting NPC components. The nodes of the nups are colored according to their membership to the NPC subcomplexes whereas their size indicates the protein size. To determine as internal value the reliability of the interactions an interaction score was introduced. The score was calculated by dividing the total number of growing spots by the actual number of growing spots in all replicas. The minimum score ranged from 0.67 for three replicas to 0.75 for four replicas. The maximum score was 1 indicating the growth of all possible spots in the prey matrix after mating with a bait construct. More than half of the interacting construct pairs revealed an interaction score of 1. Only nine interacting construct pairs resulted in the minimum interaction score of 0.67. However, all interactions of the construct pairs were analyzed.

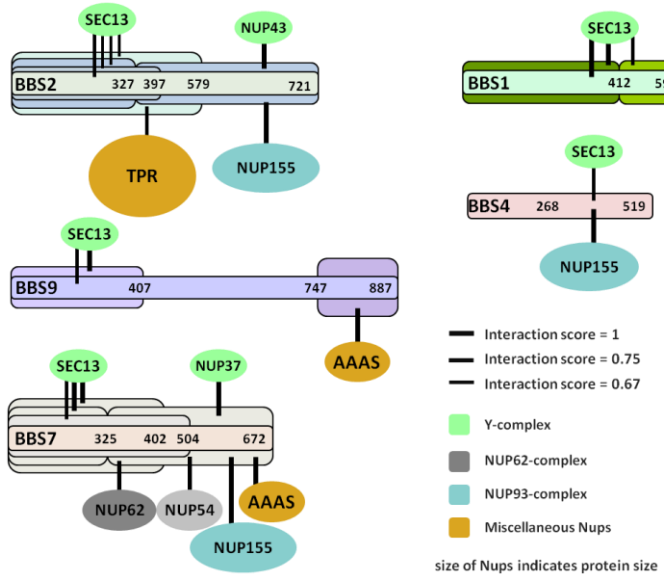


Fig 3.31 High resolution interaction map of NPC components and BBSome fragments. Shown are the interacting fragments of the BBSome components and the NPC components. All are colored according to their membership. The thickness of the links is according to the intern interaction score ranging from 0.67 to 1. The Y2H analysis revealed that most of the NPC components bind to the C-termini whereas SEC13 is mostly attached to the C-termini.

The high resolution map revealed that the NPC components interact with BBSome components at different sites. The Y-complex members NUP43 and NUP37 showed connections to the N-terminal parts of BBS2 (327-721) and BBS7 (325-672). The NUP93-complex member NUP155 is also connected to the N-terminal or middle part of BBS2 (327-721) and BBS7 (325-672). Additionally NUP155 is attached to the full length construct of BBS4 which makes it impossible to propose a specific interaction site. The members of the NUP62-complex NUP54 and NUP62 are also attached to the N-terminal part of BBS7 (325-672). In contrast to the previous described connections TPR seems to bind the C-terminal or middle part of BBS2 (1-579). AAAS is also attached to the middle or the N-terminal part of BBS9 and BBS7. Taken together BBS2 and BBS7 seem to prior interact with the NPC components with its N-terminal part and BBS9 also show two interactions at its N-terminal part to AAAS. The BBSome core seems to be connected to NPC members. The peripheral BBS components BBS1 and BBS4 are only linked to NUP155 and SEC13. One of the most conspicuous observations of this screen was done regarding SEC13, a member of the NPC scaffold. A construct of this small β -propeller protein showed interactions to constructs of all five BBSome components. One SEC13 construct (CCSB_4052) in one bait vector (pBTMcC24) resulted in all 13 interactions. These interactions could be possibly false positive or at least unspecific interactions. Nevertheless, there are lines of evidence against this apprehension. *First*, the construct did not result in interactions with all BBSome prey constructs. Thus auto-activation can be excluded. *Second*, the interaction score ranges from 0.67 to 1 showing the binding behavior is also dependent of the prey-construct. A higher interaction score indicate binding to more prey constructs. *Third*, the BBSome constructs that interacted with the SEC13 construct are overlapping and not randomly distributed over the overall

structure of the BBSome components suggesting a certain interaction domain in each BBSome protein. SEC13 showed interactions to all five BBSome components, four overlapping constructs of BBS2, three of BBS7 and two of BBS9. Additional to the fragment constructs also the full length constructs of all three BBSome components showed interactions to SEC13. In summary the screen revealed that SEC13 is C-terminal connected to the ‘inner core’ of the BBSome. With regards to the ‘peripheral’ BBSome components BBS4 and BBS1 the interaction pattern is not specific. Only the full length construct of BBS4 interacts with the SEC13 construct and with NUP155 which makes a specific determination of an interaction domain impossible. Nevertheless interactions between BBS4 and SEC13 and NUP155, both NPC scaffold components are indicated. On the other hand all three partially non-overlapping BBS1 constructs seem to interact with the construct of SEC13. Thus the full length construct, the N-terminus BBS1(aa 1-412) and the C-terminus (aa 412-593) are involved indicating the possibility of more than one SEC13 binding site. Taken together the peripheral BBSome components BBS1 and BBS4 seem to interact with two scaffold components of the NPC, SEC13 and NUP155.

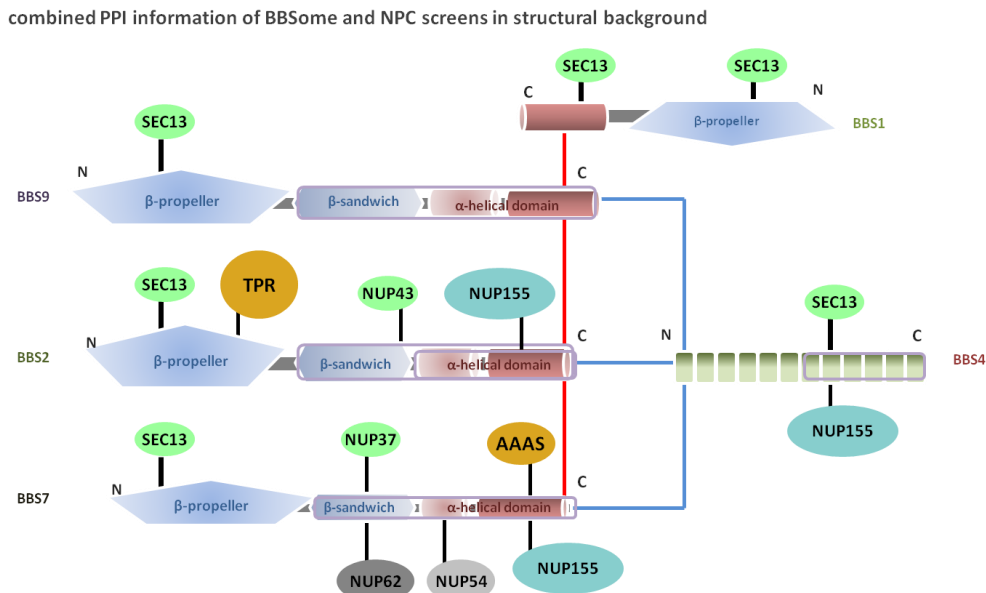


Fig 3.32 Combined interaction map of NPC components and BBSome component fragments. Shown is the domain architecture of the BBSome components, the intra-complex binding of BBSome components and the attachment of NPC components to the BBSome components. The nups are colored according to their membership in NPC: green = Y-complex, grey = NUP62-complex, blue = NUP93-complex, brown = miscellaneous nups. The Y2H analysis showed that the BBSome core complex seems to be attached via α -helical domains at their C-termini. There are β -propeller interactions between the N-termini of the BBSome core components and SEC13. All other nups are attached to either β -sandwich domains or α -helical domains at the C-termini or middle parts of the BBSome components.

3.5.5 Functional relationship between NPC and BBSome - summary

Taken together the Y2H screen revealed binary PPIs between NPC and BBSome components. The ‘inner core’ of the BBSome comprising BBS7, BBS9 and BBS7 is interconnected with the NPC components SEC13 via their N-terminus. The N-termini of the BBSome ‘inner core’ contain beta-

propeller domains. The other NPC components (NUP37 – Y-complex, NUP155 – NUP93-complex, NUP62 and NUP54 – NUP62-complex and miscellaneous nups – AAAS and TPR) are connected to the middle part or the C-terminus of the BBSome components. Based on the localization of NPC components especially FG-repeat domain containing nups a ciliary pore was proposed that controls the transport of molecules in and out of the primary cilia (Kee et al., 2012). The distribution of the C-terminal inner BBSome complex connections and the attachment of the NPC components partially on the opposite parts of the BBSome proteins (N-terminal), especially those of SEC13 indicate evidence for a biological relevance. At a first glance it could be suggested that strong β -propeller interactions seem to connect the N-terminal parts of the BBSome to build the scaffold of the CPC. The knowledge about a CPC remains largely elusive and this hypothesis is not based on any additional evidence. It has to be proven further. We only can conclude from our Y2H results that there is at least a minimal functional relationship between BBSome and NPC components.

4. Discussion

4.1 Aims and Structure of the discussion

This thesis comprises the detection of protein-protein interactions and their analysis of three known protein assemblies: the yeast and the human nuclear pore complex (NPC) and the human BBSome. The NPC was firstly described in 1959 (Watson, 1959) whereas the BBSome was only recently discovered in 2007 (Nachury et al., 2007). Using PPI data insight can be gained into their architecture. To address this two large Y2H screens were performed. In order to receive the most accurate idea of possible complex architecture via PPI information comprehensive Y2H clone sets were generated, including protein fragments of both complexes, resulting in the most comprehensive binary data sets of the NPC and the BBSome. Thus we undertook an NPC – NPC and a BBSome - BBSome Y2H screen. Key et al., 2012 suggested a ciliary pore consisting of NPC and BBSome components. A third screen was realized testing human nups against human BBSome components.

The Y2H results for the BBSome give a first insight into its architecture. In addition the Y2H screen revealed an initial insight into the functional relationship between NPC and BBSome. The structural character of the BBSome as well as the functional relationship of between BBSome and NPC is already discussed in section 3.6.4. However here are the major outcomes and their implications belonging to the BBSome are combined and summarized. The NPC Y2H screen gave high precision data that allow the arrangement of subcomplexes within the NPC. Therefore the major part of the discussion is referring to the structural arrangement of the NPC.

4.2 The PPIs of the BBSome and the functional relationship between BBSome and NPC

- The BBSome was recently discovered and therefore its architecture is poorly annotated (Nachury et al., 2007). To address this question with PPI information a comprehensive Y2H screen was performed including fragments that revealed specific PPI information regarding to interacting domains. The screen resulted in 37 interactions between 16 BBSome components. The interaction data by screening also BBSome fragments allowed assignment of certain interactions to specific domains.

- BBS1, BBS2, BBS4, BBS7, TTC8 (BBS8) and BBS9 are connected in a highly dense network comprising 37 interactions between 16 constructs combined to six PPIs between six BBS components.
- There is an ‘inner core’ observable consisting of BBS2, BBS7 and BBS9, where BBS9 and BBS7 are not directly connected with each other.
- There are also ‘peripheral’ BBSome components attached to the ‘inner core’, e.g. BBS1, BBS4 and TTC8 (BBS8).
- The Y2H screen revealed dimerizations of BBS7 and BBS9 suggesting the occurrence of two or more BBS7 and BBS9 proteins in each BBSome complex.
- BBS4 seems to bridge the ‘inner core’ members BBS9 with BBS7.
- The fragment interactions revealed a C-terminal attachment of the ‘inner core’ members and BBS1.
- BBS4 and BBS8 are attached via their N-termini to members of the ‘inner core’.
- Kee et al., 2012 proposed the presence of a CPC (ciliary pore complex) at the bottom of the cilia comprising BBSome and NPC components. Therefore a Y2H screen was performed testing human NPC constructs against human BBSome constructs. Also included in the screen are BBSome fragments revealing specific information regarding interacting BBSome domains. The major outcomes are as follows:
 - The screen resulted in 15 interactions between eight NPC proteins (SEC13, NUP37, NUP43, NUP62, NUP54, NUP155, AAAS and TPR) and five BBSome components (BBS1, BBS2, BBS4, BBS7 and BBS9).
 - Included are nups belonging to the Y-complex, the NUP62-complex and miscellaneous nups.
 - All five BBSome components interact with SEC13 moreover while the intra-complex connections of the BBSome ‘inner core’ occur with its C-termini the connection to SEC13 is made by the N-termini.
 - SEC13 is also attached to BBS1 and BBS4 but to the C-termini and in the case of BBS1 to both part
 - All other nups except TPR are attached to the C-termini of BBS2, BBS7 and BBS4.
 - Taken together the Y2H screen resulted indeed in connections between BBSome and NPC components. Moreover the results indicate a specific functional relationship between SEC13 and the BBSome.

4.3 The structure of the Nuclear Pore Complex

One of the hallmarks of evolution is the separation of the nucleus as cellular organelle. The nucleus contains the genetic material and its separation from the rest of the cell allows its controlled handling manifested through several mechanisms. One of these mechanisms is the controlled transport of molecules in and out of the nucleus such as proteins or RNA subunits. The transport occurs through specific gateways – the nuclear pores (Watson, 1959; Feldherr, 1965). They fuse the inner and the outer nuclear membrane and are formed as large nuclear pore complexes with a molecular weight of 60 MDa in yeast and 120 MDa in mammalian cells. The nuclear pore complex (NPC) is one of the largest protein assemblies of the cell (Peters, 2005). Because of its enormous size and its exposed localization on both sides of the nuclear envelope the NPC was already described in the 1950th (Watson, 1959). For a long time electron microscopy was the best technique to investigate the nuclear pores. Many different cell types were observed and it became clear that nuclear pores are conserved throughout organisms regarding their shape, symmetry and size (Kiseleva et al., 2000). They compose symmetrical octagonal rings surrounding a central channel showing less electron density (Watson et al., 1959). Although they share symmetrical similarities they look distinct from the nucleoplasmic and the cytoplasmic side (Kiseleva et al., 2000). The cytoplasmic side is characterized by basket-like structures that turned out to be cytoplasmic fibrils (Jarnik and Aebi, 1991; Goldberg and Allen, 1993). At the nucleoplasmic side a basket-like structure was observed indicated by eight filaments that join a platform-like structure to the NPC. Therefore it was called nuclear basket (Goldberg and Allen, 1993, 1996; Ris and Malecki, 1993; Rakowska et al., 1998; Stoffler et al., 1999). Both structures were visualized on cells in many organisms. It became clear that these structural characteristics are conserved. These characteristics differ in their strength of formation (Kiseleva et al., 2000, 2007). However the resolution of electron microscopy was limited. Further studies included results of cryo-electron microscopy increasing the resolution. The images of many NPCs were averaged enabling the reconstitution of the NPC scaffold. It seemed that the scaffold ring is made by thinner and thicker layers – it was called the spoke ring (Akey and Radermacher, 1993). In addition by using cryotomography it turned out that the NPC scaffold is made by three main ring structures: the cytoplasmic ring, the nucleoplasmic ring and lying in between the spoke ring (Beck et al., 2007). It appears that the layers in between the rings have a less electron density suggesting that the rings float on each other. However this could be due to poor resolution in this region. The central channel did not show any structural features moreover it seemed to be filled with an aqueous meshwork that was identified as long sequences of phenyl-alanine (FG)-repeat domains of the proteins building the NPC. In parallel to the structural studies the identification of approximately 30 nucleoporins was achieved (Rout et al., 2000; Ryan and Wente, 2000; Fahrenkrog et al., 2000; Cronshaw et al., 2002). Using immunogold electron microscopy the molecular organization of the nucleoporins was mapped to subdomains (Rout et al., 2000, Alber et al., 2007).

To date many questions regarding the structural character of the NPC could be answered such as the actual protein composition, the major structural composition and the determination of its distinct subcomplexes (Rout et al., 2000; Cronshaw et al., 2002; Alber et al., 2007). However, there remain fundamental questions to be solved surrounding the basic knowledge of each protein complex such as the structural arrangement of the distinct subcomplexes. Using panel of distinct methods, including cryo-tomography, allowed the localization of the nups and the subcomplexes (Beck et al., 2007). In addition, over the past decades much crystallization data was obtained. Initially only subdomains of nups were crystallized, but later ternary complexes of ~ 200 kDa could be solved (Berke et al., 2004; Boehmer and Schwartz, 2007; Jeudy and Schwartz, 2007; Boehmer et al., 2008; Leksa et al., 2009; Brohawn and Schwartz, 2009; Kampmann et al., 2009; Bilokapic and Schwartz, 2012). Currently 30% of the main scaffold comprising the Y-complex and the nic96-complex (NUP93-complex in vertebrates) has already been crystallized (Brohawn et al., 2009). Furthermore for the nsp1-complex (NUP62-complex in vertebrates) crystal data are available (Yoshida et al., 2011; Montpetit et al., 2011). The majority of crystal data (90%) refers to the Y-complex. This complex is *in vitro* most stable (Brohawn et al., 2009). In contrast the structural characterization of the nic96-complex (NUP93-complex in vertebrates) is much more fragmentary (Whittle et al., 2009; Schrader et al., 2008; Jeudy and Schwartz, 2007) and the arrangement of the subcomplexes remains unclear. The complete architecture of the NPC remains elusive. There are still knowledge gaps and four models try to combine all previous results and organize the NPC based on the arrangement of the Y-complex which is the largest scaffold subcomplex of the NPC: *first*, the fence pole model; *second*, the computational model; *third*, the lattice model and *forth*, a model based on cryo-tomography (Alber et al., 2007; Brohawn et al., 2008; Debler et al., 2008; Bui et al., 2013). These models were created using different experimental approaches such as Co-APs, crystallization, cryo-electron tomography (cryo-ET) and computational modeling.

Binary protein-protein interactions especially those between subcomplexes, provide insight into the direct connections between subcomplexes. Approaches to detect binary protein-protein interactions are rarely found in the experimental set ups. Most of the nups are soluble and PPI detection methods like Y2H are applicable. A comprehensive Y2H screen was performed including human and yeast NPC constructs. The evaluation of the yeast Y2H data was done against the data sets of Amlacher et al., 2011 and Leducq et al., 2012 and against the other large data sets of Alber et al., 2007. PPI networks were generated and connections within and between subcomplexes were analyzed. Selected PPIs identified in our Y2H screen could be used to hypothesize a model based on the arrangement of the Y-complex. Several PPIs were recapitulated using orthogonal techniques; for thermophoresis (MST) for yeast PPIs and split-fluorophor assay (PCA) for the human PPIs. Regarding resulting experimentally workflow the discussion comprises: *first*, a detailed analysis of the obtained binary PPIs with regards to all subcomplexes and their connections and *second*, an analysis of the obtained binary PPIs with regards to previously described models of NPC subcomplex arrangement. Taken together we set out

an Y2H screen that should reveal valid binary PPI data to support the modeling of Y-complex arrangement in the NPC.

4.3.1 Binary PPIs of the yeast and the human NPC resulting in connections between the subcomplexes

The NPC is an assembly with a dynamic character. This was firstly suggested when Akey et al. discovered in 1995 that NPCs can occur in open and in closed conformations. Two possibilities could lead to these two states. It was shown that some nups were relocalized according to their current transporting task or that they were reorganized during cell-cycle specific rearrangements of the NPC by changing their interaction partners (Fahrenkrog et al., 2002; Paulillo et al.; 2005). Another possibility of NPCs conformational change could be reasoned directly by conformational changes of the nups themselves (Makhnevych et al., 2003). For instance, structural studies revealed that nup58/nup45 forms specific dimer-dimer interfaces that form structures allowing the regulation of the diameter of the NPC by intermolecular sliding (Melcak et al., 2007). Structural studies revealed flexibility in certain domains resulting in open and closed conformations of the nic96 complex (NUP93 in vertebrates) (Sampathkumar et al., 2013). The dynamic character of the NPC was shown in several ways but it is assumed that a fixed scaffold serves as docking unit for more transiently attached nups. This was indicated by detection of different residue times of several nups within the NPC ranging from seconds over minutes to more than 70 hours (Rabut et al., 2004). In addition certain subcomplexes were suggested within the NPC scaffold component (Rout et al., 2000). A fixed scaffold is suggested within the NPC and connections between nups building this scaffold might be easier to determine. The positions of the scaffold subcomplexes were solved to resolutions of 58 Å or 32 Å using cryo-tomography (Beck et al., 2007; Bui et al., 2013). Obviously there still remains a resolution gap preventing the determination of the specific subcomplex arrangement. However, there is already structural data based on crystal data, yet these data are limited and comprise only 23 PPIs that are partially redundant (see Fig 6.2, Appendix). Another possibility to overcome the resolution gap is to use additional information based on protein-protein interactions. The Y2H screen revealed 21 novel yeast PPIs and 13 novel human PPIs that can be used to directly connect the major subcomplexes, namely the Y-complex, the nsp1-complex and the nic96-complex. Moreover connections between the linker nups and all subcomplexes were detected. All subcomplexes are assumed to be directly connected to each other. They are arranged in spatial proximity (Alber et al., 2007). However there is the assumption that the interactions building the NPC are mostly heterotypic. Only a few homotypic interactions were suggested to form the ‘keystones’ in a significantly larger number of interactions between most other nucleoporins (Alber at al., 2007). In their integrative

studies the Alber et al. arranged the subcomplexes within several symmetrical rings. The two major rings are based on the major symmetry element the ‘spoke rings’ and called the inner and the outer ring. Each is localized both at the nucleoplasmic and cytoplasmic side of the NPC whereby the outer ring is sandwiching the inner ring. These rings build the scaffold and contain the Y-complex, the nic96-complex (NUP93-complex in vertebrates) and one part of the nsp1-complex (NUP62-complex in vertebrates) (Rout et al., 2000; Alber et al., 2007; Sampathkumar et al., 2013). Moreover a membrane ring is described that is embedded in the nuclear envelope and builds the connection to the membrane containing nups that include a membrane domain. The linker nups are attached between both set of outer and inner rings. The inner channel of the NPC is filled with nups containing FG-repeat domains whereas the FG-repeats fill the inner channel and the more structural domains are anchored to the inner rings and some are connected directly to the outer ring (Alber et al., 2007). The localization of the subcomplexes can be determined within certain structural arrangements of the NPC but direct connections still remain unclear. Binary PPI data is rare and making it difficult to determine the distinct orientation of the subcomplexes. The Y2H screen performed in this study resulted in 11 PPIs between three major subcomplexes (Fig 4.3). In detail, a relationship between nic96-complex and the nsp1-complex was already shown in 1993 by Grandi et al. They purified nic96 with the inner nsp1-complex members nup49, nup57 and nsp1. Moreover several studies reconstitute nic96 into the nsp1-complex (Grandi et al., 1995; Schlaich et al., 1997). The relationship between the two subcomplexes was uncovered early by affinity purification and co-IP and the Y2H screen revealed a direct connection via the nup57/nic96 PPI suggesting that nup57 is responsible for the immunoprecipitation of nic96 (Grandi et al., 1995; Schlaich et al., 1997). Two other Y2H PPIs describe connections between both subcomplexes, namely asm4/nsp1 and asm4/nup49. Nsp1, nup57 and nup49 are part of the inner nsp1-complex and nsp1 is also part of the outer nsp1-complex. The Y2H results indicate that the nic96-complex is bridging the Y-complex and the inner channel complex, as it was previously proposed by Alber et al. and mentioned above (Alber et al., 2007). The nic96-complex does not seem to be connected to the outer nsp1-complex members except of nsp1 itself. It is difficult to determine if the nic96-complex is linked to the outer nsp1-complex. The PPIs nic96/nup57, asm4/nup49 and asm4/nsp1 might imply the connection of the nic96-complex to the inner nsp1-complex whereas the PPI asm4/nsp1 could suggest the attachment of nic96 to the outer nsp1-complex. The results might imply that asm4 (nup59) builds a connection to the inner hetero-trimeric nsp1-complex via nsp1 and nup49. The connection of asm4 to nup49 and nsp1 could also suggest that this part of the nic96-complex builds a link to both nsp1-complex subunits. Because of lack of evidence both opportunities remain possible. Taken together a connection between the nic96-complex and the nsp1-complex was previously described but the direct link was unraveled by our Y2H screen (Grandi et al., 1993). It seems that the nic96-complex bridges the inner nsp1-complex and the Y-complex whereas the Y-complex bridges the nic96-complex and the outer nsp1-complex. It was previously suggested that the

nic96-complex bridges the inner and the outer ring in the NPC arrangement proposed by Alber et al., 2007. Considering this the Y2H results reflect very well the current described NPC architecture.

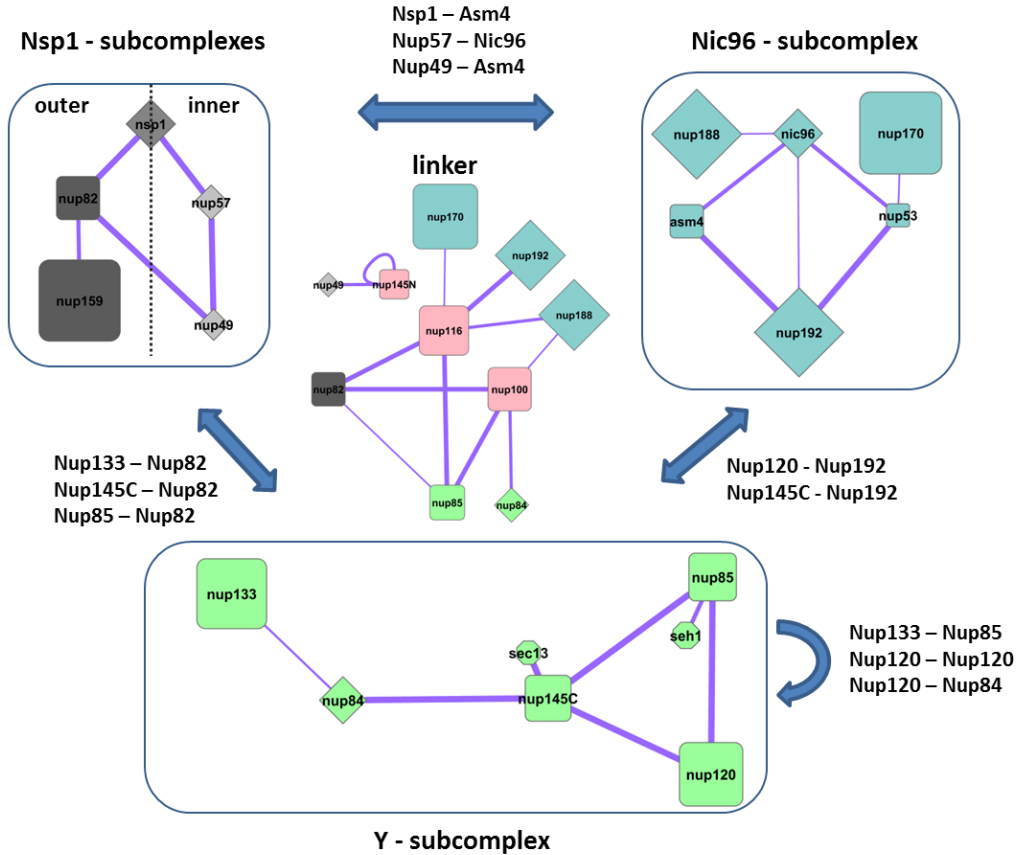


Fig 4.1 Overview of all NPC subcomplexes and their connections. Shown are the several subcomplexes (boxed) and the PPIs linking them. All subcomplexes are connected to each other. However the nic96-complex is connected to inner subunit of the nsp1-complex whereas the outer subunit is connected to the Y-complex. The Y-complex is directly attached to the nic96-complex. It seems that the Y-complex is connected to itself via three PPIs (nup133/nup85, nup120/nup120 and nup120/nup84). The linker nups are connected to all subcomplexes with at least two PPIs.

Nup116, nup100 and nup145N are similar in structural arrangement and thus build a family within the NPC nups, the linker nups. The Y2H screen revealed not only PPIs between the distinct subcomplexes also connections between the linker nups and the subcomplexes were unraveled. The architectural structure of these nups is made of mostly FG-repeat domains followed by alpha/beta-domains (Brohawn et al., 2009). They are suggested to link the subcomplexes and therefore they are assumed to be grouped between the other subcomplexes (Alber et al., 2007). In fact previously studies showed that nup116 was co-purified with nup170 and nup192 (Rout et al., 2000; Alber et al., 2007). In addition, nup116 was co-purified with nup188 also in the large data set of Alber et al. 2007. However, apart from the suggested positions and the co-immunoprecipitation unraveled by Alber et al. and Rout et al., knowledge of the linker nups remains elusive. The results of the Y2H screen provide insight into the structural arrangement of the linker nups within the NPC. First of all we could recapitulate the

previously published Co-IP data of nup116 and nup100 that are mentioned above. Furthermore the Y2H screen resulted in binary interactions of the nic96-complex members nup170, nup188 and nup192. In fact it seems that the linker nups are highly connected to the nic96-complex whereas nup100 and nup116 share the interaction partner nup188. There are more shared interaction partners of nup100 and nup116, namely nup85 and nup82 which are members of Y-complex and the nsp1-complex. Nup116 and nup100 connect the major scaffold subcomplexes whereas nup145N is attached to the inner nsp1-complex member nup49. Therefore the linker nups seem to interact with at least one member of each subcomplex. In total 11 PPIs describe the connections of all three linker nups to all three major subcomplexes including both nsp1-complexes. Taken together the hypothesis that the linker nups link all subcomplexes is well reflected in the Y2H network.

The Y-complex is directly connected to the nic96-complex (NUP93-complex in vertebrates) via two PPIs: nup192/nup120 and nup192/nup145C. Considering our Y2H results it seems that the attachment between both scaffold complexes occurs on one end of the Y-complex, namely at the ‘hub’-end. The interaction nup192/nup145C was identified earlier by Alber et al. 2007 in their large Co-AP data set. Thus an attachment of the nic96-complex to the Y-complex was already shown but the direct connection could not be determined with the Co-AP data. The nup192/nup120 PPI was not described previously. In addition neither the Leducq data set nor the Amlacher data set revealed connections between the nic96-complex and the Y-complex. Our Y2H screen unraveled a complete new connection. The connection between the Y-complex and the nsp1-complex (NUP62-complex in vertebrates) is made of three PPIs all including nup82, in detail nup82/nup85, nup82/nup145C and nup82/nup133. Nup82/nup85 was already described by Leducq. The nup82/nup133 PPI was previously identified twice in large data sets. The first identification occurred in a genome wide tandem affinity purification approach coupled to mass spectrometry (Krogan et al., 2005). It was also detected in the large Co-AP data set of Alber et al. 2007. Here several other proteins were co-purified with nup133 and nup82 preventing the determination of the direct interaction between the Y-complex and the nsp1-complex (NUP62-complex in vertebrates). Thus our Y2H screen revealed new links between the Y-complex and the nsp1-complex. The connection to the nsp1-complex occurs via the ‘end’ of the Y-complex, namely the tail, whereas the connection to the nic96-complex (NUP93-complex in vertebrates) is made via the ‘hub’-end, as described above. The Y-complex seems not to be linked to the inner nsp1-complex comprising nup49, nup57 and nsp1. There are two possibilities to explain the lack of Y2H PPIs between these two subcomplexes. *First*, the Y2H approach did not reveal this information and thus are due to false negatives of the screen or *second*, both subcomplexes are really not directly linked. In the large study of Alber et al. members of the inner nsp1 complex are localized around the major scaffold rings but a direct connection is also not shown. Moreover they propose that the nic96-complex bridges the inner and the outer ring (Alber et al., 2007). This hypothesis is well reflected in our Y2H results.

The Y-complex is the best characterized subcomplex of the NPC and the focus of many studies (Siniossoglou et al., 2000; Belgareh et al., 2001; Brohawn et al., 2008; Kampmann et al., 2009; Thierbach et al., 2013). The Y2H screen recapitulated previously known PPI information and are described as intra-molecular Y-complex connections (Rout et al., 2000; Alber et al., 2007; Brohawn et al., 2008; Thierbach et al., 2013; Bui et al., 2013). However there are some PPIs that are revealed by our screen and do not fit into previous Y-complex architecture as intra-molecular connections. We suggest that the Y2H screen also revealed intermolecular subcomplex connections that are made by the subcomplexes themselves. The architecture of the other subcomplexes is not well understood and hypothesizing a distinction between inter- and intra-molecular interactions is not possible. However, some PPIs between subcomplex components could represent inter-complex interactions. Some of these new inter molecular Y-complex PPIs are of major importance to provide insight into the NPC architecture. It was suggested that the Y-complex is largely involved in building the scaffold (Walther et al., 2003, Alber et al., 2007) and it was shown that this subcomplex is firstly recruited to the nuclear pore (Harel et al., 2003). Novel PPIs regarding the Y-complex could lead to a more advanced idea of how the NPC is structurally organized.

4.3.2 Novel PPIs in the background of two major models describing NPC structure – Alber et al., 2007 and Brohawn et al., 2008

The detailed architecture of the NPC remains under discussion (Brohawn et al., 2009). Different methods were used to emerge insight into the subcomplex arrangement such as crystallization, cryo-EM and cryo-tomography (Brohwan et al., 2008 & 2009; Beck et al., 2007; Alber et al., 2007; Kampmann et al., 2009; Bui et al., 2013). On the one hand there are crystal data available for approximately 30% of the mass of the NPC scaffold but this is currently not enough to reveal a comprehensive insight into the structural organization of the NPC (Bilokapic et al., 2012). On the other hand there is cryo-EM and cryo-tomography tackling this problem from a different angle. Beck et al. reported in 2007 the structure of the yeast NPC with a resolution of 58 Å, whereas Maimon described the structure of the human NPC at a resolution of 66 Å (Beck et al., 2007; Maimon et al., 2012). More recently Bui et al. reported the human NPC scaffold at a resolution of 32 Å (Bui et al., 2013). Investigating entire NPCs and averaging of multiple assemblies its dynamic character remains intact. An overall structure of the NPC was delineated the arrangement of the discrete subcomplexes could not be clarified reasoned by the insufficient resolution (Hrabe et al., 2012). In general crystal data can be fairly reliable fitted into the cryo-EM data that are in range of 10–15 Å. The cryo-tomography resolution is lower and therefore the data could not be matched to crystal data in atomic resolution leaving a resolution gap between both methods (Fath et al., 2007; Fotin et al., 2004; Stagg et al., 2008). Another attempt to capture the dynamic character of the NPC and create a model which is

also based on subcomplex arrangement took an integrative approach including several experiments ranging from affinity purification over immuno-EM and also including cryo-tomography (Beck et al., 2007 a/b; Fernandez-Martinez et al., 2012). The combined results of all approaches were used to create a model that is based on the likelihood of protein contacts. Likelihood does not describe a constant event but reflect the dynamic character of the NPC.

In summary three models are available all based on divergent perspectives.

Like co-crystallization that revealed direct protein contacts Y2H screens also result in binary protein-protein interactions. Y2H screens reveal information about the interaction of two proteins or protein fragments in a cellular environment. The weakest detectable interaction can be observed at K_{DS} of approximately 10-100 μ M (Mackay et al., 2008). The sensitivity of the Y2H could be adequate to detect even weaker PPIs building inter-complex connections that might be not detected earlier possibly reasoned by their dynamic character. The Y2H PPIs were validated with two independent methods to ensure their specificity (see section 3.4). Strong interactions, namely intra-complex connections which reflect the stable character of the NPC can be captured as well. Some of these interactions were described before in various IP and pull down experiments (Rout et al., 2000, Cronshaw et al., 2002; Alber et al., 2007; Onischenko et al., 2009; Fernandez-Martinez et al., 2012). Reasoned by limitations each method might unravel distinct PPIs. Therefore the knowledge about PPIs obtained by Y2H may help to define the molecular architecture of the NPC.

The previously described approaches of Alber et al., Brohawn et al. and Bui et al. resulted in models of NPC architecture based on the arrangement of subcomplexes, mostly on the arrangement of the largest subcomplex - the Y-complex. All models are not easy to reconcile. Each model still supports single features of the molecular architecture that are based on their perspectives. Our Y2H screen might reveal missing inter-complex connections that can be fitted into the models and overcome the limitations such as the resolution gap or binding affinity. As a start the models of Alber et al. and Brohawn et al. are explained in detail. They reflect very well the different directions of the NPC science and influenced long time the NPC field. Lastly the recently published model of Bui et al. will be presented.

In 2007 Alber et al. performed an integrative analysis by performing different experiments such as ultracentrifugation (determination of the protein's shape and size), quantitative immunoblotting (protein stoichiometry), affinity purification (protein composites and connectivity), overlay assay (protein contacts), electron microscopy (NPC symmetry and nuclear envelope excluded volume), immuno-electron microscopy (protein localization), bioinformatics and membrane fractionation (nuclear envelope surface localization and protein excluded volume) to obtain as much protein information as possible. To analyze the data they used a four step protocol: *first*, data generation by the experiment; *second*, translation of the data into spatial restraints; *third*, calculation of an ensemble of structures by satisfaction of these restraints and *fourth*, an analysis of an ensemble to produce the final structure. They collected large amounts of data in order to obtain sufficient spatial restraints,

introduce appropriate tolerances to avoid over-interpretation of relatively low precision data, and include the possibility of false-positives. They tried to resolve in their structural interpretation the ambiguity of the data. Multiple copies of the same protein could be present in any architecture and any single experiment is not able to determine which of the copies of the according protein is responsible for a positive result. The final data set comprised 435 contact frequencies (“Contact frequencies reflect the likelihood that a protein interaction is formed given the data considered and are calculated from the ensemble of optimized structures”) that were assigned to each protein pair reflecting interaction data. The contact frequencies range from 0 to 1 whereas 32 protein pairs obtained a contact frequency of 1 indicating a highly probable physical interaction. Using the contact frequencies they created a three-dimensional model that combines all their data and resulted in a draft model with an estimated 5 nm resolution. The major subcomplexes, the Y-complex and the nic96-complex (NUP62-complex in vertebrates) are arranged in a horizontal cytoplasmic and a nucleoplasmic ring whereby the nic96 subcomplex is arranged in two rings between the rings containing the Y-complexes. All other nups, except the miscellaneous nups, are fitted into this model and are distributed onto and between the rings composed of Y-complex and nic96-complex. One of the restrictions of this modeling is that the Y-complex is modeled as compact rod and the coat is space-filling with very small gaps that are in clear contrast to previous published crystal data (Brohawn et al., 2009). Alber et al. performed the comprehensive analysis and determined the position of single nups as well as of subcomplexes but the specific orientation of the Y-complex remains elusive. In the publication of Fernandez-Martinez et al., 2012, the structure, function and orientation of the Y-complex was analyzed based on the results of the Alber papers and with additional integrative data. In agreement with the Alber et al. version of the

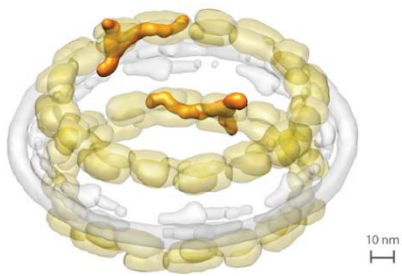


Fig 4.2 Density map of the NPC and the Y-complex (Figure of Fernandez-Martinez et al., 2012); The Y-complex structure was fitted into the NPC ensemble using the data of Alber et al., 2007 and Fernandez et al., 2012.

model, this revised model describes two Y-complexes interacting in a head-to-tail manner, but it is not described if the two Y-complexes are overlapping and where they touch each other. The Y2H results could possibly determine the touching points of the arranged Y-complexes. In total there are five validated PPIs that are suggested to be inter-Y-complex PPIs and can be fitted into the Alber model: nup120/nup120, nup120/nup84, nup85/nup133, sec13/sec13 and SEC13/SEH1. As mentioned above the Alber model suggests a head-to-tail orientation of the Y-complexes (Fig 4.2). By fitting our Y2H PPIs into this model we assume two Y-complexes that are

arranged behind each other. Both Y-complexes are connected via the PPI nup85/nup133 that was detected in the Y2H screen and validated in MST experiments and in the PCA experiments. Notably this PPI was also determined as cross species PPI with human and yeast constructs in our Y2H screen. The cross species PPI suggests a conserved function of this PPI. The hypothesis of a single ring of Y complexes in a head-to-tail orientation excludes the other four detected and validated PPIs (Fig 4.3).

The proteins are not in sufficient proximity to form interactions. If both Y-complexes are shifted upon each other the PPI nup84/nup120 could be plausible, still depending on extend of overlay. The strong β -propeller interactions of sec13/sec13 and sec13/seh1 are plausible only in a head to head overlay which allows proximity, but this prevents the nup85/nup133 interaction reasoned by the spatial distance between both proteins. According to the orientation of two overlapping Y-complexes also the PPI nup120/nup120 could be possible. In summary only the PPI nup133/nup85 is plausible and the PPI nup120/nup84 might be possible if there is a certain overlap, information that is currently missing. The three other validated PPIs: nup120/nup120, SEC13/SEC13 and SEC13/SEH1 could not be fitted into this model suggesting discordance between the model and our Y2H data.

Another model was postulated by Brohawn et al. in 2008. It is based on architectural similarities of the yeast proteins nic96, nup85, nup145C, nup84 and sec13. As discovered by Brohawn, Schwartz and co-workers, they all share a ACE fold with the occurrence of a characteristic tripartite structural element consistent of crown, trunk and tail.

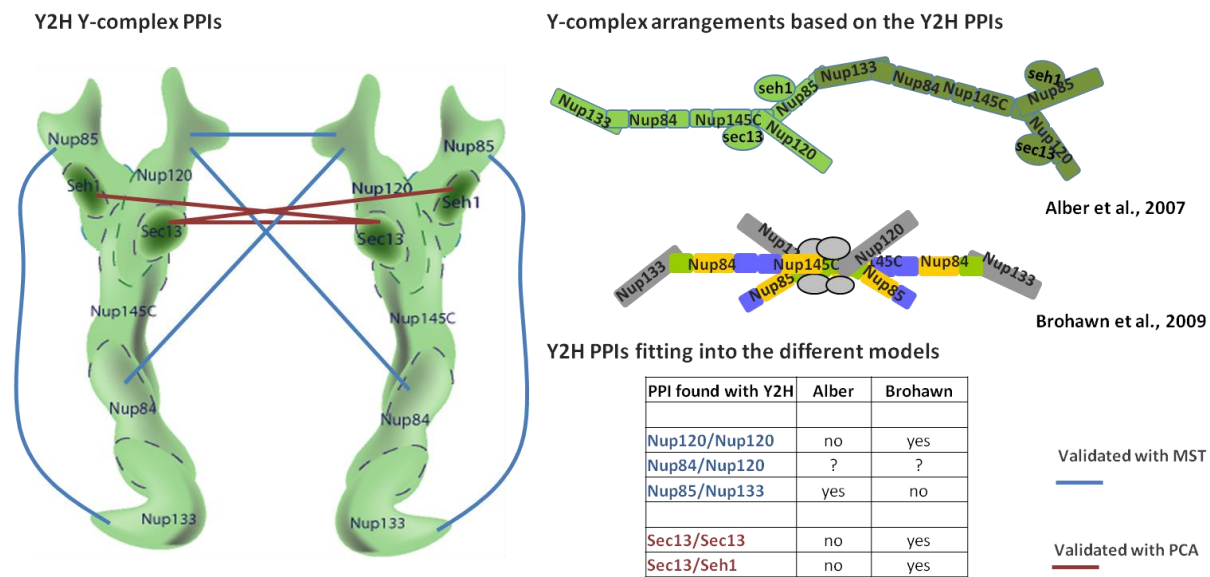


Fig 4.3 Overview of the inter-Y-complex PPIs between two Y-complexes and the models of Alber et al., 2007 and Brohawn et al., 2009; Left: there are five Y2H PPIs that are suggested to be inter-Y-complex PPIs and were validated with MST (blue links) or with PCA (red links). Right: Shown are two Y-complex arrangements based on the models of Alber and Brohawn with an overview of possible Y2H PPIs according to the model. The Y-complexes of the Brohawn model are colored according to the ACE1 elements described by Brohawn et al., 2008.

In an initial experiment the group around Brohawn solved the structure of nup85 (aa 1-564) and seh1 at a resolution of 3.5 Å. Both proteins form a heterodimer as distinct tight unit of 102 kDa. The structural studies revealed that seh1 folds into an open β -propeller structure whereby a central axis is surrounded by the six blades indicating a typical canonical β -propeller structure (Chaudhuri et al., 2008). Between the blades one and six of seh1 a β -propeller blade of the N-terminus of nup85 is inserted *in trans* that forms a three stranded blade and therefore complete the seh1 β -propeller. By following the N-terminal insertion of nup85 a cuboid structure, including 20 α -helices, forms two distinct modules comprising a trunk and a crown. The trunk is made of the α -helices 1-3 (aa 100-200) whereas the crown is made of the α -helices 4-11 (aa 362-509). The connectivity as well as the

topology of the secondary structure elements of nup85 and nup145C is remarkably similar, in contrast to the low sequence similarity of only ~10% (Brohawn et al. 2008). Nup145C also has an N-terminal three stranded β -sheet that includes a seventh blade to close the open β -propeller of sec13. The relative orientation of the domains is modestly different while the trunk and the crown modules of nup145C and nup85 are similar. Interestingly the interaction sites of sec13 and seh1 in nup145C and nup85 are the most conserved regions, indicating another similarity between both proteins. Furthermore this form of domain architecture is also found in three other proteins: nic96, nup84 and Sec31. Nic96 and nup84 are also part of the NPC whereas Sec31 is a member of the COPII coatamer. Sec31 homodimerizes and thus creates an edge element in the COPII coat where internal domains are changed between two crown molecules resulting in mixed crown modules. These mixed crown modules are identical in topology to the unmixed crowns in nup85, nup145C and nic96 (Fath et al., 2007). Since nup84 also shares module similarity that is extending beyond the trunk and the crown modules and was characterized by the Schwartz group in the C-terminus of the human homolog NUP107, the structural prediction (Phyre) also places nup84 into the group of proteins containing similar architectural modules. Because of the similarity of the architectural characteristics of crown, trunk and tail in the three nups nup145C, nup85 and nup84 as well as in the COPII coatamer protein SEC31 the tripartite structural element was called ancestral coatamer element 1 (ACE1) by Brohawn et al., 2008.

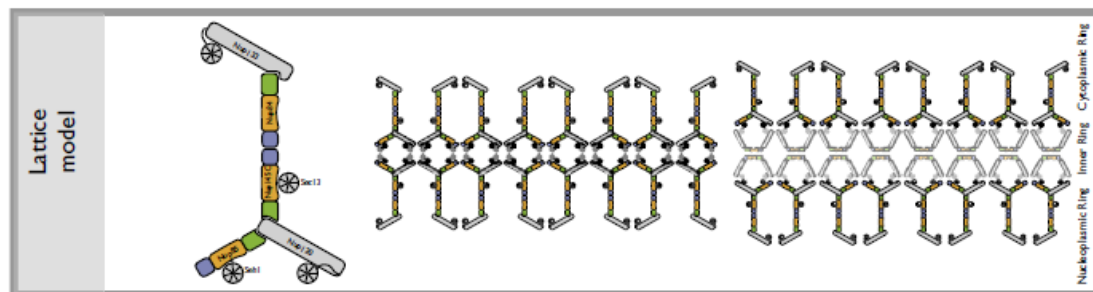


Fig 4.4 The lattice model of Brohawn et al., 2008 (Figure of Brohawn et al., 2008); The lattice model provided by Brohawn et al. is based on structural homologies represented by the ACE elements (ancestral coatamer elements) in the NPC and COPII coatamer. ACE1 proteins are colored according to their modularity: green = tail; orange = trunks; blue = crowns. Even though the illustration emphasizes the open-lattice like organization there are no specific interaction points implied. In addition the exact nature of the vertex elements remains to be seen.

While this evolutionary relationship was suggested before Brohawn et al. were able to provide strong experimental evidence (Devos et al., 2004). Predicted interaction sites (Phyre) were tested by constructing point mutations of nup84 and nup145C and experimentally validated. They found that the nup84/nup145C interaction interface is made by a crown-crown connection involving the α -helix 8 as in the SEC31 homo dimerization. In addition the tail modules of nup145C and nup85 seem to interact with nup120. In summary, two of the three interface types that are described in the COPII coat are also found in the NPC coat. Based on these similar interaction interfaces, distance constraints and stoichiometric considerations the orientation of the Y-complex was modeled: nup84 is linking nup133 with nup145C and thus connect the edge element (nup145C-sec13/nup84/nup85-seh1) containing the ACE1 element with nup133 that is pointing outward and is positioned at the periphery of the pore. The

pentamer containing nup145C-sec13/nup85-seh1/nup120 formed a symmetrical triskelion that corresponds to the vertex elements of the polygonal cages in the vesicle coats. The triskelion has approximately 20 nm distance between the tips, as measured by EM (Lutzmann et al., 2002), and when the eight Y-complexes form a ring around the central channel a diameter of 50 nm is reasonable if the edges touch at the tips (Brohawn et al., 2008) (Fig 4.4). Another possibility would include a yet unidentified adaptor protein. Because nic96 also shares an ACE1 element Brohawn et al. predicted that the inner scaffold ring is branched and lattice-like, like the peripheral rings. They postulate that the Y-complex and the nic96-complex contain vertex elements and thus build the edges in NPC scaffold architecture. In summary two Y-complexes were arranged in a head-to-head orientation in a vertical plane of the NPC (Fig 4.3). It is assumed that the NPC coat is similar to the clathrin and COP coats and as such the model is based on strong beta-propeller interactions that are also found in the COPII coatamer (Brohawn et al., 2008). Considering the Y2H and PCA results indeed these could be built by sec13/sec13 and sec13/seh1. In the model of Brohawn the small beta-propeller proteins were localized at the tip of the Y-complexes but it was suggested that sec13 and is located in the 'hub' whereas SEH1 is located close to the 'hub' (Fig 4.4)(Kampmann et al., 2009; Fernandez-Martinez et al., 2012). Therefore it is possible to arrange the Y-complexes in a head-to-head orientation but the Y-complexes must then overlap close to the 'hub'. With this overlap, two of the five inter-Y-complex PPIs could fairly match up with the model: the strong beta-propeller interaction made of the PPIs sec13/sec13 and sec13/seh1 building the basis of the model (Fig 4.3). Within this model nup120 in two Y-complexes would overlap at their N-termini, therefore come into close proximity allowing dimerization. Both N-terminal parts of nup120, aa 1-757 showed dimerization in the Y2H as well as in the MST experiments supporting the suggestion of inter Y-complex connections. The PPI nup84/nup120 is likely if there is a large overlap between two Y-complexes. Otherwise both molecules are too distant from each other to interact. Considering the PPI nup85/nup133 there is no possibility that both proteins interact indicated again by the huge distant between them. Moreover both proteins are located on the opposite sides of the two Y-complexes. The Y-complexes are orientated in a vertical plane to the NPC and nup133 would point outwards of the NPC. In summary three of the five PPIs (SEC13/SEC13, SEC13/SEH1 and nup120/nup120) fit in this model. Under certain conditions regarding the overlap of two Y-complexes, the PPI nup84/nup120 is also possible. The PPI nup85/nup133 is not plausible because nup133 is directed towards the cytoplasm and nucleoplasm and there is no possibility to connect it to nup85.

For a long time these two contrary models were used to describe the NPC subcomplex organization but obviously could not come together. The Y2H results reflect this problem very well by providing PPIs that support both models. The PPI nup85/nup133 could be fitted into the Alber model but most of the other PPIs support the model of Brohawn et al., 2008. Therefore it might be possible that there exist more than one relative Y-complex arrangement within the NPC.

4.3.4 Inter-Y-complex interactions can contribute to 16mer inner ring formation – Bui et al., 2013

As described above previous work provides substantial insight into the structural arrangement of the NPC subcomplexes (Alber et al., 2007; Brohawn et al., 2008). However the field is lacking direct structural evidence. Bui et al. named two obstacles that should overcome the determination of the arrangement of subcomplexes within the NPC: *first*, the resolution of tomography of the entire NPC should be enhanced to fit in single particle structures obtained from isolated subcomplexes and *second*, the discrimination between inter- and intra-subcomplex protein contact sites (Bui et al., 2013). To investigate the exact 3D orientation and stoichiometry of the Y-complex within the human NPC several techniques such as cryo-tomography, electron tomography, single-particle electron microscopy, and cross linking mass spectrometry were applied that should finally bridge the various length scales of tomography and high resolution data such as crystallographic data. Bui et al. distinguished inter- from intra-complex connections with cross linking MS on either isolated Y-complexes or on intact NPCs. Further phosphorylation sites were identified which seem to be responsible for NPC architecture. The sites were identified mostly at inter-subcomplex interfaces. To reconstruct the Y-complex a systematic, template-matching-based search was performed to determine the position and orientation of the highly ordered vertex within the tomographic electron optical density of one subunit of the NPC. This procedure was repeated 30 000 times with random starting positions resulting in identification of two pairs of exactly symmetric positions of the highly ordered vertex in the nuclear and cytoplasmic rings. Finally the study resulted in a model of NPC architecture based on the arrangement of the Y-complex. The resolution of the scaffold structure could be enhanced down to 32 Å (3.2 nm). Based on their results Bui et al. places eight Y-complexes in a ring. There are two rings of Y-complexes at the cytoplasmic site and two rings at the nucleoplasmic site resulting in rings of 16 copies of Y-complexes. The inner and outer Y-complexes are shifted by 11 nm along the long axis and are orientated in a 55° angle to the nuclear envelope plane. The longer arm of the Y-complex consisting of NUP160 (nup120 in invertebrates) is pointing towards the membrane whereas the shorter arm (NUP85) points toward the inner channel of the NPC (Fig 4.7). Notably this is one of the first specific models proposing touching points of the Y-complex. The Y-complex was visualized via a density map viewer in the data base EMD (entry: 2445).

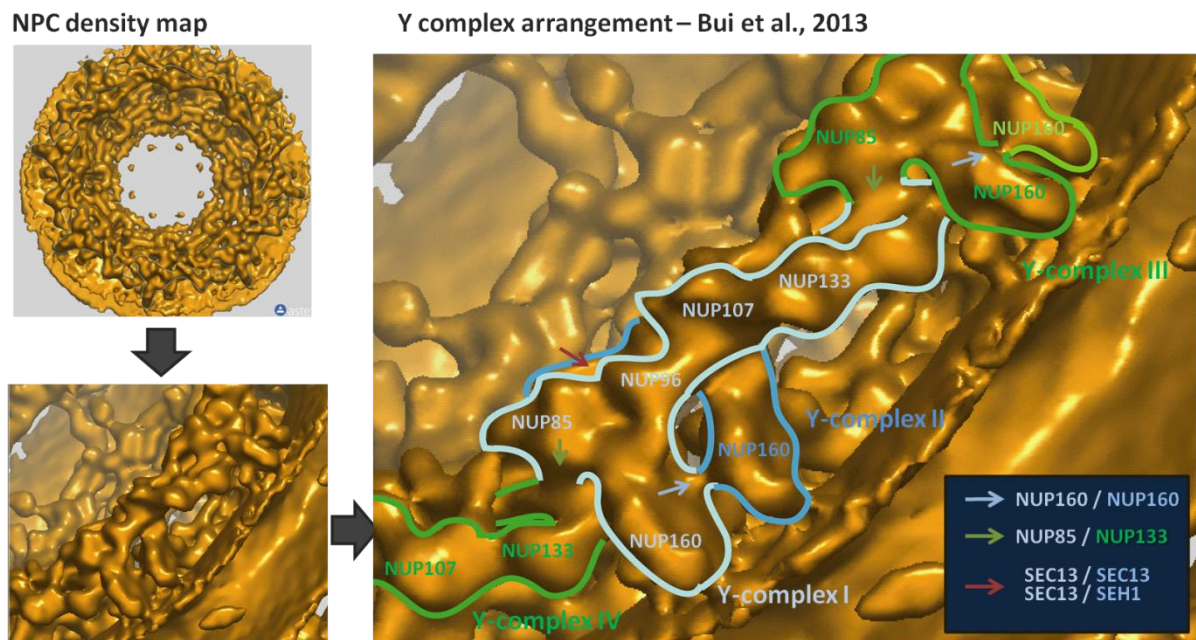


Fig 4.5 NPC density map of the cytoplasmic ring of the NPC made by Bui et al., 2013. Top left: density map of the entire NPC from the cytoplasmic side. Down left: the density map in higher resolution – the Y-complex is visible. Right: density map with visualized Y-complex indicated by different colors and the according nups. The proposed interaction sites are indicated by blue and red arrows and are listed in the box.

Even though the resolution is high enough to visualize the Y-complex within the NPC it is not high enough to reach atomic resolution and thus to see interaction sites. However, the proposed orientation is visible and connections can be suggested. The descriptions of Bui et al. suggested that the Y-complexes are arranged behind each other in an overlapping head-to-tail orientation (Fig 4.7). The overlap occurs close to the ‘hub’. The two Y-complexes are shifted towards each other by approximately 11 nm. The ‘hub’ of the inner Y-complex is located behind the stem of the outer Y-complex. Additionally the Y-complexes are not planar orientated; they are at an angle of 55° to the nuclear envelope plane. By analyzing the electron densities of the cytoplasmic side of the human NPC scaffold the Y-complex was discernible in the map viewer. Two Y-complexes (I and II) are shifted towards each other whereas the ‘hub’ of the inner Y-complex II is located behind the ‘hub’ of Y-complex I in the region of NUP96/sec13 (nup145C in invertebrates). This position enables the detected β-propeller interactions SEC13/SEH1 and SEC13/NUP37 whereas SEC13 is located at the center of the ‘hub’ and NUP37 and SEH1 are more distantly positioned directed towards the arms (see dark red arrows in Fig 4.7). However the SEC13/NUP37 and SEC13/SEH1 β-propeller interactions will likely not occur simultaneously. The arrangement of the Y-complexes I and II behind each other brings NUP160 of the inner Y-complex in proximity to NUP160 of the outer Y-complex (Y-complex I and Y-complex II) that could be visualized in the density map viewer (see blue arrows in Fig 4.7). This connection is consistent with the nup120/nup120 homo-meric PPI found in our Y2H screen and with the MST approach with a K_D of 3-5 μM. There is another PPI that is made possible by the mutual shift of the inner and outer Y-complex, namely NUP107/NUP160 (nup84/nup120 in invertebrates).

This PPI was found in our yeast Y2H screen and was recapitulated in our MST experiments with a K_D of 1-2 μM . However this connection is not visible in the density map viewer since it is hidden between the Y-complexes I and II. In summary three PPIs could be realized by the arrangement of Y-complex I and II that are both parts of two distinct rings, the inner and the outer cytoplasmic ring. However the density map also reveals connections between Y-complexes of the outer ring that are arranged behind each other, namely Y-complex I and III. Thus Y-complex III is interacting with Y-complex I at one visible point namely NUP85/NUP133 (green arrows in Fig 4.5). This PPI is one of the best characterized PPIs in the entire study. It was detected in the Y2H screen, measured with a biophysically method with an affinity of $> 3 \mu\text{M}$ and could be visualized in intact human cells at the nuclear rim. In the density map it seems to be the major bridge between Y-complex I and III and likely also between II and IV (difficult to visualize in the map). In summary it seems that the PPIs NUP160/NUP160 (nup120/nup120 in invertebrates), SEH1/SEC13, SEC13/SEC13 and NUP107/NUP160 (nup84/nup120 in invertebrates) are connecting the two shifted Y-complexes I and II whereas NUP85/NUP133 connects two Y-complexes I and III which are arranged behind each other (Fig 4.5). Thus the inter-molecular Y-complex interactions describe connections between three Y-complexes of the outer and inner cytoplasmic scaffold ring. Even though the inter-Y-complex PPIs can be well fitted into the structural model of NPC architecture proposed by Bui et al. other configurations might also be possible considering the relatively low resolution of 32 \AA° . The nucleoplasmic ring could contain a different Y-complex arrangement since the electron density and seems to be different in both NPC scaffold structures. This is in agreement with the previous idea of the dynamic structure of the NPC reasoned by different local symmetry (Brohawn et al., 2009; Grossmann et al., 2012). Taken together more configurations of Y-complex arrangement might exist than seen in the density map viewer supporting the NPC flexibility.

The model of Bui et al., builds a bridge between the head-to-head model of Brohawn et al., and the head-to-tail model postulated by Alber et al. because it arranges the Y-complex in an overlapping way where the two Y-complexes come into close proximity close to their ‘hubs’ (Fig 4.5). It suggests that more than two relative Y-complex arrangements might exist within the NPC enabling the five validated human and yeast Y2H PPIs: SEC13/SEC13, SEC13/SEH1, nup85/nup133, nup120/nup120 and nup120/nup84.

4.3.3 Summary of the investigation of the binary PPIs of the human and the yeast NPC

The nuclear pore complex is, with an estimated molecular weight of 60 MDa in yeast and 120MDa in human one of the largest protein assemblies of the cell (Peters, 2005). It controls the transport of molecules between nucleoplasm and cytoplasm whereby smaller molecules ($< 40 \text{ kDa}$) can freely

diffuse through the pore whereas larger molecules are actively transported (Cook et al., 2007). Its molecular organization is suggested to be based on the largest subcomplex, the Y-complex resulting in different models Alber et al., 2007; Brohawn et al., 2008; Bui et al., 2013). The lattice model based on evolutionary considerations places the Y-complex in a perpendicular head-to-head orientation to the nuclear envelope plane whereas the Alber model proposed a horizontal head-to-tail arrangement of the Y-complex (Alber et al., 2007; Brohawn et al., 2008). The latest model supports neither both models (Bui et al., 2013). Moreover it places the Y-complex in a 55° angle to the nuclear envelope and combines both models indicating that both previous models contains features that might reflect certain structural features of the dynamic NPC structure. The elusive knowledge is mostly reasoned by the resolution gap of previous used methods like cryo-tomography experiments (3-5 nm) and crystallization studies (atomic resolution) (Grossmann et al., 2012). To address common limitations we applied an intense Y2H screen investigating the binary protein-protein interactions which might emerge insight into the direct connections between the subcomplexes (Rout et al., 2000; Cronshaw et al., 2002; Alber et al., 2007; Brohawn et al., 2009). Besides yeast full length constructs the Y2H screen included fragments of yeast nucleoporins (nups) and several construct of human full length nups resulting in a network comprising 44 PPIs between 26 yeast nups and 16 PPIs between 15 human nups. While benchmarking of the yeast Y2H data set against different previous published data sets we confirmed highly reliable data. In addition several PPIs were recapitulated with independent cell-based and biophysical experiments (protein-complementation assay for the human PPIs and MST for the yeast PPIs). The Y2H screen revealed direct connections between all subcomplexes and the linker nups and even five novel inter-Y-complex PPIs were unraveled. The data were used to scrutinize current structural models. We could reconcile our inter Y-complex Y2H PPIs in the latest model proposed by Bui et al., though many uncertainties remain, in particular steric constraint may arise that could exclude proposed interactions in the suggested arrangements. However, our validated inter Y-complex interactions allow the conclusion that more than two relative Y-complex positions within the NPC must exist. Taken together the Y2H interaction map will assist structural work on subcomplexes and may provide crucial information to overcome the resolution gap between the structural view at atomic resolution and the supramolecular NPC assembly.

4.3.4 Zusammenfassung der Untersuchung der binären Protein-Proteininteraktionen des humanen und des Hefe-Kernporenkomplexes

Der Kernporenkomplex ist, mit einer molekularen Größe von ca. 60 MDa in Hefen und 120 MDa in Vertebraten einer der größten Proteinkomplexe der Zelle (Peters, 2005). Er kontrolliert den Molekültransport zwischen Zellkern und Zytoplasma wobei kleinere Moleküle (< 40 kDa) frei hindurch diffundieren, während größere Moleküle (> 40 kDa) aktiv transportiert werden. Der

Kernporenkomplex ist aus mehreren Kopien dreier Subkomplexe (Y-Komplex, NUP62-Komplex und NUP93-Komplex) sowie Linker-NUPS und transient angelagerte NUPS zusammengesetzt, wobei deren relative Position innerhalb des Komplexes noch diskutiert wird. Der Aufbau des gesamten Komplexes wird in verschiedenen Modellen diskutiert. Deren Grundlage ist die Position des größten Subkomplexes: des Y-Komplexes (Alber et al., 2007, Brohawn et al., 2008; Bui et al., 2013). Das „lattice-model“ schlägt eine senkrecht zur Kernmembran angeordnete Kopf-an-Kopf (head-to-head) Position zweier Y-Komplexe vor (Brohwan et al., 2008). Alber et al. hingegen postuliert eine horizontale, Kopf-zu-Schwanz (head-to-tail) Position mehrerer Y-Komplexe. Das neueste Modell positioniert Y-Komplexe in zwei horizontale Ringe, die jeweils aus acht Y-Komplexen bestehen (Bui et al., 2013). Die Y-Komplexe sind in einem Winkel von 55° zur Kernmembran angeordnet. So gesehen bildet das Bui-Modell eine Brücke zwischen Alber und Brohawn, da es Eigenschaften beider Modelle vereint. Alle Modelle basieren auf verschiedenen experimentellen Methoden. So wurde das Alber-Modell aufgrund eines integrativen Versuchsansatzes postuliert während das Brohawn-Modell auf Kristalldaten beruht. Zwischen den Ergebnissen beider Ansätze klafft eine Auflösungslücke (Cryo-Tomographie = 3-5nm; Krystallographie = atomare Auflösung) (Grossmann et al., 2012). Wir haben ein Hefe-2-Hybrid Experiment ausgeführt, welches dazu benutzt werden kann, diese Auflösungslücke zu umgehen, indem es binäre Protein-Protein Interaktionen identifiziert und damit Einblick in direkte Kontakte zwischen Subkomplexen gewährt. Neben Hefe- und Humanenproteinkonstrukten in voller Länge wurden auch Hefeproteinfragmente eingesetzt, die in ein Netzwerk aus 44 PPIs zwischen 26 Hefeproteinen und 16 PPIs zwischen 15 Humanen Proteinen resultieren. Die Validierung der Hefe Proteininteraktionen gegen zwei weitere binäre Netzwerke ergab ein zuverlässiges Hefenetzwerk. Der Hefe-2-Hybrid Versuch zeigte direkte Verbindungen innerhalb einzelner Subkomplexe sowie zwischen ihnen. Ausgewählte humane und Hefe-Proteininteraktionen, die Verbindungen zwischen zwei Y-Komplexen beschrieben, wurden zudem experimentell mit unabhängigen Zell-basierten bzw. Protein-basierten Methoden bestätigt (humane Interaktionen – Protein Komplementierungs Test; Hefe-Interaktionen – Micro-scale Thermophoresis). Die resultierenden Daten wurden benutzt, um die bestehenden Modelle eingehend zu prüfen. Dabei wurde festgestellt, dass die Hefe-2-Hybrid Proteininteraktionen vornehmlich mit dem Bui-Modell übereinstimmen. Dennoch bleiben Ungewissheiten zurück, insbesondere bezüglich der räumlichen Anordnung, die die vorgeschlagenen Interaktionen ausschließt beziehungsweise nicht eindeutig unterstützt. Dennoch erlauben erhaltenen Hefe-2-Hybrid Proteininteraktionen die Schlussfolgerung, dass es mehr als zwei mögliche Y-Komplexanordnungen innerhalb des NPC geben kann. Zusammengefasst unterstützen die gewonnenen Daten die strukturelle Arbeit am Kernporenkomplex und stellen wichtige Informationen, die die bisherige Auflösungslücke zwischen atomarer Auflösung und supramolekularer NPC Architektur überwinden können.

5. References

- Ahmed, S., and J. H. Brickner, 2007, Regulation and epigenetic control of transcription at the nuclear periphery: *Trends Genet.*, v. 23, p. 396-402.
- Andersen KR¹, Onischenko E, Tang JH, Kumar P, Chen JZ, Ulrich A, Liphardt JT, Weis K, Schwartz TU., 2013, Scaffold nucleoporins Nup188 and Nup192 share structural and functional properties with nuclear transport receptors: *Elife*, e00745.
- Akey, C., Radermacher, M., 1993, Architecture of the Xenopus nuclear pore complex revealed by three-dimensional cryo-electron microscopy: *J Cell Biol.*, v. 122, p. 1-19.
- Alber, F., S. Dokudovskaya, L. M. Veenhoff, W. Zhang, J. Kipper, D. Devos, A. Suprapto, O. Karni-Schmidt, R. Williams, B. T. Chait, M. P. Rout, and A. Sali, 2007a, Determining the architectures of macromolecular assemblies: *Nature*, v. 450, p. 683-94.
- Alber, F., S. Dokudovskaya, L. M. Veenhoff, W. Zhang, J. Kipper, D. Devos, A. Suprapto, O. Karni-Schmidt, R. Williams, B. T. Chait, A. Sali, and M. P. Rout, 2007b, The molecular architecture of the nuclear pore complex: *Nature*, v. 450, p. 695-701.
- Amlacher, S., P. Sarges, D. Flemming, V. van Noort, R. Kunze, D. P. Devos, M. Arumugam, P. Bork, and E. Hurt, 2011a, Insight into structure and assembly of the nuclear pore complex by utilizing the genome of a eukaryotic thermophile: *Cell*, v. 146, p. 277-89.
- Badano JL¹, Ansley SJ, Leitch CC, Lewis RA, Lupski JR, Katsanis N, Identification of a novel Bardet-Biedl syndrome protein, BBS7, that shares structural features with BBS1 and BBS2: *Am J Hum Genet*, v. 3, p. 650-8.
- Bagley, S., M. W. Goldberg, J. M. Cronshaw, S. Rutherford, and T. D. Allen, 2000, The nuclear pore complex: *J Cell Sci*, v. 113 (Pt 22), p. 3885-6.
- Bandyopadhyay, S.; Chiang, C. Y.; Srivastava, J.; Gersten, M.; White, S.; Bell, R.; Kurschner, C.; Martin, C. H.; Smoot, M.; Sahasrabudhe, S.; Barber, D. L.; Chanda, S. K. and Ideker, T., 2010, A human MAP kinase interactome: *Nat Methods*, v. 7, p. 801-5.
- Bailer, S. M., C. Balduf, and E. Hurt, 2001, The Nsp1p carboxy-terminal domain is organized into functionally distinct coiled-coil regions required for assembly of nucleoporin subcomplexes and nucleocytoplasmic transport: *Mol Cell Biol*, v. 21, p. 7944-55.
- Bailer, S. M., C. Balduf, J. Katahira, A. Podtelejnikov, C. Rollenhagen, M. Mann, N. Pante, and E. Hurt, 2000, Nup116p associates with the Nup82p-Nsp1p-Nup159p nucleoporin complex: *J Biol Chem*, v. 275, p. 23540-8.
- Bailer, S. M., S. Siniossoglou, A. Podtelejnikov, A. Hellwig, M. Mann, and E. Hurt, 1998, Nup116p and nup100p are interchangeable through a conserved motif which constitutes a docking site for the mRNA transport factor gle2p: *EMBO J*, v. 17, p. 1107-19.
- Braun, P.; Tasan, M.; Dreze, M.; Barrios-Rodiles, M.; Lemmens, I.; Yu, H.; Sahalie, J. M.; Murray, R. R.; Roncari, L.; de Smet, A. S.; Venkatesan, K.; Rual, J. F.; Vandenhoute, J.; Cusick, M. E.; Pawson,

T.; Hill, D. E.; Tavernier, J.; Wrana, J. L.; Roth, F. P. and Vidal, M., 2009, An experimentally derived confidence score for binary proteinprotein interactions: *Nat Methods*, v. 6, p. 91-7.

Beck, M., F. Förster, M. Ecke, J. M. Plitzko, F. Melchior, G. Gerisch, W. Baumeister, and O. Medalia, 2004, Nuclear pore complex structure and dynamics revealed by cryoelectron tomography: *Science*, v. 306, p. 1387-90.

Beck M¹, Lucić V, Förster F, Baumeister W, Medalia O., 2007, Snapshots of nuclear pore complexes in action captured by cryo-electron tomography: *Nature*, v. 449, p. 611-615.

Belgareh, N., G. Rabut, S. W. Baï, M. van Overbeek, J. Beaudouin, N. Daigle, O. V. Zatsepina, F. Pasteau, V. Labas, M. Fromont-Racine, J. Ellenberg, and V. Doye, 2001a, An evolutionarily conserved NPC subcomplex, which redistributes in part to kinetochores in mammalian cells: *J Cell Biol*, v. 154, p. 1147-60.

Belgareh, N., C. Snay-Hodge, F. Pasteau, S. Dagher, C. N. Cole, and V. Doye, 1998, Functional characterization of a Nup159p-containing nuclear pore subcomplex: *Mol Biol Cell*, v. 9, p. 3475-92.

Berke, I. C., T. Boehmer, G. Blobel, and T. U. Schwartz, 2004, Structural and functional analysis of Nup133 domains reveals modular building blocks of the nuclear pore complex: *J Cell Biol*, v. 167, p. 591-7.

Bilokapic S, Schwartz TU., 2012, 3D ultrastructure of the nuclear pore complex: *Curr Opin Cell Biol*, v. 24, p. 86-91.

Bilokapic, S., and T. U. Schwartz, 2013, Structural and functional studies of the 252 kDa nucleoporin ELYS reveal distinct roles for its three tethered domains: *Structure*, v. 21, p. 572-80.

Bilokapic, S., and T. U. Schwartz, 2013, Molecular basis for Nup37 and ELY5/ELYS recruitment to the nuclear pore: *PNAS*, v. 109 p. 15241-15246.

Bodoor, K., S. Shaikh, P. Enarson, S. Chowdhury, D. Salina, W. H. Raharjo, and B. Burke, 1999, Function and assembly of nuclear pore complex proteins: *Biochem Cell Biol*, v. 77, p. 321-9.

Boehmer, T., S. Jeudy, I. C. Berke, and T. U. Schwartz, 2008, Structural and functional studies of Nup107/Nup133 interaction and its implications for the architecture of the nuclear pore complex: *Mol Cell*, v. 30, p. 721-31.

Boehmer, T., and T. U. Schwartz, 2007, Purification, crystallization and preliminary X-ray analysis of a Nup107-Nup133 heterodimeric nucleoporin complex: *Acta Crystallogr Sect F Struct Biol Cryst Commun*, v. 63, p. 816-8.

Brohawn, S. G., N. C. Leksa, E. D. Spear, K. R. Rajashankar, and T. U. Schwartz, 2008, Structural evidence for common ancestry of the nuclear pore complex and vesicle coats: *Science*, v. 322, p. 1369-73.

Brohawn, S. G., J. R. Partridge, J. R. Whittle, and T. U. Schwartz, 2009, The nuclear pore complex has entered the atomic age: *Structure*, v. 17, p. 1156-68.

Brohawn, S. G., and T. U. Schwartz, 2009a, A lattice model of the nuclear pore complex: *Commun Integr Biol*, v. 2, p. 205-7.

Brohawn, S. G., and T. U. Schwartz, 2009b, Molecular architecture of the Nup84-Nup145C-Sec13 edge element in the nuclear pore complex lattice: *Nat Struct Mol Biol*, v. 16, p. 1173-7.

Brückner, A., C. Polge, N. Lentze, D. Auerbach, and U. Schlattner, 2009, Yeast two-hybrid, a powerful tool for systems biology: *Int J Mol Sci*, v. 10, p. 2763-88.

Bui KH¹, von Appen A, DiGuilio AL, Ori A, Sparks L, Mackmull MT, Bock T, Hagen W, Andrés-Pons A, Glavy JS, Beck M., 2013, Integrated structural analysis of the human nuclear pore complex scaffold: *Cell*, v. 155, p. 1233-1243.

Capelson, M., Y. Liang, R. Schulte, W. Mair, U. Wagner, and M. W. Hetzer, 2010, Chromatin-bound nuclear pore components regulate gene expression in higher eukaryotes: *Cell*, v. 140, p. 372-83.

Carmi R¹, Elbedour K, Stone EM, Sheffield VC., 1995, Phenotypic differences among patients with Bardet-Biedl syndrome linked to three different chromosome loci, *Am J Med Genet*, v. 59, p. 199-203.

Chaudhuri, I., J. Söding, and A. N. Lupas, 2008, Evolution of the beta-propeller fold: *Proteins*, v. 71, p. 795-803.

Chen, Y. C., S. V. Rajagopala, T. Stellberger, and P. Uetz, 2010, Exhaustive benchmarking of the yeast two-hybrid system: *Nat Methods*, v. 7, p. 667-8; author reply 668.

Chial, H. J., M. P. Rout, T. H. Giddings, and M. Winey, 1998, *Saccharomyces cerevisiae* Ndc1p is a shared component of nuclear pore complexes and spindle pole bodies: *J Cell Biol*, v. 143, p. 1789-800.

Chiang, A. P., D. Nishimura, C. Searby, K. Elbedour, R. Carmi, A. L. Ferguson, J. Secrist, T. Braun, T. Casavant, E. M. Stone, and V. C. Sheffield, 2004, Comparative genomic analysis identifies an ADP-ribosylation factor-like gene as the cause of Bardet-Biedl syndrome (BBS3): *Am J Hum Genet*, v. 75, p. 475-84.

Chien CT¹, Bartel PL, Sternglanz R, Fields S., 1991, The two-hybrid system: a method to identify and clone genes for proteins that interact with a protein of interest: *PNAS*, v. 88, p. 9578-9582.

Chook, Y. M., and G. Blobel, 2001, Karyopherins and nuclear import: *Curr Opin Struct Biol*, v. 11, p. 703-15.

Chook, Y. M., A. Jung, M. K. Rosen, and G. Blobel, 2002a, Uncoupling Kapbeta2 substrate dissociation and ran binding: *Biochemistry*, v. 41, p. 6955-66.

Chook, Y. M., A. Jung, M. K. Rosen, and G. Blobel, 2002b, Uncoupling Kapbeta2 substrate dissociation and ran binding: *Biochemistry*, v. 41, p. 6955-66.

Cook, A., F. Bono, M. Jinek, and E. Conti, 2007a, Structural biology of nucleocytoplasmic transport: *Annu Rev Biochem*, v. 76, p. 647-71.

Cook, A. G., and E. Conti, 2010, Nuclear export complexes in the frame: *Curr Opin Struct Biol*, v. 20, p. 247-52.

D'Angelo, M. A., D. J. Anderson, E. Richard, and M. W. Hetzer, 2006a, Nuclear pores form de novo from both sides of the nuclear envelope: *Science*, v. 312, p. 440-3.

D'Angelo MA¹, Hetzer MW., 2008, Structure, dynamics and function of nuclear pore complexes: *Trends Cell Biol.*, v. 18, p. 456-466.

Dange, T., D. Grünwald, A. Grünwald, R. Peters, and U. Kubitscheck, 2008, Autonomy and robustness of translocation through the nuclear pore complex: a single-molecule study: *J Cell Biol*, v. 183, p. 77-86.

Debler, E. W., G. Blobel, and A. Hoelz, 2009, Nuclear transport comes full circle: *Nat Struct Mol Biol*, v. 16, p. 457-9.

Debler, E. W., K. C. Hsia, V. Nagy, H. S. Seo, and A. Hoelz, 2010a, Characterization of the membrane-coating Nup84 complex: paradigm for the nuclear pore complex structure: *Nucleus*, v. 1, p. 150-7.

Debler, E. W., Y. Ma, H. S. Seo, K. C. Hsia, T. R. Noriega, G. Blobel, and A. Hoelz, 2008, A fence-like coat for the nuclear pore membrane: *Mol Cell*, v. 32, p. 815-26.

DeGrasse, J. A., K. N. DuBois, D. Devos, T. N. Siegel, A. Sali, M. C. Field, M. P. Rout, and B. T. Chait, 2009, Evidence for a shared nuclear pore complex architecture that is conserved from the last common eukaryotic ancestor: *Mol Cell Proteomics*, v. 8, p. 2119-30.

Devos, D., S. Dokudovskaya, F. Alber, R. Williams, B. T. Chait, A. Sali, and M. P. Rout, 2004a, Components of coated vesicles and nuclear pore complexes share a common molecular architecture: *PLoS Biol*, v. 2, p. e380.

Devos, D., S. Dokudovskaya, R. Williams, F. Alber, N. Eswar, B. T. Chait, M. P. Rout, and A. Sali, 2006a, Simple fold composition and modular architecture of the nuclear pore complex: *Proc Natl Acad Sci U S A*, v. 103, p. 2172-7.

Dingwall, C., S. Kandels-Lewis, and B. Séraphin, 1995, A family of Ran binding proteins that includes nucleoporins: *Proc Natl Acad Sci U S A*, v. 92, p. 7525-9.

Dishinger, J. F., H. L. Kee, and K. J. Verhey, 2013, Analysis of ciliary import: *Methods Enzymol*, v. 524, p. 75-89.

Doye V., 2011, Mitotic phosphorylation of nucleoporins: Dismantling NPC and beyond: *Cell*, v. 20, p. 281-282.

Dultz, E., E. Zanin, C. Wurzenberger, M. Braun, G. Rabut, L. Sironi, and J. Ellenberg, 2008, Systematic kinetic analysis of mitotic dis- and reassembly of the nuclear pore in living cells: *J Cell Biol*, v. 180, p. 857-65.

Fahrenkrog, B., and U. Aebi, 2002, The vertebrate nuclear pore complex: from structure to function: *Results Probl Cell Differ*, v. 35, p. 25-48.

Fahrenkrog, B., E. C. Hurt, U. Aebi, and N. Panté, 1998a, Molecular architecture of the yeast nuclear pore complex: localization of Nsp1p subcomplexes: *J Cell Biol*, v. 143, p. 577-88.

Fahrenkrog, B., E. C. Hurt, U. Aebi, and N. Panté, 1998b, Molecular architecture of the yeast nuclear pore complex: localization of Nsp1p subcomplexes: *J Cell Biol*, v. 143, p. 577-88.

Fahrenkrog, B., W. Hübner, A. Mandinova, N. Panté, W. Keller, and U. Aebi, 2000a, The yeast nucleoporin Nup53p specifically interacts with Nic96p and is directly involved in nuclear protein import: *Mol Biol Cell*, v. 11, p. 3885-96.

Fahrenkrog, B., W. Hübner, A. Mandinova, N. Panté, W. Keller, and U. Aebi, 2000b, The yeast nucleoporin Nup53p specifically interacts with Nic96p and is directly involved in nuclear protein import: *Mol Biol Cell*, v. 11, p. 3885-96.

Fahrenkrog, B., B. Maco, A. M. Fager, J. Köser, U. Sauder, K. S. Ullman, and U. Aebi, 2002, Domain-specific antibodies reveal multiple-site topology of Nup153 within the nuclear pore complex: *J Struct Biol*, v. 140, p. 254-67.

Fan, Y., M. A. Esmail, S. J. Ansley, O. E. Blacque, K. Boroevich, A. J. Ross, S. J. Moore, J. L. Badano, H. May-Simera, D. S. Compton, J. S. Green, R. A. Lewis, M. M. van Haelst, P. S. Parfrey, D. L. Baillie, P. L. Beales, N. Katsanis, W. S. Davidson, and M. R. Leroux, 2004, Mutations in a member of the Ras superfamily of small GTP-binding proteins causes Bardet-Biedl syndrome: *Nat Genet*, v. 36, p. 989-93.

Fath S, Mancias JD, Bi X, Goldberg J., 2007, Structure and organization of coat proteins in the COPII cage: *Cell*, v. 129, p. 1325-1236.

Fernandez-Martinez, J., J. Phillips, M. D. Sekedat, R. Diaz-Avalos, J. Velazquez-Muriel, J. D. Franke, R. Williams, D. L. Stokes, B. T. Chait, A. Sali, and M. P. Rout, 2012, Structure-function mapping of a heptameric module in the nuclear pore complex: *J Cell Biol*, v. 196, p. 419-34.

Feuerbach, F., V. Galy, E. Trelles-Sticken, M. Fromont-Racine, A. Jacquier, E. Gilson, J. C. Olivo-Marin, H. Scherthan, and U. Nehrbass, 2002, Nuclear architecture and spatial positioning help establish transcriptional states of telomeres in yeast: *Nat Cell Biol*, v. 4, p. 214-21.

Flemming, D., D. P. Devos, J. Schwarz, S. Amlacher, M. Lutzmann, and E. Hurt, 2012a, Analysis of the yeast nucleoporin Nup188 reveals a conserved S-like structure with similarity to karyopherins: *J Struct Biol*, v. 177, p. 99-105.

Flemming, D., P. Sarges, P. Stelter, A. Hellwig, B. Böttcher, and E. Hurt, 2009, Two structurally distinct domains of the nucleoporin Nup170 cooperate to tether a subset of nucleoporins to nuclear pores: *J Cell Biol*, v. 185, p. 387-95.

Fotin A, Cheng Y, Sliz P, Grigorieff N, Harrison SC, Kirchhausen T, Walz T., 2004, Molecular model for a complete clathrin lattice from electron cryomicroscopy: *Nature*, v. 432, p. 573-579.

Franz, C., R. Walczak, S. Yavuz, R. Santarella, M. Gentzel, P. Askjaer, V. Galy, M. Hetzer, I. W. Mattaj, and W. Antonin, 2007, MEL-28/ELYS is required for the recruitment of nucleoporins to chromatin and postmitotic nuclear pore complex assembly: *EMBO Rep*, v. 8, p. 165-72.

Frenkiel-Krispin, D., B. Maco, U. Aebi, and O. Medalia, 2010, Structural analysis of a metazoan nuclear pore complex reveals a fused concentric ring architecture: *J Mol Biol*, v. 395, p. 578-86.

Gall, J. G., 1967, Octagonal nuclear pores: *J Cell Biol*, v. 32, p. 391-9.

Galy, V., J. C. Olivo-Marin, H. Scherthan, V. Doye, N. Rascalou, and U. Nehrbass, 2000, Nuclear pore complexes in the organization of silent telomeric chromatin: *Nature*, v. 403, p. 108-12.

Giot, L.; Bader, J. S.; Brouwer, C.; Chaudhuri, A.; Kuang, B.; Li, Y.; Hao, Y. L.; Ooi, C. E.; Godwin, B.; Vitols, E.; Vijayadamodar, G.; Pochart, P.; Machineni, H.; Welsh, M.; Kong, Y.; Zerhusen, B.; Malcolm, R.; Varrone, Z.; Collis, A.; Minto, M.; Burgess, S.; McDaniel, L.; Stimpson, E.; Spriggs, F.; Williams, J.; Neurath, K.; Ioime, N.; Agee, M.; Voss, E.; Furtak, K.; Renzulli, R.; Aanensen, N.;

Carrolla, S.; Bickelhaupt, E.; Lazovatsky, Y.; DaSilva, A.; Zhong, J.; Stanyon, C. A.; Finley, R. L., Jr.; White, K. P.; Braverman, M.; Jarvie, T.; Gold, S.; Leach, M.; Knight, J.; Shimkets, R. A.; McKenna, M. P.; Chant, J. and Rothberg, J. M., 2003, A protein interaction map of *Drosophila melanogaster*: *Science*, v. 302 , p. 1727-36.

Goetz, S. C., and K. V. Anderson, 2010, The primary cilium: a signalling centre during vertebrate development: *Nat Rev Genet*, v. 11, p. 331-44.

Goldberg, M. W., and T. D. Allen, 1993, The nuclear pore complex: three-dimensional surface structure revealed by field emission, in-lens scanning electron microscopy, with underlying structure uncovered by proteolysis: *J Cell Sci*, v. 106 (Pt 1), p. 261-74.

Goldberg, M. W., and T. D. Allen, 1996, The nuclear pore complex and lamina: three-dimensional structures and interactions determined by field emission in-lens scanning electron microscopy: *J Mol Biol*, v. 257, p. 848-65.

Goehler, H.; Lalowski, M.; Stelzl, U.; Waelter, S.; Stroedicke, M.; Worm, U.; Droege, A.; Lindenberg, K. S.; Knoblich, M.; Haenig, C.; Herbst, M.; Suopanki, J.; Scherzinger, E.; Abraham, C.; Bauer, B.; Hasenbank, R.; Fritzsche, A.; Ludewig, A. H.; Bussow, K.; Coleman, S. H.; Gutekunst, C. A.; Landwehrmeyer, B. G.; Lehrach, H. and Wanker, E. E., 2004, A protein interaction network links GIT1, an enhancer of huntingtin aggregation, to Huntington's disease: *Mol Cell*, v. 15, p. 853-65.

Goshima N, Kawamura Y, Fukumoto A, Miura A, Honma R, Satoh R, Wakamatsu A, Yamamoto J, Kimura K, Nishikawa T, Andoh T, Iida Y, Ishikawa K, Ito E, Kagawa N, Kaminaga C, Kanehori K, Kawakami B, Kenmochi K, Kimura R, Kobayashi M, Kuroita T, Kuwayama H, Maruyama Y, Matsuo K, Minami K, Mitsubori M, Mori M, Morishita R, Murase A, Nishikawa A, Nishikawa S, Okamoto T, Sakagami N, Sakamoto Y, Sasaki Y, Seki T, Sono S, Sugiyama A, Sumiya T, Takayama T, Takayama Y, Takeda H, Togashi T, Yahata K, Yamada H, Yanagisawa Y, Endo Y, Imamoto F, Kisu Y, Tanaka S, Isogai T, Imai J, Watanabe S, Nomura N., 2008, Human protein factory for converting the transcriptome into an in vitro-expressed proteome: *Nat Methods*, v. 5, p. 1011-1017.

Grandi, P., T. Dang, N. Pané, A. Shevchenko, M. Mann, D. Forbes, and E. Hurt, 1997, Nup93, a vertebrate homologue of yeast Nic96p, forms a complex with a novel 205-kDa protein and is required for correct nuclear pore assembly: *Mol Biol Cell*, v. 8, p. 2017-38.

Grandi, P., V. Doye, and E. C. Hurt, 1993, Purification of NSP1 reveals complex formation with 'GLFG' nucleoporins and a novel nuclear pore protein NIC96: *EMBO J*, v. 12, p. 3061-71.

Grandi, P., S. Emig, C. Weise, F. Hucho, T. Pohl, and E. C. Hurt, 1995a, A novel nuclear pore protein Nup82p which specifically binds to a fraction of Nsp1p: *J Cell Biol*, v. 130, p. 1263-73.

Grandi, P., N. Schlaich, H. Tekotte, and E. C. Hurt, 1995b, Functional interaction of Nic96p with a core nucleoporin complex consisting of Nsp1p, Nup49p and a novel protein Nup57p: *EMBO J*, v. 14, p. 76-87.

Green JS, Parfrey PS, Harnett JD, Farid NR, Cramer BC, Johnson G, Heath O, McManamon PJ, O'Leary E, Pryse-Phillips W., 1989, The cardinal manifestations of Bardet-Biedl syndrome, a form of Laurence-Moon-Biedl syndrome: *N Engl J Med*, v. 321, p. 1002-1009.

Grossman E¹, Medalia O, Zwerger M., 2012, Functional architecture of the nuclear pore complex: *Annu Rev Biophys*, v. 41, p. 557-584.

Hallberg, E., R. W. Wozniak, and G. Blobel, 1993, An integral membrane protein of the pore membrane domain of the nuclear envelope contains a nucleoporin-like region: *J Cell Biol*, v. 122, p. 513-21.

Harel, A., A. V. Orjalo, T. Vincent, A. Lachish-Zalait, S. Vasu, S. Shah, E. Zimmerman, M. Elbaum, and D. J. Forbes, 2003, Removal of a single pore subcomplex results in vertebrate nuclei devoid of nuclear pores: *Mol Cell*, v. 11, p. 853-64.

Hartwell LH, Hopfield JJ, Leibler S, Murray AW, From molecular to modular cell biology: *Nature*, v. 402, p. 47-52.

Havugimana PC, Hart GT, Nepusz T, Yang H, Turinsky AL, Li Z, Wang PI, Boutz DR, Fong V, Phanse S, Babu M, Craig SA, Hu P, Wan C, Vlasblom J, Dar VU, Bezginov A, Clark GW, Wu GC, Wodak SJ, Tillier ER, Paccanaro A, Marcotte EM, Emili A., 2012, A census of human soluble protein complexes: *Cell*, v. 150, p. 1068-1081.

Hegele, A., A. Kamburov, A. Grossmann, C. Sourlis, S. Wowro, M. Weimann, C. L. Will, V. Pena, R. Lührmann, and U. Stelzl, 2012, Dynamic protein-protein interaction wiring of the human spliceosome: *Mol Cell*, v. 45, p. 567-80.

Hinshaw, J. E., B. O. Carragher, and R. A. Milligan, 1992, Architecture and design of the nuclear pore complex: *Cell*, v. 69, p. 1133-41.

Hinshaw, J. E., and R. A. Milligan, 2003, Nuclear pore complexes exceeding eightfold rotational symmetry: *J Struct Biol*, v. 141, p. 259-68.

Ho, A. K., T. X. Shen, K. J. Ryan, E. Kiseleva, M. A. Levy, T. D. Allen, and S. R. Wente, 2000, Assembly and preferential localization of Nup116p on the cytoplasmic face of the nuclear pore complex by interaction with Nup82p: *Mol Cell Biol*, v. 20, p. 5736-48.

Hoelz, A., and G. Blobel, 2004, Cell biology: popping out of the nucleus: *Nature*, v. 432, p. 815-6.

Hoelz, A., E. W. Debler, and G. Blobel, 2011, The structure of the nuclear pore complex: *Annu Rev Biochem*, v. 80, p. 613-43.

Hrabe T¹, Chen Y, Pfeffer S, Cuellar LK, Mangold AV, Förster F., 2012, PyTom: a python-based toolbox for localization of macromolecules in cryo-electron tomograms and subtomogram analysis: *J Struct Biol*, v. 178, p. 177-188.

Hsia KC¹, Stavropoulos P, Blobel G, Hoelz A., 2007, Architecture of a coat for the nuclear pore membrane: *Cell*, v. 131, p. 1313-1326.

Hu, Q., L. Milenkovic, H. Jin, M. P. Scott, M. V. Nachury, E. T. Spiliotis, and W. J. Nelson, 2010a, A septin diffusion barrier at the base of the primary cilium maintains ciliary membrane protein distribution: *Science*, v. 329, p. 436-9.

Huangfu, D., A. Liu, A. S. Rakeman, N. S. Murcia, L. Niswander, and K. V. Anderson, 2003, Hedgehog signalling in the mouse requires intraflagellar transport proteins: *Nature*, v. 426, p. 83-7.

Hurd, T. W., S. Fan, and B. L. Margolis, 2011, Localization of retinitis pigmentosa 2 to cilia is regulated by Importin beta2: *J Cell Sci*, v. 124, p. 718-26.

Iovine, M. K., J. L. Watkins, and S. R. Wente, 1995, The GLFG repetitive region of the nucleoporin Nup116p interacts with Kap95p, an essential yeast nuclear import factor: *J Cell Biol*, v. 131, p. 1699-713.

Iovine, M. K., and S. R. Wente, 1997, A nuclear export signal in Kap95p is required for both recycling the import factor and interaction with the nucleoporin GLFG repeat regions of Nup116p and Nup100p: *J Cell Biol*, v. 137, p. 797-811.

Ito, T., T. Chiba, R. Ozawa, M. Yoshida, M. Hattori, and Y. Sakaki, 2001, A comprehensive two-hybrid analysis to explore the yeast protein interactome: *Proc Natl Acad Sci U S A*, v. 98, p. 4569-74.

Jarnik, M., and U. Aebi, 1991a, Toward a more complete 3-D structure of the nuclear pore complex: *J Struct Biol*, v. 107, p. 291-308.

Jerabek-Willemsen, M., C. J. Wienken, D. Braun, P. Baaske, and S. Duhr, 2011, Molecular interaction studies using microscale thermophoresis: *Assay Drug Dev Technol*, v. 9, p. 342-53.

Jeudy, S., and T. U. Schwartz, 2007, Crystal structure of nucleoporin Nic96 reveals a novel, intricate helical domain architecture: *J Biol Chem*, v. 282, p. 34904-12.

Jin, H., S. R. White, T. Shida, S. Schulz, M. Aguiar, S. P. Gygi, J. F. Bazan, and M. V. Nachury, 2010, The conserved Bardet-Biedl syndrome proteins assemble a coat that traffics membrane proteins to cilia: *Cell*, v. 141, p. 1208-19.

Kampmann, M., C. E. Atkinson, A. L. Mattheyses, and S. M. Simon, 2011, Mapping the orientation of nuclear pore proteins in living cells with polarized fluorescence microscopy: *Nat Struct Mol Biol*, v. 18, p. 643-9.

Kampmann, M., and G. Blobel, 2009, Three-dimensional structure and flexibility of a membrane-coating module of the nuclear pore complex: *Nat Struct Mol Biol*, v. 16, p. 782-8.

Katsanis, N., 2004, The oligogenic properties of Bardet-Biedl syndrome: *Hum Mol Genet*, v. 13 Spec No 1, p. R65-71.

Katsanis, N., P. L. Beales, M. O. Woods, R. A. Lewis, J. S. Green, P. S. Parfrey, S. J. Ansley, W. S. Davidson, and J. R. Lupski, 2000, Mutations in MKKS cause obesity, retinal dystrophy and renal malformations associated with Bardet-Biedl syndrome: *Nat Genet*, v. 26, p. 67-70.

Kee, H. L., J. F. Dishinger, T. L. Blasius, C. J. Liu, B. Margolis, and K. J. Verhey, 2012a, A size-exclusion permeability barrier and nucleoporins characterize a ciliary pore complex that regulates transport into cilia: *Nat Cell Biol*, v. 14, p. 431-7.

Kim, Badano Jose L, Sonja Sibold, Munneer A Esmail, Josephine Hill, Bethan E Hoskins, Carmen C Leitch, Kerrie Venner, Stephen J Ansley, Alison J Ross, Michel R Leroux, Nicholas Katsanis & Philip L Beales, The Bardet-Biedl protein BBS4 targets cargo to the pericentriolar region and is required for microtubule anchoring and cell cycle progression: *Nature Genet*, v. 36, p. 462-470.

Kiseleva, E., M. W. Goldberg, T. D. Allen, and C. W. Akey, 1998, Active nuclear pore complexes in Chironomus: visualization of transporter configurations related to mRNP export: *J Cell Sci*, v. 111 (Pt 2), p. 223-36.

Kiseleva E., Rutherford S., Cotter LM, Allen TD, Goldberg MW, 2001, Steps of nuclear pore complex disassembly and reassembly during mitosis in early Drosophila embryos: *J Cell Sci*, v 114 (Pt 20), p. 3607-18.

Kosova, B., N. Panté, C. Rollenhagen, and E. Hurt, 1999, Nup192p is a conserved nucleoporin with a preferential location at the inner site of the nuclear membrane: *J Biol Chem*, v. 274, p. 22646-51.

Kubota, H., G. Hynes, and K. Willison, 1995, The chaperonin containing t-complex polypeptide 1 (TCP-1). Multisubunit machinery assisting in protein folding and assembly in the eukaryotic cytosol: *Eur J Biochem*, v. 230, p. 3-16.

Kwitek-Black AE¹, Carmi R, Duyk GM, Buetow KH, Elbedour K, Parvari R, Yandava CN, Stone EM, Sheffield VC., 1993, Linkage of Bardet-Biedl syndrome to chromosome 16q and evidence for non-allelic genetic heterogeneity: *Nat Genet*, v. 5, p. 392-396.

Lalonde, S.; Ehrhardt, D. W.; Loque, D.; Chen, J.; Rhee, S. Y. and Frommer, W. B., 2008, Molecular and cellular approaches for the detection of protein-protein interactions: latest techniques and current limitations: *Plant J*, v. 53, p. 610-35.

Lamesch, P., S. Milstein, T. Hao, J. Rosenberg, N. Li, R. Sequerra, S. Bosak, L. Doucette-Stamm, J. Vandenhoute, D. E. Hill, and M. Vidal, 2004a, *C. elegans* ORFeome version 3.1: increasing the coverage of ORFeome resources with improved gene predictions: *Genome Res*, v. 14, p. 2064-9.

Lamesch, P., S. Milstein, T. Hao, J. Rosenberg, N. Li, R. Sequerra, S. Bosak, L. Doucette-Stamm, J. Vandenhoute, D. E. Hill, and M. Vidal, 2004b, *C. elegans* ORFeome version 3.1: increasing the coverage of ORFeome resources with improved gene predictions: *Genome Res*, v. 14, p. 2064-9.

Laurell, E., K. Beck, K. Krupina, G. Theerthagiri, B. Bodenmiller, P. Horvath, R. Aebersold, W. Antonin, and U. Kutay, 2011, Phosphorylation of Nup98 by multiple kinases is crucial for NPC disassembly during mitotic entry: *Cell*, v. 144, p. 539-50.

Leducq, J. B., G. Charron, G. Diss, I. Gagnon-Arsenault, A. K. Dubé, and C. R. Landry, 2012a, Evidence for the robustness of protein complexes to inter-species hybridization: *PLoS Genet*, v. 8, p. e1003161.

Leksa, N. C., S. G. Brohawn, and T. U. Schwartz, 2009a, The structure of the scaffold nucleoporin Nup120 reveals a new and unexpected domain architecture: *Structure*, v. 17, p. 1082-91.

Leppert M¹, Baird L, Anderson KL, Otterud B, Lupski JR, Lewis RA., 1994, Bardet-Biedl syndrome is linked to DNA markers on chromosome 11q and is genetically heterogeneous: *Nat Genet*, v. 7, p. 108-112.

Li, S.; Armstrong, C. M.; Bertin, N.; Ge, H.; Milstein, S.; Boxem, M.; Vidalain, P. O.; Han, J. D.; Chesneau, A.; Hao, T.; Goldberg, D. S.; Li, N.; Martinez, M.; Rual, J. F.; Lamesch, P.; Xu, L.; Tewari, M.; Wong, S. L.; Zhang, L. V.; Berriz, G. F.; Jacotot, L.; Vaglio, P.; Reboul, J.; Hirozane-Kishikawa, T.; Li, Q.; Gabel, H. W.; Elewa, A.; Baumgartner, B.; Rose, D. J.; Yu, H.; Bosak, S.; Sequerra, R.; Fraser, A.; Mango, S. E.; Saxton, W. M.; Strome, S.; Van Den Heuvel, S.; Piano, F.; Vandenhoute, J.; Sardet, C.; Gerstein, M.; Doucette-Stamm, L.; Gunsalus, K. C.; Harper, J. W.; Cusick, M. E.; Roth, F. P.; Hill, D. E. and Vidal, M., 2004, A map of the interactome network of the metazoan *C. elegans*: *Science*, v. 303, p. 540-3.

Liu X¹, Mitchell JM, Wozniak RW, Blobel G, Fan J., 2012, Structural evolution of the membrane-coating module of the nuclear pore complex: Proc Natl Acad Sci, v 41, p. 16498-503

Loiodice I¹, Alves A, Rabut G, Van Overbeek M, Ellenberg J, Sibarita JB, Doye V., 2004, The entire Nup107-160 complex, including three new members, is targeted as one entity to kinetochores in mitosis: Mol. Biol. Cell, v. 15, p. 3333-3344.

Loktev, A. V., Q. Zhang, J. S. Beck, C. C. Seaby, T. E. Scheetz, J. F. Bazan, D. C. Slusarski, V. C. Sheffield, P. K. Jackson, and M. V. Nachury, 2008, A BBSome subunit links ciliogenesis, microtubule stability, and acetylation: Dev Cell, v. 15, p. 854-65.

Lutzmann M¹, Kunze R, Buerer A, Aebl U, Hurt E., 2002, Modular self-assembly of a Y-shaped multiprotein complex from seven nucleoporins: EMBO, v. 3, p. 387-97.

Lutzmann, M., R. Kunze, K. Stangl, P. Stelter, K. F. Tóth, B. Böttcher, and E. Hurt, 2005, Reconstitution of Nup157 and Nup145N into the Nup84 complex: J Biol Chem, v. 280, p. 18442-51.

Macara IG., 2001, Transport in and out of the nucleus: Microbiol. Mol. Biol. Rev, v. 65, p. 570-594.

Macaulay C¹, Meier E, Forbes DJ., 1995, Differential mitotic phosphorylation of proteins of the nuclear pore complex: J Biol Chem, v. 270, p 254-262.

Mackay JP, Sunde M, Lowry JA, Crossley M, Matthews JM., 2007, Protein interactions: is seeing believing?: Trends Biochem Sci, v. 32, p. 530-531.

Magliery, T. J.; Wilson, C. G.; Pan, W.; Mishler, D.; Ghosh, I.; Hamilton, A. D. and Regan, L., 2005, Detecting proteinprotein interactions with a green fluorescent protein fragment reassembly trap: scope and mechanism: J Am Chem Soc, v. 127, p. 146-57.

Maimon T¹, Elad N, Dahan I, Medalia O., 2012, The human nuclear pore complex as revealed by cryo-electron tomography: Structure, v. 20, p. 998-1006.

Makio T¹, Stanton LH, Lin CC, Goldfarb DS, Weis K, Wozniak RW., 2009, The nucleoporins Nup170p and Nup157p are essential for nuclear pore complex assembly: J Cell Biol., v. 185, p. 459-473.

Mans BJ, Anantharaman V, Aravind L, Koonin EV., 2004, Comparative genomics, evolution and origins of the nuclear envelope and nuclear pore complex: Cell Cycle, v. 3, p. 1612–37.

Mansfeld, J., S. Güttinger, L. A. Hawryluk-Gara, N. Panté, M. Mall, V. Galy, U. Haselmann, P. Mühlhäuser, R. W. Wozniak, I. W. Mattaj, U. Kutay, and W. Antonin, 2006a, The conserved transmembrane nucleoporin NDC1 is required for nuclear pore complex assembly in vertebrate cells: Mol Cell, v. 22, p. 93-103.

Marelli M¹, Aitchison JD, Wozniak RW., 1998, Specific binding of the karyopherin Kap121p to a subunit of the nuclear pore complex containing Nup53p, Nup59p, and Nup170p: J Cell Biol, v. 143, p. 1813-1830.

Maruyama Y¹, Kawamura Y, Nishikawa T, Isogai T, Nomura N, Goshima N., 2012, HGPD: Human gene and protein database, 2012 update: Nucleic Acid Res, v. 40, p. 924-929.

McLane, L. M., and A. H. Corbett, 2009, Nuclear localization signals and human disease: IUBMB Life, v. 61, p. 697-706.

Melcák I, Hoelz A, Blobel G., 2007, Structure of Nup58/45 suggests flexible nuclear pore diameter by intermolecular sliding: *Science*, v. 315, p. 1729-1732.

Michnick SW¹, Ear PH, Manderson EN, Remy I, Stefan E., Universal strategies in research and drug discovery based on protein-fragment complementation assays: *Nat Rev Drug Discov*, v. 6, p. 569-582.

Montpetit B, Thomsen ND, Helmke KJ, Seeliger MA, Berger JM, Weis K., 2011, A conserved mechanism of DEAD-box ATPase activation by nucleoporins and InsP6 in mRNA export: *Nature*, v. 472, p. 238-242.

Mykytyn, K., R. F. Mullins, M. Andrews, A. P. Chiang, R. E. Swiderski, B. Yang, T. Braun, T. Casavant, E. M. Stone, and V. C. Sheffield, 2004, Bardet-Biedl syndrome type 4 (BBS4)-null mice implicate Bbs4 in flagella formation but not global cilia assembly: *Proc Natl Acad Sci U S A*, v. 101, p. 8664-9.

Nachury, M. V., 2008, Tandem affinity purification of the BBSome, a critical regulator of Rab8 in ciliogenesis: *Methods Enzymol*, v. 439, p. 501-13.

Nachury, M. V., A. V. Loktev, Q. Zhang, C. J. Westlake, J. Peränen, A. Merdes, D. C. Slusarski, R. H. Scheller, J. F. Bazan, V. C. Sheffield, and P. K. Jackson, 2007, A core complex of BBS proteins cooperates with the GTPase Rab8 to promote ciliary membrane biogenesis: *Cell*, v. 129, p. 1201-13.

Nachury, M. V., E. S. Seeley, and H. Jin, 2010, Trafficking to the ciliary membrane: how to get across the periciliary diffusion barrier?: *Annu Rev Cell Dev Biol*, v. 26, p. 59-87.

Nachury, M., 2010, Maxence Nachury: a transporting view of the primary cilium. Interview by Ben Short: *J Cell Biol*, v. 191, p. 436-7.

Nagai, T.; Ibata, K.; Park, E. S.; Kubota, M.; Mikoshiba, K. and Miyawaki, A., 2002, A variant of yellow fluorescent protein with fast and efficient maturation for cell-biological applications: *Nat Biotechnol*, v. 20, p. 87-90.

Nagy, V., K. C. Hsia, E. W. Debler, M. Kampmann, A. M. Davenport, G. Blobel, and A. Hoelz, 2009a, Structure of a trimeric nucleoporin complex reveals alternate oligomerization states: *Proc Natl Acad Sci U S A*, v. 106, p. 17693-8.

Nagy, V., K. C. Hsia, E. W. Debler, M. Kampmann, A. M. Davenport, G. Blobel, and A. Hoelz, 2009b, Structure of a trimeric nucleoporin complex reveals alternate oligomerization states: *Proc Natl Acad Sci U S A*, v. 106, p. 17693-8.

Nagy, V., K. C. Hsia, E. W. Debler, M. Kampmann, A. M. Davenport, G. Blobel, and A. Hoelz, 2009c, Structure of a trimeric nucleoporin complex reveals alternate oligomerization states: *Proc Natl Acad Sci U S A*, v. 106, p. 17693-8.

Nakayama, M.; Kikuno, R. and Ohara, O., 2002, Protein-protein interactions between large proteins: two-hybrid screening using a functionally classified library composed of long cDNAs: *Genome Res*, v. 12, p. 1773-84.

Nehrbass, U., M. P. Rout, S. Maguire, G. Blobel, and R. W. Wozniak, 1996, The yeast nucleoporin Nup188p interacts genetically and physically with the core structures of the nuclear pore complex: *J Cell Biol*, v. 133, p. 1153-62.

Neumann, N., D. Lundin, and A. M. Poole, 2010, Comparative genomic evidence for a complete nuclear pore complex in the last eukaryotic common ancestor: PLoS One, v. 5, p. e13241.

Niforou KM¹, Anagnostopoulos AK, Vougas K, Kittas C, Gorgoulis VG, Tsangaris GT., 2008, The proteome profile of the human osteosarcoma U2OS cell line: Cancer Genomics Proteomics, v. 5, p. 63-78.

Obado, S. O., and M. P. Rout, 2012a, Ciliary and nuclear transport: different places, similar routes?: Dev Cell, v. 22, p. 693-4.

Onischenko, E., L. H. Stanton, A. S. Madrid, T. Kieselbach, and K. Weis, 2009, Role of the Ndc1 interaction network in yeast nuclear pore complex assembly and maintenance: J Cell Biol, v. 185, p. 475-91.

Ou G, Blacque OE, Snow JJ, Leroux MR, Scholey JM., 2005, Functional coordination of intraflagellar transport motors: Nature, v. 436, p. 583-587.

Palancade, B., X. Liu, M. Garcia-Rubio, A. Aguilera, X. Zhao, and V. Doye, 2007, Nucleoporins prevent DNA damage accumulation by modulating Ulp1-dependent sumoylation processes: Mol Biol Cell, v. 18, p. 2912-23.

Paoli, M., 2001, Protein folds propelled by diversity: Prog Biophys Mol Biol, v. 76, p. 103-30.

Pascual-Garcia, P., and M. Capelson, 2014, Nuclear pores as versatile platforms for gene regulation: Curr Opin Genet Dev, v. 25C, p. 110-117.

Paulillo, S. M., E. M. Phillips, J. Köser, U. Sauder, K. S. Ullman, M. A. Powers, and B. Fahrenkrog, 2005, Nucleoporin domain topology is linked to the transport status of the nuclear pore complex: J Mol Biol, v. 351, p. 784-98.

Peters, R., 2005, Translocation through the nuclear pore complex: selectivity and speed by reduction-of-dimensionality: Traffic, v. 6, p. 421-7.

Rabut, G., V. Doye, and J. Ellenberg, 2004, Mapping the dynamic organization of the nuclear pore complex inside single living cells: Nat Cell Biol, v. 6, p. 1114-21.

Rakowska, A., T. Danker, S. W. Schneider, and H. Oberleithner, 1998, ATP-Induced shape change of nuclear pores visualized with the atomic force microscope: J Membr Biol, v. 163, p. 129-36.

Rasala Beth A., Orjalo Arturo V., Shen Zhouxin, Briggs Steven, . Forbes Douglass J, 2006, ELYS is a dual nucleoporin/kinetochore protein required for nuclear pore assembly and proper cell division: PNAS, v. 103, p. 17801-17806.

Ratner, G. A., A. E. Hodel, and M. A. Powers, 2007, Molecular determinants of binding between Gly-Leu-Phe-Gly nucleoporins and the nuclear pore complex: J Biol Chem, v. 282, p. 33968-76.

Reboul J¹, Vaglio P, Rual JF, Lamesch P, Martinez M, Armstrong CM, Li S, Jacotot L, Bertin N, Janky R, Moore T, Hudson JR Jr, Hartley JL, Brasch MA, Vandenhoute J, Boulton S, Endress GA, Jenna S, Chevet E, Papasotiropoulos V, Tolias PP, Ptacek J, Snyder M, Huang R, Chance MR, Lee H, Doucette-Stamm L, Hill DE, Vidal M., 2003, C. elegans ORFeome version 1.1: experimental verification of the genome annotation and resource for proteome-scale protein expression: Nat Genet, v. 34, p. 35-41.

Remy I, Michnick SW., 2004, Mapping biochemical networks with protein-fragment complementation assays, *Methods Mol Biol*, v. 261, p. 411-426.

Reichelt, R., A. Holzenburg, E. L. Buhle, M. Jarnik, A. Engel, and U. Aebi, 1990, Correlation between structure and mass distribution of the nuclear pore complex and of distinct pore complex components: *J Cell Biol*, v. 110, p. 883-94.

Ribbeck, K., and D. Görlich, 2001, Kinetic analysis of translocation through nuclear pore complexes: *EMBO J*, v. 20, p. 1320-30.

Ris H¹, Malecki M., 1993, High-resolution field emission scanning electron microscope imaging of internal cell structures after Epon extraction from sections: a new approach to correlative ultrastructural and immunocytochemical studies: *J Struct Biol*, v. 111, p. 148-157.

Rout, M. P., J. D. Aitchison, A. Suprapto, K. Hjertaas, Y. Zhao, and B. T. Chait, 2000a, The yeast nuclear pore complex: composition, architecture, and transport mechanism: *J Cell Biol*, v. 148, p. 635-51.

Rout, M. P., and G. Blobel, 1993, Isolation of the yeast nuclear pore complex: *J Cell Biol*, v. 123, p. 771-83.

Rual, J. F., T. Hirozane-Kishikawa, T. Hao, N. Bertin, S. Li, A. Dricot, N. Li, J. Rosenberg, P. Lamesch, P. O. Vidalain, T. R. Clingingsmith, J. L. Hartley, D. Esposito, D. Cheo, T. Moore, B. Simmons, R. Sequerra, S. Bosak, L. Doucette-Stamm, C. Le Peuch, J. Vandenhoute, M. E. Cusick, J. S. Albala, D. E. Hill, and M. Vidal, 2004, Human ORFeome version 1.1: a platform for reverse proteomics: *Genome Res*, v. 14, p. 2128-35.

Ruthenburg AJ¹, Li H, Patel DJ, Allis CD., 2007, Multivalent engagement of chromatin modifications by linking binding modules: *Nat Rev Mol Cell Biol*, v. 8, p. 983-994.

Ryan KJ¹, Wente SR, Isolation and characterization of new *Saccharomyces cerevisiae* mutants perturbed in nuclear pore complex assembly: *BMC Genet*, v. 3:17.

Sampathkumar P¹, Kim SJ, Upla P, Rice WJ, Phillips J, Timney BL, Pieper U, Bonanno JB, Fernandez-Martinez J, Hakhverdyan Z, Ketaren NE, Matsui T, Weiss TM, Stokes DL, Sauder JM, Burley SK, Sali A, Rout MP, Almo SC., 2013, Structure, dynamics, evolution, and function of a major scaffold component in the nuclear pore complex: *Structure*, v. 4, p. 560-71.

Schlaich, N. L., M. Häner, A. Lustig, U. Aebi, and E. C. Hurt, 1997a, In vitro reconstitution of a heterotrimeric nucleoporin complex consisting of recombinant Nsp1p, Nup49p, and Nup57p: *Mol Biol Cell*, v. 8, p. 33-46.

Schrader, N., P. Stelter, D. Flemming, R. Kunze, E. Hurt, and I. R. Vetter, 2008, Structural basis of the nic96 subcomplex organization in the nuclear pore channel: *Mol Cell*, v. 29, p. 46-55.

Seo, H. S., Y. Ma, E. W. Debler, D. Wacker, S. Kutik, G. Blobel, and A. Hoelz, 2009a, Structural and functional analysis of Nup120 suggests ring formation of the Nup84 complex: *Proc Natl Acad Sci U S A*, v. 106, p. 14281-6.

Seo, S., Q. Zhang, K. Bugge, D. K. Breslow, C. C. Searby, M. V. Nachury, and V. C. Sheffield, 2011, A novel protein LZTFL1 regulates ciliary trafficking of the BBSome and Smoothened: *PLoS Genet*, v. 7, p. e1002358.

Siniossoglou, S., M. Lutzmann, H. Santos-Rosa, K. Leonard, S. Mueller, U. Aebi, and E. Hurt, 2000, Structure and assembly of the Nup84p complex: *J Cell Biol*, v. 149, p. 41-54.

Siniossoglou, S., C. Wimmer, M. Rieger, V. Doye, H. Tekotte, C. Weise, S. Emig, A. Segref, and E. C. Hurt, 1996, A novel complex of nucleoporins, which includes Sec13p and a Sec13p homolog, is essential for normal nuclear pores: *Cell*, v. 84, p. 265-75.

Solmaz, S. R., R. Chauhan, G. Blobel, and I. Melčák, 2011, Molecular architecture of the transport channel of the nuclear pore complex: *Cell*, v. 147, p. 590-602.

Spiess, C., A. S. Meyer, S. Reissmann, and J. Frydman, 2004, Mechanism of the eukaryotic chaperonin: protein folding in the chamber of secrets: *Trends Cell Biol*, v. 14, p. 598-604.

Stagg SM, LaPointe P, Balch WE., 2007, Structural design of cage and coat scaffolds that direct membrane traffic: *Curr Opin Struct Biol*, v. 17, p. 221-228.

Stavru, F., B. B. Hülsmann, A. Spang, E. Hartmann, V. C. Cordes, and D. Görlich, 2006a, NDC1: a crucial membrane-integral nucleoporin of metazoan nuclear pore complexes: *J Cell Biol*, v. 173, p. 509-19.

Stavru, F., G. Naustrup-Pedersen, V. C. Cordes, and D. Görlich, 2006b, Nuclear pore complex assembly and maintenance in POM121- and gp210-deficient cells: *J Cell Biol*, v. 173, p. 477-83.

Stelzl, U., and E. E. Wanker, 2006, The value of high quality protein-protein interaction networks for systems biology: *Curr Opin Chem Biol*, v. 10, p. 551-8.

Stelzl, U., U. Worm, M. Lalowski, C. Haenig, F. H. Brembeck, H. Goehler, M. Stroedicke, M. Zenkner, A. Schoenherr, S. Koeppen, J. Timm, S. Mintzlaff, C. Abraham, N. Bock, S. Kietzmann, A. Goedde, E. Toksöz, A. Droege, S. Krobitsch, B. Korn, W. Birchmeier, H. Lehrach, and E. E. Wanker, 2005, A human protein-protein interaction network: a resource for annotating the proteome: *Cell*, v. 122, p. 957-68.

Stein A¹, Mosca R, Aloy P., 2011, Three-dimensional modeling of protein interactions and complexes is going 'omics: *Curr Opin Struct Biol*, v. 21, p.200-208.

Stoetzel, C., J. Muller, V. Laurier, E. E. Davis, N. A. Zaghloul, S. Vicaire, C. Jacquelain, F. Plewniak, C. C. Leitch, P. Sarda, C. Hamel, T. J. de Ravel, R. A. Lewis, E. Friederich, C. Thibault, J. M. Danse, A. Verloes, D. Bonneau, N. Katsanis, O. Poch, J. L. Mandel, and H. Dollfus, 2007, Identification of a novel BBS gene (BBS12) highlights the major role of a vertebrate-specific branch of chaperonin-related proteins in Bardet-Biedl syndrome: *Am J Hum Genet*, v. 80, p. 1-11.

Stoffler, D., B. Fahrenkrog, and U. Aebi, 1999a, The nuclear pore complex: from molecular architecture to functional dynamics: *Curr Opin Cell Biol*, v. 11, p. 391-401.

Stoffler, D., B. Fahrenkrog, and U. Aebi, 1999b, The nuclear pore complex: from molecular architecture to functional dynamics: *Curr Opin Cell Biol*, v. 11, p. 391-401.

Stoffler, D., B. Feja, B. Fahrenkrog, J. Walz, D. Typke, and U. Aebi, 2003, Cryo-electron tomography provides novel insights into nuclear pore architecture: implications for nucleocytoplasmic transport: *J Mol Biol*, v. 328, p. 119-30.

Strambio-De-Castillia, C., M. Niepel, and M. P. Rout, 2010, The nuclear pore complex: bridging nuclear transport and gene regulation: *Nat Rev Mol Cell Biol*, v. 11, p. 490-501.

Strawn, L. A., T. Shen, N. Shulga, D. S. Goldfarb, and S. R. Wente, 2004, Minimal nuclear pore complexes define FG repeat domains essential for transport: *Nat Cell Biol*, v. 6, p. 197-206.

Tarassov, K.; Messier, V.; Landry, C. R.; Radinovic, S.; Serna Molina, M. M.; Shames, I.; Malitskaya, Y.; Vogel, J.; Bussey, H. and Michnick, S. W., 2008, An in vivo map of the yeast protein interactome: *Science* 320, p. 1465-70.

Theerthagiri G, Eisenhardt N, Schwarz H, Antonin W., 2010, The nucleoporin Nup188 controls passage of membrane proteins across the nuclear pore complex: *J Cell Biol*, v. 189, p. 1129-1142.

Teixeira, M. T., E. Fabre, and B. Dujon, 1999, Self-catalyzed cleavage of the yeast nucleoporin Nup145p precursor: *J Biol Chem*, v. 274, p. 32439-44.

Teixeira, M. T., S. Siniossoglou, S. Podtelejnikov, J. C. Bénichou, M. Mann, B. Dujon, E. Hurt, and E. Fabre, 1997, Two functionally distinct domains generated by in vivo cleavage of Nup145p: a novel biogenesis pathway for nucleoporins: *EMBO J*, v. 16, p. 5086-97.

Theisen, U., A. Straube, and G. Steinberg, 2008, Dynamic rearrangement of nucleoporins during fungal "open" mitosis: *Mol Biol Cell*, v. 19, p. 1230-40.

Thierbach K, von Appen A, Thoms M, Beck M, Flemming D, Hurt E., 2013, Protein interfaces of the conserved Nup84 complex from *Chaetomium thermophilum* shown by crosslinking mass spectrometry and electron microscopy: *Structure*, v. 21., p. 1672-1682.

Tong, A. H., M. Evangelista, A. B. Parsons, H. Xu, G. D. Bader, N. Pagé, M. Robinson, S. Raghibizadeh, C. W. Hogue, H. Bussey, B. Andrews, M. Tyers, and C. Boone, 2001, Systematic genetic analysis with ordered arrays of yeast deletion mutants: *Science*, v. 294, p. 2364-8.

Townsend D, Tew K, 2003, The role of glutathione-S-transferase in anti-cancer drug resistance: *Oncogene*, v. 22, p. 7369-7375.

Uetz, P., L. Giot, G. Cagney, T. A. Mansfield, R. S. Judson, J. R. Knight, D. Lockshon, V. Narayan, M. Srinivasan, P. Pochart, A. Qureshi-Emili, Y. Li, B. Godwin, D. Conover, T. Kalbfleisch, G. Vijayadamodar, M. Yang, M. Johnston, S. Fields, and J. M. Rothberg, 2000, A comprehensive analysis of protein-protein interactions in *Saccharomyces cerevisiae*: *Nature*, v. 403, p. 623-7.

Uetz, P., and R. E. Hughes, 2000, Systematic and large-scale two-hybrid screens: *Curr Opin Microbiol*, v. 3, p. 303-8.

Unwin PN, Milligan RA., 1982, A large particle associated with the perimeter of the nuclear pore complex: *J Cell Biol*, v. 93, p. 63-75.

Ulrich, A., J. R. Partridge, and T. U. Schwartz, 2014a, The stoichiometry of the Nup62 subcomplex of the nuclear pore in solution: *Mol Biol Cell*.

Ulrich, A., J. R. Partridge, and T. U. Schwartz, 2014b, The stoichiometry of the Nup62 subcomplex of the nuclear pore in solution: *Mol Biol Cell*.

Vasu S, Shah S, Orjalo A, Park M, Fischer WH, Forbes DJ., 2001, Novel vertebrate nucleoporins Nup133 and Nup160 play a role in mRNA export: *J. Cell. Biol.*, v. 155, p. 339-353.

Venkatesan, K.; Rual, J. F.; Vazquez, A.; Stelzl, U.; Lemmens, I.; Hirozane-Kishikawa, T.; Hao, T.; Zenkner, M.; Xin, X.; Goh, K. I.; Yildirim, M. A.; Simonis, N.; Heinzmann, K.; Gebreab, F.; Sahalie, J. M.; Cevik, S.; Simon, C.; de Smet, A. S.; Dann, E.; Smolyar, A.; Vinayagam, A.; Yu, H.; Szeto, D.; Borick, H.; Dricot, A.; Klitgord, N.; Murray, R. R.; Lin, C.; Lalowski, M.; Timm, J.; Rau, K.; Boone, C.; Braun, P.; Cusick, M. E.; Roth, F. P.; Hill, D. E.; Tavernier, J.; Wanker, E. E.; Barabasi, A. L. and Vidal, M., 2009, An empirical framework for binary interactome mapping: *Nat Methods*, v. 6, p. 83-90.

Vidal M, Cusick ME, Barabási AL, 2011, Interactome networks and human disease: *cell*, v. 144, p. 986-998.

Vogel, S. S.; Thaler, C. and Koushik, S. V., 2006, Fanciful FRET: *Sci STKE* 2006, v.331, p. re2.

Vollmer, B., and W. Antonin, 2014a, The diverse roles of the Nup93/Nic96 complex proteins - structural scaffolds of the nuclear pore complex with additional cellular functions: *Biol Chem*, v. 395, p. 515-28.

Vollmer, B., and W. Antonin, 2014b, The diverse roles of the Nup93/Nic96 complex proteins - structural scaffolds of the nuclear pore complex with additional cellular functions: *Biol Chem*, v. 395, p. 515-28.

Wagstaff, K. M., and D. A. Jans, 2009, Importins and beyond: non-conventional nuclear transport mechanisms: *Traffic*, v. 10, p. 1188-98.

Walhout, A. J., and M. Vidal, 1999, A genetic strategy to eliminate self-activator baits prior to high-throughput yeast two-hybrid screens: *Genome Res*, v. 9, p. 1128-34.

Walther, T. C., A. Alves, H. Pickersgill, I. Loiodice, M. Hetzer, V. Galy, B. B. Hülsmann, T. Köcher, M. Wilm, T. Allen, I. W. Mattaj, and V. Doye, 2003a, The conserved Nup107-160 complex is critical for nuclear pore complex assembly: *Cell*, v. 113, p. 195-206.

Walther, T. C., A. Alves, H. Pickersgill, I. Loiodice, M. Hetzer, V. Galy, B. B. Hülsmann, T. Köcher, M. Wilm, T. Allen, I. W. Mattaj, and V. Doye, 2003b, The conserved Nup107-160 complex is critical for nuclear pore complex assembly: *Cell*, v. 113, p. 195-206.

Walther, T. C., A. Alves, H. Pickersgill, I. Loiodice, M. Hetzer, V. Galy, B. B. Hülsmann, T. Köcher, M. Wilm, T. Allen, I. W. Mattaj, and V. Doye, 2003c, The conserved Nup107-160 complex is critical for nuclear pore complex assembly: *Cell*, v. 113, p. 195-206.

Walther, T. C., P. Askjaer, M. Gentzel, A. Habermann, G. Griffiths, M. Wilm, I. W. Mattaj, and M. Hetzer, 2003d, RanGTP mediates nuclear pore complex assembly: *Nature*, v. 424, p. 689-94.

Walther, T. C., P. Askjaer, M. Gentzel, A. Habermann, G. Griffiths, M. Wilm, I. W. Mattaj, and M. Hetzer, 2003e, RanGTP mediates nuclear pore complex assembly: *Nature*, v. 424, p. 689-94.

Watson ML., 1959, Further observations on the nuclear envelope of the animal cell: *J Biophys Biochem Cytol.*, v.6, p. 147-156.

Wei Q¹, Zhang Y, Li Y, Zhang Q, Ling K, Hu J., 2012, The BBSome controls IFT assembly and turnaround in cilia: *Nat Cell Biol*, v. 14, p. 950-957.

Wente, S. R., and G. Blobel, 1993, A temperature-sensitive NUP116 null mutant forms a nuclear envelope seal over the yeast nuclear pore complex thereby blocking nucleocytoplasmic traffic: *J Cell Biol*, v. 123, p. 275-84.

Wente, S. R., M. P. Rout, and G. Blobel, 1992, A new family of yeast nuclear pore complex proteins: *J Cell Biol*, v. 119, p. 705-23.

Whittle, J. R., and T. U. Schwartz, 2009, Architectural nucleoporins Nup157/170 and Nup133 are structurally related and descend from a second ancestral element: *J Biol Chem*, v. 284, p. 28442-52.

Wimmer, C., V. Doye, P. Grandi, U. Nehrbass, and E. C. Hurt, 1992, A new subclass of nucleoporins that functionally interact with nuclear pore protein NSP1: *EMBO J*, v. 11, p. 5051-61.

Worseck, J. M., A. Grossmann, M. Weimann, A. Hegele, and U. Stelzl, 2012, A stringent yeast two-hybrid matrix screening approach for protein-protein interaction discovery: *Methods Mol Biol*, v. 812, p. 63-87.

Worseck, J., 2012, Characterization of phosphorylation-dependent interactions involving neurofibromin 2 (NF2, merlin) isoforms and the Parkinson protein 7 (PARK7, DJ1), PhD Thesis

Wozniak, R. W., G. Blobel, and M. P. Rout, 1994, POM152 is an integral protein of the pore membrane domain of the yeast nuclear envelope: *J Cell Biol*, v. 125, p. 31-42.

Yang, Q., M. P. Rout, and C. W. Akey, 1998, Three-dimensional architecture of the isolated yeast nuclear pore complex: functional and evolutionary implications: *Mol Cell*, v. 1, p. 223-34.

Yoshida, K., H. S. Seo, E. W. Debler, G. Blobel, and A. Hoelz, 2011, Structural and functional analysis of an essential nucleoporin heterotrimer on the cytoplasmic face of the nuclear pore complex: *Proc Natl Acad Sci U S A*, v. 108, p. 16571-6.

Yu, H., P. Braun, M. A. Yildirim, I. Lemmens, K. Venkatesan, J. Sahalie, T. Hirozane-Kishikawa, F. Gebreab, N. Li, N. Simonis, T. Hao, J. F. Rual, A. Dricot, A. Vazquez, R. R. Murray, C. Simon, L. Tardivo, S. Tam, N. Svrzikapa, C. Fan, A. S. de Smet, A. Motyl, M. E. Hudson, J. Park, X. Xin, M. E. Cusick, T. Moore, C. Boone, M. Snyder, F. P. Roth, A. L. Barabási, J. Tavernier, D. E. Hill, and M. Vidal, 2008, High-quality binary protein interaction map of the yeast interactome network: *Science*, v. 322, p. 104-10.

Zabel, U., V. Doye, H. Tekotte, R. Wepf, P. Grandi, and E. C. Hurt, 1996, Nic96p is required for nuclear pore formation and functionally interacts with a novel nucleoporin, Nup188p: *J Cell Biol*, v. 133, p. 1141-52.

Zhang Q¹, Yu D, Seo S, Stone EM, Sheffield VC., 2012, Intrinsic protein-protein interaction-mediated and chaperonin-assisted sequential assembly of stable bardet-biedl syndrome protein complex, the BBSome: *J Biol Chem*, v. 287, p. 20625-35.

6. Appendix

Protein-protein interactions of the Amlacher data set and the Leducq data set

Amlacher et al., 2011

ProteinA	ProteinB
nup53	nup170
nup53	nup192
nup157	nup170
nup192	asm4
nup188	nic96
nup53	nic96
nup192	nic96
nup170	nup170
nup53	nup53
nup157	nup53
asm4	nup85
nup170	nup133
nup170	nup145C
nup53	nup85
asm4	nup84
nup133	nup84
nup145C	nup84
nup145C	sec13
nup85	seh1

Leducq et al., 2012

ProteinA	ProteinB	Leducq_score	ProteinA	ProteinB	Leducq_score
Nup57	Nup49	7.756	Nup49	Nup116	1.805
Nup57	Nsp1	4.885	Nsp1	Nup100	1.642
Nup57	Nup57	4.786	Nup57	Nup100	1.474
Nup49	Nsp1	4.569	Nup116	Nup100	4.159
Nup82	Nup82	4.299	Nup116	Nup116	2.622
Nup49	Nup49	3.669	Nup116	Nup157	3.602
Nup159	Nup159	4.081	Nup192	Nup192	1.595
Nup82	Nup159	2.806	Nup49	Nup192	2.160
Nup82	Nsp1	2.613	Nup57	Nup192	2.016
Nup159	Nsp1	2.328	Nup82	Nup120	3.277
Nsp1	Nsp1	2.069	Nup82	Nup85	2.171
Nup57	Nup159	1.936	Nsp1	Nup120	1.666
Nup159	Nup157	1.880	Nup82	Nup145	1.503
Nup49	Nup159	1.606	Nup85	Nup145	3.901
Nup82	Nup157	1.571	Nup85	Nup120	3.234
Nup82	Nup116	5.075	Nup120	Nup145	2.271
Nup159	Nup116	4.179	Nup100	Nup120	2.409
Nup82	Nup100	3.846	Nup100	Nup85	2.160
Nup159	Nup100	3.319	Nup116	Nup120	1.493
Nsp1	Nup116	2.978	Nup100	Nup145	1.633
Nup157	Nup100	2.661	Nup100	Nup1	1.497
Nup57	Nup116	2.485	Nup60	Nup60	1.417

Figure 6.1

Shown are the binary protein-protein interactions of the yeast nuclear pore complex of the Amlacher data set and the Leducq data set. The proteins are colored according to their subcomplex membership: blue: nic96-complex; green: Y-complex; grey: nsp1-complex; pink: linker nups; golden brown: miscellaneous nups. The Amlacher data set comprises 19 PPIs of two major scaffold subcomplexes of the NPC that were obtained by Y2H. 14 PPIs describe connections within the nic96-complex (NUP93-complex in vertebrates) and within the Y-complex. 5 PPIs revealed connections between both subcomplexes. The Leducq data set comprises 44 PPIs that were obtained by a protein complementation assay (PCA). 15 PPIs describe connections within the nsp1-complex, three within the Y-complex, one within the nic96-complex and two between the linker nups. All other PPIs reveal connections between subcomplexes. Leducq et al., 2012 introduced an interaction score that is called Leducq score.

Crystallization data of nucleoporins collected with PDB:

ProteinA	ProteinB	ProteinA_Residue	ProteinB_Residue	Organism	PDB_ID	Pubmed_ID
Nup145C_Sec13	Nup84	731-1158	1-460	S.c.	3IKO	19855394
Nup159	Nup82	1425-1460	1-452	S.c.	3TKN	21930948
Nup82	Nup116	1-452	967-1113	S.c.	3PBP	21930948
Nup82	Nup159	1-452	1425-1460	S.c.	3PBP	22480613
Seh1	Nup85	1-349	1-564	S.c.	3EWE	18974315
Nup84	Nup145C	1-460	731-1158	S.c.	3IKO	19805193
Sec13	Nup145C	1-297	731-1158	S.c.	3JRP	19855394
Nup159	Gle1	2-387	244-538	S.c.	3RRM	21441902
NUP133	NUP107	935-1156	658-925	H.s.	3CQC	18570875
NUP133	NUP107	517-1156	658-925	H.s.	3I4R	19674973
NUP62	NUP54	362-425	346-407	R.n.	3T97	22036567
Nup53	kap121	401-448	1-1078	S.c.	3W3Y	23541588
NUP98	RAE1	158-213	1-368	H.s.	3MMY	20498086
KAP2	NUP2	88-530	1-51	H.s.	1UN0	14532109
KAP2	NUP2	88-541	1-51	H.s.	2C1T	16222336
KAP95	NUP1	1-861	974-1012	H.s.	2BPT	15878174
NUP54	NUP58	445-494	327-415	R.n.	3T98	22036567
KAP2	NUP50	75-498	1-46	M.m.	2C1M	16222336
NUP37	Nup120	1-394	1-961	Ss.p.	4FHM	22955883
NUP37	Nup120	1-393	1-950	Ss.p.	4GQ2	23019579
Nup82	NUP98	1-452	732-880	S.c./M.m.	3TKN	22480613
RAN	NUP153	1-216	703-754	R.n./H.s	3CH5	18611384
KAP1	Nsp1	1-442	497-608	H.s./S.c.	1O6O	12372823

Figure 6.2

Shown are the crystallization data that were collected in the PDB data base. The PDB-ID is depicted for each crystallization study. In all there were 23 crystals collected that could be summarized to 19 PPIs.

Y2H interactions of the yeast NPC:

SymbolA	SymbolB	GeneIDA	GeneIDB	ConstructA	ConstructB	Ranking	Count	Config
nup57	nic96	853016	850552	nup57(271-541)	nic96(1-200)	1	2	BP
nup57	nup49	853016	852703	nup57(271-541)	nup49(269-472)	3	11	VV
nup82	nup49	853385	852703	nup82(1-452)	nup49(269-472)	1	3	PB
nsp1	nup57	853409	853016	nsp1(600-823)	nup57(271-541)	2	6	PB
nsp1	nup82	853409	853385	nsp1(600-823)	nup82(452-end)	3	6	PB
nup159	nup82	854691	853385	nup159(1131-1460end)	nup82(1-452)	2	3	BP
nup85	nup82	853499	853385	nup85(1-744end)	nup82(1-452)	2	3	BP
nup133	nup82	853957	853385	nup133(881-1157end)	nup82(1-452)	3	3	BP
nup145C	nup82	85278802	853385	nup145C(606-1317)	nup82(1-452)	1	3	BP
nup145C	sec13	85278802	850905	nup145C(606-1317)	sec13(f.l.)	3	12	PB
nup145C	sec13	85278802	850905	nup145C(735-1317)	sec13(f.l.)	3	12	PB
nup145C	nup84	85278802	851441	nup145C(783-1160)	nup84(1-726end)	3	3	BP
nup145C	nup84	85278802	851441	nup145C(783-1317)	nup84(1-726end)	2	6	BP
nup145C	nup84	85278802	851441	nup145C(735-1317)	nup84(1-726end)	2	2	BP
nup145C	nup84	85278802	851441	nup145C(606-1317)	nup84(1-726end)	2	4	BP
nup145C	nup85	85278802	853499	nup145C(606-1317)	nup85(1-744end)	3	4	VV
nup145C	nup85	85278802	853499	nup145C(606-1317)	nup85(533-744end)	3	17	VV
nup145C	nup120	85278802	853808	nup145C(1140-1317)	nup120(f.l.)	3	3	BP
nup145C	nup120	85278802	853808	nup145C(606-1317)	nup120(f.l.)	3	13	VV
nup145C	nup120	85278802	853808	nup145C(735-1317)	nup120(f.l.)	3	6	BP
nup145C	nup120	85278802	853808	nup145C(735-1317)	nup120(1-757)	1	2	PB
nup145C	nup120	85278802	853808	nup145C(783-1160)	nup120(1-757)	2	2	PB
nup145C	nup120	85278802	853808	nup145C(783-1317)	nup120(f.l.)	3	11	VV
nup145C	nup120	85278802	853808	nup145C(783-1317)	nup120(1-757)	2	3	PB
nup120	nup85	853808	853499	nup120(f.l.)	nup85(1-744end)	3	13	VV
nup120	nup85	853808	853499	nup120(f.l.)	nup85(533-744end)	3	16	VV
nup120	nup85	853808	853499	nup120(822-1037end)	nup85(533-744end)	2	2	PB
nup120	nup120	853808	853808	nup120(f.l.)	nup120(1-757)	3	9	DMPB
nup120	nup120	853808	853808	nup120(1-757)	nup120(f.l.)	3	9	DMPB
nup120	nup84	853808	851441	nup120(1-757)	nup84(1-726end)	3	9	BP
nup120	nup84	853808	851441	nup120(822-1037end)	nup84(1-726end)	3	9	BP
nup133	nup85	853957	853499	nup133(881-1157end)	nup85(101-543)	3	3	BP
nup133	nup85	853957	853499	nup133(881-1157end)	nup85(1-744end)	3	3	BP
nup133	nup84	853957	851441	nup133(881-1157end)	nup84(1-726end)	3	2	BP
nup85	seh1	853499	852778	nup85(1-744end)	seh1(f.l.)	2	4	PB
nup192	asm4	853410	851470	nup192(1-1133)	nup59(f.l.)	3	9	BP
nup192	asm4	853410	851470	nup192(1-1680)	nup59(f.l.)	2	3	BP
asm4	nic96	851470	850552	nup59(f.l.)	nic96(f.l.)	2	6	PB
nup53	nic96	855184	850552	nup53(f.l.)	nic96(f.l.)	3	6	PB
nup53	nup192	855184	853410	nup53(f.l.)	nup192(1-1133)	3	9	PB
nup82	nup53	853385	855184	nup82(1-452)	nup53(f.l.)	2	6	BP
nsp1	asm4	853409	851470	nsp1(600-823)	nup59(f.l.)	1	3	PB
nup49	asm4	852703	851470	nup49(269-472)	nup59(f.l.)	1	2	PB

SymbolA	SymbolB	GeneIDA	GeneIDB	ConstructA	ConstructB	Ranking	Count	BP	Config
nup120	nup192	853808	853410	nup120(f.l.)	nup192(1-1680)	2	6	BP	
nup145C	nup192	85278802	853410	nup145C(606-1317)	nup192(1-1680)	2	4	BP	
nup85	nup100	853499	853796	nup85(101-543)	nup100(800-end)	1	2	BP	
nup85	nup100	853499	853796	nup85(101-543)	nup100(560-end)	3	8	BP	
nup85	nup100	853499	853796	nup85(1-744end)	nup100(560-end)	3	9	BP	
nup85	nup116	853499	855066	nup85(101-543)	nup116(736-end)	3	9	BP	
nup85	nup116	853499	855066	nup85(1-744end)	nup116(736-end)	3	8	BP	
nup84	nup100	851441	853796	nup84(1-726end)	nup100(800-end)	3	6	BP	
nup145N	nup145N	85278801	85278801	nup145N(457-605)	nup145N(457-605)	2	3	DM	
nup116	nup170	855066	852199	nup116(736-end)	nup170(89-473)	1	2	BP	
nup116	nup192	855066	853410	nup116(736-end)	nup192(1-1133)	1	6	PB	
nup100	nup188	853796	854868	nup100(560-end)	nup188(181-1655)	1	2	PB	
nup116	nup188	855066	854868	nup116(736-end)	nup188(181-1655)	2	5	BP	
nup100	nup82	853796	853385	nup100(560-end)	nup82(1-452)	3	9	BP	
nup116	nup82	855066	853385	nup116(736-end)	nup82(1-452)	3	9	BP	
nup145N	nup49	85278801	852703	nup145N(1-605)	nup49(269-472)	2	2	PB	
nup145C	ndc1	85278802	854977	nup145C(735-1317)	ndc1(250-655)	2	9	PB	
nup145C	ndc1	85278802	854977	nup145C(606-1317)	ndc1(250-655)	3	9	PB	
gle1	ndc1	851320	854977	gle1(f.l.)	ndc1(250-655)	2	2	BP	
nup42	gle1	851774	851320	nup42(f.l.)	gle1(f.l.)	3	11	VV	
nup42	gsp1	851774	851000	nup42(f.l.)	ran(f.l.)	1	2	PB	
nup2	gsp1	851048	851000	nup2(570-end)	ran(f.l.)	1	2	PB	
nup2	gsp1	851048	851000	nup2(592-end)	ran(f.l.)	2	5	PB	

Figure 6.3

Shown are the interactions of the Y2H screen of the yeast NPC. The proteins are colored according to their subcomplex membership: blue: nic96-complex; green: Y-complex; grey: nsp1-complex; pink: linker nups; golden brown: miscellaneous nups. To evaluate the interactions internal judgments in form of the Count (number of growing spots), the ranking (interaction score – number of growing spots dependent on occurrence of the constructs in the screening set up) and the Configuration (the direction of the interaction – BP: bait/prey, PB: prey/bait; VV: both directions; DMBP/DMPB: dimerization) were listed. The higher the Count and the Ranking, the more often was this interaction found in the Y2H screen. The Ranking is increased as well if an interaction occurs in both directions or as dimer.

Y2H interactions of the human NPC:

SymbolA	SymbolB	GeneIDA	GeneIDB	Ranking	Count	Config
SEC13	SEC13	6396	6396	3	18	DM
NUP107	NUP133	57122	55746	3	65	VV
NUP37	SEC13	79023	6396	3	16	PB
SEH1L	SEC13	81929	6396	3	15	PB
SEC13	NUPL2	6396	11097	1	2	BP
NUP133	AAAS	55746	8086	1	6	BP
NUP133	RAE1	55746	8480	2	5	BP
NUP43	TPR	348995	7175	1	2	PB
NUP37	TPR	79023	7175	3	5	PB
SEC13	POM121	6396	9883	1	4	BP
NUP54	POM121	53371	9883	1	4	PB
NUP54	NUP133	53371	55746	3	7	PB
NUP62	SEC13	23636	6396	1	5	PB
NUP54	NUP62	53371	23636	2	4	PB
NUP54	NUP54	53371	53371	3	21	DM
NUP35	NUP93	129401	9688	2	3	BP

Figure 6.4

Shown is the PPI network of the human Y2H screen. The Y2H screen resulted in 16 PPIs between 15 proteins. PPIs within and between three major scaffold subcomplexes are shown. Green: Y-complex; grey: NUP62-complex; blue: NUP93-complex. There were also connections to the membrane via POM121 (yellow), to the nuclear basket (sand) and the cytoplasmic fibrils unraveled (golden brown). The PPIs differ in configurations. Most of the PPIs are one-directed interactions either in bait-prey direction (BP) or in prey-bait direction (PB). One interaction was measured in both directions and two proteins form homo dimers (SEC13 and NUP54). The count implies the number of grown colonies. The higher the number of colonies the higher is the internal judgment, namely the rank.

Y2H interactions between human and yeast nucleoporins:

Yeast Protein	Human Protein	Yeast GenelD	Human GenelD	Yeast Construct	Human Construct	Ranking	Count	Config
nup170	AAAS	852199	8086	nup170(1252-1502)	ALADIN	1	4	BP
nup192	AAAS	853410	8086	nup192(1-1680)	ALADIN	2	2	BP
nup192	AAAS	853410	8086	nup192(1-1133)	ALADIN	2	4	BP
nic96	NUP54	850552	53371	nic96	NUP54	2	2	BP
nup170	NUP54	852199	53371	nup170(89-473)	NUP54	1	2	PB
nup192	NUP54	853410	53371	nup192(1-1133)	NUP54	3	17	BP
nup53	NUP37	855184	79023	nup53	NUP37	1	2	BP
nup192	NUP133	853410	55746	nup192(1-1680)	NUP133	3	10	PB
nup85	NUP133	853499	55746	nup85(1-744end)	NUP133	3	14	PB
nup85	NUP133	853499	55746	nup85(533-744end)	NUP133	3	49	VV
nup145C	SEC13	85278802	6396	nup145C(606-1317)	SEC13	3	19	VV
nup145C	SEC13	85278802	6396	nup145C(735-1317)	SEC13	3	17	VV
nup145C	NUP43	85278802	348995	nup145C(606-1317)	NUP43	1	2	PB
nup100	NUP37	853796	79023	nup100(560-end)	NUP37	3	6	BP
nup100	NUP43	853796	348995	nup100(560-end)	NUP43	3	13	BP
nup116	NUP37	855066	79023	nup116(736-end)	NUP37	2	2	BP
nup116	NUP43	855066	348995	nup116(736-end)	NUP43	2	3	BP
kap95	NUP37	851061	79023	kap95	NUP37	2	4	PB
kap114	NUP54	852610	53371	kap114	NUP54	1	2	BP
kap95	NUP62	851061	23636	kap95	NUP62	2	2	BP
kap95	NUP54	851061	53371	kap95	NUP54	2	4	BP
nup49	NUP54	852703	53371	nup49(269-472)	NUP54	3	13	VV
nup49	TMEM48	852703	55706	nup49(269-472)	NDC1	1	2	PB

Figure 6.5

Shown are the binary protein-protein interactions of the yeast and human nups. The proteins are colored according to their subcomplex membership: blue: nic96-complex; green: Y-complex; grey: nsp1-complex; pink: linker nups; golden brown: miscellaneous nups. To evaluate the interactions internal judgments in form of the Count (number of growing spots), the Ranking (interaction score – number of growing spots dependent on occurrence of the constructs in the screening set up) and the Configuration (the direction of the interaction – BP: bait/prey, PB: prey/bait; VV: both directions; DMBP/DMPB: dimerization) were listed. The higher the Count and the Ranking, the more often was this interaction found in the Y2H screen. The Ranking is increased as well if an interaction occurs in both directions or as dimer.

Y2H interactions of the human BBSome:

Protein B	Protein P	GenelD B	GenelD P	Construct B	Construct P	Count
BBS7	BBS2	55212	583	BBS7(1-504)	BBS2(324-721)	6
BBS7	BBS2	55212	583	BBS7(325-672)	BBS2(324-721)	6
BBS7	BBS2	55212	583	BBS7(325-672)	BBS2(579-721)	3
BBS7	BBS7	55212	55212	BBS7(325-672)	BBS7(325-672)	6
BBS7	BBS4	55212	102774	BBS7(325-672)	BBS4(1-519)	4
BBS8	BBS9	123016	27241	TTC8(1-271)	BBS9(1-410)	3
BBS8	BBS9	123016	27241	TTC8(1-531)	BBS9(1-410)	3
BBS8	BBS9	123016	27241	TTC8(1-271)	BBS9(1-890)	6
BBS9	BBS9	27241	27241	BBS9(407-890)	BBS9(1-890)	3
BBS9	BBS9	27241	27241	BBS9(407-890)	BBS9(407-890)	2
BBS9	BBS9	27241	27241	BBS9(407-890)	BBS9(747-890)	2
BBS9	BBS9	27241	27241	BBS9(1-890)	BBS9(1-890)	5
BBS9	BBS1	27241	582	BBS9(1-890)	BBS1(412-593)	3
BBS9	BBS1	27241	582	BBS9(407-890)	BBS1(412-593)	6
BBS9	BBS2	27241	583	BBS9(407-890)	BBS2(324-721)	6
BBS9	BBS2	27241	583	BBS9(407-890)	BBS2(579-721)	6
BBS9	BBS2	27241	583	BBS9(1-890)	BBS2(324-721)	4
BBS9	BBS2	27241	583	BBS9(1-890)	BBS2(579-721)	3
BBS9	BBS4	27241	102774	BBS9(407-890)	BBS4(1-268)	3
BBS9	BBS4	27241	102774	BBS9(407-890)	BBS4(1-519)	3

Figure 6.6

Shown are the binary protein-protein interactions of the human BBSome obtained with our Y2H screen. The six BBSome proteins are indicated by different colors. The screen resulted in 20 interactions between 13 BBSome constructs. Beside PPI information between full length proteins the screen resulted in interaction data between BBSome fragments indicating the interaction domain.

Y2H interactions between BBSome components and NPC components:

Protein A	Protein B	GeneID A	GeneID B	ConstructA	Construct B	Count
SEC13	BBS1	6396	582	SEC13	BBS1(1-593)	3
SEC13	BBS1	6396	582	SEC13	BBS1(1-413)	3
SEC13	BBS1	6396	582	SEC13	BBS1(412-593)	2
NUP43	BBS2	348995	583	NUP43	BBS2(324-721)	3
SEC13	BBS2	6396	583	SEC13	BBS2(1-721)	2
SEC13	BBS2	6396	583	SEC13	BBS2(1-327)	2
SEC13	BBS2	6396	583	SEC13	BBS2(1-397)	2
SEC13	BBS2	6396	583	SEC13	BBS2(1-583)	2
BBS4	SEC13	102774	6396	BBS4(1-519)	SEC13	2
BBS4	SEC13	102774	6396	BBS4(1-519)	SEC13	3
BBS7	SEC13	55212	6396	BBS7(1-327)	SEC13	3
BBS7	SEC13	55212	6396	BBS7(1-402)	SEC13	3
BBS7	SEC13	55212	6396	BBS7(1-504)	SEC13	2
BBS9	SEC13	27241	6396	BBS9(1-890)	SEC13	2
BBS9	SEC13	27241	6396	BBS9(1-410)	SEC13	3
NUP37	BBS7	79023	55212	NUP37	BBS7(325-672)	4
BBS7	NUP54	55212	53371	BBS7(325-672)	NUP54	4
BBS7	NUP54	55212	53371	BBS7(325-672)	NUP54	3
BBS7	NUP54	55212	53371	BBS7(325-672)	NUP54	4
BBS7	NUP62	55212	23636	BBS7(325-672)	NUP62	3
BBS7	NUP155	55212	9631	BBS7(325-672)	NUP155	3
NUP155	BBS2	9631	583	NUP155	BBS2(324-721)	3
TPR	BBS2	7175	583	TPR	BBS2(1-327)	2
BBS4	NUP155	102774	9631	BBS4(1-519)	NUP155	3
BBS7	AAAS	55212	8086	BBS7(325-672)	aladin	4
BBS9	AAAS	27241	8086	BBS9(747-890)	aladin	4

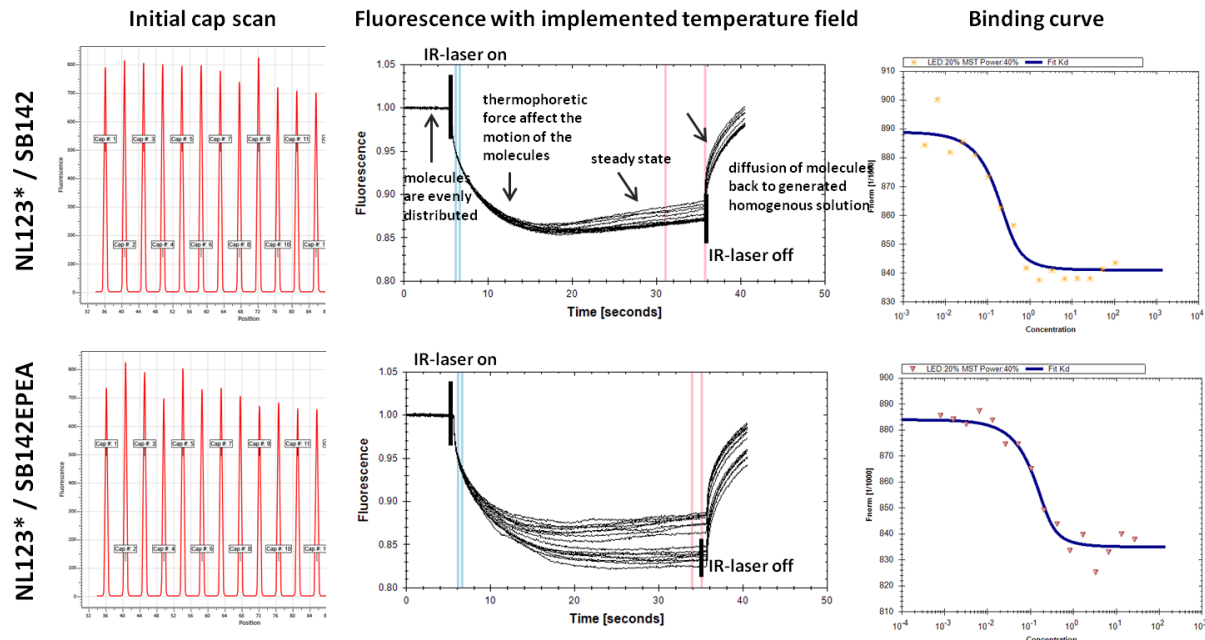
Figure 6.7

Shown are the binary interactions of BBSome fragments with human full length constructs. The Y2H screen resulted in 26 interactions between the human BBSome and the human NPC. The NPC components are colored according to their NPC subcomplex membership: blue: NUP93-complex; green: Y-complex; grey: NUP62-complex; golden brown: miscellaneous nups. The several BBSome components are indicated by different colors.

Micro-scale thermophoresis – Validation of selected yeast PPIs

[nup145C(34-712)/nup120/sec13]*::[nup85/seh1]

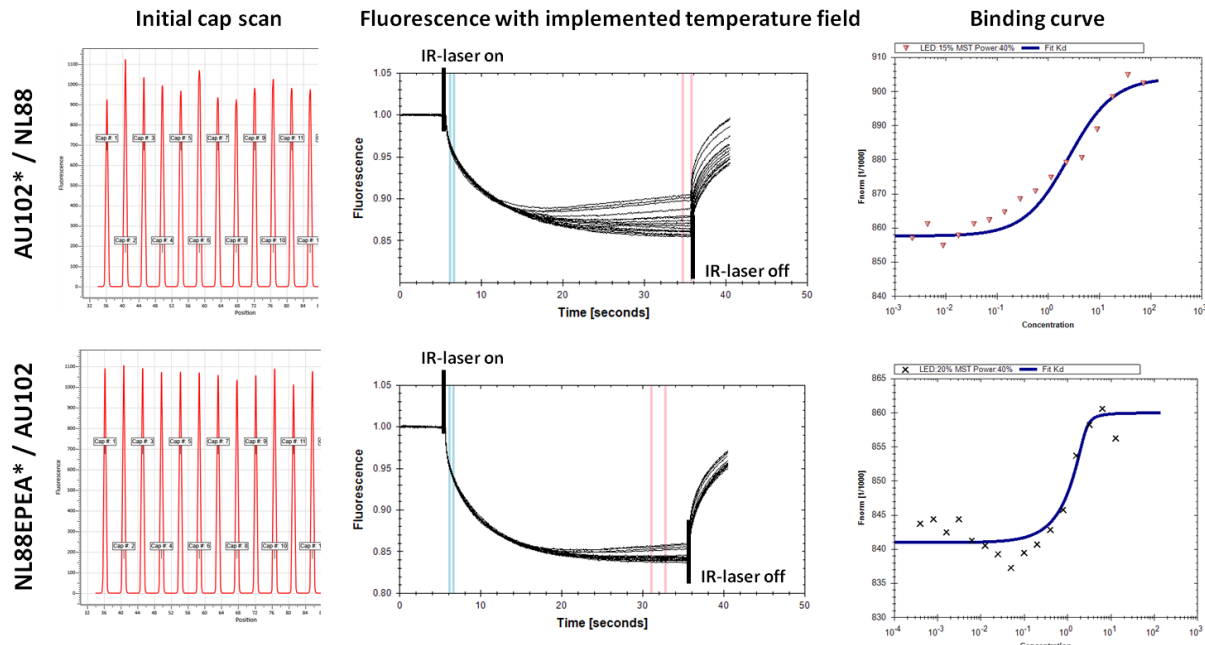
„Y-complex hub“



$$K_D = 0.16 - 0.17 \mu\text{M}$$

[nup120(1-757)]*::[nup133(521-1157)/nup84]

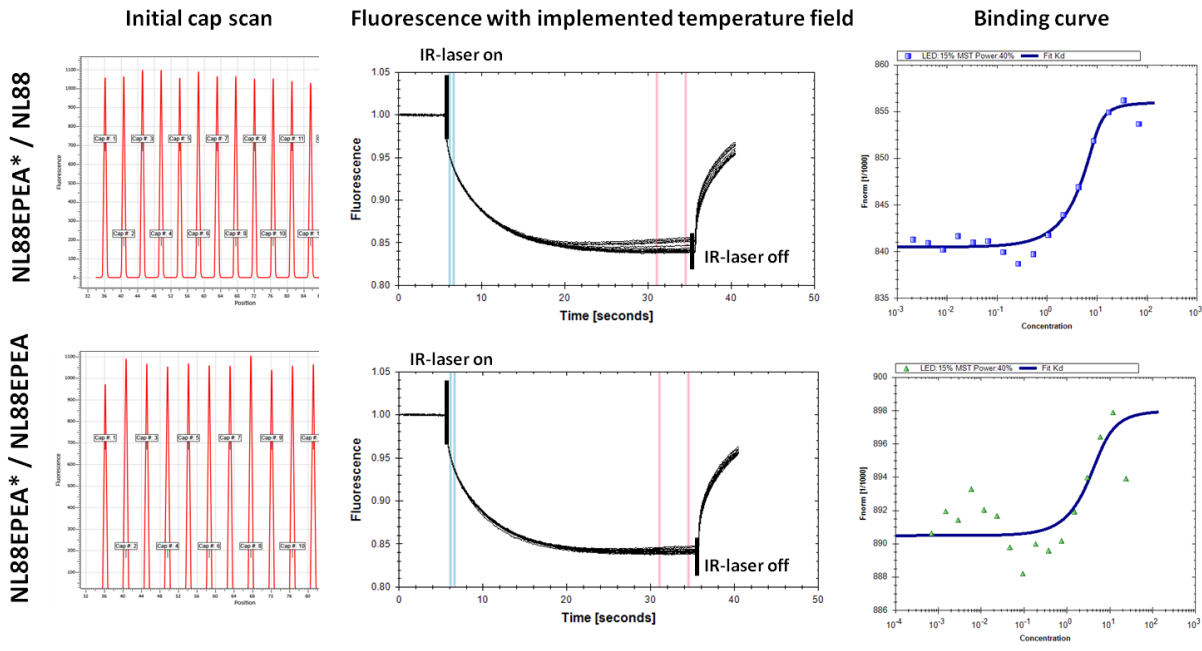
nup120-nup84



$$K_D = 1 - 2 \mu\text{M}$$

[nup120(1-757)]*::[nup120(1-757)]

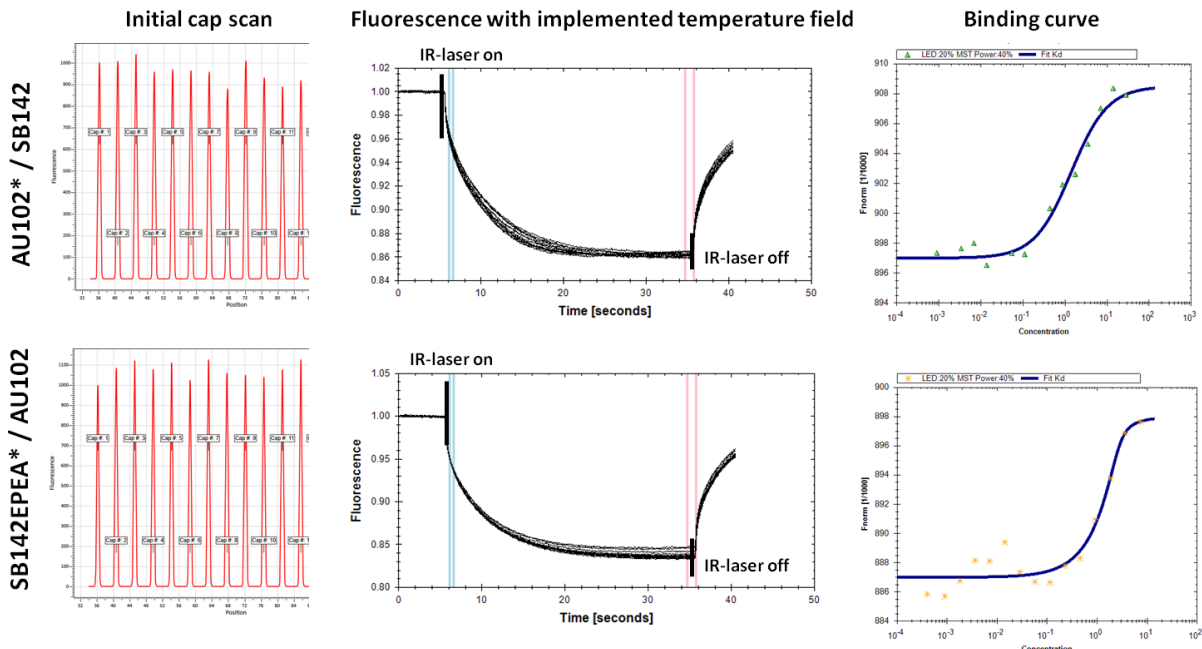
nup120-nup120



$$K_D = 3 - 4 \mu\text{M}$$

[nup85/seh1]*::[nup133(521-1157)/nup84]

nup85-nup133



$$K_D = 2 - 3 \mu\text{M}$$

Figure 6.8 Shown are the capillary scans, the initial fluorescence and the resulting binding curves of the “Y-complex hub” interactions nup85/nup145C or nup120/nup145C, the homo dimerization nup120 (aa 1-757)/nup120 (aa 1-757), nup85/nup133 and nup84/nup120.

The samples are filled in MST capillaries by capillary force. The intensity of the fluorescently labeled protein construct is measured with the initial cap scan to ensure that the fluorescently labeled molecule is kept constant throughout all 16 capillaries. The local change of fluorescence intensity due to the motion of labeled molecules is observed while the IR-laser implements a temperature gradient. The motion of fluorescently labeled molecules is divided in different phases: the molecules are evenly distributed and diffuse freely in the solution. By switching on the IR-laser the thermophoretic force affects the molecules that change their motions, typically they move out of the heated spot. A steady state phase followed in that the molecule flow is balanced. By turning off the IR-laser the molecules diffuse back to generated again a homogenous solution. The fluorescence measurements result finally in the binding curve. Using this curve a K_D can be determined (see section 3.3.1.3).

Protein Complementation Assay – Validation of selected PPIs of the human NPC:

Protein_1	Protein_2	ProtID_1	ProtID_2	Vector_1	Vector_2	PPI localization
NUP62	SEC13	RZPDo839E01149	CCSB_4052	pVEN_F1C	pVEN_F2N	Nuclear rim
NUP62	SEC13	RZPDo839E01149	CCSB_4052	pVEN_F1C	pVEN_F2N	Nuclear rim
SEC13	NUP62	CCSB_4052	RZPDo839E01149	pVEN_F1N	pVEN_F2C	Nuclear rim
SEC13	NUP62	CCSB_4052	RZPDo839E01149	pVEN_F1N	pVEN_F2N	Nuclear rim
SEC13	NUP62	CCSB_4052	RZPDo839E01149	pVEN_F1N	pVEN_F2N	Nuclear rim
SEC13	SEC13	CCSB_4052	CCSB_4052	pVEN_F1N	pVEN_F2N	Nuclear rim
SEC13	SEC13	CCSB_4052	CCSB_4052	pVEN_F1N	pVEN_F2N	Nuclear rim
SEC13	SEC13	CCSB_4052	CCSB_4052	pVEN_F1N	pVEN_F2N	Nuclear rim
SEC13	SEH1	CCSB_4052	CCSB_632	pVEN_F1N	pVEN_F2N	Nuclear rim
SEC13	SEH1	CCSB_4052	CCSB_632	pVEN_F1N	pVEN_F2N	Nuclear rim
SEC13	SEH1	CCSB_4052	CCSB_632	pVEN_F1N	pVEN_F2C	Nuclear rim
SEC13	SEH1	CCSB_4052	CCSB_632	pVEN_F1N	pVEN_F2C	Nuclear rim
SEH1	SEC13	CCSB_632	CCSB_4052	pVEN_F1C	pVEN_F2N	Nuclear rim
SEH1	SEC13	CCSB_632	CCSB_4052	pVEN_F1C	pVEN_F2N	Nuclear rim
SEH1	SEC13	CCSB_632	CCSB_4052	pVEN_F1N	pVEN_F2N	Nuclear rim
NUP107	NUP133	FLJ11217AAAN	FLJ95222AAAF	pVEN_F1C	pVEN_F1C	Nuclear rim
NUP107	NUP133	FLJ11217AAAN	FLJ95222AAAF	pVEN_F1C	pVEN_F2C	Nuclear rim
NUP107	NUP133	FLJ11217AAAN	RZPDo839H0993	pVEN_F1C	pVEN_F2C	Nuclear rim
NUP133	NUP107	FLJ95222AAAF	FLJ11217AAAN	pVEN_F1C	pVEN_F2C	Nuclear rim
NUP133	NUP85	FLJ95222AAAF	CCSB_3256	pVEN_F1C	pVEN_F2N	Nuclear rim
NUP133	NUP85	FLJ95222AAAF	CCSB_3256	pVEN_F1C	pVEN_F2C	Nuclear rim
NUP133	NUP107	RZPDo839H0993	FLJ11217AAAN	pVEN_F1C	pVEN_F2C	Nuclear rim
NUP133	NUP107	RZPDo839H0993	FLJ11217AAAN	pVEN_F1C	pVEN_F2C	Nuclear rim
NUP133	NUP85	RZPDo839H0993	CCSB_3256	pVEN_F1C	pVEN_F2N	Nuclear rim
NUP85	NUP133	CCSB_3256	RZPDo839H0993	pVEN_F1C	pVEN_F2C	Nuclear rim
NUP85	NUP133	CCSB_3256	RZPDo839H0993	pVEN_F1C	pVEN_F2C	Nuclear rim

Figure 6.9

Shown are the PPIs of all constructs that were used in the PCA approach and showed nuclear rim staining. The nups are colored according to their subcomplex membership: green: Y-complex, grey: NUP62-complex. More than one protein construct pair for each PPI resulted in staining of the nuclear rim indicating the PPI within the NPC. All constructs were negatively controlled and resulted in other pairings in no fluorescence. The vectors differ in the position of the splitted YFP fragment: pVEN_F1/2C: N-terminal; pVEN_F1/2N: C-terminal. The Prot_ID indicate the different constructs.

Formulars:

Frequency Distribution of the Copurification Scores, related to Fig 3.7 and 3.8

$$C(p,q) = \frac{\sum_i \frac{K_{ip} K_{iq}}{\sum_j K_{ij} - 1}}{\sqrt{\sum_i K_{ip} \sum_i K_{iq}}}$$

K = binary matrix
 p = protein p
 q = protein q

The normalized co-purification score was calculated for the protein pairs of the co-AP data set of Alber et al., 2007. All containing complex data were summarized in a binary matrix K with columns representing the purifications and rows representing the different proteins. If a protein p was detected in a purification i, then $K_{ip} = 1$; otherwise $K_{ip} = 0$. Based on this matrix, the co-purification score $C(p,q)$ was calculated for all pairs of proteins p and q.

The co-occurrences of the two protein were counted and each co-occurrence was divided by the total number of proteins in the according composite (purification). This was subtracted minus one to favor co-occurrences in more stringent purifications containing fewer proteins. The specificity of the two proteins is involved in the denominator by the geometric mean of the number of complexes containing p and q and favors the co-occurrence of more specific proteins.

The Z-score calculation from a raw score, related to Fig 3.8

$$Z = \frac{X - \mu}{\sigma}$$

μ = mean of a distribution
 σ = standard deviation of a distribution
 X = raw value

Y2H data set:

$$Z = \frac{0.19 - 0.09}{0.015}$$

$$\begin{aligned} X &= 0.19 \\ \mu &= 0.09 \\ \sigma &= 0.015 \end{aligned}$$

$$Z = 6.7$$

Amlacher data set:

$$Z = \frac{0.19 - 0.11}{0.026}$$

$$\begin{aligned} X &= 0.19 \\ \mu &= 0.11 \\ \sigma &= 0.03 \end{aligned}$$

$$Z = 3.3$$

Leducq data set:

$$Z = \frac{0.14 - 0.11}{0.011}$$

$$\begin{aligned} X &= 0.11 \\ \mu &= 0.14 \\ \sigma &= 0.011 \end{aligned}$$

$$Z = 2.7$$